CRANFIELD UNIVERSITY

Giacomo Struzziero

Optimisation of the VARTM process

School of Aerospace, Transport & Manufacturing (formerly SAS)

PhD Thesis
Academic Years: 2010-2014

Supervisor: Dr Alexandros A. Skordos
August 2014

CRANFIELD UNIVERSITY

Giacomo Struzziero

Optimisation of the VARTM process

School of Aerospace, Transport & Manufacturing (formerly SAS)

PhD Thesis
Academic Years: 2010-2014

Supervisor: Dr Alexandros A. Skordos
August 2014

This thesis is submitted in partial fulfilment of the requirements for the degree of PhD

ABSTRACT

This study focuses on the development of a multi-objective optimisation methodology for the vacuum assisted resin transfer moulding composite processing route. Simulations of the cure and filling stages of the process have been implemented and the corresponding heat transfer and flow through porous media problems solved by means of finite element analysis. The simulations involved material sub-models to describe thermal properties, cure kinetics and viscosity evolution. A Genetic algorithm which constitutes the foundation for the development of the optimisation has been adapted, implemented and tested in terms of its effectiveness using four benchmark problems. Two methodologies suitable for multi-objective optimisation of the cure and filling stages have been specified and successfully implemented. In the case of the curing stage the optimisation aims at finding a cure profile minimising both process time and temperature overshoot within the part. In the case of the filling stage the thermal profile during filling, gate locations and initial resin temperature are optimised to minimise filling time and final degree of cure at the end of the filling stage. Investigations of the design landscape for both curing and filling stage have indicated the complex nature of the problems under investigation justifying the choice for using a Genetic algorithm. Application of the two methodologies showed that they are highly efficient in identifying appropriate process designs and significant improvements compared to standard conditions are feasible. In the cure process an overshoot temperature reduction up to 75% in the case of thick component can be achieved whilst for a thin part a 60% reduction in process time can be accomplished. In the filling process a 42% filling time reduction and 14% reduction of degree of cure at the end of the filling can be achieved using the optimisation methodology. Stability analysis of the set of solutions for the curing stage has shown that different degrees of robustness are present among the individuals in the Pareto front. The optimisation methodology has also been integrated with an existing cost model that allowed consideration of process cost in the optimisation of the cure stage. The optimisation resulted in process designs that involve 500 € reduction in process cost. An inverse scheme has been developed based on the optimisation

methodology aiming at combining simulation and monitoring of the filling stage for the identification of on-line permeability during an infusion. The methodology was tested using artificial data and it was demonstrated that the methodology is able to handle levels of noise from the measurements up to 5 s per sensor without affecting the quality of the outcome.

Keywords:

Infusion, Cure, Inverse procedure, Genetic algorithm, Optimisation, Multi-objective, Temperature overshoot, Degree of cure, Filling time

When you have eliminated the impossible,

Whatever remains, however improbable, must be the truth.

(Sir Arthur Conan Doyle)

Lo duca e io per quel cammino ascoso
intrammo a ritornar nel chiaro mondo;
e sanza cura aver d'alcun riposo,

salimmo sù, el primo e io secondo,
tanto ch'i' vidi de le cose belle
che porta 'l ciel, per un pertugio tondo.

E quindi uscimmo a riveder le stelle.

(Dante Alighieri)

ACKNOWLEDGEMENTS

My deepest gratitude goes to my supervisor Dr. A. Skordos for his priceless guidance, moral support through hard times, patience, caring, advices and for the crucial discussions about work and life which have been a turning point during this adventure.

I'm very thankful to Dr. G. Dell'Anno and Dr. D. Ayre for their precious help and for introducing me to the correct approach and discipline to mechanical testing.

I'm very grateful to Dr. E. Costa for being always available and willing to clarify my doubts. I would like to warmly thank Mr. J. Hurley for introducing me to the VARTM technique and for his technical assistance.

Special thanks go to my father Domenico, my sister Giulia and my brother in law Danilo. You have been there throughout it all and I couldn't have got through without you.

My sweetest thoughts go to my little niece Gaia and my little nephew Gioele.

I thank all my friends, the ones who have been rooting for me from Cesenatico for their constant support and encouragement and the ones who have shared this experience at Cranfield University with me.

This journey would have not been the same without my fellow mates Diego, Paul, Tassos, Thomas and Vincenzo who were there through the good and bad times.

Thanks to my volleyball mates and friends Mike and Stefan. I will always treasure the fabulous moments spent together on and off the volleyball court.

Special mention goes to my oldest friends Alessandro, Andrea, Danilo, Fabio, Fabio G., Michele, Francesco, Giacomo, Ruben and Valentina. I have always felt privileged to have you all right by my side.

A last thought goes to those who would have loved seeing this coming true but that unfortunately have not been given enough time.

TABLE OF CONTENTS

LIST OF FIGURES

LIST OF TABLES

LIST OF EQUATIONS

LIST OF ABBREVIATIONS

ANN	Artificial Neural Network
BP	Back Propagation
BBS	Branch and Bound Search
CMC	Cranfield Monitoring and Control system
CO	Cascaded Optimisation
DSC	Differential Scanning Calorimetry
EA	Evolutionary Algorithm
ES	Evolutionary Strategy
FEA	Finite Element Analysis
FE/CV	Finite Element/Control Volume
FEM	Finite Element Method
GA	Genetic Algorithm
GLO	Global Local Optimiser
IQR	Interquartile Range
LCO	Local Criterion Optimisation
LCM	Liquid Composite Moulding
LRI	Liquid Resin Infusion
MES	Modified Evolutionary Strategy
MOGA	Multi Objective Genetic Algorithm
NSGA	Non-dominated Sorted Genetic Algorithm
PISA	Platform and Programming Language Independent Interface for Search Algorithms
RES	Robust Evolutionary Strategy
RIFT	Resin Infusion under Flexible Tooling
RTM	Resin Transfer Moulding
SA	Simulated Annealing
SPEA	Strength Pareto Evolutionary Algorithm
SQP	Sequential Quadratic Programming
VARTM	Vacuum Assisted Resin Transfer Moulding
VEGA	Vector Evaluated Genetic Algorithm
WP	Work Package

1 Overall Introduction

1.1 Motivations and goals

Composite materials have been widely used by humans throughout history in structural applications because of their versatility in providing tailored mechanical behaviour. This has been the case of cellulose reinforced by lignin (wood) and steel reinforced by concrete. Nowadays modern composites maintain an edge in mechanical performance associated with a cost penalty due to their complex manufacturing. The cost implications are intensified as the size and complexity of the final part increase. In the past 60 years composite materials have gradually broadened their application fields becoming widely used in a variety of different industries. Modern composite materials were first introduced in the late 1950s and their superior mechanical performance associated with a low specific weight was immediately noticed by the aerospace industry with particular attention paid by the military field. The necessity for best performance in the aerospace military field led to quick adoption of composite materials in military aircraft industry exploiting the potential of these new materials regardless of process cost. In 1969 boron epoxy rudders were installed on an F-4 jet made by General Dynamics. Also the F-14 (US Navy) and F-15 (US Air Force) used boron epoxy composites for the empennage [1]. With time the potential of composites became attractive for commercial aviation and other industry fields such as automotive, naval and high level competitive sports. As space and military demand declined developments in the field of composites focused more on the requirements of these industrial sectors with the process and materials cost gaining increasing importance. Today the percentage use of composites by weight in aircraft has reached 50% with Boeing 787 and 53% with Airbus 350 [2], Figure 1-1.

Figure 1-1 Composite fuselage for the A350 XWB (© Airbus/M. Lindner), [2]

Following the trend for improved process efficiency, predictive process modelling, process monitoring, optimisation and automation have become highly relevant objectives of research. In this perspective Liquid Composite Moulding (LCM) has begun to be considered a viable alternative to the expensive autoclave process route due to its potential for easier automation and control. The earliest aerospace application of liquid moulding was the manufacture of radomes. The Concorde radome was one of the first components in service manufactured by means of Resin Transfer Moulding (RTM). The Concorde incorporated also the first use of high performance epoxy resins given its supersonic regime and associated temperatures up to 200 ºC. Since 1960s RTM has been used for fabrication of propeller blades; some examples are Fokker F50 and Saab S340. In the 1980s composite materials have been introduced to manufacture lightweight and low cost airframes in place of aluminium alloys with subsequent reduction in weight and manufacturing costs. Several airframe parts have been manufactured by RTM for the F-22 and F117-A fighters. Engine and nacelle components have also been produced by RTM. In the aerospace industry the most important factors are weight and performance, requiring volume fibre fraction often higher than 60%. The epoxy resin used needs several hours for cure ending in a very low production rate (100s parts per year). In the automotive industry structural parts require fibre volume fraction higher than 35%, it follows that high quality components can be produced economically with a production rate up to 10000 parts per year; for example the DB7 Aston Martin has the hood, fenders and

deck-lid manufactured by RTM. Other examples of structural parts produced by RTM in the automotive are convertible hard tops for the Alpha Romeo Spider (Italy) and body panels for the BMW Z-1 (Germany) [3; 4].

Vacuum Assisted Resin Transfer Moulding (VARTM) has started to be put forward as a high potential alternative in recent years. In VARTM the compaction pressure is provided by the atmosphere by means of vacuum applied within the vacuum bag which is sealed to the mould. Once the vacuum within the bag is reached and stabilised the resin is injected and the flow is driven by the negative pressure gradient between the inlet and the outlet. The impregnation ends when the resin reaches the outlet gate; Figure 1-2 illustrates a schematic of the process. A flow media is applied on one or two sides of the reinforcement stack to enhance the flow speed, while a peel ply is used to facilitate the removal of the flow media after infusion [5].

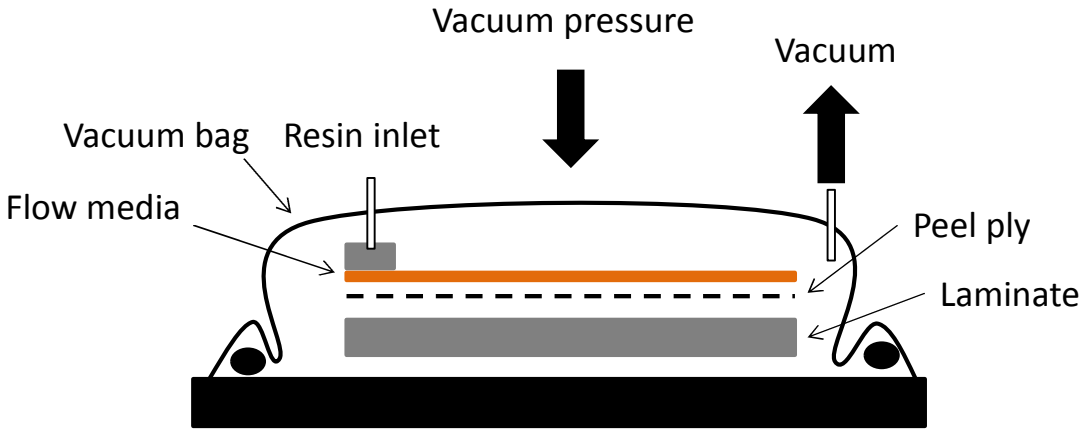

Figure 1-2 Schematic of VARTM process

VARTM is significantly less expensive than RTM due to its lower tooling cost corresponding to the use of a flexible bag on one side and the lower requirements in terms of pressure application. The absence of an autoclave for curing and the presence of a flexible bag also make the process able to handle large structures without generating prohibitive scale up costs. These combined characteristics make the process attractive to the aerospace industry. Nevertheless, in addition to increased significance of production costs, the aerospace industry has very stringent requirements in terms of quality.

The complex nature of the VARTM process makes a trial and error approach to process design inefficient. Furthermore, the compressed time scale of development highlights the pivotal importance of the design stage leaving no room for mistakes at this step. It is at this phase of the process that cost and quality are determined. Therefore, the design/development stage is where the choices are made to comply with the desired specifications whilst satisfying targets related to process efficiency. In such a scenario, conformity with specifications cannot be addressed at the end of the production line because even though such change might be feasible, rework costs can be prohibitive. The more issues avoided and prevented early on through a carefully designed process the fewer problems will appear at later stages.

A variety of causes can result in a poor manufacturing quality of composite parts; namely degradation of resin due to exothermic effects, dry spots and porosity due to air entrapment or incomplete filling, distortion after removal from the tool and thickness variations. Therefore a systematic approach capable of both taking into account the large set of variables and phenomena involved and investigating new feasible optimised design solutions is needed in order to make the process realise its full potential. Simulation and optimisation of the process are required in order to predict the effect of design choice on the final product and to set the process choosing optimised parameters able to maximise the quality of the product, minimise defects, maximise production rate for a specific geometry and minimise process cost. Furthermore, reliable process optimisation contributes to scrap and waste material reduction making the process more environmentally sustainable by decreasing both the need for recycling composite materials and the number of processes run with subsequent energy saving.

1.2 Aim and objectives

The overall aim of the present work is to achieve an efficient and high quality automated design of the infusion process addressing high end applications. This is accomplished by the following objectives:

- Cure and filling simulations for both stages of VARTM to give an insight of the relations among variables playing an important role within the process;
- Identification and selection of key parameters to be optimised for both the cure and filling stages;
- Identification of competitive objectives, which need to be quality and cost relate and are affected significantly by the parameters selected;
- Investigation of the landscape of the cure and filling problems;
- Development/adaptation of a suitable optimisation tool to deal with the aforementioned landscapes;
- Testing of the optimisation method against benchmarks and established software to prove reliability, robustness and performance;
- Building interfaces capable to handle and solve the multi-objective problem sets;
- Finding out and quantifying trade-off for both filling and cure process.
- Evaluation of the process performance benefits that can be achieved using optimisation;
- Development of an inverse routine capable to perform on-line estimation of permeability;
- Testing of the robustness of the inverse scheme against different levels of artificial noise;

1.3 Project setting

The work in this thesis is part of the INFUCOMP FP7 European project. The aim of the project was to develop the appropriate simulation tools to automate Liquid Resin Infusion (LRI) technologies as a low-cost and high performance alternative to metal and prepreg composite solutions. The focus of the project was the aerospace industry. A group of partners comprising universities and companies with expertise in relevant fields spread in eight countries collaborated at the project: ESI GmbH (Germany), ARMINES (France), Cranfield University (UK), DAHER Aerospace (France), ESI group (France), Hexcel (France), Katholieke Universiteit Leuven (Belgium), Patras University

(Greece), Swerea SICOMP AB (Sweden), Bombardier Aerospace (UK), Israel Aerospace Industry (Israel), INASCO (Greece), Institute for Aircraft Design (Germany) and Piaggio Aero Industries S.p.a. (Italy).

The work within the project was divided in nine different work packages addressing different aspects of the process:

- WP1 Project management, dissemination and exploitation;
- WP2 Fabric deformation characterisation: Mechanical fabric testing to gather data for fabric deformation laws have been undertaken. Results have been implemented in the FE draping software;
- WP3 Viscosity and permeability characterisation: resin viscosity testing for predicting viscosity behaviour has been carried out and results implemented in the LRI infusion software;
- WP4 Preform tooling and assembly simulation: Deformation in fabric affects permeability and therefore infusion. Methodologies to address the coupled problem have been developed;
- WP5 Infusion simulation development: New developments for thick, large scale components simulation have been developed and validated;
- WP6 Cost analysis and cost optimisation: Cost analysis simulation and optimisation of the overall process have been undertaken;
- WP7 Post infusion defects prediction: Influence of defects like residual stresses and void content upon mechanical performances have been experimentally and numerically investigated;
- WP8 Process optimisation: Optimisation technique (evolutionary) have been developed to optimise both cure and infusion stage. An inverse scheme for on-line estimation of permeability has been also developed;
- WP9 Industrial validation: three demonstrator parts have been fabricated for industrial validation

The work packages this work has contributed to were WP8 in which the development of methodologies capable to address the optimisation of the two stages involved in the process and on line estimation of parameters such as permeability were addressed and WP6 in which the development of a

cost/quality optimisation methodology was developed in collaboration with the University of Patras and Bombardier Aerospace..

1.4 Road map

The main body of this thesis is structured as follows:

- Chapter 2 reviews the state of the art concerning optimisation of composite materials manufacturing, describing briefly the different typology of optimisation and describing in detail the effort made by the scientific community in the field up to date;
- Chapter 3 presents the genetic algorithm adapted in this study and the tests carried out to prove its reliability, robustness and reproducibility;
- Chapter 4 reports the modelling methodology applied and the constitutive material models;
- Chapters 5 presents the work on optimisation of the cure stage of the process taking into account both process time and maximum temperature within the part;
- Chapter 6 addresses the optimisation of the filling stage of the process minimising both filling time and degree of cure at the end of the filling stage;
- Chapter 7 describes the optimisation of cost and performance related to the cure stage;
- Chapter 8 presents the inverse scheme able to estimate unknown properties of the material such as permeability.

Chapters 9-11 report the overall discussion of the work, conclusions and suggestions for areas further of development on the topic of this study.

2 Numerical optimisation of composites processing

2.1 Introduction

This chapter reviews the state of the art on optimisation of composites manufacturing. The continuous pursuit of performance, robustness and efficiency in the aerospace, automotive, marine and energy industries has been reflected in shifting the scale, production rate and part complexity requirements that the composites manufacturing sector has to respond to. The process design challenges associated with this transition are significant and can be partially met by the integration of manufacturing simulation in the design loop. The potential benefits of simulation are enhanced a great deal by the adoption of computational optimisation to determine efficient processing parameters. The focus of relevant research has been on single-objective problems with multi-objective setups starting to receive attention in recent years. Flow and curing have concentrated most of the research effort on the topic, with optimisation schemes developed for both continuous and batch processing. The majority of optimisation problems have been tackled using heuristic methods.

2.2 Design and performance of composites processing

Nowadays composite materials have become one of the most important material options in a wide variety of fields because of their high mechanical performance. First consequence of this great diffusion is a renewed interest in processing. During the last fifty years different techniques have been developed in order to improve the quality of manufacture. Several different processes to fabricate composite materials have been devised, most of them involving some common steps which accomplish broadly the forming/deposition of the reinforcement, filling/consolidation of the assembly and curing/cooling of the matrix. Differences in aspects of the processes can be pointed out, e.g. different ways of reinforcement deposition (manual lay-up, filament winding, pultrusion), different ways of impregnate fabrics, different means of heating to initiate the curing reaction.

In the last decade the increasing interest in keeping the process cost and time as low as possible without compromise the quality and the performance, has led to a focus on the optimisation of these key aspects. The importance of optimising taking into account more than one objective within a certain process was dictated by the complexity of the links between the variables that govern the different stages of manufacture and the close interdependencies of certain variables. The optimisation of composite processes has been addressed using both gradient based technique and stochastic search algorithm; the benefits and drawbacks of each of these techniques led to the development of hybrid techniques.

In composite processing a large number of design variables impact process performances. The choice of design parameters affects the governing phenomena. In turn the evolution of governing phenomena determines the manifestation of process issues and the quality of the final product, as depicted in Figures 2-1, 2-2. Figure 2-1 illustrates which governing phenomena are affected by changes in design parameters within the process. The heat transfer problem is affected by changes in cure profile and initial mould and resin temperature. A change in these parameters results in a different heat transfer problem with subsequent different temperature distribution therefore different gradient temperature and overshoot. Cure kinetics is affected by the same design parameters with the initial resin temperature influencing the initial state of the resin. A satisfactory mould filling is influenced by an appropriate design of gate and vent locations together with a suitable initial resin and mould temperature as these have a direct effect on resin viscosity. Injection pressure or flow front speed, depending on which control flow strategy has been selected, must be chosen aiming to achieve a complete filling before the resin viscosity increases dramatically. Flow front speed has also an effect on the quality of impregnation and can generate micro and macro-voids so that constraints are imposed to the selection of this parameter [6].

Figure 2-2 depicts which process defects due to different governing phenomena. Altering the heat transfer and cure kinetics phenomena causes

different degree of cure evolution and different minimum degree of cure. Furthermore, these might trigger a very fast cure reaction with subsequent high level of overshoot leading to non-uniformity in cure, residual stresses and in extreme cases degradation of the part. Non-uniformity in cure is also caused by inadequate impregnation which also leads to void formation.

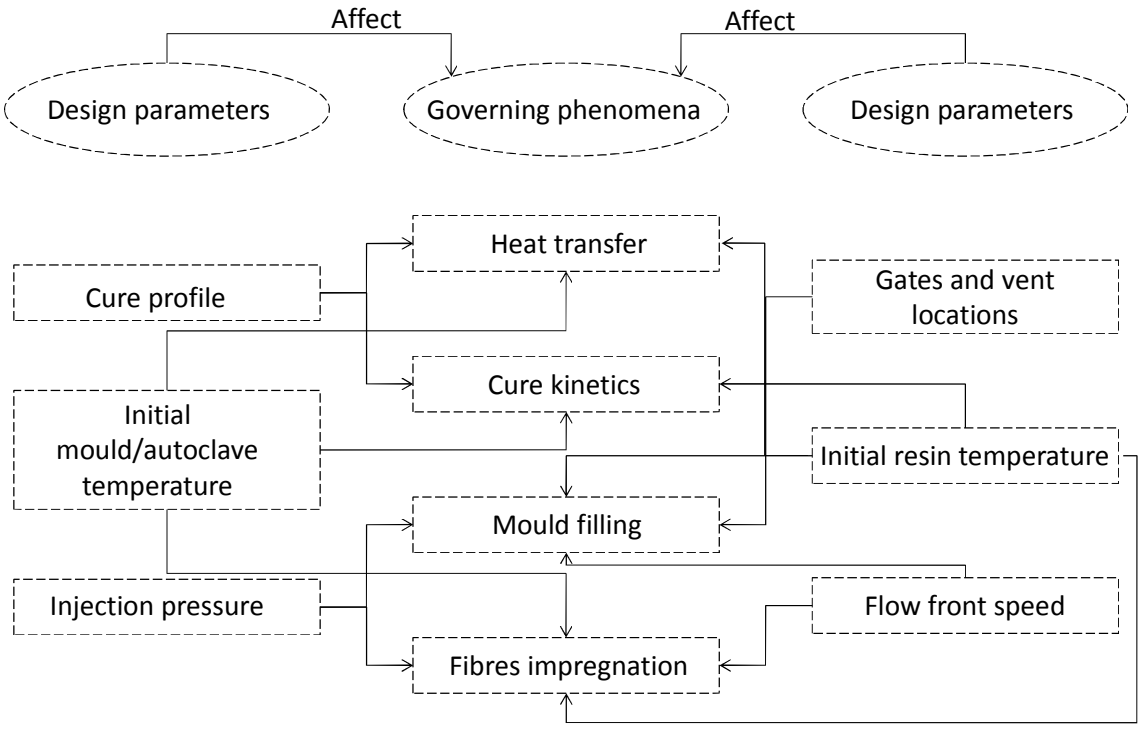

Figure 2-1 Relationship between design parameters and governing phenomena

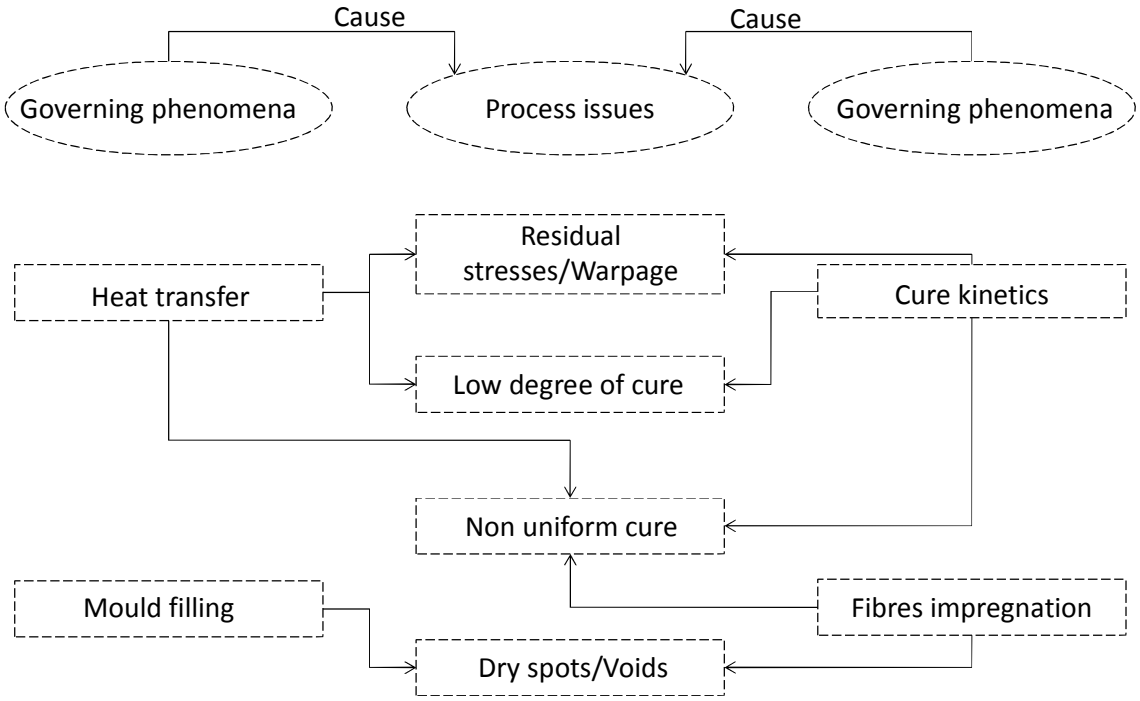

Figure 2-2 Relationship between governing phenomena and process issues

2.3 Overview of the research landscape on composites process optimisation

Figure 2-3 presents an overview of research on composites processing optimisation. Three major fields have been addressed in the literature concerning composites process optimisation: cure, impregnation and drape optimisation. Filament winding optimisation has received limited coverage and since in these articles the objectives are strictly correlated with final shape and drape, it is possible to include them within this category

Within each category there is a further division between single and multi-objective optimisation. Cure optimisation has been carried for two principal variations: pultrusion and batch processes. In works dealing with single-objective optimisation, residual stresses and process time have been optimised in both processes mainly using gradient based techniques. In works addressing multi-objective optimisation pull speed and energy consumption have been dealt with for the pultrusion process, whereas for batch processes three different objective combinations have been used: process time and degree of

cure, process time and maximum exotherm, process cost and process time. All multi-objective cure problems have been implemented using a Genetic Algorithm (GA).

In impregnation related problems only the RTM process has been addressed. Voids, filling time and filling distance have been taken into account for single-objective optimisation tackled mostly using a GA; multi-objective treated combinations of voids and filling time, filling time and vents number, gates number and vents number, implemented by either evolutionary strategies or a cascaded algorithm. Filament winding process has been studied under only single-objective optimisation addressing slippage, process time and process cost. In draping/forming, wrinkling and warpage minimisation have been dealt separately using GA, whilst multi-objective optimisation using GA has addressed the combination of maximum shear angle and minimum average shear angle.

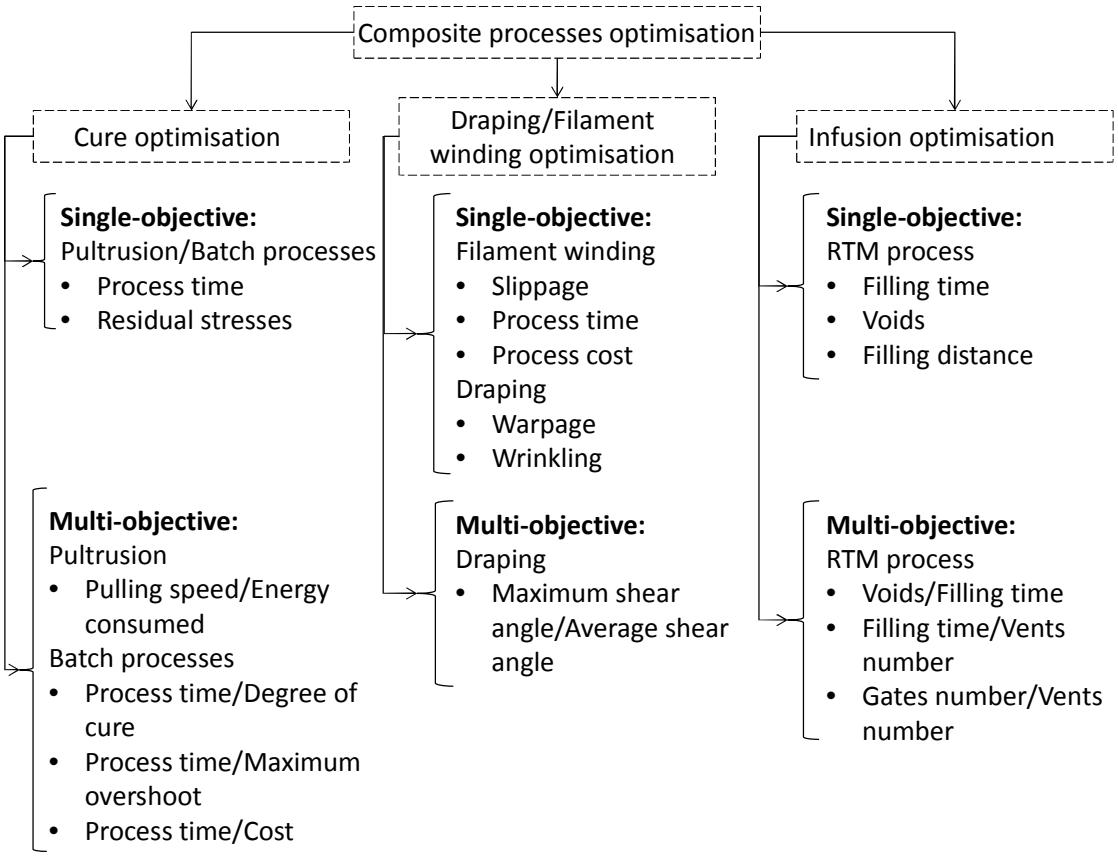

Figure 2-3 Composite process optimisation landscape

2.4 Optimisation problem

2.4.1 Single and multi-objective optimisation

Solving an optimisation problem means finding the minimum point of a prescribed objective function, (if the problem requires finding a maximum point the same formalism can be used with a decreasing function of the objective), under some equality and inequality constraints [8]. A single-objective optimisation problem has the following form:

Minimise *f(x)* subject to:

$$g_i(x_1, x_2 \dots x_n) \geq 0 \text{ with } i = 1,2 \dots r \tag{2-1}$$

$$h_j(x_1, x_2 \dots x_n) = 0 \text{ with } j = 1,2 \dots p \tag{2-2}$$

A mathematical representation of multi-objective optimisation can be expressed as follows:

Minimise

$$f_m(x_1, x_2 \dots x_n) \text{ with } m = 1,2 \dots s \tag{2-3}$$

Subject to:

$$l_n \leq x_n \leq u_n$$

$$g_i(x_1, x_2 \dots x_n) \geq 0 \text{ with } i = 1,2 \dots r \tag{2-4}$$

$$h_j(x_1, x_2 \dots x_n) = 0 \text{ with } j = 1,2 \dots p$$

Here x_n is the n^{th} parameter, f_m is the m^{th} objective, g_i is the i^{th} inequality constraint and h_j is the j^{th} equality constraint, s is the number of objectives, n is the number of parameters, r is the number of inequality constraints and p is the number of equality constraints. A feasible point in the design space is Pareto optimal if there are no other feasible points in the design space with all the objectives being equal or better than it. A mathematical definition of such point for a minimisation problem is as follows:

$(x_1, x_2 \dots x_n)$ is Pareto optimal iff

there is no $(x'_1, x'_2 \dots x'_n)$ such that

$$\forall i \in \{1,2 \dots m\}, f_i(x'_1, x'_2 \dots x'_n) \leq f_i(x_1, x_2 \dots x_n) \quad (2\text{-}5)$$

and

$$\exists i \in \{1,2 \dots m\}, f_i(x'_1, x'_2 \dots x'_n) < f_i(x_1, x_2 \dots x_n)$$

All the Pareto optimal solutions form collectively the Pareto optimal set. Any point within the Pareto optimal set is an optimal solution and therefore a non-dominated solution. Figure 2-4 (a) illustrates the Pareto optimal set and the feasible region of solutions and Figure 2-4 (b) depicts the dominance criterion for a minimisation problem.

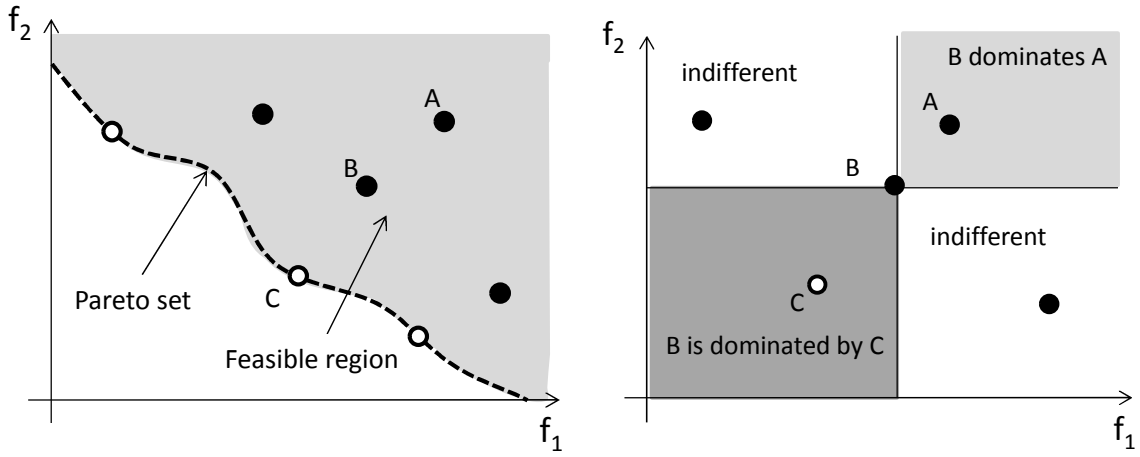

Figure 2-4 a) Pareto set and feasible region b) Dominance definition

2.4.2 Gradient based technique

The idea of gradient based techniques is to decrease the value of the objective function at each step in order to achieve a minimum, using only the information from the function and from its gradient. Gradient based technique can be used with confidence only when the landscape of the problem is well known and without local minima therefore when the landscape has a convex space. Otherwise the outcome of this algorithm depends strongly on the initial point

selection and a position close to local minima will make the algorithm fail in reaching the global minima. An algorithm of this kind starts by selecting a starting design point x^0, and initialising the iteration counter *k=0,* after that a search direºtion d_k must be defined in the design space. Then a positive step size α_k in the direction d_k is selected. The next point for the iteration is defined as:

$$x^{k+1} = x^k + \alpha_k d^k \tag{2-6}$$

In a minimisation problem a desirable direction is the one able to reduce the current value of the objective function as:

$$f(x^{k+1}) < f(x^k) \tag{2-7}$$

Substituting Eq. 2.6 in Eq. 2.7 and applying Taylor's expansion the following equation is obtained:

$$f(x^k) + \alpha_k(c^k \cdot d^k) < f(x^k) \tag{2-8}$$

$$c^k = \nabla f(x^k) \tag{2-9}$$

The condition to satisfy is therefore:

$$c^k \cdot d^k < 0 \tag{2-10}$$

Since the gradient of the function is known it is possible to define a desirable direction as any d_k satisfying Eq. 2.10. The Steepest descent method is the oldest first order method introduced by Cauchy in 1847 [7]. The method is based on a fundamental property of the gradient of a function to point in the direction of maximum increase [8]. Consequently, the direction of maximum decrease is the opposite. The negative gradient vector is then the direction of steepest descent:

$$d = -c \tag{2-11}$$

2.4.3 Stochastic algorithm

Stochastic algorithms are based on a random search in all the space of the feasible solutions. The idea is to choose many solutions randomly and then evaluate them; the best solution will be the result of the random search. The Simulated Annealing (SA) is a stochastic search method based on statistical mechanics and in particular on the Boltzmann distribution. It can determine a near global optimum solution in a large search space which could have several local minima. The method is based on the search of the minimum energy state within the system. The SA tries to emulate a physical annealing process which allows atoms to reach a minimum energy configuration after reaching an elevated energy state during heating up. The algorithm starts from a high temperature (control parameter) that allows a great range of variation to the inputs. As the algorithm gradually progresses the temperature decreases and the range of input variations reduces its gap. This behaviour leads to better solutions [9].

Genetic algorithms are a type of random search algorithm based on concepts of natural selection, where the basic rule is the survival of the fittest. A population of individuals (strings of bits), each representing a solution, forms a generation. At each generation the goodness of every solution is evaluated assigning fitness, the current generation evolves in the next one by applying some mathematical operators (reproduction, cross-over, mutation), which aim to bias positively the survival of the fittest solution of the old generation [10].

2.4.4 Genetic algorithm for multi-objective optimisation

The use of GAs for single-objective optimisation can be extended to multi-objective optimisation as well, forming the Evolutionary Algorithms (EA) class. One of the first algorithms was Vector Evaluated Genetic Algorithm (VEGA) developed by Schaffer and it is still considered a foundation for this category [11]. The basic idea of it is creating a sub-population based on the evaluation of one single-objective problem at a time since the minimum of such problem is a Pareto optimal point. One of the major drawbacks of VEGA is the clustering of solutions in the vicinity of this minimum point. The multi-objective Genetic

Algorithm (MOGA) introduced the Pareto ranking concept [12]. The algorithm carries out a dominance check, pointing out the non-dominated solutions; all non-dominated solutions receive a rank equal to 1. Subsequently, this set of points is removed and the new non-dominated solutions are assigned a rank equal to 2. The algorithm continues until every solution has been ranked and fitness values are assigned according to the ranking. The Non-dominated Sorted Genetic Algorithm (NSGA) introduced the idea of fitness sharing, in order to avoid clustering and to have a more uniform distribution, penalising fitness value of points in crowded area [13].

2.5 Process simulation model

The manufacturing of composite materials involves many stages; the simulation of each stage has been addressed resulting in a set of models describing the phenomena occurring during processing. The cure is governed by a heat conduction equation with generation of heat due to chemical reaction occurring during the cure process [14-20]. The rate of heat generation is proportional to the rate of reaction calculated by the resin cure kinetics model. The cure kinetics takes into account the glass transition development which is a function of degree of cure described by Di Benedetto's equation [21-23]. The residual stress model development predicts the generation of process stresses within the part due to chemical shrinkage and expansion/contraction anisotropy and inhomogeneity [24-29]. The development of stress is of importance once the mechanical properties have reached a certain level and it can no longer allow stress relaxation [30].

Filling simulation has been performed following Darcy's law, which states that resin flow is proportional to the pressure gradient, to model the resin flow through porous media [31-35]. The simulation of consolidation describes how the applied pressure is distributes in the resin and reinforcement obtaining the real driving pressure for the flow [36-42].

Draping/forming simulation has been addressed either using kinematic models which do not take into account the mechanical response of the reinforcement of the draping [43-46] or using finite element modelling which is capable to

simulate mechanical effects in detail with the drawback of high computational cost [47-50]

2.6 Application of optimisation to composite processing

2.6.1 Optimisation of curing in pultrusion

In the process of pultrusion there are two variables which play a fundamental role in order to improve quality: the die temperature, the pull speed. The simultaneous optimisation of these variables is the key to obtain the best final product in terms of the final degree of cure and uniformity of cure. The selection of an optimum cure cycle is necessary to obtain the best match between these two design parameters. Table 2-1 summarises the research carried out on topic of optimisation of pultrusion cure.

A relationship between the degree of cure in the thickness and the die temperature during the pultrusion process and an optimisation which related the die temperature and the uniformity of cure were carried out for a graphite-epoxy resin C-section part [51]. Any changes in the die temperature lead to a variation of the degree of cure and this is taken into account in the objective function. The results show how an optimisation procedure can be useful to improve the uniformity and the degree of cure. The pull speed was kept constant (5 mm/s) the required degree of cure was 0.9 and the maximum allowed temperature was 240 °C. To avoid the degradation of the resin the optimisation algorithm stops when it reaches the maximum temperature allowed. The optimisation problem was solved using the steepest descend method. In the case studied an improvement of 75% in the uniformity of cure (that is to say lower standard deviation) was observed with respect to the non-optimised case, which implies an improvement in the mechanical performance. In order to optimise the pultrusion process it is important to consider both the pull speed and die temperature. Following this, a subsequent work added to the optimisation parameters the pull speed [52]. The mean degree of cure in the cross-section at the exit of the die decreases as the pull speed increases and so does the standard deviation ending in higher variation in the degree of cure in the cross-section for higher pull speed. The optimisation led to an improvement of 52% in

the uniformity of cure. Constraints for the maximum temperature (240 ^{0}C) and for the desired degree of cure (0.9) were imposed. The maximum temperature allowed is a fundamental constraint in the process. When the process overcomes it the solution is rejected. The effect of initial composite temperature, variable pull speed and die cooler temperature were studied separately to investigate their effects in a glass fibre-epoxy resin C-section [53]. A steepest descend method was implemented to minimise residual stresses increasing the uniformity in cure. Using initial composite temperature as parameters the standard deviation of uniformity of cure was improved by 73% with respect to the starting configuration. Optimisation with both pulling speed and heater temperature was implemented; the improvement in degree of cure was 22% (0.892) and its standard deviation reduced by 95%.

A hybrid technique which combines a GA and the simplex method has been applied to optimisation of curing in pultrusion for a C-section [54]. This work was carried out taking only into account the heater die temperature as a variable and assuming the pull speed is constant. The minimum degree of cure required (0.9) was the constraint applied. The fitness function considered was the difference between the desired degree of cure and the one at the node location, for each node. Using a GA has the advantage of avoiding the local minima, whereas the simplex method increases the speed of algorithm convergence. The reason for applying the simplex method only near the optimal solution is to avoid the local optima in which the simplex method could be trapped. The uniformity of cure resulted with the hybrid method in an improvement in standard deviation of about 86% with respect to the reference value (with 177 ^{0}C temperature for all the three die heaters) and 71% compared to GA optimisation. Another work considered the optimisation of the pultrusion under uncertainty [55]. A stochastic model was developed and the uncertainty of the process parameters was represented using a Gaussian distribution. A Nelder-Mead algorithm [56] coupled with SA was implemented. The objective was to optimise the cycle temperature in order to minimise the process time for a glass fibre polyester composite rod. The constraints applied were the maximum temperature allowed, the maximum difference temperature in the cross-section

allowed and the minimum degree of cure required (0.97). Three optimisations, with three different temperatures (120 ^{0}C, 140 ^{0}C and 160 ^{0}C), were executed. The results showed that cure time increases as the temperature decreases and that cycles with higher temperature involve longer initial ramp. Furthermore, increasing the level of uncertainty makes the cure time longer. A subsequent work addressed the same problem for a fibre/ polyester resin system implementing a Sequential Quadratic Programming (SQP) algorithm coupled with a SA, obtaining the same trends [57]. A Gaussian method was implemented to optimise the die temperature aiming to minimise the process time of a rod composite. The maximum temperature allowed within the part and a minimum degree of cure were the constraints imposed. A comparison between six different resin compositions was carried out [58]. A stochastic optimisation algorithm was used to find the optimal temperature profile to minimise process cost for a vinyl-ester glass fibre I-beam [59]. The result was an improvement by 26% in energy consumption compared with the model proposed by Liu [60]. The impregnation stage within pultrusion process has not been addressed in the context of optimisation.

.

Table 2-1 Research on optimisation of pultrusion process

Papers	Objective	Parameters	Constraints	Optimisation	Main Results
[51]	Uniformity of cure	Die temperature	Maximum temperature Minimum degree of cure	Steepest descend	75% improvement in the uniformity of cure
[52]	Uniformity of cure	Die temperature Pull speed	Maximum temperature Minimum degree of cure	Steepest descend	52% improvement in the uniformity of cure
[53]	Uniformity of cure	Die temperature Pull speed	Maximum temperature Minimum degree of cure	Steepest descend	Influence of pull speed
[54]	Uniformity of cure	Die temperature	Minimum degree of cure	GA	86% improvement in uniformity of cure
[55]	Process time	Die temperature	Maximum temperature Minimum degree of cure	Nelder-Mead SA	Increasing level of uncertainty make the cure time longer
[57]	Process time	Die temperature	Maximum temperature Minimum degree of cure	SQP	SQP showed reliability
[58]	Process time	Die temperature	Maximum temperature Minimum degree of cure	Gaussian method	Comparison between 6 different resins
[59]	Process cost	Die temperature	Minimum degree of cure	Stochastic algorithm	26% reduction in energy consumption

2.6.2 Cure cycle optimisation of batch curing to minimise process time

Table 2-2 summarises the research on process time minimisation in batch processes. Finding the optimal cure cycles involves obtaining the optimal temperature profile and the optimal pressure profile in order to fabricate a part with an acceptable degree of cure, state of stress and void content. The aspects to address are five:

- The degree of cure must achieve a minimum prescribed value (e.g. 0,9) in the minimum time;
- The temperature inside the part must be kept under the maximum temperature allowed;
- The residual stresses must be minimised;
- The percentage of the void must be acceptable;
- Any excess resin must be removed to guarantee a uniform consolidation.

The first three items can be addressed through the optimisation of the temperature cycle and the last two through the optimisation of the pressure profile. One of the goals of the optimisation of batch curing is the minimisation of the process time and by imposing the constraints the limitation of the final residual stresses and of the degradation of the resin. In this type of optimisation typical constraints are: the maximum exothermic temperature allowed inside the part in order to avoid the degradation of the resin and the maximum gradient of temperature allowed in order to have uniformity in the cure. The problem has high dimensionality and for this reason it is computationally intensive.

The ‘look ahead’ strategy has been used in order to minimise the cure process time of a thick polyester/carbon fibre composite laminate [61]. This method tries to find a trade-off between two techniques, a simple gradient based descent method and a heuristic search, finding a near-optimum solution. The basic idea is that using the ‘look ahead’ strategy the original problem is approximated with one which has local optimisation criteria; therefore the technique is called Local Criterion Optimisation (LCO). For every time step a heuristic function h is evaluated for every possible choice, the one which gives the minimum value is

chosen for that step. Large computational time is required. This issue could be overcome using parallel computation. A comparison with recommended cure profile proved a reduction in cure time from 300 min down to 170 min (43%), lower exotherm and temperature gradient within the part reduced.

Choosing the best dwell temperature is a complex problem. If the part is thin the influence of the number of dwells on the quality of the final product is negligible, if the part is thick the scenario is influenced by the number of dwells. A thin and a thick laminate composite with epoxy resin cure profile optimisation were compared using an SQP algorithm based on thermochemical analysis [62]. For a thin part (2 mm) optimal cure time resulted in 588 s with one dwell and 582 s with two dwells. For a thick part (40 mm) optimal cure profile resulted in 5024 s (one dwell), 3702 s (two dwells) and 1544 s (three dwells) The results pointed out that finding an optimal cure profile in a thick part is not trivial and that selecting the number of dwells, the cooling and heating rate is more important in a thick part where heat dissipation is more problematic. Using a carefully selected cure cycle in this case can bring significant benefits in terms of cure time. Consolidation analysis has been added in a follow up work [63]. The results showed that cure profile found applying only thermochemical considerations work for thin laminates which result in fully cured and consolidated part. In the case of the thick part, not taking into account consolidation leads to partially consolidated parts. Considering the consolidation leads to optimal cure cycle capable to produce fully cured and consolidated parts with improvement in cure time between 48% and 63%. SQP algorithm was also implemented to find the temperature profile of a cure cycle involving five stages among heating and cooling zones for a polyester glass fibre system [64]. The optimisation proved to be better than a heuristic method (by 56%) and standard profile (by 80%).

Optimal cure profile for thick carbon fibre-epoxy resin prepreg composites laminates, 5 cm and 10 cm, have been found using GAs taking into account maximum temperature and maximum heating rate allowed as constraints [65]. The results showed the power and flexibility of GAs algorithms. For the 5 cm

laminates there is a reduction in cure time one of 62% between the initial cure cycle and the optimised. The improvement is 67% for the 10 cm component. A simple but reliable iterative gradient based procedure to optimise cure profile of a thick carbon fibre-epoxy resin prepreg laminates was carried out and verified experimentally; highlighting how the process time saved increases with the thickness of the part [66]. The cure time, according to standard profile, for 12.5, 25 and 50 mm is 275, 782 and 1532 min respectively. The corresponding optimised cure time found are 175, 200 and 312 min, i.e. cure time reduction of 36%, 74% and 80% respectively. A reduction of cure time (26%) with respect to the standard cure profile was obtained using a GA to optimise the cure profile of a carbon fibre-epoxy resin system [67]

Cure optimal profile and pressure optimal profile have been found using an SQP algorithm for a thick graphite-epoxy laminate, solving for the temperature profile first and subsequently finding the smallest pressure profile to apply in order to keep the void content under certain limits [68]. The cure time optimised found was compared with the one found by Criscioli [15], the reduction was about 45%.

The Levenberg Marquardt algorithm [69] was implemented to optimise the cure profile of a thick composite laminate [70]. Constraints to ensure quality were imposed according to what has been pointed out in [61] that is residual stresses arise when the surface cures before the centre. Maximum temperature difference between centre and surface was also used. An optimal cure profile respecting the constraints was found ending in 162 minutes which is better compared to the 170 minutes found by Pillai for the same composite system using LCO [61].

Optimisation of heat generation using resistive heating elements and providing supplemented heating obtained significant improvement in cure cycle time and uniformity of cure [71]. The optimisation was carried out by SA combined with a simplex method when the algorithm was close to the solution. Two different material systems were addressed: glass fibre epoxy and glass fibre polyester. The optimal cure time for the epoxy resin system without embedded resistive

heating elements was 1710 s. The cure time decrease as the number of heating mats increases: 1002 s for one mat, 961 s for two mats and 948 s for three mats. The same behaviour was found for the other system.

In a recent effort a simulation based optimisation that unified an SA with the Nelder-Mead method was carried out for a carbon fibre-epoxy resin composite thick (50 mm) laminate, pointing out that combining with the SA improves the capability of the Nelder-Mead method [72].

2.6.3 Optimal cure cycle of batch curing to minimise residual stress

The problem of residual stress arises during cure due to the different thermal expansion and shrinkage of laminates. Table 2-3 summarises the research on minimisation of residual stresses in batch processes.

A first effort towards an optimisation of the problem pointed out the parameters that influenced the presence of residual stresses in the final part, concluding that a cure at lower temperatures reduced the residual stresses. A slow cooling rate is useful to increase the stress relaxation while increasing cool down pressure had no effect on residual stresses [73]. The optimal cure profile to minimise the residual stress under the constraints of minimum degree of cure (0.9) and process time, was solved through a graphical method. The parameters of the optimisation were the cure dwell temperature and duration. Two composite carbon/epoxy systems were taken into account. The method is able to find a cure profile that minimise residual stress both for single composite material and co-curing of two materials [74].

An optimisation was conducted to investigate the relationship between residual stress and cure profile; the result of the optimisation was not only to reduce the residual stresses (by more than 30%) but also the cure time (by about 20%) [75]. An inverse procedure based on a gradient technique, with the only constraint of maximum temperature allowed, was set to minimise the residual stress reducing the thermal gradient through the thickness in a polyester-glass fibre composite. The procedure is able to find a cure profile that result in a quasi-uniform temperature [76].

Process induced residual stresses generated in an autoclave process have been investigated to minimise the warpage after mould removal. The mould tool geometry to fabricate an L-shape part has been optimised in order to minimise the warpage. The problem has been addressed using the Broyden-Fletcher-Goldfarb-Shannon optimisation algorithm [77], a gradient based technique and GAs [78; 79].

Table 2-2 Research on process time minimisation in batch curing process

Papers	Objective	Parameters	Constraints	Optimisation	Main Results
[61]	Process time	Cure profile	Maximum temperature Minimum degree of cure	Heuristic approach	43% cure time reduction
[62]	Process time	Cure profile	Maximum temperature Minimum degree of cure	SQP	Optimal cure cycle for thick and thin part depending on number of dwells
[64]	Process time	Cure profile	Minimum degree of cure	SQP	Improvement for process time compared to heuristic optimisation (56%) and standard solution (80%)
[65]	Process time	Cure profile	Maximum temperature Heating rate	GA	Significant reduction in cure time of thick components, about 65%
[66]	Process time	Cure profile	Maximum temperature Minimum degree of cure	Iterative method	Process time saved increases with the thickness, up to 80%
[67]	Process Time	Cure profile	Maximum thermal gradient	GA	26% reduction in curing time
[68]	Process time	Cure profile	Max temperature and void Minimum degree of cure	SQP	Considerable improvement in reduction of process time (45%)
[63]	Process time	Cure profile	Maximum temperature Fibres volume fraction	Standard gradient based optimisation	Process time reduction up to 63%
[70]	Process time	Cure profile	Maximum temperature difference between surface and centre	Gradient based technique	A cure cycle of 162 min was found to fabricate quality composite
[71]	Process time	Cure and current profile	Maximum temperature allowed Minimum degree of cure	SA Simplex method	Improvements in process time
[72]	Process time	Cure profile	Technological constraints	SA Nelder-Mead algorithm	SA improves the performance of the Nelder-Mead algorithm

Table 2-3 Research on residual stress minimisation in batch curing process

Papers	Objective	Parameters	Constraints	Optimisation	Main Results
[73]	Residual stress	Cure profile		Towards process optimisation	Reduction of residual stress up to 30%
[74]	Residual stress	Cure profile	Minimum degree of cure Process time	Graphic approach three dimensional diagram	Reduction of about 30% of residual stresses presence
[75]	Residual stress	Cure profile	Maximum temperature Minimum degree of cure	Max/Min approach	Reduction of about 30% of residual stresses And about 20% of cure time
[76]	Residual stress	Cure profile	Maximum temperature allowed	Gradient based technique	A cycle achieving a quasi-uniform temperature through the thickness was found
[78]	Residual stress/Warpage	Cure profile	Maximum residual stress allowed	BFGS	Reduction of the final angle
[79]	Residual stress/Warpage	Cure profile	Maximum residual stress allowed	GA	Comparison with non-linear programming showed that the GA find the better solution in terms of warpage

2.6.4 Optimisation of liquid moulding processes to minimise voids and dry spots

The goal of all liquid moulding processes is to fabricate a composite part without voids or dry spots. Table 2-4 reports the research on optimisation of liquid moulding to minimise voids content and dry spots. In early investigations the formation of micro and macro voids has been related to the capillary number [80; 81]. An iterative optimisation algorithm based on the analysis of the capillary number at the fluid front position using an FE/CV approach to advance the flow front was carried out [6].The constraints were the maximum injection rate and pressure allowed. The result, tested on a three dimensional part filled non-isothermally, showed a reduction of the percentage of voids from 4% to 2% for the same filling time.

A mesh distance based-model (e.g. triangular mesh) has been used to optimise pipes, inlet and outlet arrangement to minimise dry spots in a RIFT process [82] A GA was implemented in this case. The fitness function aims to reduce the dry spots content by reducing the maximum filling distance between either pipes or inlet with outlets. The number of inlets is fixed at one and the number of pipes is a user input whilst the algorithm finds the optimal number and location of outlets and the optimal length of pipes. This procedure is mostly important when the geometry of the part is complex. A pilot seat for a glider was taken into account, the optimal configuration required nine vents and three pipes, giving a minimum fill distance of 0.21 m. A similar approach was used for the RTM process in order to obtain an optimum arrangement of outlet locations to reduce voids and dry spots content [83]. GAs was implemented for this purpose. A fitness function was set to minimise the filling distance between inlet and outlets and therefore the possibility of voids formation and dry spots. The advantage of this effort is that it is able to handle the problem of multiple vents and could handle multiple gates as well.

Table 2-4 Research on optimisation of liquid moulding processes to minimise voids and dry spots

Papers	Objective	Parameters	Constraints	Optimisation	Main Results
[6]	Micro/Macro voids	Injection rate	Maximum injection rate Maximum injection pressure Maximum resin speed	Iterative optimisation algorithm based on the capillary number	Reduction from 4% to 2% of void percentage
[82]	Minimise dry spots	Number of gates, vents and pipes	No constraints	GA	Possibility to find the optimum scenario (Number of inlet, outlet and pipe)
[83]	Minimise dry spots	Number of gates, vents	No constraints	GA	The resulting arrangement led to satisfactory process performance

2.6.5 Optimisation in RTM to minimise filling time

Table 2-5 recaps the research on minimisation of filling time in RTM process. The optimisation problem of gate and vent location has the aim to minimise the filling time imposing the constraint of maximum percentage of dry spots allowed. Powell's method, a gradient based technique, was adopted to find the optimal initial resin and mould temperature (assumed to be equal) and initial speed of the resin to minimise the amount of filling time and cure time; a set of 13 constraints were applied to preserve the quality and respect technological limits [84]. A successful optimisation complying with the constraints was found obtaining an optimal mould/resin temperature of 154 ºC and an optimal resin velocity of 24 cm/s resulting in a cure time of 33 s and a filling time around 20 s. A heuristic method called graph-based two-phase heuristic was used for the RTM process to treat optimal gate and vent location [85]. The maximum percentage of voids was considered as constraint. The results showed the efficiency of the algorithm compared to others heuristic methods as GAs and Branch and Bound Search (BBS) in terms of computational efficiency. The filling time of a flat and an uneven plate was optimised using the Global Local Optimiser (GLO) code, which contains different strategies: Quasi Newton, Random global search and GA. Both examples involved three gates and a total of six parameters corresponding to *x* and *y* locations of each inlet [86]. The Quasi-Newton method showed to have a good convergence and to improve the final filling time; while GAs, because of a lack in constraint definition, resulted in overlapping gates in many simulations. In an early work by Young GA was applied to solve a single gate problem [87]. A U-shaped part was considered in four different optimisation cases [88]. The objective was to solve the problem of optimum gate and vent location minimising a performance index that related the flow pattern and the filling time. Case 1: constant flow equal to 2 cm^3/s, one gate and one vent; Case 2: constant flow equal to 2 cm^3/s, one gate and two vents; Case 3: constant pressure equal to $2.0 \cdot 10^5$ Pa, one gate and one vent; Case 4: constant pressure equal to $2.0 \cdot 10^5$ Pa, one gate and two vents. A GA has been adopted. The result showed that with constant flow injection strategy

the best vent is the last node filled, constant pressure strategy leads to a short flow path process while constant flow strategy yields a vent oriented flow path. The minimisation of the filling time could be improved, without sacrificing part quality, using multiple injection gates especially when the geometry becomes complex. Following this idea, a GA was implemented for three injection cases: single, simultaneous and sequential injection [89; 90]. The parameters of optimisation were the gate locations. It was shown that a correct set up of the sequential injection results in the best solution. The sequential injection scheme was proved to be the best configuration in order to reduce the filling time without adversely affecting the quality part in terms of void content. A GA trained with Artificial Neural Network (ANN) has been implemented to address the same optimisation problem [91]. A resin flow index, sensitive to filling time, has been formulated, feasible regions for gates and vents and allowed ranges of injection pressure and mould temperature were defined. The use of Neural Network, which can predict future parameters based on the past results, between the simulator and GA accelerates the convergence.

A BBS method has been proposed for single gate location problem to minimise filling time [92]. BBS converges to the optimal solution dividing the solution set in smaller sets cancelling the one that are less likely to have the optimal solution. BBS performances were compared with existing ES and GAs showing its ability to achieve quality results with 90% less computations. A Hill Climbing algorithm was implemented taking into account constraints concerning prohibited positions for the gates; the routine was able to handle constraints that forbid the presence of gates in particular areas (no gate constraint) and on the border (edge gate constraint) [93].

In recent studies optimal vents location were found for fixed gate location by means of combinatorial search [94-96]. A Cascade Optimisation (CO) algorithm was implemented for the multi-objective optimisation of liquid moulding [97]. The optimisation took into account gate and vent locations to minimise filling time and number of vents considering also a probabilistic forecast of race-tracking and maximising a success rate. In the definition of the objective

function 15% of the weight is assigned both to filling time and number of vents while 70% is given to the success rate, which reflects the quality of the infusion for a given scenario. The algorithm gives priority to the selection of gate location. Two separated loops are implemented for these two problems. The methodology is superior because it also takes into account race-tracking, and gives the best vents and gates configuration. The capability of combining gate and vent configuration and the race-tracking modelling to achieve an optimum injection design, demonstrated the power and robustness of this methodology. CO was demonstrated on three parts: a window pane, a rectangular component with an L-shaped insert and a component with ribs. In the window pane model when the gate location was fixed the maximum success rate reached was 48.2% with two vents and it was 88% with four vents. Using the CO algorithm which optimises also the gate location the success rate reached with two vents was equal to 94.5%.

The complexity of the RTM processes leads to long computational times using a search algorithm and no reliable solutions using gradient search methods [98]. A hybrid global-local optimisation for the gate location has been implemented coupling GAs effectiveness with gradient search efficiency showing to have a faster convergence and an inferior number of simulation required than GAs. The filling time was investigated using a globalized Nelder-Mead optimisation algorithm considering the maximum pressure allowed. The optimisation showed the link existing between injection time and maximum mould pressure [99].

2.6.6 Optimisation of filament winding

There are not many efforts in the optimisation of the filament winding process. Table 2-6 reviews the research on optimisation of the filament winding process. The winding is always performed with pre-tensioning under an external load. An optimal preload distribution was found for the winding of cylindrical and spherical pressure vessels [100]. Moreover the influence of the rheological characteristics of the material on optimal pre-tensioning was studied numerically. A software code named AL was developed in order to achieve the optimum alignment by the selection of the best variables values among wind

angles, band width, mandrel dimension and a test case, a scaled-down rocket case manufactured with CFRP prepreg, was used to validate the reliability of the software [101]. Dynamic programming was used to find the optimum path which minimises process time considering constraints related to winding velocity and acceleration [102]. A process cost optimisation was attempted. The process was modelled using the WITNESS package. A GA able to choose among 375000 different setups was implemented and compared with a random search algorithm showing to reach best optimal solutions concerning the process cost and better convergence time [103].

Table 2-5 Research on filling time minimisation

Papers	Objective	Parameters	Constraints	Optimisation	Main Results
[84]	Overall time	Resin temperature Resin injection speed	13 constraints for performance and process limitations	Gradient based technique	The optimisation found the optimal resin temperature and speed to minimise cycle time
[85]	Filling time	Gate and vent	Maximum void content	Graph based	The new method had a better computational efficiency compared to GA and BB
[86]	Filling time	Gate and vent	No constraints	GLO code	GA overlapped gates due to a lack of constraints
[87]	Filling time	Gate and vent	Single gate	GA	GA is suited to solve this problem
[88]	Filling time	Gate and vent	Constant flow injection	GA	The best vent is the last node filled
[89,90]	Filling time	Gate and vent	Injection pressure and mould temperature	GA	Sequential injection reduced filling time without increasing void content
[91]	Filling time	Gate and vent	Feasible region for gate/vent	ANN-GA	ANN enhance algorithm convergence
[92]	Filling time	Gate and vent	Single Gate	BBS	BBS recommended for big model size
[93]	Filling time	Gate and vent	Feasible region for gate	Hill climbing	Hill climbing handle no-gate and edge gate constraint
[94]	Filling time	Gate and vent	Dry spots	Cascaded algorithm	Optimal vents configuration for fixed gate
[96]	Filling time	Gate and vent	Dry spots	Cascaded algorithm	Optimal vents configuration for fixed gate
[97]	Filling time	Gate and vent	Dry spots	Cascaded algorithm	Optimal vents and gates configuration
[98]	Filling time	Gate and vent	Limit in flow front speed	Hybrid algorithm	Better result compared to GA
[99]	Filling time	Gate and vent	Maximum pressure allowed	Nelder-Mead	Link between injection time and maximum pressure

Table 2-6 Research on filament winding optimisation

Papers	Objective	Parameters	Constraints	Optimisation	Main Results
[100]	Slippage	Pre-tensioning load	Maximum stress gradient allowed	Lagrange multipliers	Optimal pre-tensioning was studied numerically
[101]	Slippage and dwell angle	Winding angle Band width	Overlap tolerance	AL code	Development and testing of AL code
[102]	Process time	Spindle rotational position Feed eye roller inclination Cross carriage position Carriage position	Winding speed and acceleration	Dynamic programming	Improvement in the reduction of process time
[103]	Process cost	Parameter to manage different set up and way to assembly the process	No constraints	GA	The algorithm is able to find the optimum set up among 375000 different possible assemblies. GA showed to act better than random search

2.6.7 Drape optimisation

Table 2-7 outlines the works on drape optimisation. The wrinkling of the fibres degrades the quality of the final part. Minimisation of wrinkling can be carried out by optimising the distribution of the holding force. The close relationship between wrinkling and holding force dictates the choice of GAs which works on the holding force drapes. A hemisphere form was modelled and then validated. The objective is to minimise total wrinkling strain varying the holding force vector intensity and profile. A comparison between the optimised holding force profile with a uniform one showed that the optimised profile results in the elimination of concentrated buckling tows [104]. A woven carbon-epoxy prepreg helicopter pilot helmet forming has been addressed both experimentally and numerically using GA. The optimisation showed that wrinkling can be minimised increasing the peripheral force at positions diagonal to the location of concentrated buckling. Improvements in total wrinkling strain up to 50% can be reached [105]. The Method of Moving Asymptotes [106], a gradient based technique, was adopted to optimise draping process on a curved C-spar [107]. Overall, eight optimisations were carried out. Two optimisations of process cost: one aimed to minimise fibre angle deviations and the other to minimise material consumption and two optimisations of weight: one minimising fibre angle deviation and the other minimising material consumption. These four optimisations were run both for unidirectional fibre and a plain weave prepreg. As expected the best value in terms of cost was achieved by minimising the material consumption while the optimisation of the weight led always to a higher manufacturing cost. Plane weave prepreg showed a better drapability

Table 2-7 Research on drape optimisation

Papers	Objective	Parameters	Constraints	Optimisation	Main Results
[104]	Wrinkling	Holding force	No constraints	GA	Elimination of concentrated buckling tows
[105]	Wrinkling	Holding force	No constraints	GA	50% in wrinkling strain improvement
[107]	Cost/Weight	Material consumption and fibre angle deviation	No constraints	Method of moving asymptotes	The plain weave prepreg behaves better than the unidirectional concerning drapability

2.6.8 Multi-objective optimisation

Table 2-8 summarises the research on multi-objective optimisation in composites processing. Multi-objective optimisation has been applied to the pultrusion process, gate and vent location, draping problem, and curing. A multi-objective problem in pultrusion process addressed minimisation of process time, maximising pull speed, and minimisation of power of the die. The constraints imposed concern the minimum degree of cure (0.9), the range of temperature for the various heaters and the range for the pull speed [108]. GAs combined with an ANN strategy called Back Propagation (BP) were implemented in order to solve the bi-objective problem for a carbon fibre-epoxy resin rod. The best results were found giving higher weight to die temperature in the definition of the objective function obtaining an increase in pull speed around 10% and a decrease in the three heaters respectively of 7%, 1% and 2% in comparison with the current set applied for such process. Simulated annealing combined with SQP has been used successfully to optimise the pull speed and the temperature profile with constraints such as minimum degree of cure and resin degradation for pultrusion process of a rod made by glass fibre and vinyl ester resin [109]. The optimal temperature profile differed in values with respect to previous non-optimised conditions but had the same tendency.

A multi-objective optimisation has been applied to the problem of gate location for a simple test part and for a complex one, a catamaran shell [110]. One objective aims to minimise the filling time. In order to allow the air to be expelled it is desirable to have a good match between the last area to be filled and the vents location. The second objective, to be maximised, has been devised to deal with this aspect. This problem was solved using GAs. Gaussian mutation probability was chosen coupled with six different cross-over probabilities, including one without cross-over. Hypercube cross-over proved to be the fastest in reaching an acceptable approximation of the Pareto front. Using cross-over also proved to induce stagnation in non-dominated set evolution in complex case suggesting that for complex case the only mutation operator is preferable. Optimisation of gate and vent configuration to minimise filling time and dry spots

taking into account the presence of race-tracking using a GA has been carried out for RTM [111]. Maximum percentage of voids and maximum time allowed were imposed as constraints. A challenging part has been selected to illustrate the potential of GAs. The part is a 2D approximation of a vehicle bed with wheel wells. The solution gave satisfactory results. In the no race-tracking case the algorithm was able to find the optimal gate and vent configuration, with a filling time equal to 4407 s and 0.006% of dry spot volume, evaluating only 40 out of 16256 possible configurations, for the race-tracking case the GA found a near optimal solution after only 48 simulations out of 83000 possible evaluations, placing the gate in a race-tracking area. A graph based, two phase heuristic algorithm approach was used to solve the impregnation problem for a seat, helicopter manifold lid and boat deck part manufactured by RTM, to seek the best gate and vent location configuration in order to minimise the number of gates and vents and a dispersion value that quantifies the ending location variation. Constraints, limiting the feasible gate location and maximum filling time allowed to preserve the quality of the part, were also applied [112]. A GA was adopted to optimise gate and vent location to minimise both bobbles and filling time to manufacture a spar with U-shape cross-section via RTM. First results pointed out the necessity to increase the size of the population, in fact the solution lacked of heterogeneity. However, the method allows optimising design and manufacturing phases [113].

The draping multi-objective optimisation of a pilot helmet was undertaken aiming to minimise the maximum absolute shear angle and the average absolute shear angle. A GA is suited to solve this problem, handling pre-shear, starting point and direction of draping. It was showed that GA is more efficient when the design space is wide and that GA led to a reduction in the computational time compared to an exhaustive search around 30% for the full helmet case [114].

An objective function that minimises the processing time and the difference of temperature inside the part was carried out for two resin system (epoxy and unsaturated polyester) with glass fibres, for RTM process. The part was a

rectangular mould of 2 cm thickness. Based on previous analysis the range for design parameters was chosen. Design parameters were filling temperature, heating rate, curing temperature and resin injection temperature. GAs showed to be able to find the optimal set of design parameters to minimise process time and temperature difference [115]. A Robust Evolutionary Strategy (RES) was developed and applied to find the optimal cure cycle for RTM of a thick composite laminate (2.5 cm) to minimise process time and maximise degree of cure with the constraint of minimum degree of cure required [116]. The algorithm showed to produce only 11% poor quality parts. A Modified Evolutionary Strategy (MES) has been used to solve the problem of finding the optimal cure profile maximising the degree of cure and minimising the maximum temperature inside the part giving weighting factors to the constraints (maximum heating and cooling rate allowed, maximum temperature, minimum degree of cure required). Two test cases were chosen with different thickness, 5 mm and 25 mm. Both in the thin and thick part a comparison with a Box algorithm showed that MES was able to converge faster and to a lower value of objective function. A comparison with other conventional ES showed the better behaviour of MES [117-119]. An ES has been adopted to optimise the cure cycle of thin and thick parts taking into account seven design parameters describing cure profile (dwell times and heating rates). This optimisation methodology was used to minimise the cure time and residual stresses in a thin (2 mm) and in a thick (20 mm) composite plate made by glass fibres and polyester [120; 121].

Table 2-8 Research on multi-objective optimisation

Papers	Objectives	Parameters	Constraints	Optimisation	Main Results
[108]	Max speed/Min die power	Range pull speed Range temperature heaters	Minimum degree of cure	GA	Significant improvement in pull speed (10%) and die temperature heaters (7%)
[109]	Max pull speed/Min power consumed to provide heater	Temperature profile	Minimum degree of cure Maximum exotherm	SA/SQP	Optimal cure profile found
[110]	Min fill time/Max matching last area to fill and outlet position	Inlet gates	Feasible location gate	NSGA	NSGA performance using different cross-over coupled with mutation
[111]	Min fill time/Min voids content	Gate and vent location	Maximum time and percentage of void	GA	GA finds optimal solution with few evaluations
[112]	Min number of gates and vents Dispersion value	Gate and vent location	Maximum filling time Feasible location gate	Graph based two phase (heuristic algorithm)	Optimising the dispersion value led to reduce the sensitivity of the process to the changing of material and process parameter
[113]	Min bobbles/Min filling time	Gate and vent location	No constraints	GA	First results pointed out the necessity to increase the size of the population
[114]	Max shear angle/Min average shear angle	Pre-shear Starting point Direction of draping	No constraints	GA	Significant reduction in computational time compare with an exhaustive search (30%)
[115]	Min process time/ Min difference of temperature	Mould heating rate Mould temperature Resin filling Curing temperature	No constraints	GA	It is shown that GA can efficiently determine the design parameters for optimal cycle

[116]	Min process time/Max degree of cure	Cure profile	Minimum degree of cure	ES	ES showed better behaviour compare to others stochastic search algorithms
[118]	Max degree of cure/Min maximum exotherm	Cure profile	Maximum heating rate Maximum cooling rate	MES	Comparing with Box algorithm, MES showed having a smooth convergence and at lower values of the objective
[119]	Max degree of cure/Min maximum exotherm/Min process time	Cure profile	Maximum cooling and heating rate	MES	Comparison between ES, MES and box algorithm performance
[120]	Cure time/Residual stresses	Cure profile	Maximum cooling and heating rate	GA	Optimal cure profile found successfully
[121]	Cure time/Residual stresses	Cure profile	Maximum cooling and heating rate	GA	Optimal cure profile found successfully

2.7 Conclusions

This chapter has reviewed the literature on optimisation of composite materials processes. The present review pointed out that each process has been addressed in both single-objective optimisation and multi-objective optimisation setups except for the filament winding process which has been addressed only with single-objective and VARTM process which has not been addressed so far.

Considering cure process the objectives optimised have been cure time and residual stresses. In pultrusion the parameters used were pull speed and energy consumed whereas in batch curing process, like autoclave, the parameters governing the cure profile are used. In multi-objective cure optimisation both cure time and quality of the final part have been optimised. Single-objective optimisation of infusion process has been addressed widely regarding filling time optimisation changing gates and vents locations. Multi-objective infusion optimisation has been studied only for RTM process optimising mostly both filling time and voids percentage within the parts. Minimising the temperature difference between two nodes has been used to minimise the warpage, while in forming optimisation wrinkling minimisation has been achieved optimising the holding force. In the filament winding process, process time and slippage have been addressed separately in single-objective optimisation.

The literature survey undertaken pointed out how technologies of infusion processes like VARTM have not been the focus of optimisation research yet. Infusion technologies are nowadays the most promising processes to fabricate high quality composite manufacture with low production cost. Nevertheless, lack of knowledge in the field makes this process still rely on empirical information. A feasible path to make the process stand out among the others is to provide the VARTM process with a complete simulation/optimisation chain describing the complex nature of the infusion problem and dealing with parameter changes to achieve optimal design conditions of the process. Such a tool will increase the knowledge and awareness of the process which is necessary to master it. Furthermore given the high non-linearity of the physical processes involved in

cure and infusion, the review highlighted how evolutionary methods, often combined with gradient based technique, give the best results in terms of performance, robustness and reliability.

3 Multi-objective optimisation methodology

3.1 Introduction

An existing methodology for multi-objective optimisation [105] has been adapted to cure and infusion problem, implemented and evaluated in terms of its performance and efficiency. The methodology is based on a GA and it has been tested using four multi-objective optimisation benchmark problems.

3.2 Genetic algorithm for multi-objective optimisation

Genetic algorithms are stochastic search algorithm a branch of evolutionary algorithm. The basic idea behind them is to emulate the natural selection process that occurs in nature and that rules the survival of the fittest. A GA begins by creating a first set of random individuals forming the population belonging to the first generation of the GA. Each individual corresponds to a solution in the search space of solutions, called objective space, of the optimisation problem investigated. A quality function, called fitness, indicating the goodness of the solution, is then assigned to each individual. The fitness function depends on the problem investigated and it changes for different optimisation problems. Individuals with higher fitness function have a higher likelihood to be selected as parents for the next population. Two selected individuals generate a new individual through two mathematical operators: cross-over and mutation. These operations are repeated until a new population has generated. The algorithm stops either when a certain convergence criterion is met or a maximum number of generations has been reached [122].

GAs are appropriate to treat optimisation problems dealing with a single-objective; however most real world cases have to cope with more than one objective simultaneously in which more than one optimal solution coexists. In order to adapt a GA to the needs of multi-objective optimisation new operators must be introduced. General ideas developed over the years can be summarised as follows [13; 123-129]:

- Fitness of an individual is increased as a function of the number of individuals that it dominates (Dominance ranking);

- Fitness of an individual is decreased as a function of the number of individuals that are close to it (Sharing ranking);
- A number of best individuals is chosen for the next generation (strong elitism);
- A Pareto optimal archive is updated at each generation.

The most important benefits of using an evolutionary such a GA for a multi-objective optimisation problem are as follows [10]:

- They do not require a deep knowledge about the problem studied;
- They are capable to deal with multiple solutions (individuals in the population) simultaneously;
- They can be easily combined with gradient based techniques to enhance their performance;
- They are easy to implement and use.

3.3 Implementation of the Genetic algorithm

The algorithm adapted in this work accepts input such as the number of generations, the number of individuals in each generation, the reproduction and elite number, the size of the Pareto front, the number of objectives, the number of the optimisation parameters and their ranges and the probability of cross-over and mutation. The output of the algorithm is the value of the objectives for all individuals and the Pareto front for each generation.

The algorithm starts by creating an initial random population of feasible solutions which are encoded in binary strings to enable subsequent operations of the GA and an archive for the Pareto set. Each individual within the population is assigned a partial fitness; each partial fitness corresponds to the value of one objective. A partial rank is computed, every individual is checked against the others in the population and when an individual is dominated its rank is decreased by a fixed value (equal to 5 in this implementation) corresponding to each time an individual is dominated, Figure 3-1 a). A sharing ranking is also used with the purpose of having a well distributed Pareto set in the domain. Individuals contained within a defined radius are penalised by one,

Figure 3-1 b). The idea behind it is to favour those solutions with no close neighbours in the objective space and penalise the others. In this way it will be less likely having overlapping solution in the Pareto front.

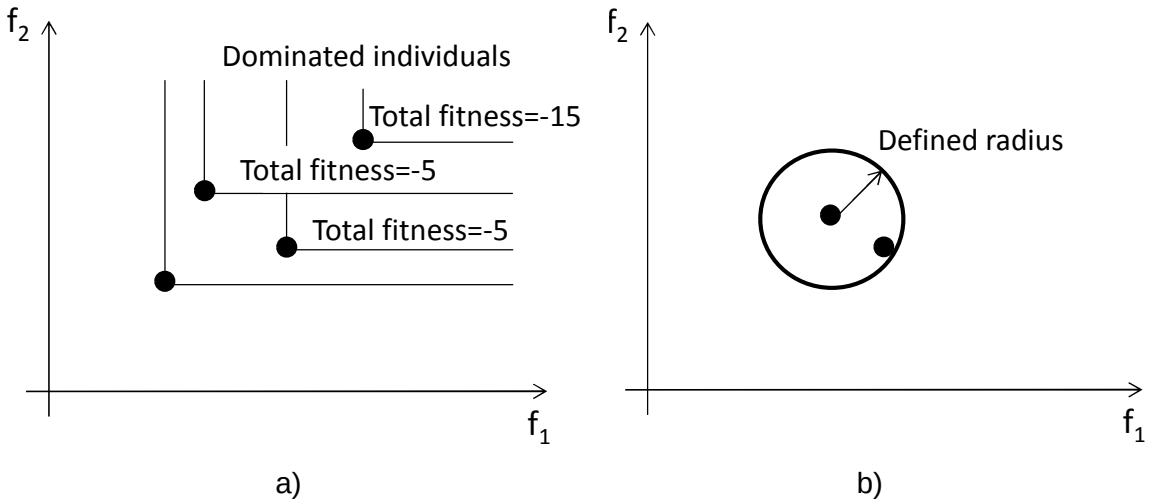

a) b)

Figure 3-1 a) Dominance rank b) Sharing rank

Once all the individuals are assigned with fitness the population is sorted according to it. After that the best individuals are sent directly to the next generation while for the others a tournament procedure is executed. The selection of two parents for the generation of new offspring is based on a tournament selection based on four individuals. The number of individuals taking part at the selection is set in the individuals reproduction number input. The winner among these four individuals is selected as first parent. The same procedure is repeated for the second parent. The two parents generate a new individual using uniform cross-over so that the bits of the new individual are taken from the corresponding bits of one of the parents. The new individual undergoes then mutation that flips bits with a very low probability. The tournament ends when the population has reached the number of individual desired. At this point the population just created undergoes the dominance and sharing rank. The procedure is repeated until a maximum number of generations has been met. Figure 3-2 shows schematically the operation of the algorithm.

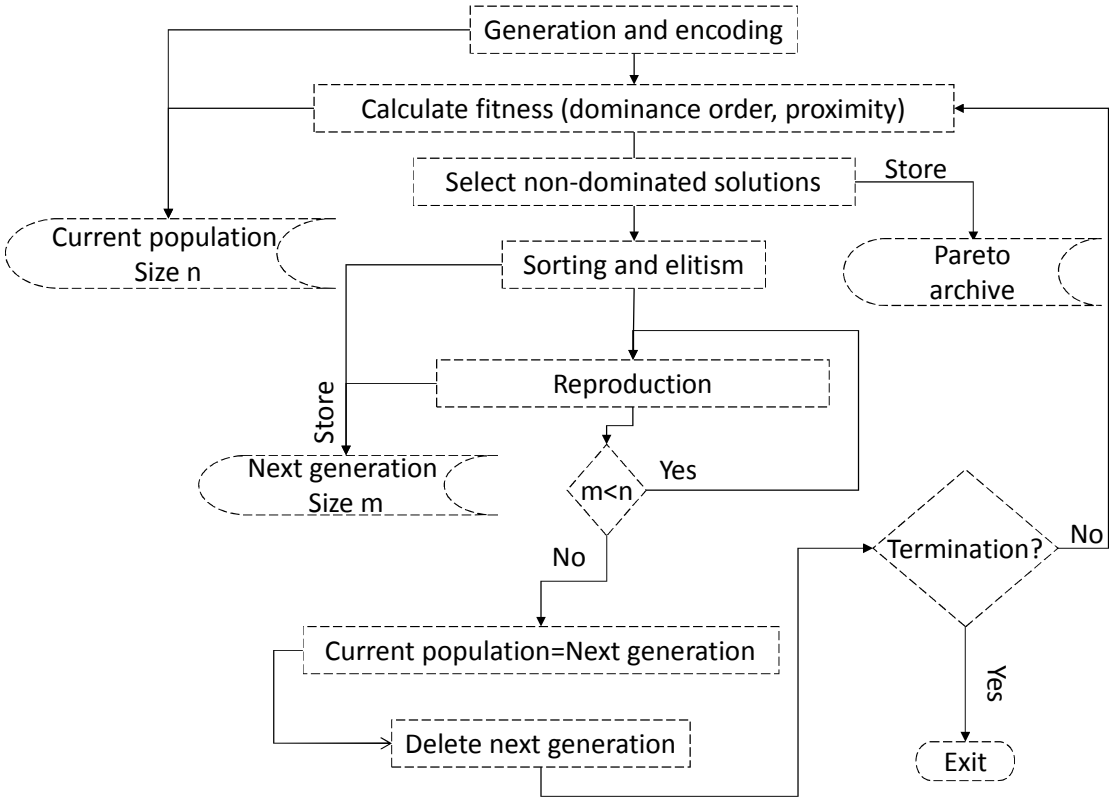

Figure 3-2 GA flow chart

Regarding the filling of the Pareto archive, each non-dominated individual belonging to the current generation is compared with individuals already in the Pareto archive. Four different scenarios can occur. They are illustrated in Figure 3-3 and listed as follows:

a) Any individual in the archive dominates the ones in the current generation, therefore, the Pareto archive does not change;
b) An individual is not dominated by any individuals in the archive and it dominates one of them; as a consequence it replaces it;
c) The archive is not filled yet and no dominance occurs then the individual is simply added to the archive;
d) The archive is completed and no dominance occurs, then one individual of the pair of individuals with the smallest distance in the Pareto archive is replaced by the new individual. The metric distance is calculated using an Euclidean norm.

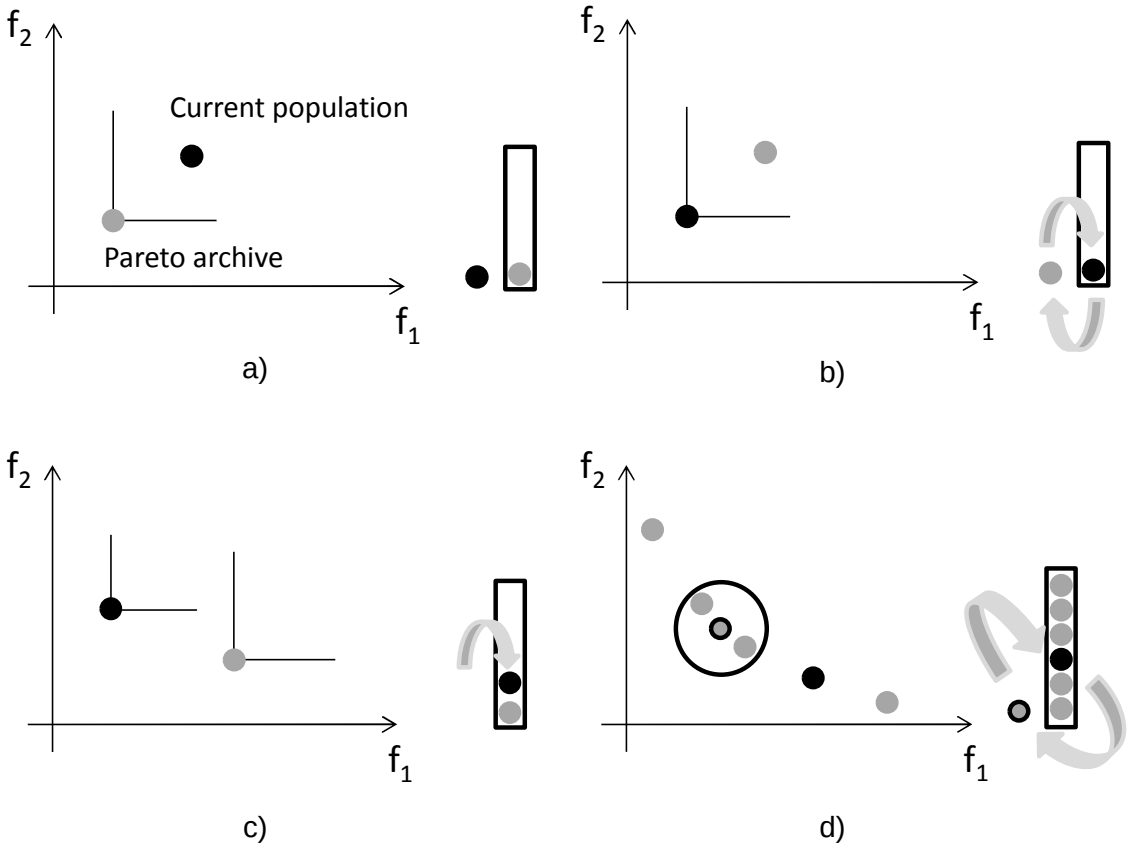

Figure 3-3 Updating Pareto archive

3.4 Analytical benchmark problems

Reliability test to prove the goodness of the methodology previously described have been carried out using four analytical multi-objective optimisation problems. The four benchmark problems have been selected from the literature. The Schaffer problem is a simple convex problem nevertheless it constitutes a stepping stone for testing GAs [130]. The two Zitzler problems chosen are benchmark test functions for studying convex (Zitzler-1) and non-convex problems (Zitzler-2) [131] and the Fonseca problem is a non-convex function good to test GA since it has a large and non-linear trade-off curve that challenges the GA to find and maintain the Pareto [132].The first benchmark (Schaffer) was proposed by Schaffer [11] and it takes into account one parameter (x) and two objectives (f_1, f_2):

$$f_1 = x^2$$

$$f_2 = (x-2)^2 \tag{3-1}$$

$$-10.0 \leq x \leq 10.0$$

The Pareto optimal front is:

$$0.0 \leq x \leq 2.0 \tag{3-2}$$

The second and third benchmarks (Zitzler-1 and Zitzler-2) were proposed by Zitzler et al. [123] and both take into account thirty parameters ($x_i, i = 1 \dots 30$) and two objectives (f_1, f_2). Zitzler-1 problem is expressed as follows:

$$f_1 = x_1$$

$$f_2 = g\left(1 - \sqrt{\frac{x_1}{g}}\right) \tag{3-3}$$

$$g = 1 + 9\sum_{2}^{30}\frac{x_i}{29}, 0.0 \leq x_i \leq 1.0, i \in \{1,2 \dots 30\}$$

while Zitzler-2 problem is:

$$f_1 = x_1$$

$$f_2 = g\left(1 - \left(\frac{x_1}{g}\right)^2\right) \tag{3-4}$$

$$g = 1 + 9\sum_{2}^{30}\frac{x_i}{29}, 0.0 \leq x_i \leq 1.0, i \in \{1,2 \dots 30\}$$

Both problems created by Zitzler have the same Pareto set defined as:

$$g = 1.0 \tag{3-5}$$

The fourth benchmark (Fonseca) was proposed by Fonseca and Fleming [124]. It involves eight parameters ($x_i, i = 1 \dots 8$) and two objectives (f_1, f_2):

$$f_1 = 1 - e^{-\sum_1^8\left(x_i - \frac{1}{\sqrt{8}}\right)^2}$$

$$f_2 = 1 - e^{-\sum_1^8\left(x_i + \frac{1}{\sqrt{8}}\right)^2} \tag{3-6}$$

$$-2.0 \leq x_i \leq 2.0$$

The Pareto optimal set in Fonseca is as follows:

$$x_1 = x_2 = \cdots = x_8, \qquad \frac{-1}{\sqrt{8}} \leq x_i \leq \frac{1}{\sqrt{8}} \tag{3-7}$$

3.5 Reliability testing

Tests to prove reliability, reproducibility, robustness and effectiveness of the methodology have been carried out. Different combinations of input parameters have been applied. The input parameters for the four benchmarks reported in Table 3-1 are the ones that showed the best compromise between approximation of final Pareto set and computational time elapsed. In all cases the cross-over probability was equal to 0.5 and mutation probability to 0.005.

Table 3-1 Input for benchmarks

Benchmark	Generations	Individuals	Reproduction Individuals	Chromosome size	Pareto set	Elite
Schaffer	50	100	70	10	50	4
Zitzler-1	400	100	70	10	50	4
Zitzler-2	400	100	70	10	50	4
Fonseca	400	200	105	15	50	15

3.5.1 Pareto set approximation test

The results concerning the approach of the theoretical front are depicted in Figure 3-4. The Schaffer problem, which is a fairly simple convex problem, was successfully addressed by the GA, showing to overlap the theoretical Pareto front after only five generations. The range of the parameter x in the final Pareto front complied with the theoretical range in Eq. 3.2. Regarding the two benchmarks proposed by Zitzler similar conclusions about the Pareto front approximation can be drawn, although one is a convex problem (Zitzler-1) and

the other is a non-convex problem (Zitzler-2). The methodology is able to approach the theoretical Pareto front successfully; after 100 generations the approximation is already satisfactory while after 400 generations the two fronts are nearly identical. Comparing the two final fronts of the Zitzler benchmarks with the corresponding theoretical fronts leads to the conclusion that the GA behaves consistently in both the convex and the non-convex problem. Furthermore, the approaching of the Pareto occurs evenly along the front as the generation number increases. The 30 parameters corresponding to the Pareto front points complied successfully with the range predicted theoretically (Eq. 3.5). For both problems the value of function g tends to the final value and it ends very close to one. Fonseca benchmark requires a higher number of individuals per generation and also a higher number of individuals picked for reproduction and elite. The chromosome size has been also increased allowing more variety in the first random population. As the number of generations increases, the non-dominated set of solutions approaches the theoretical one. However unlike the aforementioned benchmarks in the Fonseca problem not all the individuals approach the Pareto front evenly. After 50 generations the top end of the theoretical front has been already reached by the GA. This part is characterised by parameter values ranging in the proximity of the upper limit predicted in Eq. 3.7 while the other regions, especially the central part lag behind having at least two parameters well beyond the optimal range. After 100 generations the individuals corresponding to the bottom edge are now aligned with the others and present all the parameters within the theoretical range. The individuals in the central part show improvements in the parameter range although some are still out of the range expected. After 400 generations all the individuals have parameters complying with the range predicted; however the front is not evenly distributed. Although at the last generation the two fronts are not perfectly overlapped the trend followed by the front indicates that an increase in generations number and individuals per population would result in further improvement. Nevertheless the performance can be considered overall satisfactory. Concerning the parameter ranges predicted by theory almost all the points in the objective space correspond to parameter values within the

range in Eq. 3.7. Among the four benchmarks the Fonseca problem proved to be the most challenging for the methodology under study.

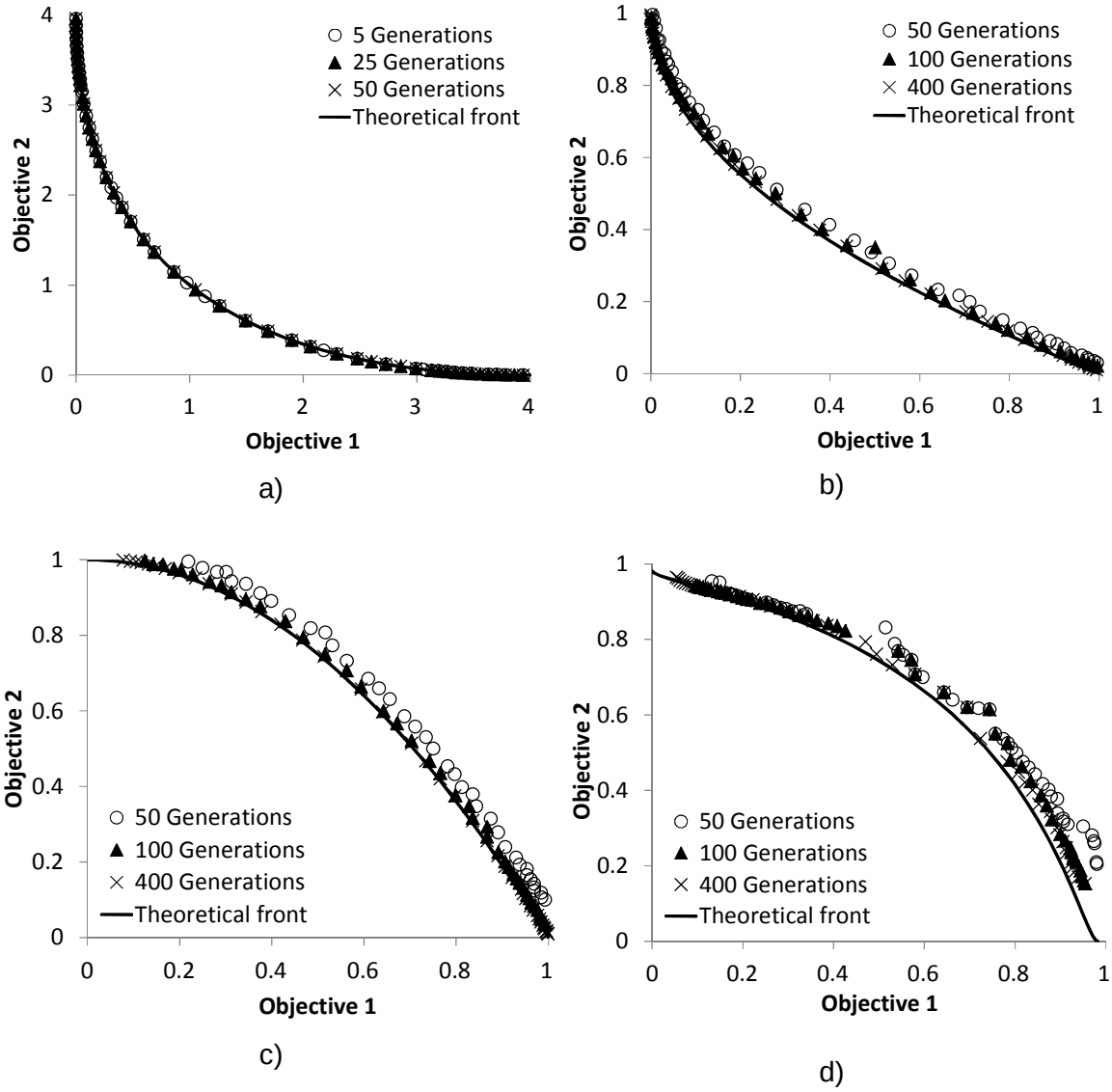

Figure 3-4 Pareto front at different generations: a) Schaffer b) Zitzler-1 c) Zitzler-2 d) Fonseca

3.5.2 Reproducibility test

The algorithm was tested for reproducibility of the approximation applying different deterministic random seeds to generate the starting population. The idea of this test is to verify if starting from different potential solutions at the first generation the algorithm is still capable to approach the final front successfully for the different seeds applied. Figure 3-5 illustrates the Pareto front at last

generation for different random seeds. The reproducibility of the solution was very good for three benchmarks out of four, the Schaffer and the two Zitzler's problems, showing that for these three problems changing random seed does not affect the behaviour and the final Pareto fronts are nearly identical.

In the case of the Fonseca problem changing the seed has a slight influence on the distribution of the solutions along the front. In particular one out of the three random seeds applied resulted in a well spread Pareto front while for the other two seeds the individuals in the last Pareto front were clustered toward the edges of the Pareto front. Nevertheless for all seeds the Pareto individuals found were very close to the front

It can be observed that the most challenging area for the algorithm corresponds to the zone involving higher values of objective 1 and lower values of objective 2. In this particular region the individuals tend to be further from the theoretical front. However taking into account the behaviour depicted in Figure 3-4, increasing the number of generations would result in solutions closer to the theoretical front in this region. In light of these considerations the algorithm proved its reproducibility, showing to approach successfully and consistently in all cases the theoretical front without being affected by the initial random seed choice.

Evaluation of the evolution of the Fonseca problem for the different seeds shows that for all seeds after 50 generations the top part of the front has been already identified. The run with seed 2 does not include significant improvements in the following generations as all the individuals are clustered in the top region. Seed 1 and seed 3 have instead individuals in the bottom part of the front and this part undergoes improvements by the generations ending in a closer position to the theoretical front. Regarding the two Zitzler's problems the final Pareto front is approached evenly by the generations for all three seeds without showing preferential parts; the whole front is approached uniformly even though the initial distance is different. The evolution of Shaffer's problem is not affected by the change in random seed.

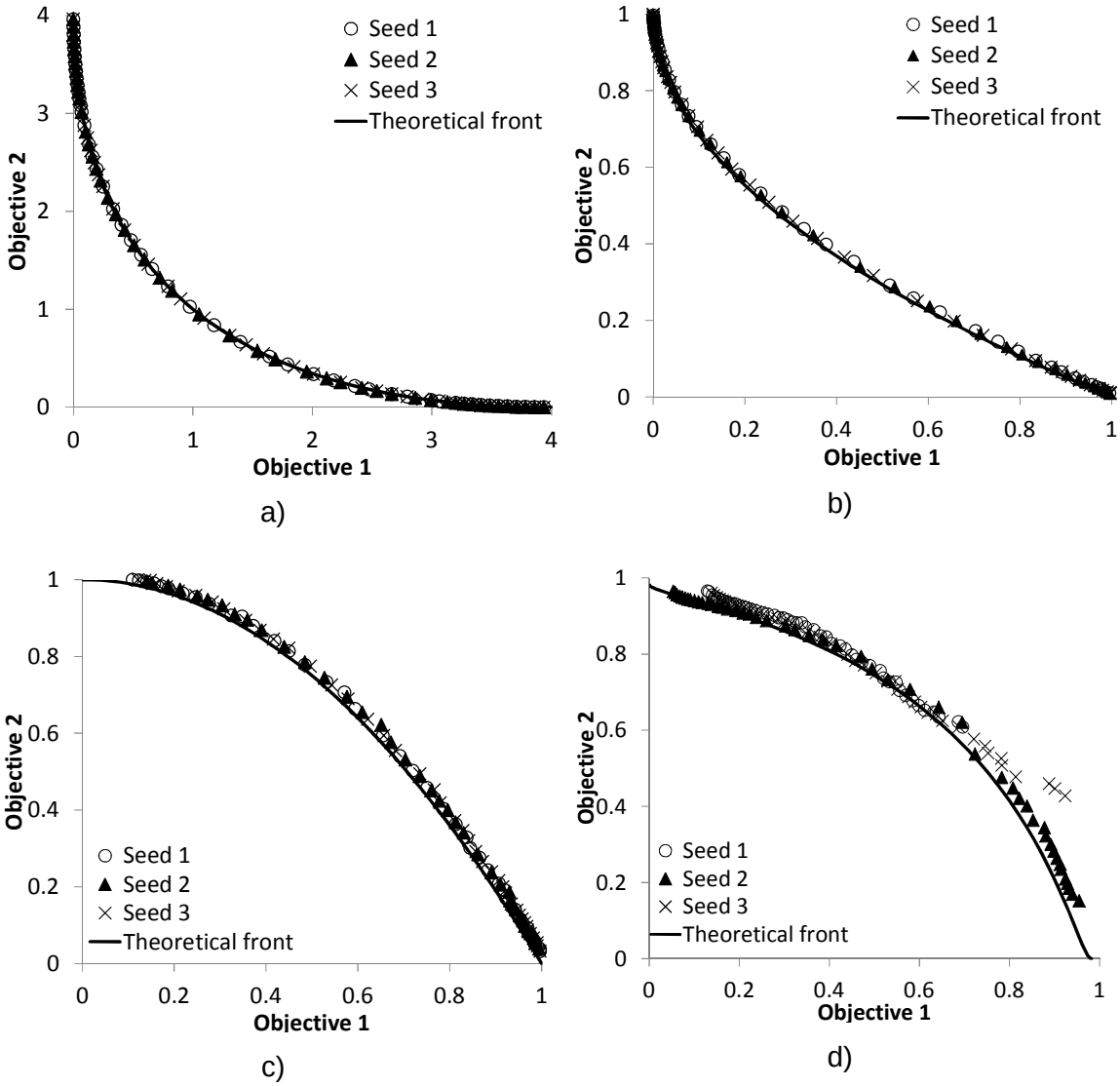

Figure 3-5 Pareto front with different seeds: a) Schaffer b) Zitzler-1 c) Zitzler-2 d) Fonseca

3.5.3 Convergence test

Evaluation of the quality of an algorithm convergence is required to prove its capability to converge within a reasonable number of generations. A metric has to be defined to quantify the distance between the Pareto front at each generation and the theoretical Pareto front. A geometric metric has been developed and implemented in Microsoft Excel VBA and the results are illustrated in Figure 3-6. The metric operates by calculating the distance between each individual in the current generation front against each point in the theoretical front and selecting the minimum distance. An average of these

minimum distances provides the distance of the current generation from the theoretical Pareto front. Calculation of distance between individuals is as follows

$$d = \sqrt{(x_2 - x_1)^2 + (y_2 - y_1)^2} \tag{3-8}$$

Where x_1, y_1 are the coordinates of the individual in the current generation and x_2, y_2 are the coordinates of the individual on the theoretical front. For each individual in the current generation front this distance is calculated against all the individuals in the theoretical front. The minimum among these distances is selected. This represents the distance between that specific individual and the theoretical front. The procedure is repeated for all the individuals in the current generation. At the end an average of the minimum distances is used as a representation of the distance between the two fronts.

It can be observed that changing the seed does not affect the convergence. The distance gradually decreases. After a hundred generations all the benchmarks converge to the theoretical front. The Schaffer problem converges after only 15 generations, where for the two Zitzler problems 100 generations are sufficient. In the case of the Fonseca problem convergence is slightly slower at around 150 generations. The residual distance in all the benchmarks after convergence is not equal to zero due to the way the metric was defined. Using a set of discrete set of points for the theoretical front means that the minimum distance found might not be exact. The metric found is influenced by the fact that the theoretical front is not made by an infinite number of individuals. Furthermore since 50 individuals have been used to represent the theoretical front and since the Schaffer problem has a larger domain the average distance between individuals in this problem is bigger (0.13) than for the others problems (0.03). This explains why the Schaffer problem settles with a higher residual than the two Zitzler problems. The two fronts in Schaffer are obviously overlapped but the use of a finite number of points in the theoretical front leads to a calculated distance different from zero because the individual that would give zero distance is missing. For the same reason a light oscillation can be observed in seed 2 of the Fonseca problem. Here a rearrangement of the individuals in the front due to sharing ranking causes modification in the calculated distance.

Increasing the number of individuals forming the Pareto would help to obtain residual values closer to zero. A different situation occurs in the Fonseca problem. The residual distance found at the end of the convergence cannot be attributed to the discretisation of the theoretical front. In this case even though the majority of individuals overlap with the theoretical front few individuals remain far from it causing an increase in the residual.

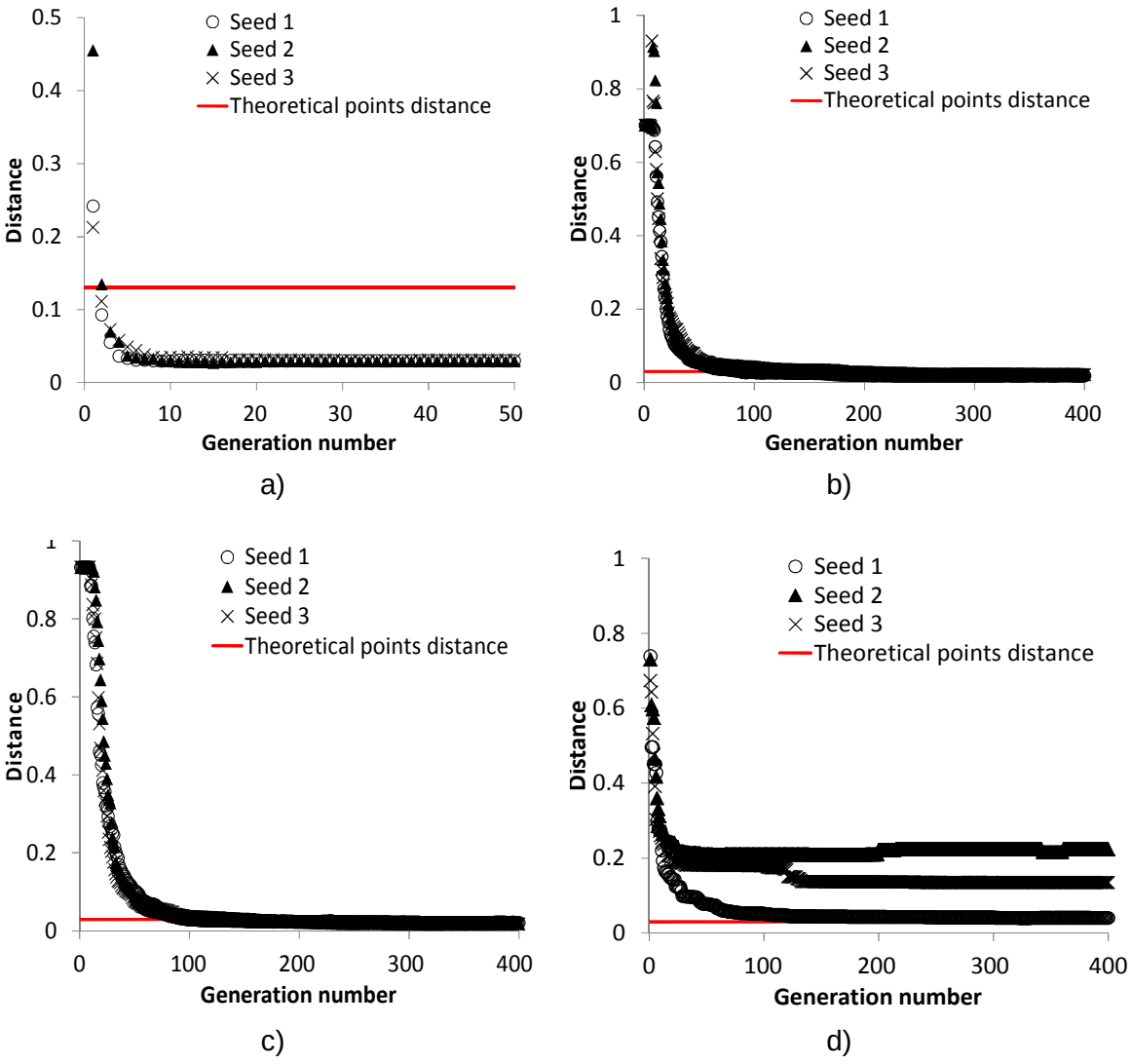

Figure 3-6 Quality of convergence: a) Schaffer b) Zitzler-1 c) Zitzler-2 d) Fonseca

3.6 Comparison with established software

The methodology developed here was compared with an established platform to evaluate its efficiency in terms of computational effort and accuracy of solutions compared to the current state of the art. The PISA (A Platform and

Programming Language Independent Interface for Search Algorithms) platform has been selected [133]. In PISA the user can choose among different optimisation algorithms and among different optimisation problems. The comparison has been carried out using three benchmarks (Zitzler-1, Zitzler-2 and Fonseca problems) evaluating each problem with three different optimisation strategies: the GA used in this study and two selected from the implementations in PISA, Strength Pareto Evolutionary Algorithm (SPEA) [134] and Non-dominated Sorted Genetic Algorithm (NSGA-II) [135]. Table 3-2 reports the input parameters for the three different algorithms. In order to make the comparison meaningful the input parameters have been chosen equal to the parameters used in the in-house GA tests. For the in-house GA the mutation probability was equal to 0.005 while the cross-over probability was equal to 0.5. Regarding the two strategies selected in PISA the cross-over was set equal to 0.5 while two different mutation probabilities have been applied one equal to 0.005 and another one equal to 0.05. The two Zitzler problems ran for a total of 40000 evaluations while Fonseca ran for 80000 evaluations.

Table 3-2 Input parameters for the PISA and GA comparison tests

Benchmark	Generation	Individual	Reproduction	Chromosome size	Pareto size	Elite
Zitzler-1	400	100	70	10	50	4
Zitzler-2	400	100	70	10	50	4
Fonseca	400	200	105	15	50	15

3.6.1 Final Pareto front comparison

The Pareto fronts reached at the last generation using the different methods are depicted in Figure 3-7 for Zitzler-1 problem, in Figure 3-8 for Zitler-2 problem and in Figure 3-9 for Fonseca problem. The comparison is illustrated evaluating the GA against each of the other two strategies for each benchmark. The computational effort used by all three algorithms for the three different benchmarks was similar, with the Fonseca problem requiring longer execution times due to the higher number of evaluations. The convex Zitzler benchmark

was successfully addressed by all three algorithms reaching the same final Pareto front. Slightly better solutions are found in SPEA and NSGA II strategy compared to the GA developed here. The results of the non-convex problem proposed by Zitzler highlights the difficulties of SPEA and NSGA II to distribute uniformly the solutions along the front ending up with a final Pareto front concentrated around the top part of the front for SPEA and around the bottom part of the front for NSGA II. It is necessary to increase the mutation probability to 5% to achieve a well distributed Pareto front. However increasing the mutation probability to 5% means losing the GA features and making the algorithm a random search strategy instead which might prevent the convergence to an optimum. The GA on the other hand achieves a good accuracy and distribution of the final Pareto front even with 0.5% of mutation probability. Concerning the Fonseca problem addressed with SPEA the solution with 0.5% mutation probability shows few individuals far from the others affecting the quality of the approximation while when addressed with NSGA II and 0.5% mutation probability the bottom part is left uncovered with the totality of individuals clustered in the upper part. The in-house GA showed a better and more uniform behaviour along the front. Summarising it can be concluded that when the comparison is carried out with same mutation probability value, the GA performed at same level as SPEA-2 and NSGA-II for the Zitzler-1 problem and Fonseca problem, and better in Zitzler-2. Increasing mutation probability makes SPEA-2 and NSGA-II approaching perfectly the theoretical front; however increasing this parameter means moving away from an evolutionary method and moving towards random search strategy.

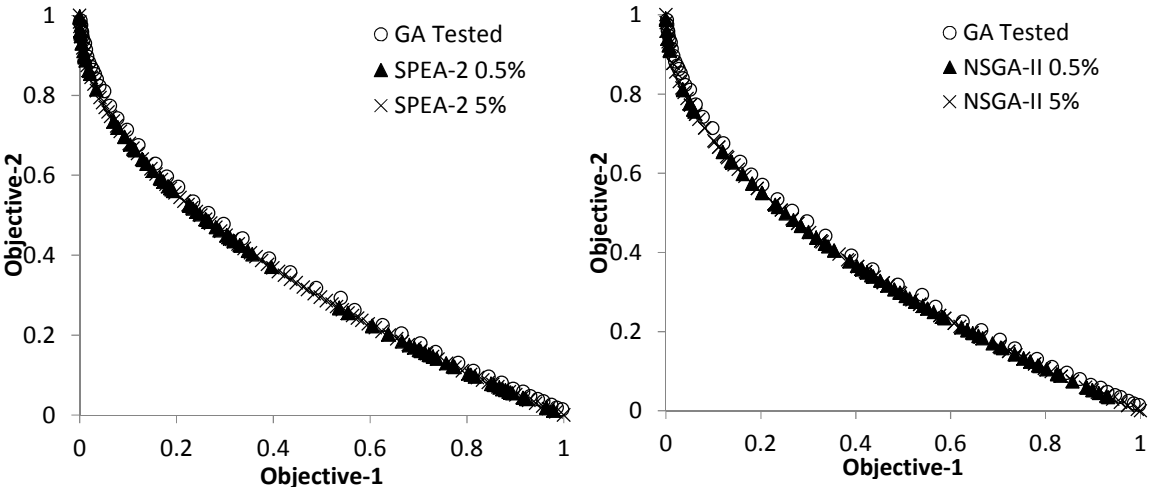

Figure 3-7 Zitzler-1 final Pareto front comparison with PISA platform a) SPEA-2 b) NSGA-II

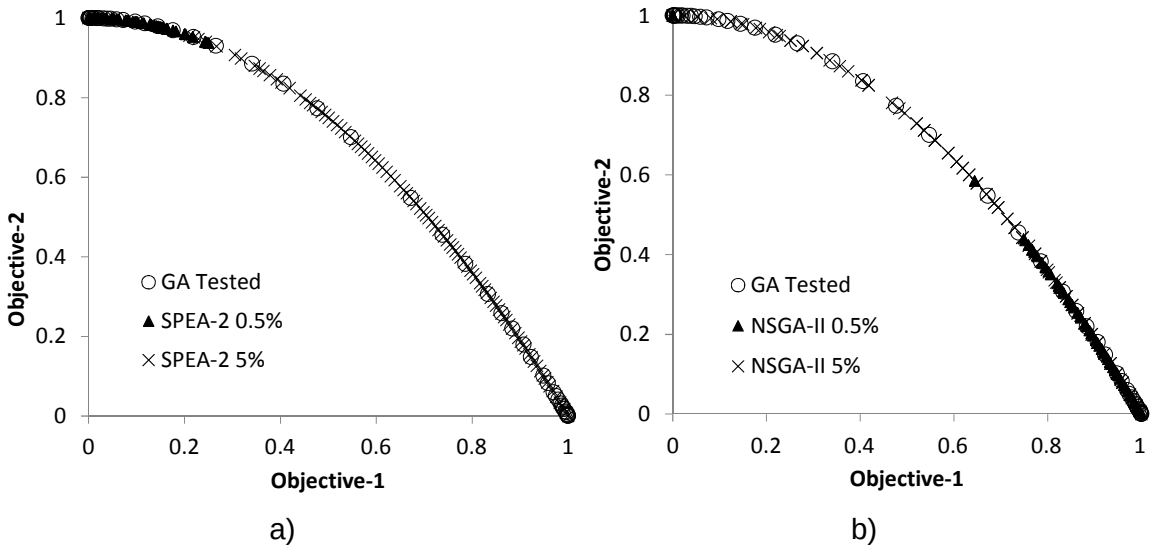

Figure 3-8 Zitzler-2 final Pareto front comparison with PISA platform a) SPEA-2 b) NSGA-II

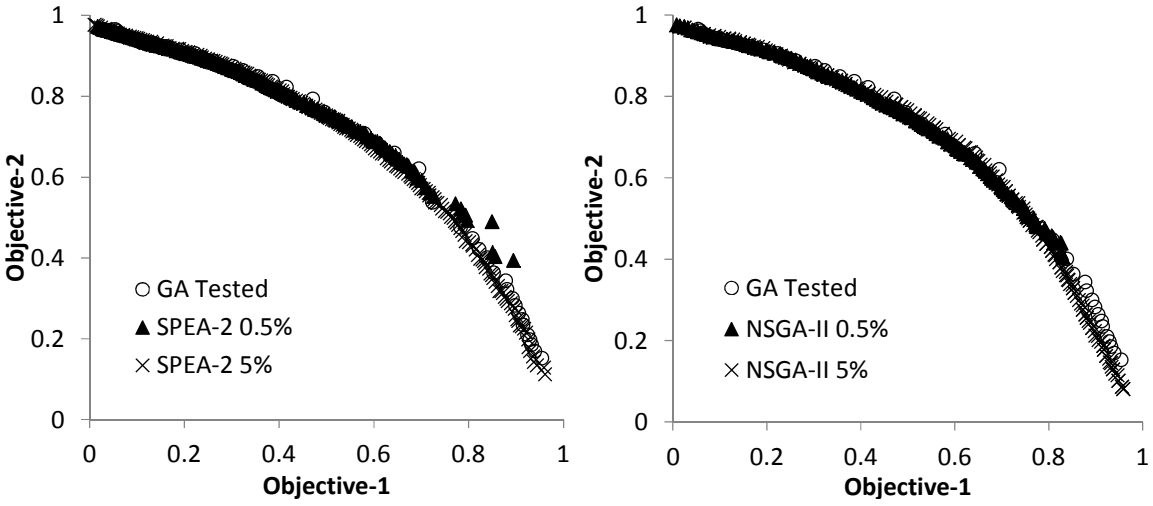

Figure 3-9 Fonseca final Pareto front comparison with PISA platform a) SPEA-2 b) NSGA-II

3.6.2 Distance distribution

The distribution of distances between the GA and PISA solutions and the theoretical fronts for the different benchmark problems has been examined. The distances have been calculated using the procedure described in Section 3.5.3. The results are illustrated in the form of box whiskers plots in Figure 3-10. These show the quartiles representing 25%, 50% and 75% which are respectively the first quartile (Q_1) the second quartile (Q_2) and the third quartile (Q_3) of the distribution while the ends of the whisker correspond to the minimum and maximum values in the distribution. Important information regarding the distribution is given by the dimension of the box itself. This is contained in the Interquartile Range (IQR) which is given by the difference between the third and first quartile. The ends of the whisker depict the minimum and maximum value in the distribution without taking into account the outliers which are calculated as follows:

$$\text{Top outliers} = Q_3 + 1.5 * \text{IQR} \tag{3-9}$$

$$\text{Bottom outliers} = Q_1 - 1.5 * \text{IQR} \tag{3-10}$$

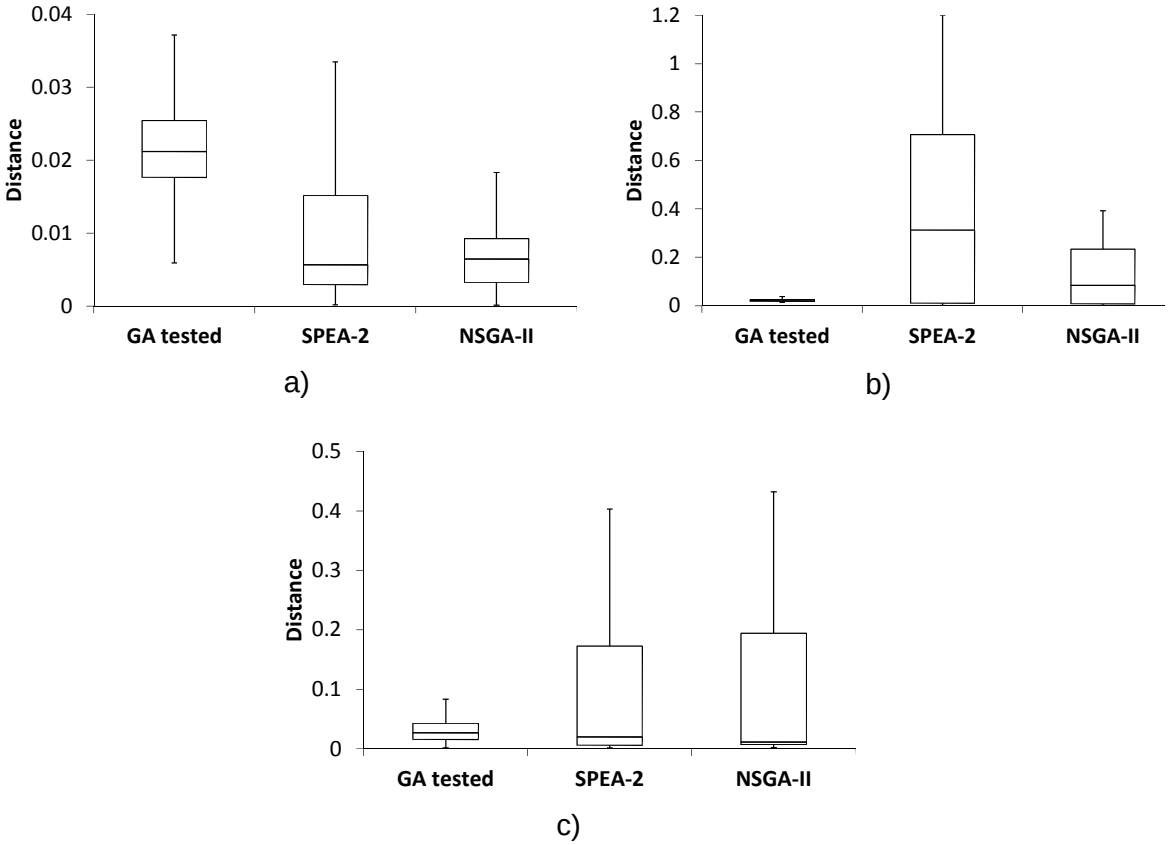

Figure 3-10 Box whiskers plot: (a) Zitzler-1; (b) Zitzler-2; (c) Fonseca

Table 3-3 Values of quartiles for each problem

	Min value	Q1 (25%)	Q2 (50%)	Q3 (75%)	Max value	IQR
Zitzler-1						
GA tested	0.0022	0.018	0.021	0.025	0.037	0.007
SPEA-2	0.00015	0.0029	0.0056	0.015	0.082	0.012
NSGA-II	0.00012	0.0032	0.0064	0.0092	0.076	0.006
Zitzler-2						
GA tested	0.013	0.017	0.019	0.025	0.039	0.008
SPEA-2	0	0.009	0.31	0.71	1.2	0.70
NSGA-II	0	0.007	0.083	0.23	0.39	0.23
Fonseca						
GA tested	0.00084	0.015	0.026	0.042	0.15	0.027
SPEA-2	0.001	0.0051	0.019	0.17	0.40	0.17
NSGA-II	0.0017	0.0063	0.011	0.19	0.43	0.19

Table 3-3 reports the quartile values for the three problems studied and the minimum and maximum values within the distribution plus the IQR value. It can be observed that for the Zitzler-1 benchmark the GA finds a median value about 27% higher than the other two established strategies. On the other hand the maximum value reached by the GA tested is 55% lower than the maximum value found by SPEA and 51% lower with respect to the NSGA II. Furthermore, the GA ends in a very compact distribution signalled by a low IQR which is similar to the value found by NSGA II and 42% better than SPEA. Moreover, the magnitude of the difference in minimum distance is negligible. Concerning Zitzler-2, the GA behaves better than the two established ones. The GA performs 93% better with respect to SPEA-2 and 77% with respect to NSGA-II in terms of the median values. In addition to higher accuracy with respect to the

median value the distribution results in a very small IQR, about 90% smaller than SPEA and NSGA II meaning that all the points belonging to the final Pareto are well close to the theoretical values. Also the maximum value is close to the distribution (0.039) whilst for the other two methodologies this value is far from the box especially for SPEA (1.2). In the Fonseca problem the average values are similar and comparable. However, for the GA the quartile values are more compact. This is reflected by a better IQR value (0.027) which is around 80% better than the IQR for the other two strategies. The maximum value of the distribution for the GA is 0.15 around 60% lower than maximum values obtained by SPEA and NSGA II.

The GA performs uniformly across the different problems; approaching the Pareto at the same speed, reaching the same average value. This confirms its reliability and robustness. In contrast, the two established codes seem to be biased towards specific types of problems addressed. The whisker box plot analysis showed that the in-house GA is a reliable optimisation tool able to perform consistently throughout different objective spaces whether convex or non-convex showing good performance comparable with established software.

Figure 3-11 depicts the minimum distance distribution for the Zitzler-1 problem with the three different strategies. The same range of distance values has been selected in order to compare the distribution in the same range of values. The presence of some spikes far from the average value reveal some flaws in the Pareto front in the final configuration which were not revealed by the whiskers box plot. It is noticeable that 66% of the individuals in the GA distribution are in the range between 0.02 and 0.028 but also the totality of individuals is contained in the range up to 0.036 distances. The calculated average distance in the GA distribution is 0.022. Both established strategies have four points further than 0.36 and up to a maximum equal to 0.76 for NSGA-II and equal to 0.82 for SPEA-2. For SPEA, 68% of the individuals are in the range up to 0.016 distance, nevertheless the wider distribution makes the average distance slipping at the edge of the range having a 0.014. Regarding the NSGA II, 82%

of the individuals have a distance lower than 0.012; nonetheless a wider distribution leads to an average distance of about 0.013.

Figure 3-12 reports the minimum distance distribution for the Zitzler-2 problem with the three different methodologies. In the GA distribution all the individuals have a distance up to 0.04. The SPEA strategy results in only 30% of the individuals with distance lower than 0.04 resulting in an average distance of 0.42. The NSGA II strategy has 36% of individuals falling into the 0.04 range and a more compact distribution with an average distance equal to 0.16.

Figure 3-13 illustrates the minimum distance distribution for the Fonseca problem for the three different approaches. The three strategies, in-house GA, SPEA and NSGA II showed to have the 76%, 62% and 66% of individuals up to 0.045 distance respectively. Nevertheless the in-house GA has a narrower range of distribution resulting in a better average distance equal to 0.06, whereas for the other two strategies the average distance is about 0.13.

The distance distribution analysis confirms that the in-house GA gives comparable performance with established strategy in convex problems and better behaviour in non-convex problems. Furthermore, it has supported the feature that makes the GA stand out with respect to the standard strategies, i.e. its ability to deal with different objective spaces maintaining good performance throughout them.

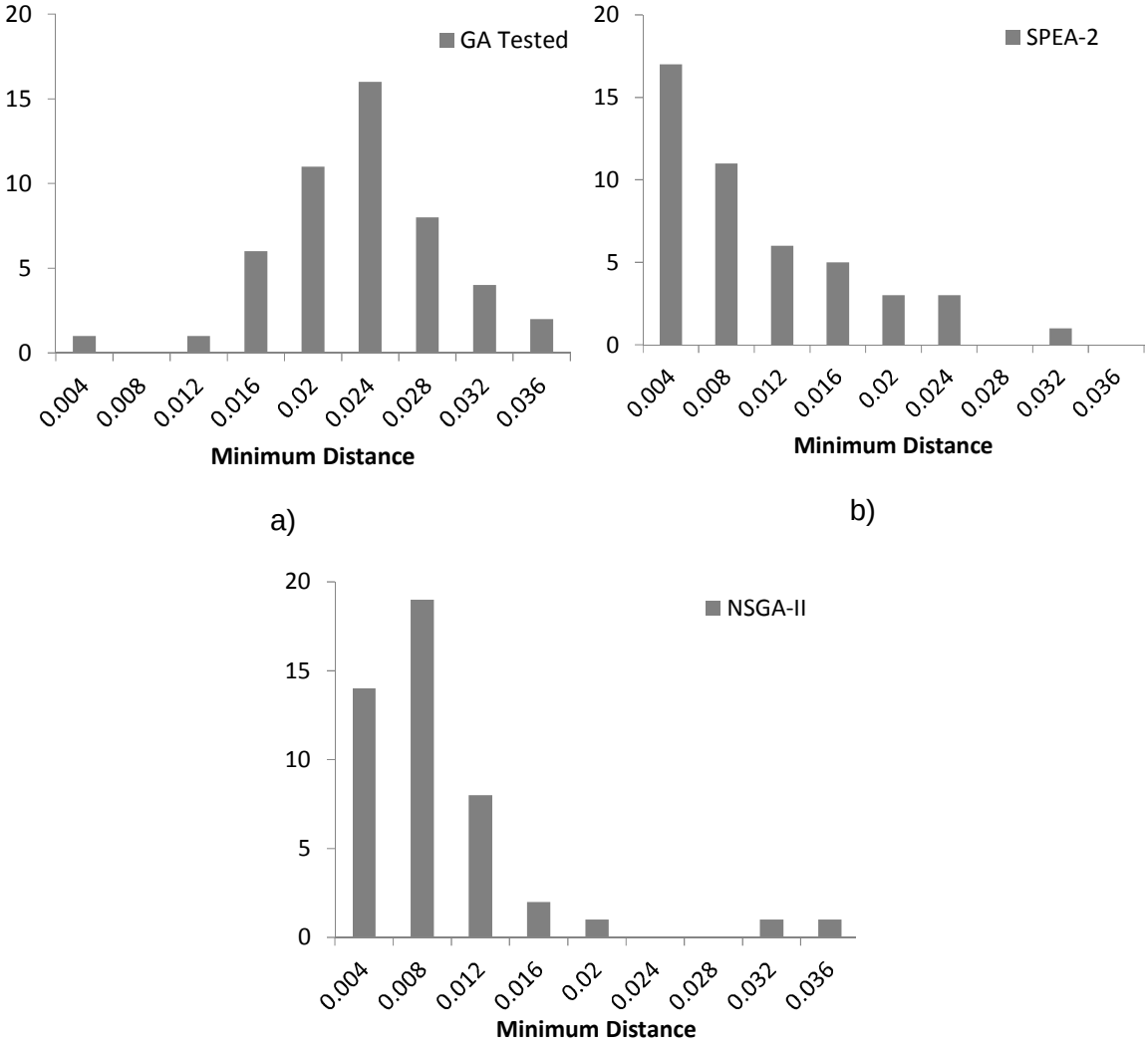

Figure 3-11 Minimum distance distribution for Zitzler-1 with three strategies a) GA tested b) SPEA-2 c) NSGA-II

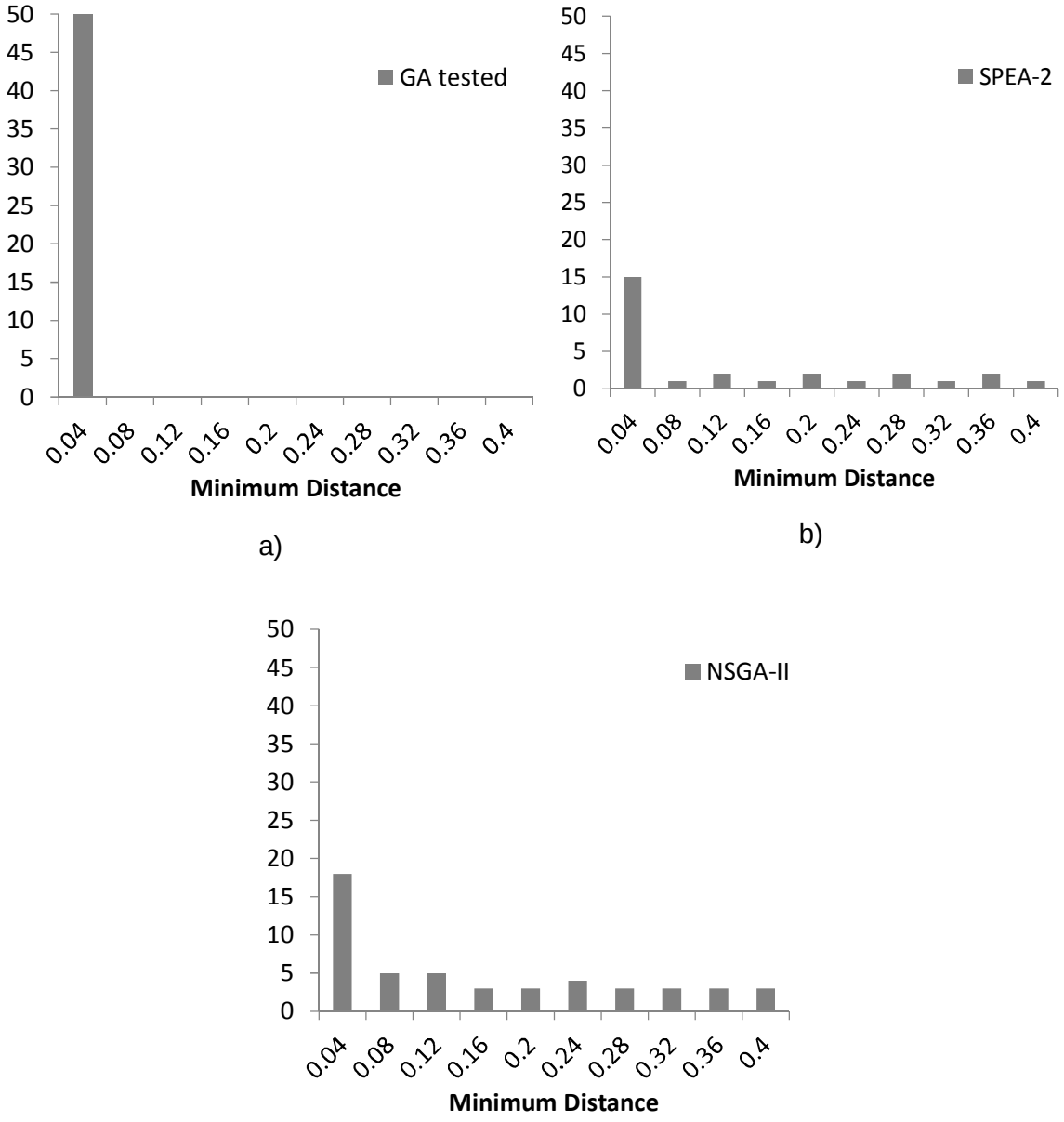

Figure 3-12 Minimum distance distribution for Zitzler-2 with three strategies a) GA tested b) SPEA-2 c) NSGA-II

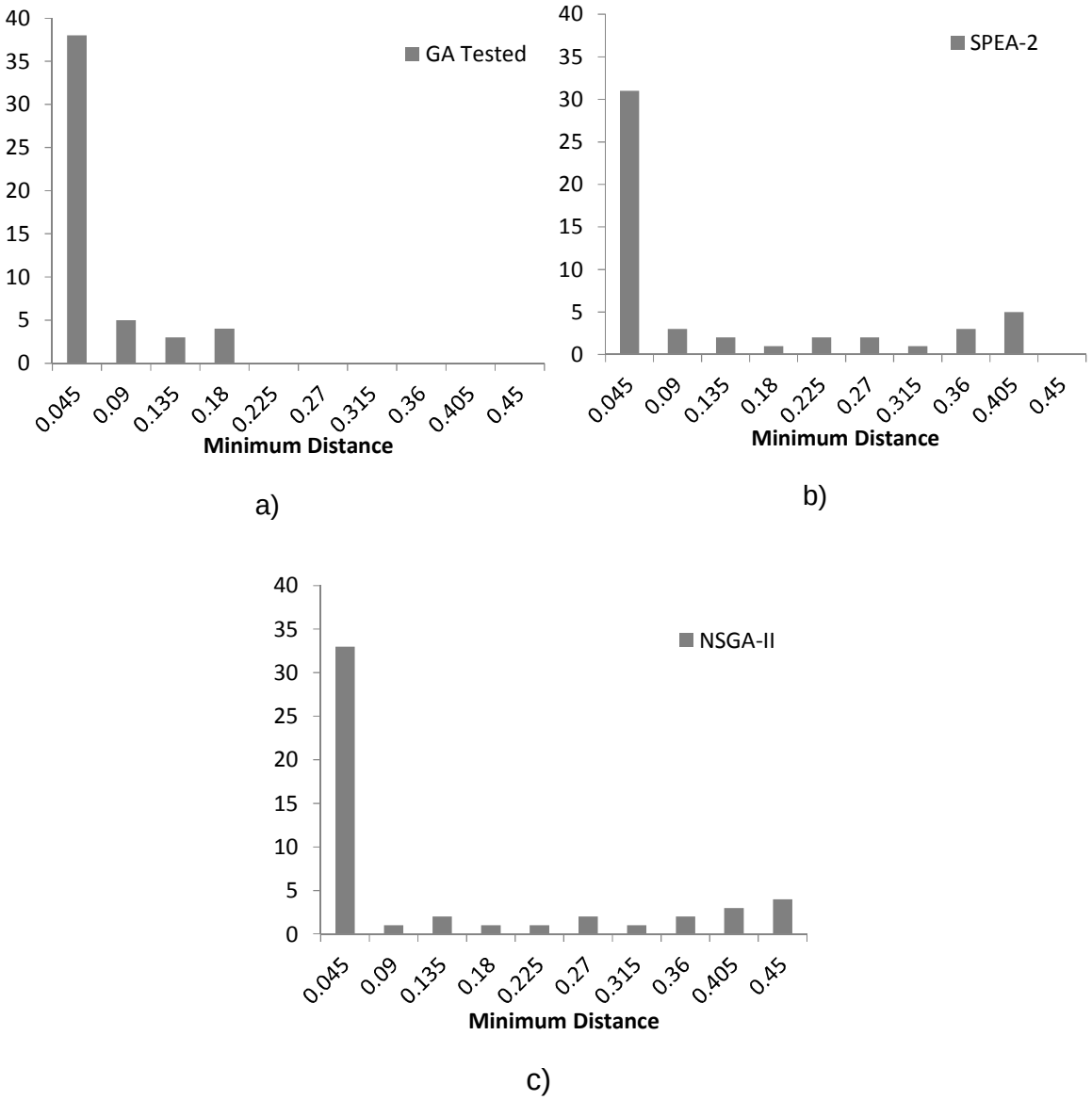

Figure 3-13 Minimum distance distribution for Fonseca with three strategies a) GA tested b) SPEA-2 c) NSGA-II

3.7 Conclusions

Evolutionary algorithms are suitable for the solution of optimisation problems with a high level of non-linearity. However, their behaviour toward different problems can vary significantly. Therefore, it is important to test their performance against different landscape problems to prove their consistency. The GA developed in this work which is the basis of the methodology for

VARTM optimisation has been tested using four benchmark problems. The GA performed very well showing good and reliable outcomes in approaching the final Pareto front, robustness against different random seeds and a good and uniform rate of convergence. Its performance has been also compared with the performance of state of the art implementations showing comparable or better behaviour depending on the type of the problem as well as independence to the test problem use in contrast to current methods. Therefore, the GA developed here can be considered a highly performing and versatile method. This latter feature makes the GA preferable with respect to the standard methodologies since evolutionary algorithms behave differently when the objective space or landscape change and that some of them might perform well in some problems and very poorly in others. In light of the results obtained the consistency and robustness in performance throughout different problems makes the in-house GA an appropriate choice for the purposes of this study.

4 Modelling methodology

4.1 Heat transfer problem

The heat transfer problem corresponding to composites cure can be described as follows:

$$\rho_c c_{pc} \frac{\partial T}{\partial t} = \frac{\partial}{\partial x}\left(K_{cxx} \frac{\partial T}{\partial t}\right) + \frac{\partial}{\partial y}\left(K_{cyy} \frac{\partial T}{\partial t}\right) + \frac{\partial}{\partial z}\left(K_{czz} \frac{\partial T}{\partial t}\right) + \rho_r \varepsilon_r H_r \frac{\partial \alpha}{\partial t} \quad (4\text{-}1)$$

Here, ρ_c is the density of the composite, c_{pc} is the specific heat capacity of the composite. K_{cxx}, K_{cyy} and K_{czz} is the thermal conductivity in the x, y and z direction of the composite and T is the temperature. The heat rate generation due to the cure of the resin is a function of the resin density ρ_r, ε_r is the porosity, H_r is the heat generated by the cure reaction and $\frac{\partial \alpha}{\partial t}$ is the cure reaction rate, α is the degree of cure which is defined as follows:

$$\alpha(t) = \frac{H(t)}{H_T} \quad (4\text{-}2)$$

where $H(t)$ is the heat of reaction up to time t and H_T is the total heat of the reaction. Initial conditions for the heat transfer problem are on temperature and degree of cure as follows:

$$T(0) = T_i \quad (4\text{-}3)$$

$$\alpha(0) = \alpha_i \quad (4\text{-}4)$$

whilst boundary conditions include the prescribed temperature:

$$T(x, t) = T_1 \quad (4\text{-}5)$$

and the natural air convection:

$$[K] \cdot \frac{\partial T}{\partial n} = h(T_{wall} - T_\infty) \quad (4\text{-}6)$$

Where $[K]$ is the thermal conductivity, n the vector normal to the surface, h the convection coefficient, T_{wall} the temperature at the surface and T_{∞} the temperature of the fluid at infinity.

4.2 Heat transfer modelling methodology

The heat transfer problem has been solved by means of Finite Element Analysis (FEA) using the commercial software Marc.Mentat® [136]. The modelling strategy used in this study is based on the use of 3D elements. The element is an isoparametric 8-node brick composite for heat transfer analysis. The element allows the representation of multiple plies which might differ in thickness and fibre orientation [137]. Thermal material properties are applied by means of table driven input whilst the cure kinetics is implemented using the UCURE user subroutine [138]. Initial conditions on temperature and degree of cure are required. Fixed temperature boundary condition depending on time is implemented via FORCDT user subroutine whilst natural air convection is applied using UFILM user subroutine [138].

4.3 Flow through porous media problem

The infusion stage is modeled using Darcy's law:

$$\bar{u} = -\frac{\tilde{K}}{\eta} \cdot \nabla P \tag{4-7}$$

where $\tilde{K}$ is the permeability tensor of the preform which depends on the geometry of the fabric, P is the pressure, η is the viscosity and $\bar{u}$ is the velocity vector. Knowledge of heat transfer exchange during the process and thermal gradients developed is also crucial as the resin viscosity is affected by changes in temperature and it appears in Darcy's too. The pressure distribution can also be found substituting Darcy's law into the continuity equation:

$$\nabla \cdot \bar{u} = \nabla \cdot \left(\frac{\tilde{K}}{\eta} \cdot \nabla P \right) = 0 \tag{4-8}$$

Initial conditions for the flow through porous media problem are as follows:

$$T(0) = T_i \tag{4-9}$$

$$\alpha(0) = \alpha_i \tag{4-10}$$

Whilst boundary conditions are prescribed pressure and temperature:

$$T(x,t) = T_1 \tag{4-11}$$

$$P(x,t) = P_1 \tag{4-12}$$

4.4 Flow modelling methodology

The flow through porous media has been solved using the commercial software PAM-RTM® [139]. A 2D element has been used for the modelling strategy. The element allows to define multiple plies with different fibre orientation and thickness. Thermal material properties, viscosity evolution and cure kinetics have been implemented by means of table driven input. A fixed temperature boundary condition depending on time has been defined using table driven input. Natural air convection has been also applied. The viscosity model with degree of cure as state variable has been implemented via table driven input. Proflot® libraries have been used to implement the viscosity model using viscosity at reference temperature as state variable [140].

4.5 Constitutive models

The materials used in this study are two resin epoxy systems (RTM6 and 890RTM) [141; 142] and carbon fibre (G1157) [143]. Cure kinetics model for the two epoxy resins used are presented. Thermal material properties for the carbon fibre and the two epoxy resins are reported. The thermal properties for the composite are computed through the rule of mixtures. Two viscosity models for RTM6 epoxy resin are also reported: one using degree of cure as state variable and the other using the viscosity at a reference temperature.

4.5.1 Cure kinetics and glass transition development for RTM6 epoxy resin

The cure kinetics model describing the evolution of the cure rate reactions depending on current temperature and degree of cure for RTM6 follows the

equation proposed by Karkanas and Partridge [21-23]. The cure kinetics model takes as input time and temperature set of data and outputs the reaction rate and the degree of cure of the resin during the cycle though integration of the following differential equation

$$\frac{d\alpha}{dt} = k_1(1-\alpha)^{n_1} + k_2\alpha^m(1-\alpha)^{n_2} \tag{4-13}$$

where k_1 and k_2 are reaction rate constants, α is the fractional conversion and m, n_1 and n_2 are reaction orders. The rate constants are defined as follows [144]:

$$\frac{1}{k_i} = \frac{1}{k_{ic}} + \frac{1}{k_d} \quad i = 1,2 \tag{4-14}$$

Where k_{ic} are Arrhenius functions of temperature corresponding to the chemical reaction and k_d is a diffusion rate constant representing the deceleration of the reaction rate as the fractional conversion approaches the maximum degree of cure at a given temperature. These are expressed as follows

$$k_d = A_d \exp\left(\frac{-E_d}{RT}\right) exp\left(\frac{-b}{f}\right) \tag{4-15}$$

$$k_{ic} = A_i \exp\left(\frac{-E_i}{RT}\right) \quad i = 1,2 \tag{4-16}$$

where A_i, A_d are pre-exponential factors, b is a parameter, E_i, E_d are the activation energy for chemical reaction and diffusion respectively, T the temperature and f the equilibrium fractional free volume expressed as follows for the resin system of this study [21]:

$$f = 0.00048 \cdot (T - T_g) + 0.025 \tag{4-17}$$

In the Eq. 4.17 T_g is the glass transition temperature following the Di Benedetto's equation:

$$T_g = T_{g0} + \frac{(T_{g\infty} - T_{g0})\lambda\alpha}{1-(1-\lambda)\alpha} \tag{4-18}$$

where T_{g0} denotes the glass transition temperature of the uncured material, $T_{g\infty}$ the glass transition temperature of the fully cured material and λ is a fitting constant which controls the convexity of this non-linear dependence.

4.5.2 Thermal properties for the G1157 carbon fibre/RTM6 epoxy resin system

Thermal material property models are based on published experimental data [67; 145; 146]. The carbon fibres and RTM6 epoxy resin specific heat are defined as follows and coefficient values are reported in Table 4-1. The material models here developed will be used for the development of FEA models in Chapter 5 and 6. The specific heat of carbon fibre (c_{pf}) follows a linear dependence on temperature whilst the specific heat capacity of the resin (c_{pr}) depends on both temperature and degree of cure with the latter one expressed by dependence on the instantaneous glass transition temperature of the resin.

$$c_{pf} = A_{fcp}T + \ B_{fcp} \tag{4-19}$$

$$c_{pr} = A_{rcp} + B_{rcp}T - \frac{C_{rcp}}{1 + exp\left(c\left(T - T_g - \sigma\right)\right)} \tag{4-20}$$

where A_{fcp} and B_{fcp} are respectively the slope and the intercept of the linear function. A_{rcp} and B_{rcp} are constants governing the linear dependence on the temperature and C_{rcp}, c and σ are the strength, the width and the temperature shift of the transition around the glass transition temperature.

Table 4-1 G1157 carbon fibres and RTM6 specific heat coefficient

Properties	Parameters	Values	Units
c_{pf} ($J{\cdot}^oC^{-1}{\cdot}kg^{-1}$)	A_{fcp}	2.3	$J{\cdot}^oC^{-2}{\cdot}kg^{-1}$
	B_{fcp}	765	$J{\cdot}^oC^{-1}{\cdot}kg^{-1}$
c_{pr} ($J{\cdot}^oC^{-1}{\cdot}kg^{-1}$)	A_{rcp}	1800	$J{\cdot}^oC^{-1}{\cdot}kg^{-1}$
	B_{rcp}	2.5	$J{\cdot}^oC^{-2}{\cdot}kg^{-1}$
	C_{rcp}	-250	$J{\cdot}^oC^{-1}{\cdot}kg^{-1}$
	C	1.1	$^oC^{-1}$
	σ	16.5	^oC

The specific heat for the composite is found applying the rule of mixture as follows:

$$c_p = w_f c_{pf} + \left(1 - w_f\right) c_{pr} \tag{4-21}$$

$$c_p = AT + B + \frac{C}{1 + exp\left(c\left(T - T_g - \sigma\right)\right)} \tag{4-22}$$

where c_p is the specific heat capacity of the composite w_f is the fibre weight fraction defined as follows:

$$w_f = \frac{v_f \rho_f}{\rho_c} \tag{4-23}$$

where v_f is the volume fibre fraction, ρ_f the density of fibre and ρ_c the composite density. A and B are constants controlling the linear dependence on temperature. C, c and σ are respectively the strength, the width and the temperature shift of the transition around the glass transition temperature. Their values are computed accounting for both resin and fibre effect through Eq. 4.21 and are as follows:

$$A = A_{fcp} w_f + B_{rcp}\left(1 - w_f\right) \tag{4-24}$$

$$B = B_{fcp} w_f + A_{rcp}\left(1 - w_f\right) \tag{4-25}$$

$$C = C_{rcp}\left(1 - w_f\right) \tag{4-26}$$

The thermal conductivity of the fibres in the longitudinal direction (K_{lf}) is a linear function of temperature while the transverse (K_{tf}) can be considered constant, [146]:

$$K_{lf} = A_{lf} T + \ B_{lf} \tag{4-27}$$

$$K_{tf} = B_{tf} \tag{4-28}$$

where A_{lf} and B_{lf} are the slope and the intercept of the linear function and B_{tf} a constant. The thermal conductivity for RTM6 (K_r) is a function of degree of cure and temperature and can be expressed as follows [67]:

$$K_r = a_{Kr}T\alpha^2 + b_{Kr}T\alpha + c_{Kr}T + d_{Kr}\alpha^2 + e_{Kr}\alpha + f_{Kr} \quad (4\text{-}29)$$

where a_{Kr}, b_{Kr}, c_{Kr}, d_{Kr}, e_{Kr} and f_{Kr} are the coefficients of the polynomial function. Table 4-2 reports the thermal conductivity values for both RTM6 and the pseudo UD G1157 carbon fibre.

Table 4-2 G1157 carbon fibres and RTM6 thermal conductivity coefficient

Properties	Parameters	Values	Units
K_f ($W{\cdot}^oC^{-1}{\cdot}m^{-1}$)	A_{lf}	0.0074	$W{\cdot}^oC^{-2}{\cdot}m^{-1}$
	B_{lf}	9.7	$W{\cdot}^oC^{-1}{\cdot}m^{-1}$
	B_{tf}	0.84	$W{\cdot}^oC^{-1}{\cdot}m^{-1}$
K_r ($W{\cdot}^oC^{-1}{\cdot}m^{-1}$)	a_{kr}	0.0008	$W{\cdot}^oC^{-2}{\cdot}m^{-1}$
	b_{kr}	-0.0011	$W{\cdot}^oC^{-2}{\cdot}m^{-1}$
	c_{kr}	-0.0002	$W{\cdot}^oC^{-2}{\cdot}m^{-1}$
	d_{kr}	-0.0937	$W{\cdot}^oC^{-1}{\cdot}m^{-1}$
	e_{kr}	0.22	$W{\cdot}^oC^{-1}{\cdot}m^{-1}$
	f_{kr}	0.12	$W{\cdot}^oC^{-1}{\cdot}m^{-1}$

In the longitudinal (K_{11}) and transverse direction (K_{22},K_{33}) the thermal conductivity for the composite can be computed, assuming the two transverse directions equals, as follow, [145]:

$$K_{11} = v_f K_{lf} + (1 - v_f)K_r \quad (4\text{-}30)$$

$$K_{22} = K_{33} = v_f K_r \left(\frac{K_{tf}}{K_r} - 1\right) + K_r \left(\frac{1}{2} - \frac{K_{tf}}{2K_r}\right) + K_r \left(\frac{K_{tf}}{K_r} - 1\right) \sqrt{v_f^2 - v_f + \frac{\left(\frac{K_{tf}}{K_r} + 1\right)^2}{\left(\frac{2K_{tf}}{K_r} - 2\right)^2}} \quad (4\text{-}31)$$

The thermal conductivity for the composite in the longitudinal and transverse directions has a polynomial shape depending on temperature and degree of cure:

$$K_i = A_i + B_i T + C_i T\alpha^2 + D_i T\alpha + E_i\alpha^2 + F_i\alpha \quad i = l, t \quad (4\text{-}32)$$

The coefficients for both longitudinal and transverse thermal conductivity have been computed combining Eqs. 4.27 – 4.31. Coefficients for the composite longitudinal thermal conductivity can be evaluated as follows:

$$A_l = v_f B_{lf} + (1 - v_f) f_{Kr} \tag{4-33}$$

$$B_l = v_f A_{lf} + (1 - v_f) c_{Kr} \tag{4-34}$$

$$C_l = (1 - v_f) a_{Kr} \tag{4-35}$$

$$D_l = (1 - v_f) b_{Kr} \tag{4-36}$$

$$E_l = (1 - v_f) d_{Kr} \tag{4-37}$$

$$F_l = (1 - v_f) e_{Kr} \tag{4-38}$$

the coefficients for the composite transverse thermal conductivity can be calculated as follows:

$$A_t = v_f f_{Kr} \left(\frac{B_{tf}}{f_{Kr}} - 1\right) + f_{Kr} \left(\frac{1}{2} - \frac{B_{tf}}{2 f_{Kr}}\right) + f_{Kr} \left(\frac{B_{tf}}{f_{Kr}} - 1\right) \sqrt{v_f^2 - v_f + \frac{\left(\frac{B_{tf}}{f_{Kr}} + 1\right)^2}{\left(\frac{2B_{tf}}{f_{Kr}} - 2\right)^2}} \tag{4-39}$$

$$B_t = -v_f c_{Kr} + \frac{c_{Kr}}{2} - c_{Kr} \sqrt{v_f^2 - v_f + 0.25} \tag{4-40}$$

$$C_t = -v_f a_{Kr} + \frac{a_{Kr}}{2} - a_{Kr} \sqrt{v_f^2 - v_f + 0.25} \tag{4-41}$$

$$D_t = -v_f b_{Kr} + \frac{b_{Kr}}{2} - b_{Kr} \sqrt{v_f^2 - v_f + 0.25} \tag{4-42}$$

$$E_t = -v_f d_{Kr} + \frac{d_{Kr}}{2} - d_{Kr} \sqrt{v_f^2 - v_f + 0.25} \tag{4-43}$$

$$F_t = -v_f e_{Kr} + \frac{e_{Kr}}{2} - e_{Kr}\sqrt{v_f^2 - v_f + 0.25} \tag{4-44}$$

It has to be highlighted that thermal properties have been also implemented via user subroutine to check the goodness of Eqs. 4.24 – 4.26 and Eqs. 4.33 – 4.44.

The density of the model is calculated using the rule of mixture. Two phases contribute to the density of composite: fibers density and resin density. The fibers density was considered without binder. The fibers volume fraction is 60%.

$$\rho_c = v_f \rho_f + (1 - v_f)\rho_r \tag{4-45}$$

where ρ_r is the resin density, ρ_f the fibre density and ρ_c the composite density. The density values for fibre and resin are reported in Table 4-3. Table 4-4 reports the parameters for the carbon composite with RTM6 epoxy resin

Table 4-3 Density values

Properties	Values	Units
ρ_f	1760	$kg \cdot m^{-3}$
ρ_r	1110	$kg \cdot m^{-3}$

Table 4-4 Material models parameters for carbon composite with RTM6 epoxy resin

Properties	Parameters	Value	Unit
Cure Kinetics	A_1	17580	s^{-1}
	A_2	21525	s^{-1}
	A_d	$6.48 \cdot 10^{18}$	s^{-1}
	E_1	70500	$J \cdot mol^{-1}$
	E_2	59050	$J \cdot mol^{-1}$
	E_d	136800	$J \cdot mol^{-1}$
	m	1.16	
	n_1	1.8	
	n_2	1.32	
	b	0.467	
	T_{g0}	-11	ºC
	$T_{g\infty}$	206	ºC
	λ	0.435	
c_p ($J \cdot ºC^{-1} \cdot kg^{-1}$)	A	2.4	$J \cdot ºC^{-2} \cdot kg^{-1}$
	B	1072	$J \cdot ºC^{-1} \cdot kg^{-1}$
	C	-74	$J \cdot ºC^{-1} \cdot kg^{-1}$
	c	1.1	$ºC^{-1}$
	σ	16.5	ºC
K_l ($W \cdot ºC^{-1} \cdot m^{-1}$)	A_l	5.87	$W \cdot ºC^{-1} \cdot m^{-1}$
	B_l	0.00436	$W \cdot ºC^{-2} \cdot m^{-1}$
	C_l	0.00032	$W \cdot ºC^{-2} \cdot m^{-1}$
	D_l	-0.00044	$W \cdot ºC^{-2} \cdot m^{-1}$
	E_l	-0.0375	$W \cdot ºC^{-1} \cdot m^{-1}$
	F_l	0.088	$W \cdot ºC^{-1} \cdot m^{-1}$
K_t ($W \cdot ºC^{-1} \cdot m^{-1}$)	A_t	0.398	$W \cdot ºC^{-1} \cdot m^{-1}$
	B_t	0.00004	$W \cdot ºC^{-2} \cdot m^{-1}$
	C_t	-0.00016	$W \cdot ºC^{-2} \cdot m^{-1}$
	D_t	0.00022	$W \cdot ºC^{-2} \cdot m^{-1}$
	E_t	0.0187	$W \cdot ºC^{-1} . m^{-1}$
	F_t	0.044	$W . ºC^{-1} \cdot m^{-1}$

4.5.3 Cycom 890RTM epoxy resin

4.5.3.1 Differential scanning calorimeter (DSC)

A heat flux DSC has been used to obtain experimental data for the cure kinetics model of 890RTM epoxy resin. A DSC comprises a heated chamber containing two bases one supporting the reference pan and the other the sample pan. Temperature differences between the reference and sample are monitored by means of two thermocouples. The heat flow required to balance the temperature differential can be determined using an appropriate calibration. The rate of the exothermic reaction can then be determined as follows:

$$\frac{d\alpha}{dt} = \frac{dH}{dt}\frac{1}{H_{tot}} \tag{4-46}$$

In which H is the exothermic heat flow due to kinetics processes and H_{tot} the total heat emitted during the curing reaction.

4.5.3.2 Cure kinetics

The cure kinetics of Cycom 890RTM epoxy resin has been successfully modelled using the model proposed by Khoun et al. [147]. The reaction rate for this epoxy system follows the following law:

$$\frac{d\alpha}{dt} = \frac{Ae^{\left(\frac{-E}{RT}\right)}}{1 + e^{C(\alpha-\alpha_c-\alpha_T T)}}(1-\alpha)^n\alpha^m \tag{4-47}$$

Here E is the activation energy, C is a constant controlling the transition from chemical to diffusion control of the kinetics, m and n are reaction orders and α_c and α_t are coefficients governing the dependence of the transition degree of cure on temperature.

The experimental data obtained using DSC are illustrated in Figure 4-1. It can be observed from the typical bell shape of isothermal data that the model describing the cure kinetics is autocatalytic. Furthermore as the temperature of the isothermal test increases both cure reaction rate slope and maximum cure reaction rate reached increase accelerating the reaction with consequent higher heat flux involved.

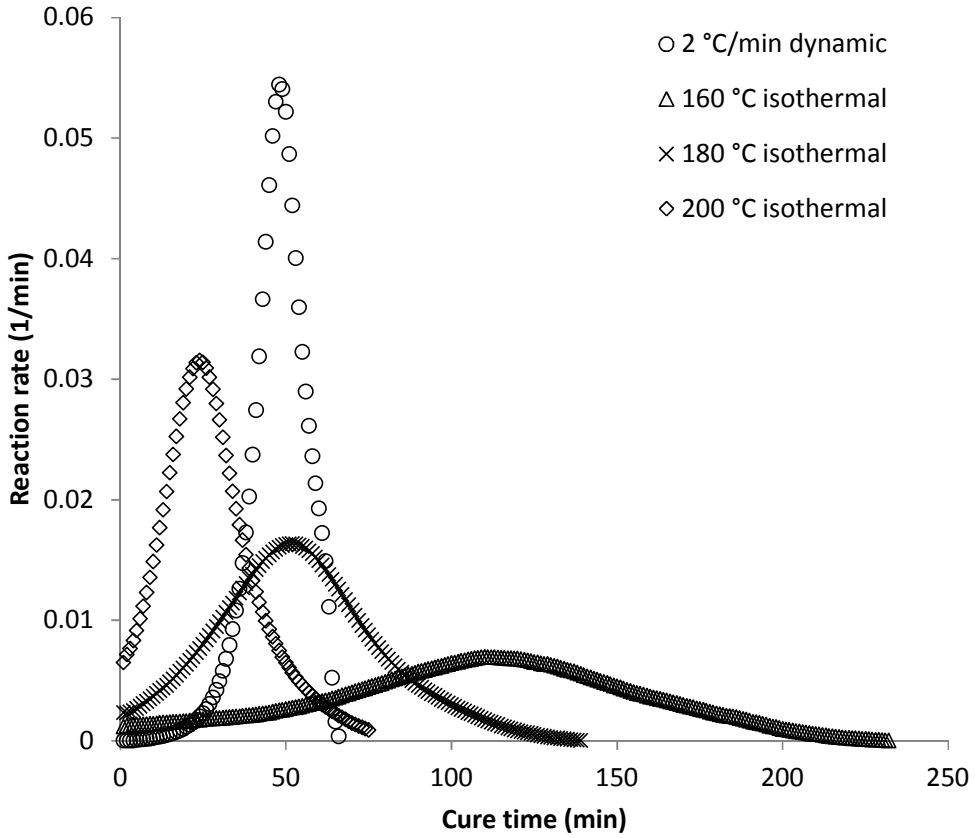

Figure 4-1 Cure reaction rate versus cure time for 890RTM epoxy resin

The experimental data are compared with the original model presented by Khoun et al [147] in Figure 4-2. It can be observed that the parameters reported in [147] do not perform well in predicting the degree of conversion.

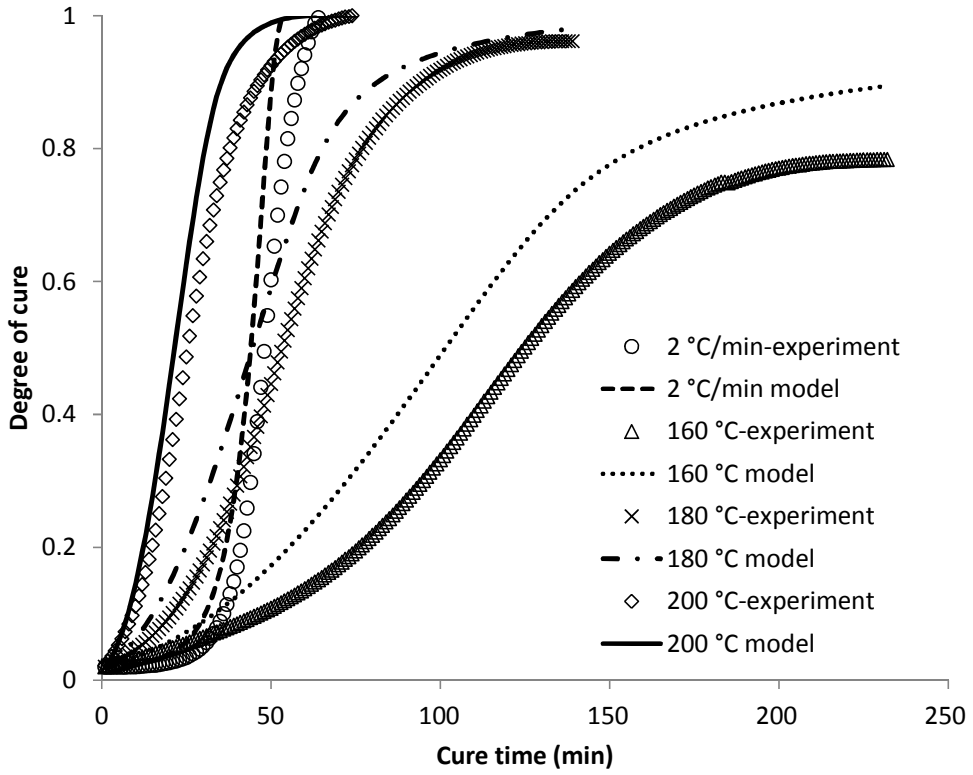

Figure 4-2 Degree of cure versus cure time: Comparison between Khoun's model and experimental results

Based on these differences a new parameter estimation was carried using the Generalised Reduced Gradient Nonlinear Optimisation method implemented in Microsoft Excel [148]. The parameters obtained are reported and compared with the original parameters [147] in Table 4-5. It can be noted that the new set of parameters results in similar value of activation energy and pre-exponential factor whilst differences are noticeable in the reaction orders, in α_c and α_t which control the dependence of transition degree of cure on temperature and in C which controls the width of the transition from chemical to diffusion control of the kinetics. The new fit shows significant improvements fitting accurately both isothermal and dynamic test results as illustrated in Figure 4-3.

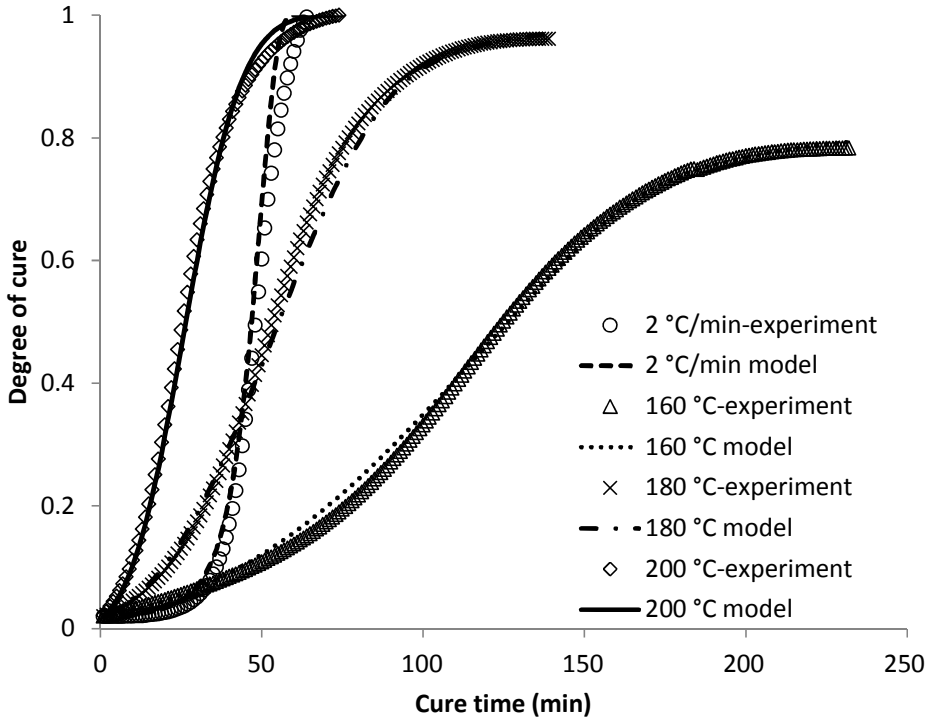

Figure 4-3 Cure time versus degree of cure: Fitting with new parameters

Table 4-5 Cure kinetics parameters values

Properties	Parameters	Khoun's Values	New Values	Units
Cure Kinetics	A	58528	58500	s^{-1}
	E	68976	68970	$J{\cdot}mol^{-1}$
	m	0.63	0.83	
	n	0.6	0.72	
	α_T	0.0039	0.0103	K^{-1}
	α_c	-0.9	-3.73	
	C	15.66	28.5	

4.5.3.3 Thermal properties for the G1157 carbon fibre/890RTM epoxy resin system

The specific heat capacity of the 890RTM epoxy resin follows the same law presented regarding RTM6 epoxy resin and it is presented in Eq. 4.20. The coefficient for the specific heat of the G1157 carbon fibres are reported in Table 4-1. The parameters of the constitutive model for the 890RTM were obtained

using a modulated DSC experiment on the fully cured material. The specific heat capacity of the 890RTM epoxy resin depends on both temperature and degree of cure with the latter dependence expressed by a dependence on the instantaneous glass transition of the resin, Eq. 4.20.

The aforementioned equation has a linear dependence on temperature and a step transition around glass transition temperature. In Figure 4-4 the comparison between experiment and constitutive model is depicted .The fitting coefficients found are reported in Table 4-6.

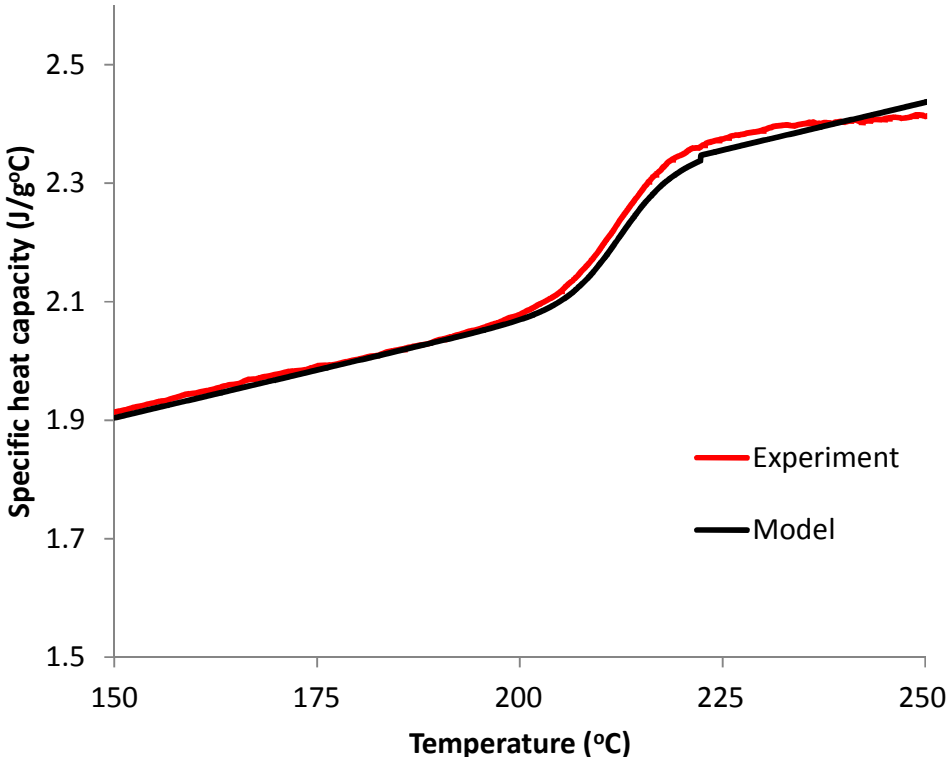

Figure 4-4 Specific heat capacity of fully cured 890RTM: comparison between experiment and constitutive model

Table 4-6 890RTM specific heat coefficient

Properties	Parameters	Values	Units
c_{pr} ($J.^0C^{-1}.kg^{-1}$)	A_{rcp}	1630	$J.^0C^{-1}.kg^{-1}$
	B_{rcp}	3.3	$J.^0C^{-2}.kg^{-1}$
	C_{rcp}	-210	$J.^0C^{-1}.kg^{-1}$
	C	0.31	$^0C^{-1}$
	σ	-12.7	^0C

The specific heat capacity of the composite is affected by two factors, one given by the specific heat capacity of the fibres and the other by the specific heat capacity of the resin. Through the rule of mixture the specific heat of the composite is found as illustrated in Eqs. 4.21, 4.22. The coefficients for the composite material A, B and C have been calculated using Eqs. 4.24 – 4.26 using coefficient values reported in Table 4-1 for G1157 carbon fibre and in Table 4-6 for 890RTM epoxy resin and are reported in Table 4-7. The thermal conductivity for the composite in the longitudinal and transverse direction can be represented as in Eq. 4.32.

It has to be noted that the data presented in [67] for RTM6 are the only values reported in literature describing the dependence of the thermal conductivity of an epoxy system on temperature and degree of cure. Therefore the same values have been used for 890RTM. The constitutive material properties for the 890RTM epoxy and carbon fibre G1157 composite are used in the model developed in Chapter 7.

Table 4-7 Cure kinetics and material properties for carbon composite with 890RTM epoxy resin

Properties	Parameters	Values	Units
c_p ($J{\cdot}^oC^{-1}{\cdot}kg^{-1}$)	A	2.6	$J{\cdot}^oC^{-2}{\cdot}kg^{-1}$
	B	1024	$J{\cdot}^oC^{-1}{\cdot}kg^{-1}$
	C	-63	$J{\cdot}^oC^{-1}{\cdot}kg^{-1}$
	c	0.31	$^oC^{-1}$
	σ	-12.7	^oC
	T_{g0}	-15	^oC
	$T_{g\infty}$	225	^oC
	λ	0.583	
K_l ($W{\cdot}^oC^{-1}{\cdot}m^{-1}$)	A_l	5.87	$W{\cdot}^oC^{-1}{\cdot}m^{-1}$
	B_l	0.00436	$W{\cdot}^oC^{-2}{\cdot}m^{-1}$
	C_l	0.00032	$W{\cdot}^oC^{-2}{\cdot}m^{-1}$
	D_l	-0.00044	$W{\cdot}^oC^{-2}{\cdot}m^{-1}$
	E_l	0.0375	$W{\cdot}^oC^{-1}{\cdot}m^{-1}$
	F_l	0.088	$W{\cdot}^oC^{-1}{\cdot}m^{-1}$
K_t ($W{\cdot}^oC^{-1}{\cdot}m^{-1}$)	A_t	0.398	$W{\cdot}^oC^{-1}{\cdot}m^{-1}$
	B_t	0.00004	$W{\cdot}^oC^{-2}{\cdot}m^{-1}$
	C_t	-0.00016	$W{\cdot}^oC^{-2}{\cdot}m^{-1}$
	D_t	0.00022	$W{\cdot}^oC^{-2}{\cdot}m^{-1}$
	E_t	0.0187	$W{\cdot}^oC^{-1}{\cdot}m^{-1}$
	F_t	0.044	$W{\cdot}^oC^{-1}{\cdot}m^{-1}$

4.5.4 Viscosity model of RTM6 epoxy resin with degree of cure as state variable

The evolution of viscosity using the degree of cure as state variable, which is used in Chapter 6, is described in [22] and implemented as follows:

$$ln\frac{\eta}{\eta_g} = -\frac{C_1(T - T_r - T_g)}{C_2 + T - T_r - T_g} \tag{4-48}$$

where η_g is the viscosity at the glass transition temperature, while the other parameters for RTM6 [22] are:

$$T_r(°C) = -145 + 1.239T \tag{4-49}$$

$$lnC_1 = 2.908 + 291.8T^{-1} \quad (4\text{-}50)$$

$$lnC_2 = -5.485 + 3562T^{-1} \quad (4\text{-}51)$$

4.5.5 Viscosity model of RTM6 epoxy resin using viscosity at reference temperature as state variable

The viscosity model here described, and used for the work developed in Chapter 8, adopts a new idea for modelling resin viscosity. Traditionally resin viscosity model has used degree of cure as state variable [22] that means that the viscosity model has to be coupled with cure kinetics model. In simulation of liquid composite moulding this approach leads to errors since the filling infusion stage of the process is strongly affected by the viscosity value which changes with temperature and is weakly affected by the degree of cure which during this stage undergoes small changes. The viscosity model applied here uses the viscosity at a reference temperature as state variable (η_0) instead of degree of cure [149]. The reference viscosity is governed by its own kinetics as follows:

$$\frac{d\ ln\ \eta_0}{dt} = Ae^{\frac{-E}{RT}}\left(ln\frac{\eta_0}{\gamma}\right)^m \quad (4\text{-}52)$$

The dependence of the reference viscosity on temperature (T) follows Arrhenius dependence, A and E are the pre-exponential factor and the activation energy of the Arrhenius function respectively. The rate of change depends on the logarithm of reference viscosity, with m being the order of this dependence and γ a coefficient.

The viscosity can be evaluated at any temperature using the value of reference viscosity obtained from the integration of Eq. 4.52:

$$\eta = \eta_0 e^{D\left(\frac{1}{T}-\frac{1}{T_0}\right)} \quad (4\text{-}53)$$

Here T_0 is the reference temperature and D is the temperature dependence coefficient. The behaviour of the model at five different isothermal temperatures is shown in Figure 4-5. Increasing the temperature decreases the initial

viscosity. However, it also causes the reaction to be faster and more intense explaining the quicker increase in viscosity.

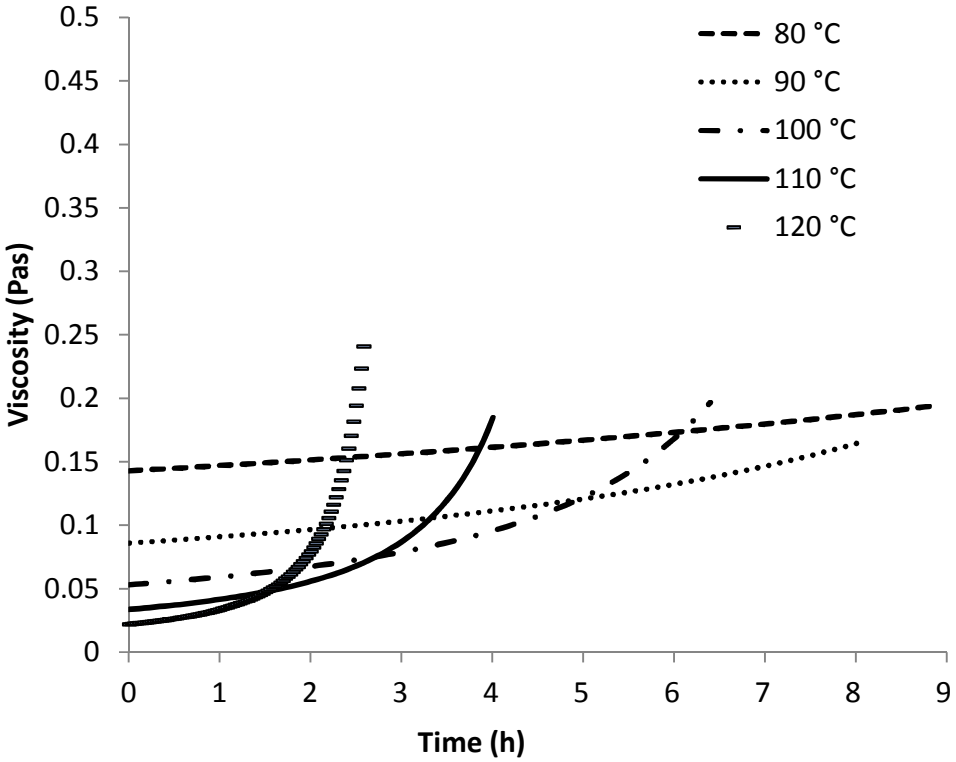

Figure 4-5 Isothermal behaviour of the viscosity model

The behaviour of the model with two different dynamic tests is reported in Figure 4-6. It is possible to observe that higher temperature rate allows reaching a minimum in viscosity sooner.

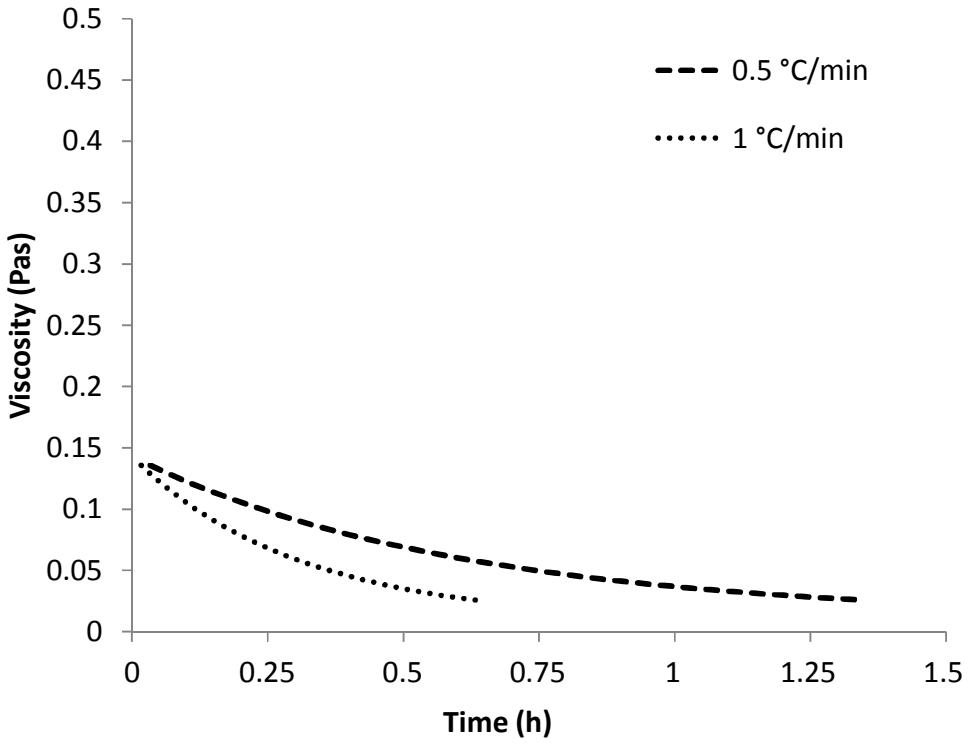

Figure 4-6 Dynamic behaviour of the viscosity model

The number of parameter necessary to solve the model is only five and they are reported in Table 4-8, [149]:

Table 4-8 Parameters of the viscosity model

	A (1/s)	E (J/mol)	m	D (1/K)	γ (Pa·s)
RTM6	600000	70500	2.11	6710	0.032

5 Multi-objective optimisation of VARTM cure

5.1 Introduction

The curing step of the VARTM process involves a number of challenges related to product quality, cost and environmental impact. The overall aim of satisfying requirements for an efficient and robust process is addressed only partially by the use of standard cure profiles that are developed based on empirical information. Standard cure profiles fail to provide optimised solution. Trying to avoid an excessive temperature overshoot that can cause resin degradation, they perform slow cure that results in longer process time and production rate. Nevertheless, they can even be inappropriate for the manufacturing of thick components. The low through thickness thermal conductivity combined with the heat generation due to the chemical reaction can result in thermal overshoot in a short period of time and this might cause thermal degradation of the resin, pre-cracking due to high thermal gradients, and non-uniform mechanical properties. Within this context, optimisation capable to investigate the wide horizon of possible design choices is essential as due to the high non-linearity of the problem the margin for error at the design stage is small. An optimisation approach can determine the best cure profile in order to achieve a prescribed degree of cure in minimum time, while keeping temperature overshoots as low as possible.

The single-objective version of the cure optimisation problem has been addressed as analysed in Sections 2.6.2, 2.6.3 using both gradient based and stochastic search techniques. Simple gradient techniques, Sequential Quadratic Programming, the Levenberg Marquard algorithm and GAs have been used to minimise cure time [61; 64; 67; 72] in a single-objective optimisation setting.

Investigation of multi-objective optimisation of composite cure has been relatively limited as reported in Section 2.6.8. The problems of minimising processing time and thermal gradients, maximising degree of cure and minimising duration as well as minimising maximum temperature and minimising duration have been addressed using EA [116; 118-121].

The work presented in this chapter describes a multi-objective methodology for cure optimisation based on the GA developed. The objectives of process time and exothermic effects minimisation are addressed. The methodology is demonstrated on three generic geometries; a flat panel, an L-shaped component and a T-joint using three different thicknesses for each model.

5.2 Cure optimisation methodology

The GA reported in Chapter 3 has been coupled with the FEM solver Marc.Mentat® [136]. The aim of the cure optimisation is to find the optimal cure profile capable to minimise both process time and maximum temperature within the model, the two objectives of the optimisation are directly related with cost and quality of the process. The process time is evaluated as the time in which every element within the model has reached a minimum value equal to 0.88. This is the degree of cure resulting from the recommended cure cycle of the epoxy system used (RTM6). The general shape of the cure profile adopted is illustrated in Figure 5-1. The standard cure profile for RTM6 comprises two dwells at two different temperatures linked by two ramps. The cure profile for the optimisation problem has been characterised by four parameters able to modify the cure profile but maintaining the same general shape. The four parameters selected are the two dwell temperatures, the ramp rate and the duration of the first dwell. Table 5-1 reports the parameter ranges used in the optimisation. The temperature of the first dwell has been chosen around the standard temperature for RTM6 which is 160 ºC. The temperature of the second dwell is the temperature of post-cure which must be higher than the glass transition temperature reached during the first dwell. The standard post-cure temperature is set at 180 ºC, and the range has been selected up to 210 ºC. The first dwell duration spans from 30 to 180 minutes aiming to produce a wide range of different degree of cure levels at the end of the first dwell. The standard first dwell duration is set to 75 minutes. The standard ramp rate is 1 °C/min and the the range chosen is up to 4 ºC/min.

Table 5-1 Design parameter ranges

Parameters	Range
T_1 (ºC)	145-175
T_2 (ºC)	180-210
Dwell duration (s)	1800-10800
Ramp (ºC/min)	1-4

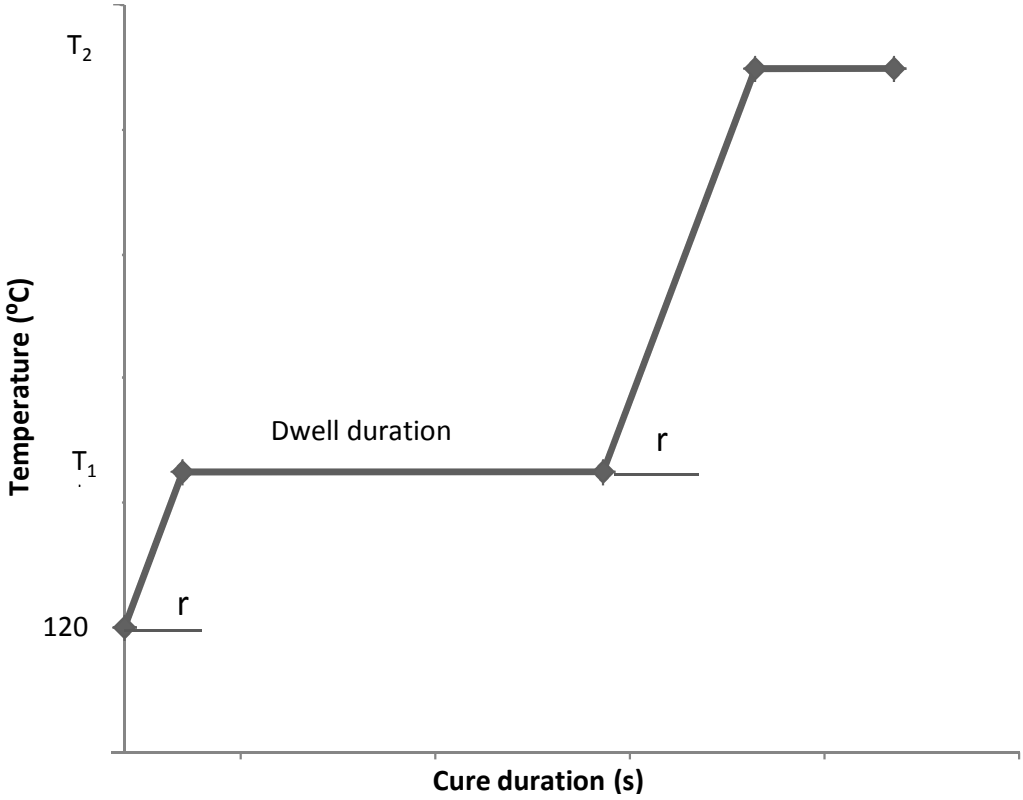

Figure 5-1 General cure profile

The process optimisation tool developed requires an interface linking the GA to the FEM solver. The interface has been implemented in C++ and its functionality is illustrated in Figure 5-2. The GA generates the new set of parameters (the two dwell temperatures, the duration of first dwell and the ramp rate) defining the new cure profile which are fed to the interface. The interface read the input file generated by Marc.Mentat® of the cure simulation model built for the optimisation and identifies the location where the new set of parameters is inserted. Subsequently, a new input file with the new set of parameters is written by the interface and it constitutes the new Marc.mentat® input template. A script file is then used to call the solver Marc.Mentat® and execute the

simulation with the new input file. At the end of the simulation the interface opens and reads the output file of Marc.Mentat®. The locations containing the quantity of interest (process time and maximum temperature overshoot within the model) are identified and read. The outputs are then sent to the GA. The loop is then repeated until a stop criterion - maximum number of generations reached in this case - is met.

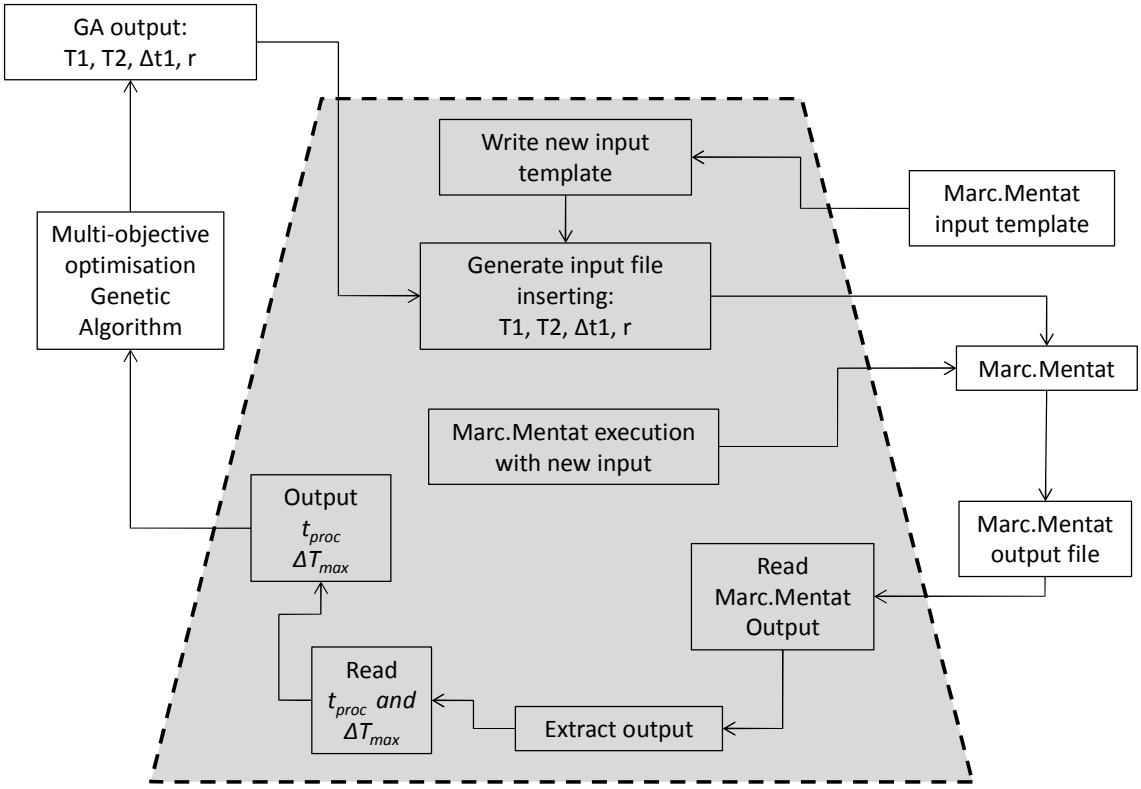

Figure 5-2 Interface for cure problem

The GA parameters used in the optimisation are reported in Table 5-2. The values of the parameters have been fine-tuned for the 48 mm T-joint model, described in Section 5.3, which is the most demanding case in terms of both geometry and thickness for the GA to converge to solution. Once the set of parameters chosen showed convergence in this case the same parameters have been adopted for all others. The assumption made has been later verified by observing earlier convergence in simpler cases.

Table 5-2 GA parameters used for cure optimisation

GA input	Values
Number of generations	50
Individuals per population	50
Individuals per reproduction	40
Elite individuals	4
Size of Pareto	30
Mutation probability	0.005
Cross-over probability	0.5

5.3 Case studies

Three different geometries, a flat panel, an L-shape geometry and a T-joint, fabricated by infusion using carbon fibre [143] and epoxy resin RTM6 [141] have been used. Typical dimensions for the geometries were based on [150-152]. For each geometry a thickness of 3 mm, 24 mm and 48 mm has been considered; Table 5-3 summarises the specific of the nine models. The three different geometries are illustrated in Figure 5-3 for the 48 mm case. The three geometries have been selected in order to show an increasing level of geometrical complexity which together with the increasing thickness contributes to a more challenging heat transfer situation. Boundary conditions of a fixed temperature provided by the cure profile at the nodes in contact with the mould and air convection on the surfaces in contact with the vacuum bag have been applied. Initial temperature of 120 ºC at all nodes in the model and initial degree of cure of 0.02 at all nodes and elements has been applied. The FEM solver Marc.Mentat® was used to solve the heat transfer problem. The lay up for the flat panel, the L-shape and T-joint were respectively:

$$[0/90/90/0]_s$$

$$[0/\pm 45/90/90/\pm 45/0]_s$$

$$[0/90/0/90/0]_s$$

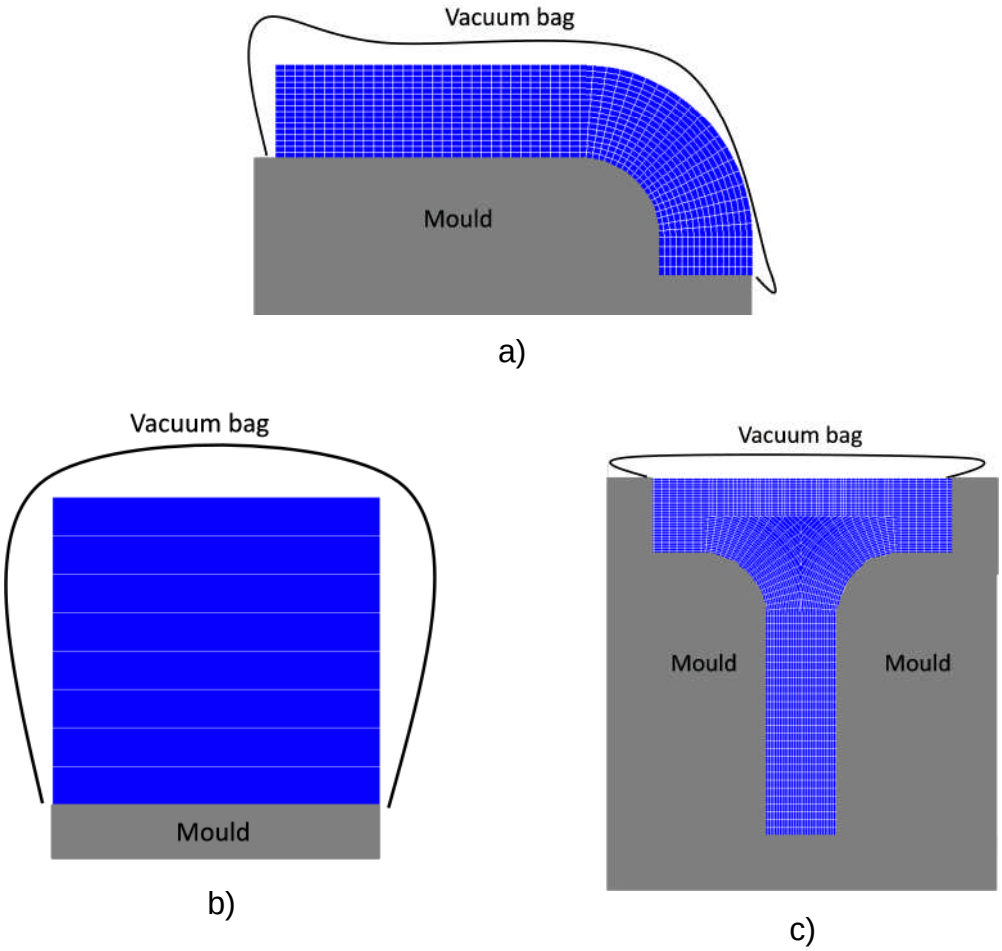

Figure 5-3 Case studies: (a) L-shape; (b) Flat panel; (c) T-joint.

Table 5-3 FEM model characteristics

Model	Nodes number	Elements number	Thickness elements
Flat panel 3 mm	36	8	8
Flat panel 24 mm	36	8	8
Flat panel 48 mm	36	8	8
L-shape 3 mm	630	248	4
L-shape 24 mm	2176	1008	16
L-shape 48 mm	2176	1008	32
T-joint 3 mm	1220	519	4
T-joint 24 mm	3272	1527	16
T-joint 48 mm	6008	2871	32

5.4 Cure optimisation results

Figures 5-4 – 5-6 illustrate the optimisation results at the 50th generation for the three flat panels, the three L-shape and the three T-joint cases. Table 5-4 presents the cure results applying a standard cure profile, comprising a ramp at 1 ^{0}C/min from 120 ^{0}C up to 160 ^{0}C, a first dwell at 160 ^{0}C for 4500 s, a second ramp at 1 ^{0}C/min up to 180 ^{0}C and a second dwell at 180 ^{0}C for 7200 s.

Table 5-4 Standard results

Model	Process time (s)	Temperature overshoot (ºC)
Flat panel 3 mm	8213	1
Flat panel 24 mm	8255	11
Flat panel 48 mm	7962	131
L-shape 3 mm	8625	1
L-shape 24 mm	9211	8
L-shape 48 mm	10091	113
T-joint 3 mm	9602	15
T-joint 24 mm	11720	27
T-joint 48 mm	7911	194

The standard cure profile results in low temperature overshoots (in the range of a few ^{0}C) for 3 mm and 24 mm thickness, in the L-shape and flat panel cases, and process times in the region of 8000 s for the flat panel and 9000 s for the L-shape. The T-joint cases for thickness of 3 mm and 24 mm present a significant temperature overshoot due to a less effective heat dissipation by the natural air convection acting on the lower face of the flange. The ultra-thick component (48 mm) is subject to a high temperature overshoot in all three cases. In the flat ultra-thick panel the temperature overshoot is 131 ^{0}C. The temperature overshoot is lower in the L-shape case (113 ^{0}C) and higher in the T-joint case (194 ^{0}C). It should be noted that at very high overshoots the maximum temperature obtained by the model does not necessarily represent the real temperature seen in the component as the model does not take into account phenomena related to resin degradation once the temperature reached very high levels. The degradation of the polymer constitutes an additional heat

release mechanism, whilst the degradation reactions are different than the crosslinking reaction with a different reaction enthalpy. Therefore, in cases where the temperature exceeds the onset of degradation (around 330 ^{0}C for RTM6 [153]) the maximum temperature reached by the model corresponds only to a proxy of the severity of the exotherm. Whilst this is appropriate for the purposes of optimisation, the temperature presented cannot be considered an accurate prediction of the real temperature observed in the component in cases of a highly exothermic event.

The differences in temperature overshoot for geometries of the same thickness can be explained by considering a ratio of the surface area heated and the area cooled down by the air convection. This ratio is equal to one for the flat panel, higher than one (2.4) for the T-joint model and lower than one (0.45) for the L-shape case. This justifies the lower temperature overshoot value predicted in L-shape and the higher value predicted in the T-joint. There is a clear dependence of overshoot on thickness with overshoot increasing as a function of part thickness. This is due to the combination of a greater heat release due to increased volume and less efficient heat dissipation due to increased distance to the surface as the thickness increases.

The trade-off surfaces observed in Figures 5-4 – 5-6 show that overshoot and process duration are negatively correlated. This is due to the nature of the cure reaction. Higher temperature results in more intense reaction therefore the degree of cure evolution is quicker and the end process criterion set at 0.88 degree of cure is reached earlier resulting in a shorter process time. The dependence tends to be non-linear with sensitivity of overshoot on process duration reducing with increasing duration. This can be explained by the fact that a long process duration solutions are characterised by lower temperature and lower reaction rate. Combining these two effects leads to a smaller temperature gradient across the thickness as the material is given more time to reach a thermal equilibrium. This behaviour results in a shape of the Pareto front that resembles an L, which allows to distinguish between a region of the design space in which there are significant benefits in terms of process duration

with small improvement in temperature overshoot and a region of significant benefits in temperature overshoot with small improvements in process duration. The conventional cure profile for the 3 mm and 24 mm models is in the area of low sensitivity of temperature overshoot on process parameters but at a significant distance from the point where benefits in terms of process duration can be obtained (Figures 5-4 – 5-6 a) and b)). For the 3 mm models maximum benefit in the range of 50-60% can be achieved in process duration which translates to around 4500 s reduction, whilst for the 24 mm the maximum benefit without considering worsening in temperature overshoot swings between 45% and 60% which translates to about 4000 s to 7000 s. Standard cure profiles are designed in a conservative way aiming to keep the solution away from possible dangerous overshoots which can degrade the quality of the part. Only for very thick components the solution proposed by the standard profile has an acceptable efficiency. In contrast the conventional cure profile for the 48 mm models is in the region of low sensitivity of process time and significant benefits in terms of temperature overshoot can be obtained (Figures 5-4 – 5-6 c)). The flat panel can reach a maximum of 87% of temperature overshoot reduction (114 ºC), the L-shape 90% (100 ºC) and the T-joint 82% (150 ºC). It has to be highlighted that the cure kinetics model used in this study does not take into account for degradation of the resin. Therefore the overshoot temperatures reported are not to be intended as absolute values but as an indication of the occurrence of an intense exotherm. The new methodology developed here for the multi-objective optimisation of the cure problem proved to be effective and to lead to significant improvements in terms of temperature overshoot and process time reduction.

In multi-objective optimisation there is not only one optimal solution but several. All of the optimal solutions are represented by the Pareto front. Among these solutions the designer has to choose the best candidate for the specific case so that different fields, different companies will probably end up choosing different individuals according to their preferences in terms of process cost and quality requirements. A natural engineering choice would be to select a process design

close to the corner of the Pareto front, in order to combine significant benefits in both objectives. Following this approach there can be significant simultaneous benefits in terms of process duration and temperature overshoot. For the flat panel case selecting a design close to the corner of the Pareto L for the 3 mm and 24 mm thickness results in a 60% and 30% reduction in process time compared to the standard profile respectively (Figure 5-4 a) and b)). For the 48 mm thick flat panel a 50% temperature overshoot reduction and a 20% process time reduction can be achieved (Figure 5-4 c)). Further benefits in temperature reduction can be achieved with a slight increase in process time in comparison to the corner point, whilst still outperforming the standard cure profile. For example, accepting a worsening in process time by 12% the temperature overshoot can be reduced up to 75%.

In the 3 mm thick flat panel (Figure 5-4 a)) the process designs at the end of the optimisation corresponds to a first dwell temperature around 175 ºC with the completion of the cure occurring before reaching the second dwell. In the 24 mm thick panel (Figure 5-4 b)) the horizontal part of the trade-off surface (high cure duration sensitivity) is dominated by a first dwell temperature in the 145-150 ºC range, high ramp rate (around 3 ºC/min), second dwell temperature higher than 202 ºC and first dwell duration greater than 5000 s. The vertical region (high overshoot temperature sensitivity) is characterised by a higher first dwell temperature between 165-175 ºC, higher ramp rate (around 4 ºC/min), second dwell temperature of about 209 ºC and first dwell duration lower than 5000 s. In the 48 mm flat panel (Figure 5-4 c)) the second dwell temperature is always around 209 ºC, the ramp rate higher than 3.5 ºC/min for all the individuals, the dwell duration for points belonging to the horizontal zone are higher than 7000 s and the temperature for the first dwell is between 145-155 ºC. The individuals belonging to the vertical region are characterised by a higher first dwell temperature (160-175 ºC) and a lower first dwell duration (lower than 4000 s).

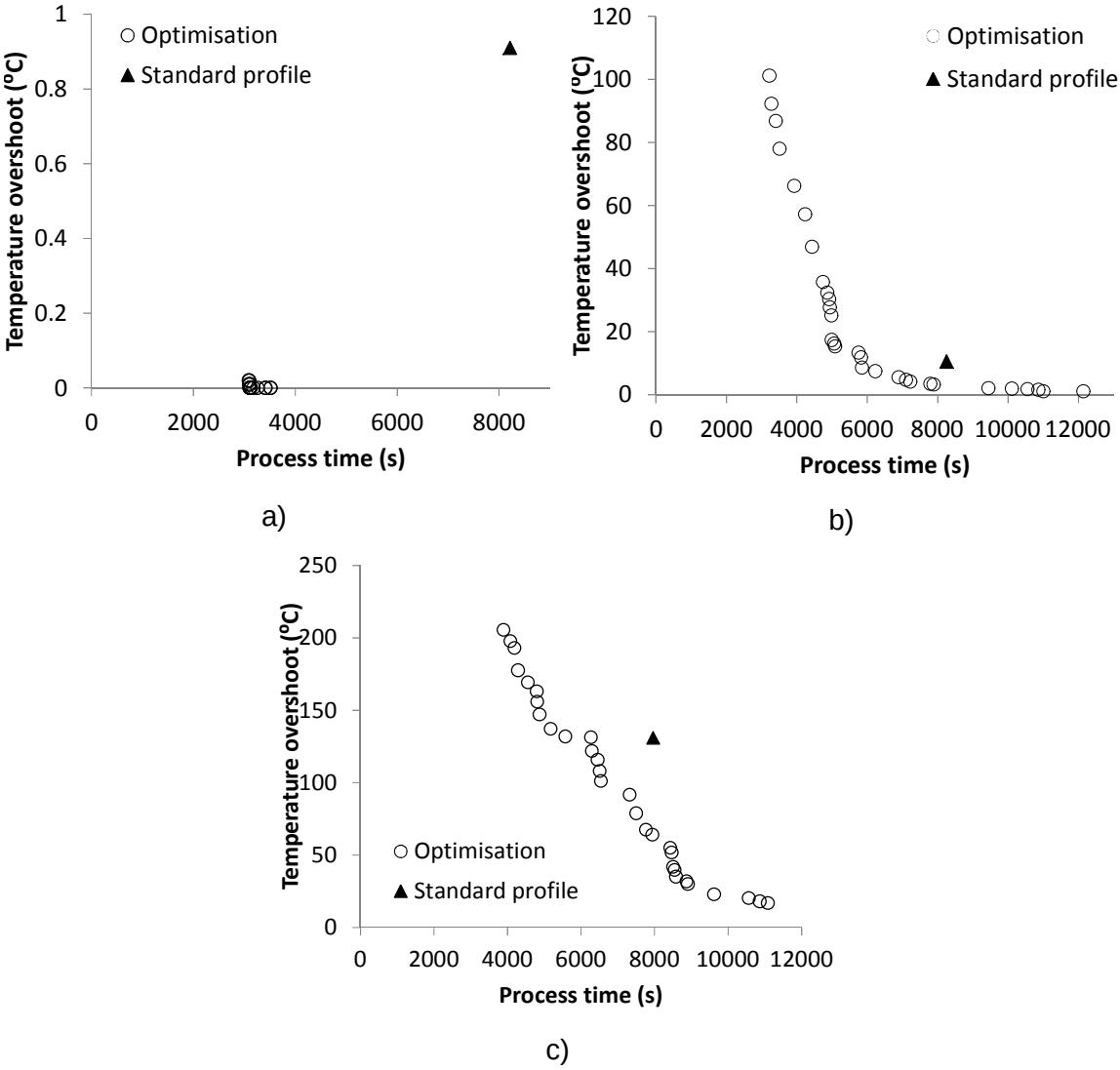

Figure 5-4 Flat panel results: (a) 3 mm; (b) 24 mm; (c) 48 mm

In the L-shape 3 mm and 24 mm thick cases models (Figure 5-5 a) and b)) significant process time reductions are possible up to 60% and 30% respectively without penalising temperature overshoot. In the 48 mm case a simultaneous reduction of about 80% in overshoot temperature and 13% in process time can be achieved. In the L-shape 3 mm model (Figure 5-5 a)) the individuals in the Pareto are characterised by an isothermal profile at a temperature between 170-175 ºC as the part reaches the target degree of cure before the second ramp. In the 24 mm L-shape component (Figure 5-5 b)) the solutions lying on the vertical part correspond to a ramp rate close to 4 ºC/min, first dwell temperature around 175 ºC, second dwell temperature around 205 ºC

and first dwell duration lower than 4000 s. Solutions in the horizontal part have lower ramp rate (lower than 3 ºC/min), first dwell temperature of about 155 ºC, first dwell duration higher than 4000 s and second dwell temperature of 210 ºC. In the 48 mm thick L-shape case (Figure 5-5 c)) the first dwell temperature is around 175 ºC and the second dwell temperature higher than 205 ºC for all optimal solutions whilst the ramp rate governs whether a solution is in the high process duration or temperature overshoot sensitivity region. Solutions in the horizontal region correspond to ramp rates lower than 2 ºC/min, whereas the vertical region of the front is dominated by process design involving ramp rates greater than this value.

In the case of the 3 mm thick T-joint (Figure 5-6 a)) a 50% process duration reduction and a 40% temperature overshoot reduction can be achieved. For a thickness of 24 mm (Figure 5-6 b)) the process time reduction is similar (52%) but led to lower improvements in temperature overshoot (11%). In the 48 mm case (Figure 5-6 c)) the improvement in process time is about 30%, whilst the temperature overshoot can be reduced about 75%. The solutions for the 3 mm case (Figure 5-6 a)) correspond to a short first dwell duration (lower than 2000 s), high second dwell temperature (about 209 ºC) and first dwell temperature in the range of 165-175 ºC for all individuals, whilst is the ramp rate to differentiates the two sections of the trade-off surface, being lower than 2 ºC/min for the horizontal part and between 3 and 4 ºC/min for the vertical part. For the 24 mm T-joint (Figure 5-6 b)) the horizontal part contains only three solutions with a ramp rate of around 1 ºC/min with the point ending in a process time around 12000 s characterised by conservative parameters, long first dwell duration (5000 s) and low first and second dwell temperature, 145 ºC and 193 ºC respectively. The other two individuals are characterised by a higher first and second dwell temperature (165 ºC and 205 ºC) and shorter first dwell duration (lower than 3000 s). Individuals belonging to the vertical region have high ramp rate (higher than 3.5 ºC/min) and higher first and second dwell temperature (around 170 ºC and 208 ºC respectively). In the 48 mm T-joint case (Figure 5-6

c)) the three individuals in the horizontal part have ramp rate of around 2 ºC/min except for the furthest individuals which have a ramp rate of around 1 ºC/min and a longer first dwell duration (about 5000 s). The other two individuals have instead a first dwell duration of about 3000 s. The first dwell temperature is lower than 165 ºC and the second dwell temperature in the range of 180-190 ºC. The individuals in the vertical zone have very high ramp rate (higher than 3.5 ºC/min), first dwell duration shorter than 3000 s, first dwell temperature higher than 165 ºC and second dwell temperature between 205 ºC and 210 ºC.

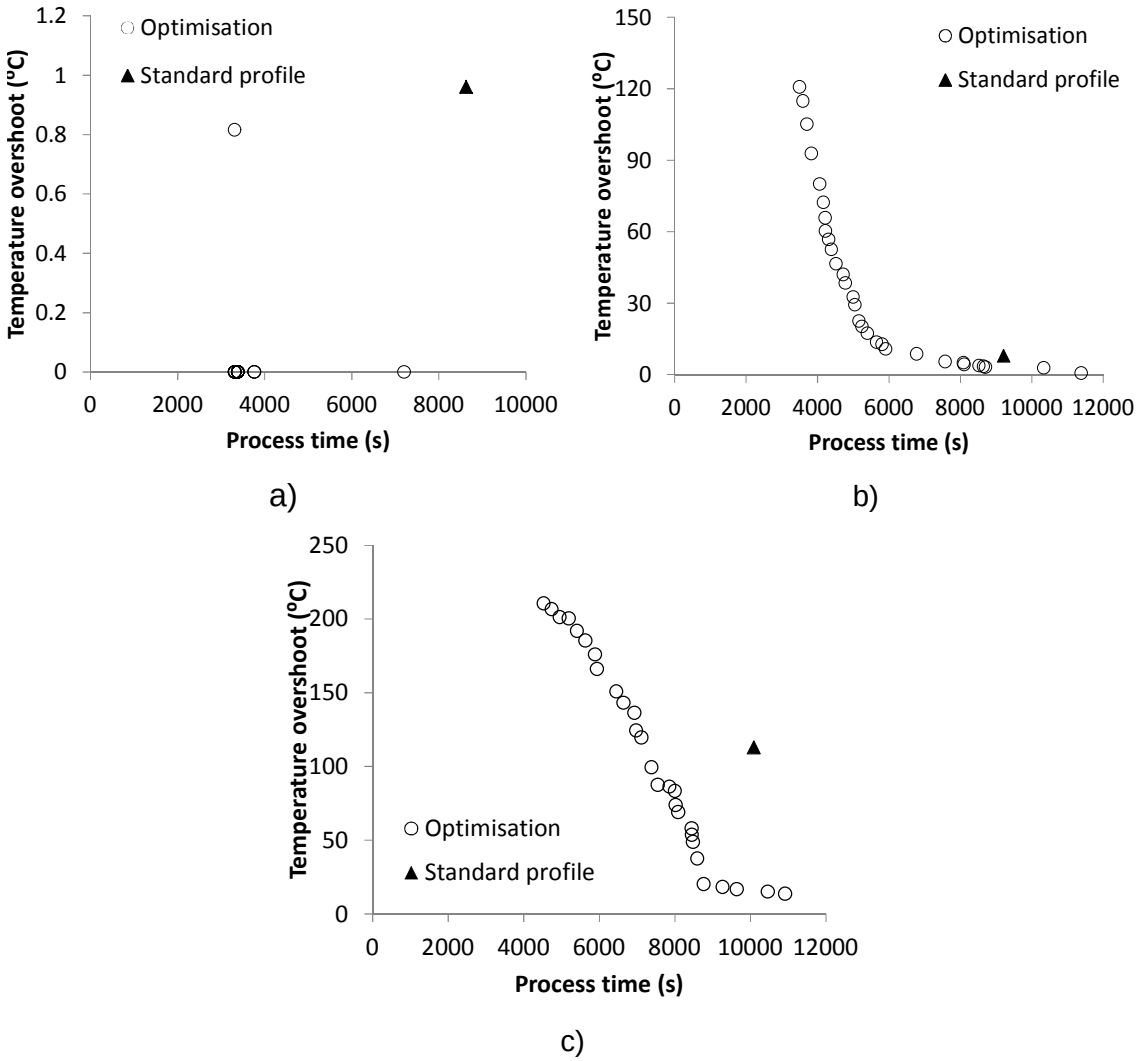

Figure 5-5 L-shape results: (a) 3 mm; (b) 24 mm; (c) 48 mm

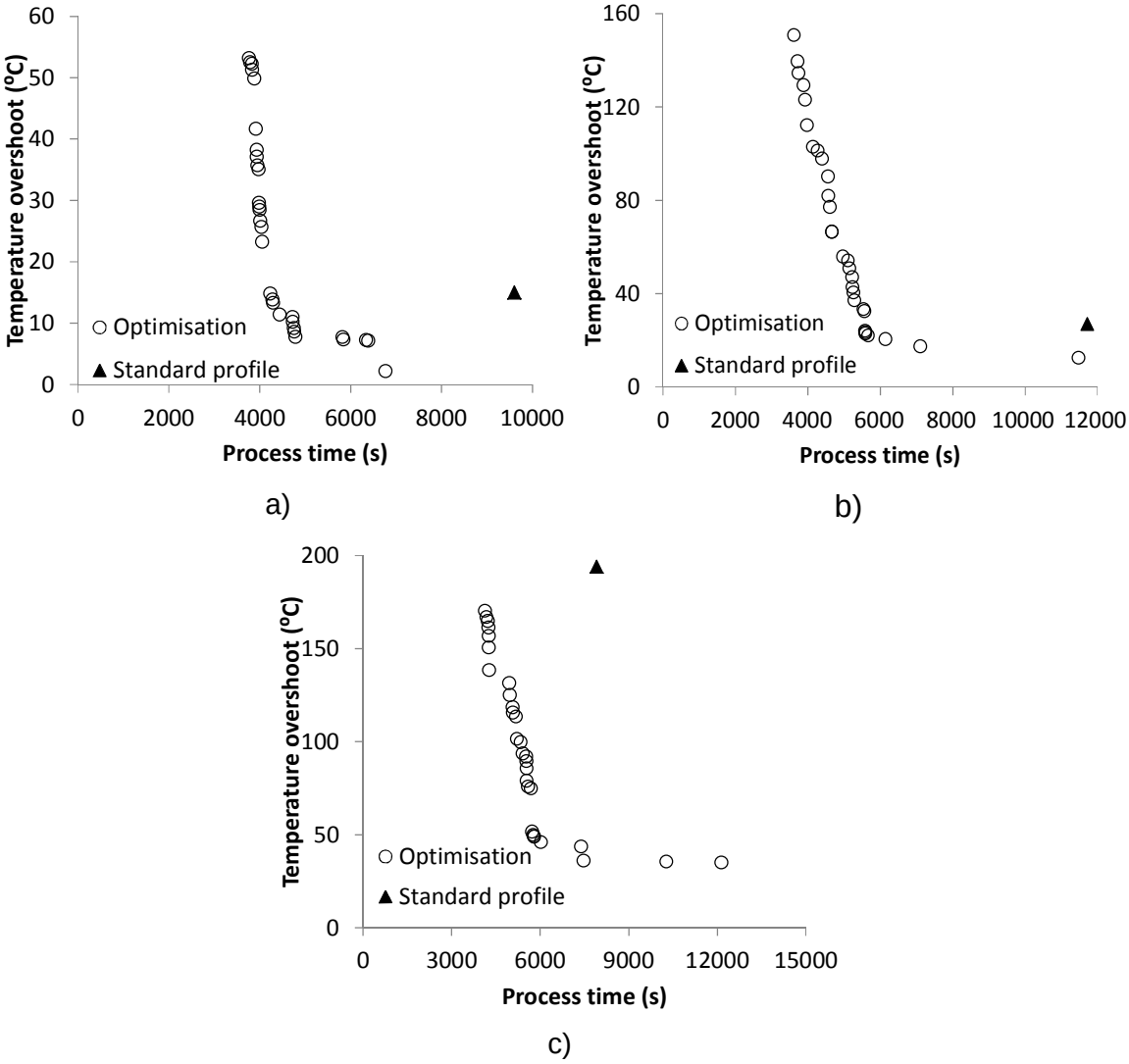

Figure 5-6 T-joint results: (a) 3 mm; (b) 24 mm; (c) 48 mm

The sensitivity of the Pareto front on thicknesses is depicted in Figure 5-7. It is possible to notice the influence of thickness on process time and overshoot temperature. In specific increasing thickness make shift the Pareto front towards higher process time and higher overshoot temperature. This is due to less effective dissipation of the heat generated by the chemical reaction as the thickness increases. The convection becomes less and less effective for thicker parts in the central part of the thickness since the distance is increased, resulting in higher temperature and higher likelihood of higher temperature overshoot. Increasing the thickness increases the diversification of individuals in the Pareto front. The solution for the 3 mm flat panel and the L-shape model (Figure 5-7 a) and b)) results in several overlapping individuals and no

distribution in the temperature overshoot direction. For these two cases the problem is in reality a single-objective optimisation problem. As the thickness increases new possible trade-off individuals arise and fill the Pareto front generating a variety of possible optimal design points. In the 3 mm T-joint model (Figure 5-7 c)) a less effective dissipation of heat characterised by a ratio between heated surface and cooled surface larger than 2. This results in a more challenging scenario compared to the other two 3 mm models which produces a larger variety of possible optimal compromise solutions.

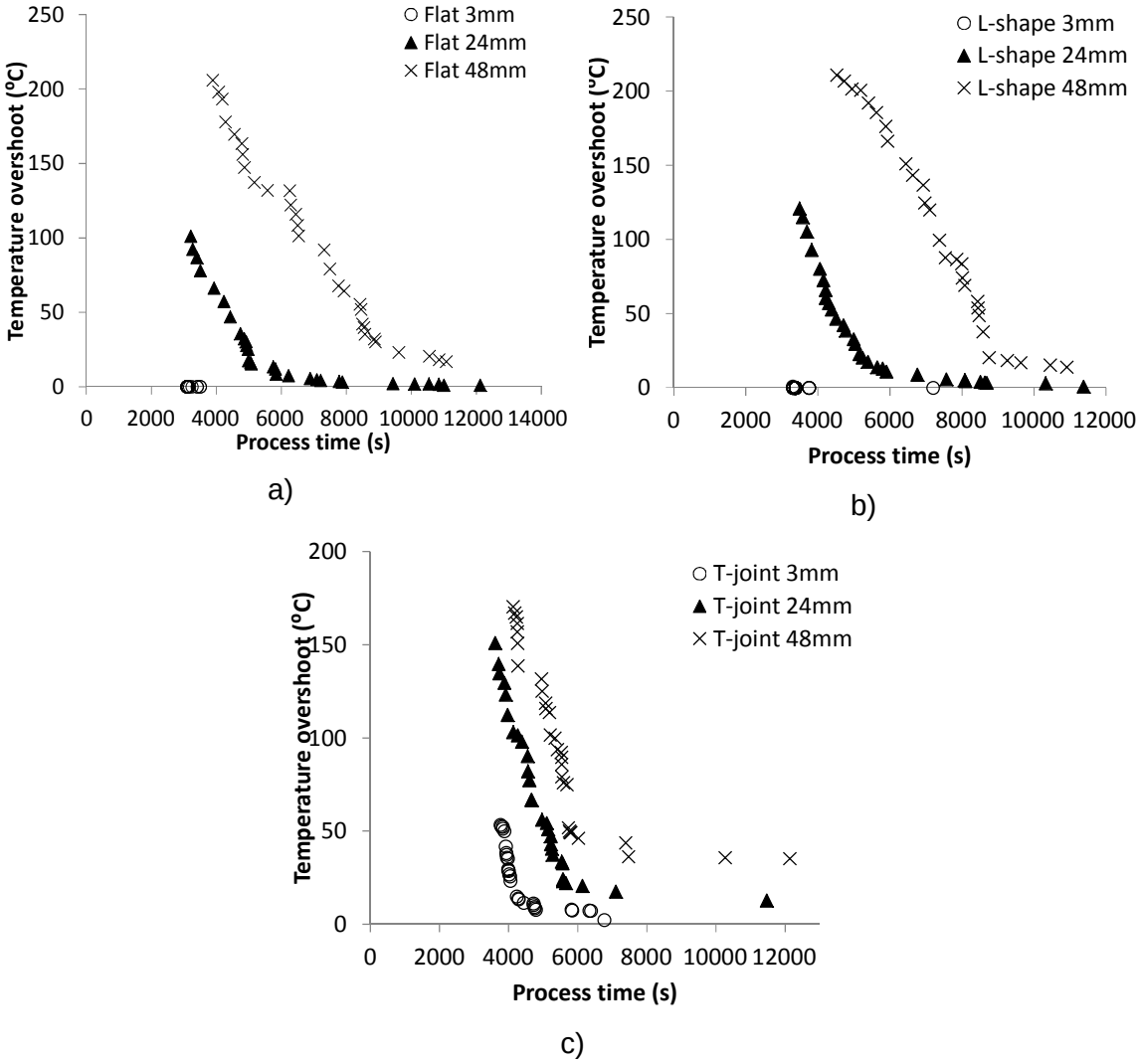

Figure 5-7 Sensitivity of the trade-off surface on thicknesses: (a) Flat panel; (b) L-shape; (c) T-joint

5.5 Detailed investigation of the L-shape 24 mm model

The outcome of the optimisation in terms of objectives and their trade-off is sufficient for uncovering ways to improve the efficiency and quality of the process through appropriate selection of its parameters. However, the results of optimisation can be explored further in order to verify their quality, learn more about what is driving the process and eventually governs the trade-off of interest and analyse further the characteristic of the design problem. The case of the 24 mm thick L-shape was selected as it provides a good compromise between negligible and extreme exothermic effects, its geometry is representative of a wider variety of composite components in comparison to the rest of the cases considered and the solution of the corresponding optimisation problem is sufficiently rich.

The evolution of temperature distribution, degree of cure and rate of reaction for five nodes across the thickness is illustrated in Figure 5-8. The peculiar development through the thickness, after that exotherm is occurred, can be explained looking at the evolution of degree of cure, temperature profile and reaction rate for nodes at different thickness locations. In Figure 5-8 a) point A lies on the fixed temperature boundary condition therefore it follows the cure profile closely. The convection (applied in point E) has a great influence on this point and that can be noticed by the increasing drop in temperature right after the initial point. Therefore, before the exotherm occurs the thermal profile through the thickness has its highest temperature at point A (fixed temperature boundary condition) and its lowest temperature at point E (air convection boundary condition). This results in different reaction rate evolution (Figure 5-8 b)). Therefore, the reaction at points C, D and E has not progressed when the second ramp is reached (7000 s). At about 8000 s the exotherm occurs at points C, D and E (Figure 5-8 b)). Point E shows the highest peak in reaction rate but its proximity to the convection boundary makes its temperature lower. Point B has a degree of cure lower than point A, because it experiences a lower thermal profile due to dissipation and it is not close enough to the location where the exotherm happens to be affected by it (Figure 5-8 c)). Although points C and D experience a lower thermal history compared to the boundary

they are close to the exothermic phenomenon which boost their temperature resulting in a higher degree of cure than point B. Point E is influenced by the exotherm effect but being in contact with the air convection boundary make its temperature the lowest in the part which results in the lowest degree of cure.

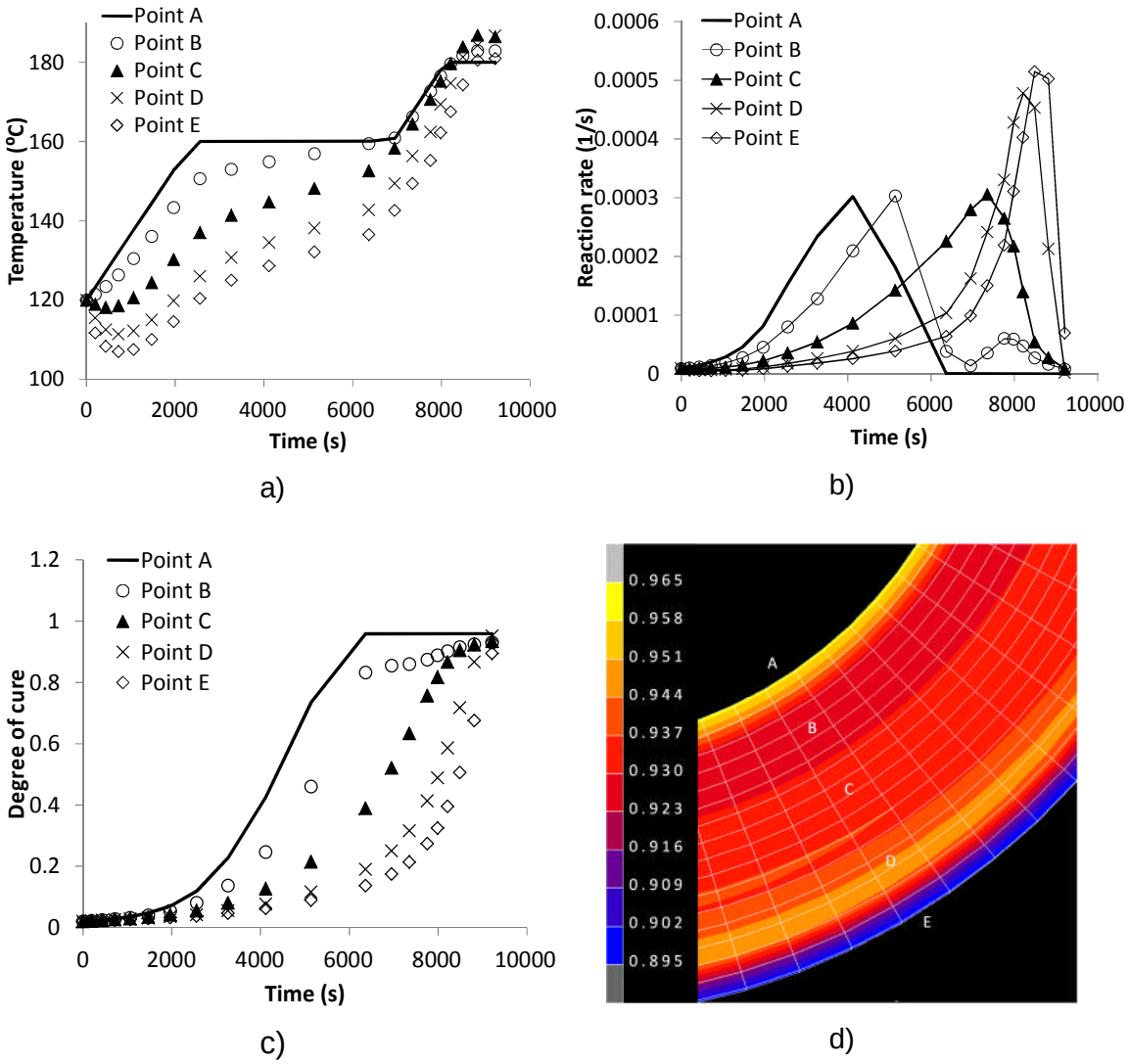

Figure 5-8 Thickness behaviour investigation a)Temperature profile b) Rate of reaction c) Degree of cure (d) Degree of cure contour map

As reported in Table 5-4 the standard solution for the L-shape 24 mm model results in 9211 s process time and 8 ºC of temperature overshoot. To investigate how the optimiser copes with such individual it is reasonable to compare this solution with individuals in the Pareto front next to it. Three sample

individuals are taken and reported in Table 5-5 together with the standard solution. The optimiser deals with the standard solution by decreasing the first dwell temperature by 5 ºC and by increasing the first dwell duration. This modification leads to a more uniform evolution of temperature across the thickness and also tends to result in an almost complete reaction before the beginning of the second ramp. In this way the optimiser can increase the ramp rate without the occurrence of an exotherm.

Table 5-5 Parameters comparison between standard solution and samples individuals

Solution	T_1 (^{0}C)	T_2 (^{0}C)	Dwell duration (s)	Ramp (^{0}C/min)	Process time (s)	Temperature overshoot (^{0}C)
Standard	160	180	4500	1	9211	8
Individual 1	155	209	6194	3.4	8515	3.9
Individual 2	155	209	6264	3.4	8695	3.2
Individual 3	155	205	6194	3.1	8640	3.5

An exhaustive search to verify and evaluate the efficiency of the GA solution has been carried out. Results are presented in Figure 5-9. The exhaustive search was set to perform 10000 evaluations. The four parameters involved in the optimisation have been divided in ten increments giving a total of 10^4 permutations. The results of the exhaustive search are compared with the final front identified by the GA for the case of 24 mm thick L-shape. It can be observed that the GA results a better final front in 2500 evaluations. The processor used had a speed of 2.93 GHz able to compute 2500 evaluation in 2.5 days and 10000 evaluations in 10 days. It should be noted that the increments used in the exhaustive search are relatively large. The discretisation chosen has been dictated by computational time restrictions and therefore the increment selected is not fine enough to represent detailed features of the optimisation landscape. A finer exhaustive search able to cover it would have taken about 10^7 evaluations which using the same processor would have taken

10000 days assuming linear scaling. Bearing this in mind the GA performance can be considered higher than the 25% showed here compared to the exhaustive search.

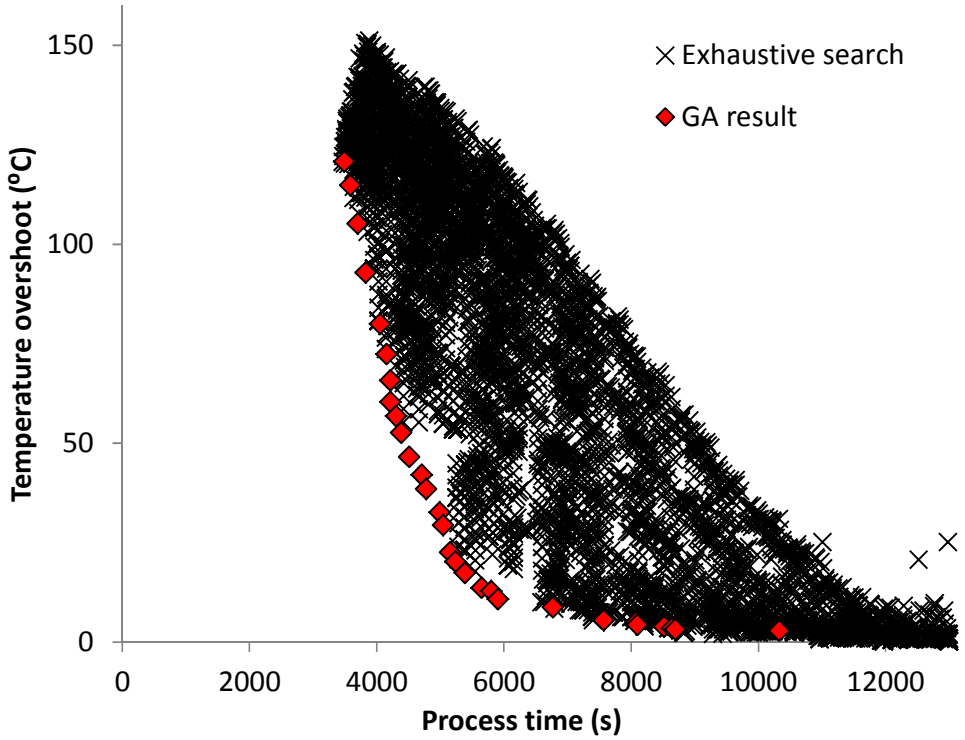

Figure 5-9 Exhaustive search result compared with GA

The exhaustive search allowed an investigation of the landscape of the optimisation surface of the cure process pointing out the necessity to address the problem via GAs since the problem revealed the presence of local minima and it would be likely to be trapped in local minima if a gradient based technique was adopted. Figure 5-10 a) and b) depicts the temperature overshoot and process time behaviour with respect to ramp rate and first dwell duration variations. The label stating 'not real solutions' indicates those solutions that have been penalised and discarded; for these solutions the process time was considered unacceptably high. It can be seen that temperature overshoot increases when the duration of the first dwell decreases (Figure 5-10 a)). Process time increases as duration of first dwell increases and it decreases as the ramp rate increases. Some smooth local minima appear at about 8000 s of first dwell duration (Figure 5-10 b)). Figure 5-11 a) and b) illustrates the temperature overshoot and process time as a function of the first dwell duration

and the first dwell temperature. The temperature overshoot increases non-linearly as the temperature of the first dwell increases (Figure 5-11 a)). The process time decreases as the temperature of the first dwell increases (Figure 5-11 b)). Figure 5-12 a) and b) reports the temperature overshoot and process time dependence on first dwell duration and temperature of second dwell. The temperature of the second dwell affects weakly both the process time and temperature overshoot (Figure 5-12 a) and b)). Figure 5-13 a) and b) shows the temperature overshoot and process time behaviour as ramp rate and temperature of first dwell vary. Both temperature overshoot and process time present a very complicated landscape rich in local maxima and minima. A gradient based technique would probably fail to reach a global minimum with such landscape. Figure 5-14 a) and b) shows the temperature overshoot and process time behaviour as a function of the temperatures of first and second dwell. Figure 5-14 a) illustrates how complex the interaction between the two dwell temperatures is unveiling new local minima in the landscape. Figure 5-15 a) and b) illustrates the temperature overshoot and process time behaviour with respect to ramp rate and temperature of second dwell. Figure 5-15 a) shows new local minima arising from variation of ramp rates and second dwell temperature. All the figures depicting the landscape highlighted the competitive nature of the two objectives.

The landscape analysis pointed out that overshoot temperature has very high dependence on ramp rate and first dwell temperature. Process time presents local minima and a slight dependence on the same process parameters, although the local minima are less pronounced, therefore a stability and robustness analysis is recommended.

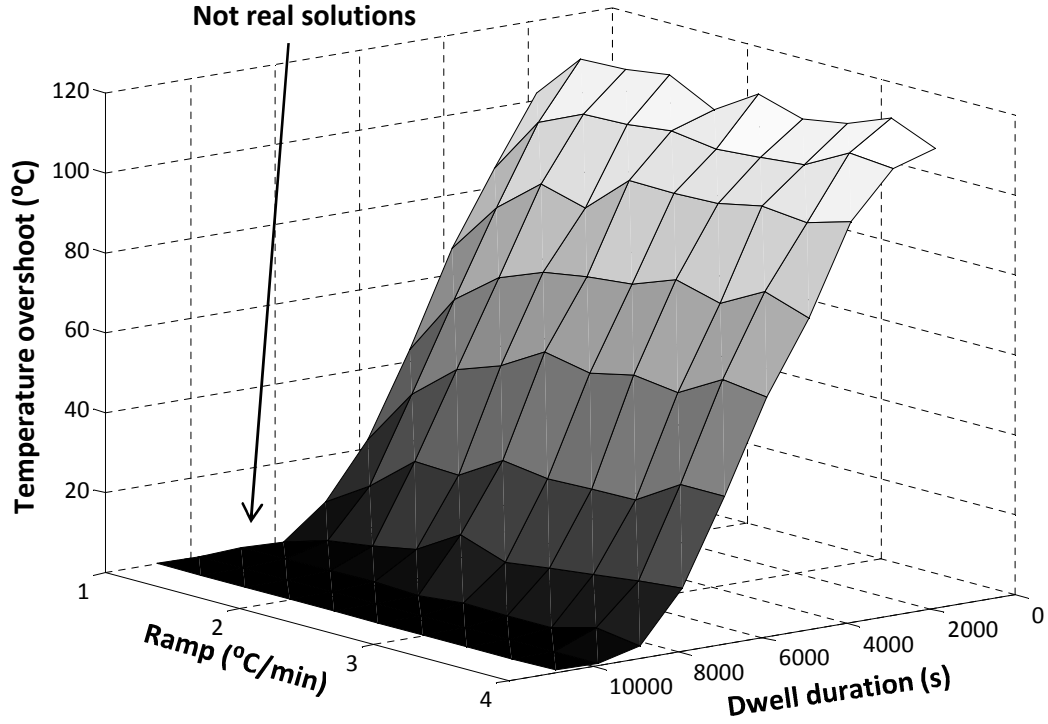

a)

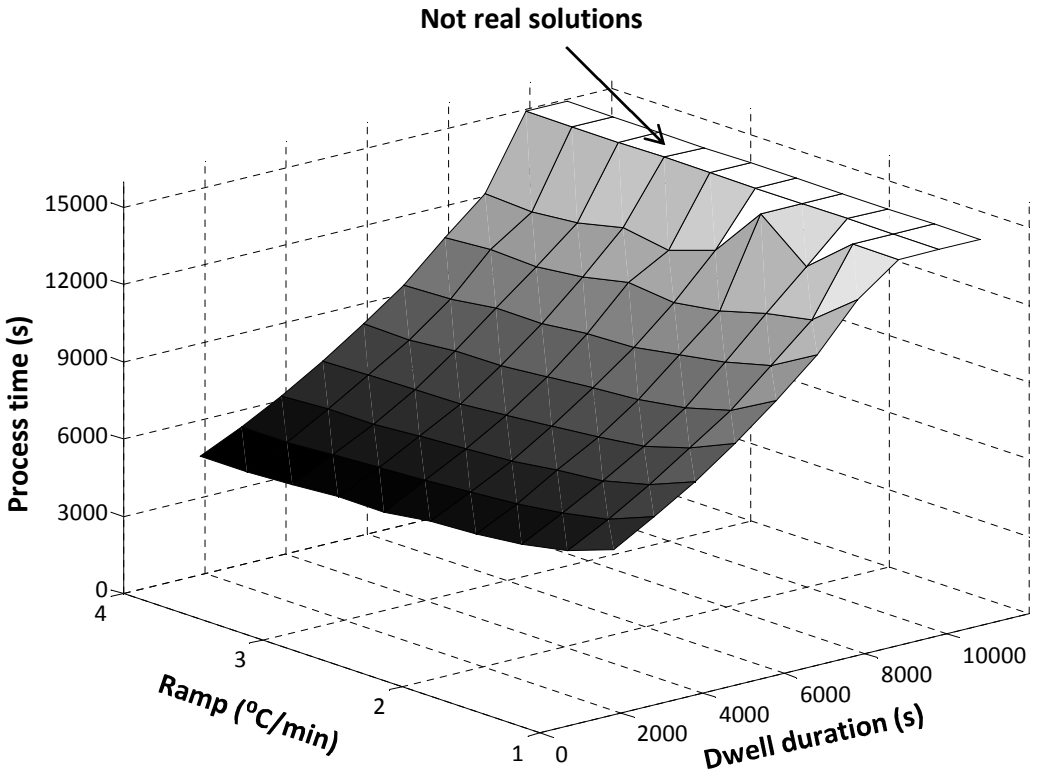

b)

Figure 5-10 Landscape of the cure problem: Ramp rate vs Dwell duration a) Temperature overshoot b) Process time

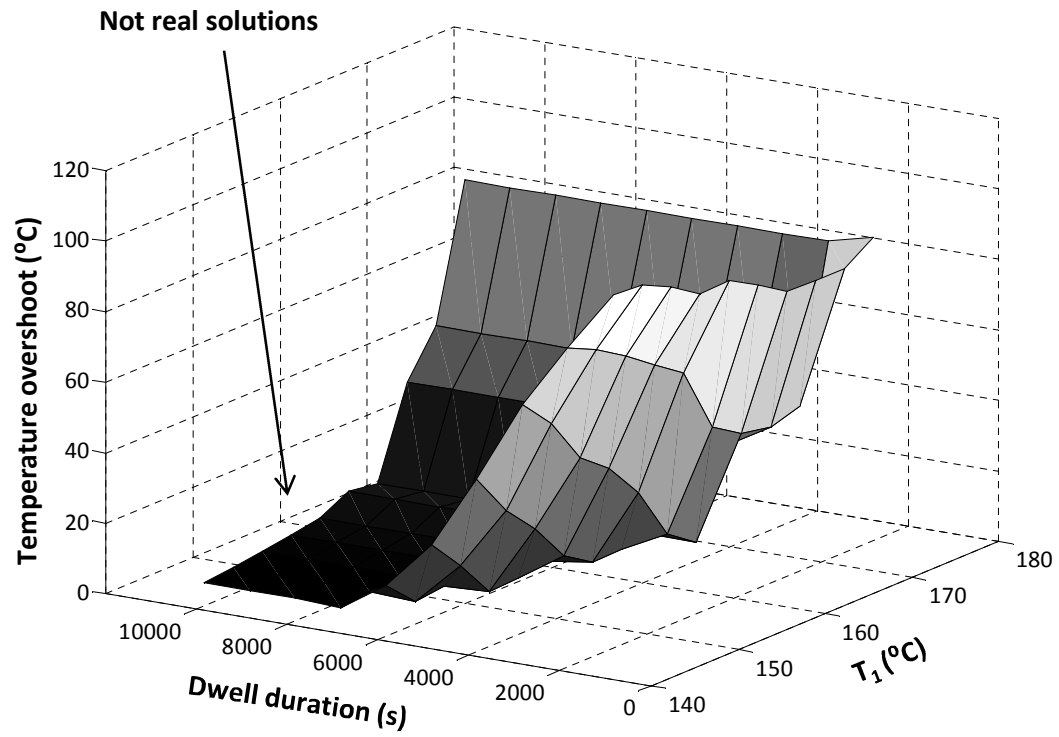

a)

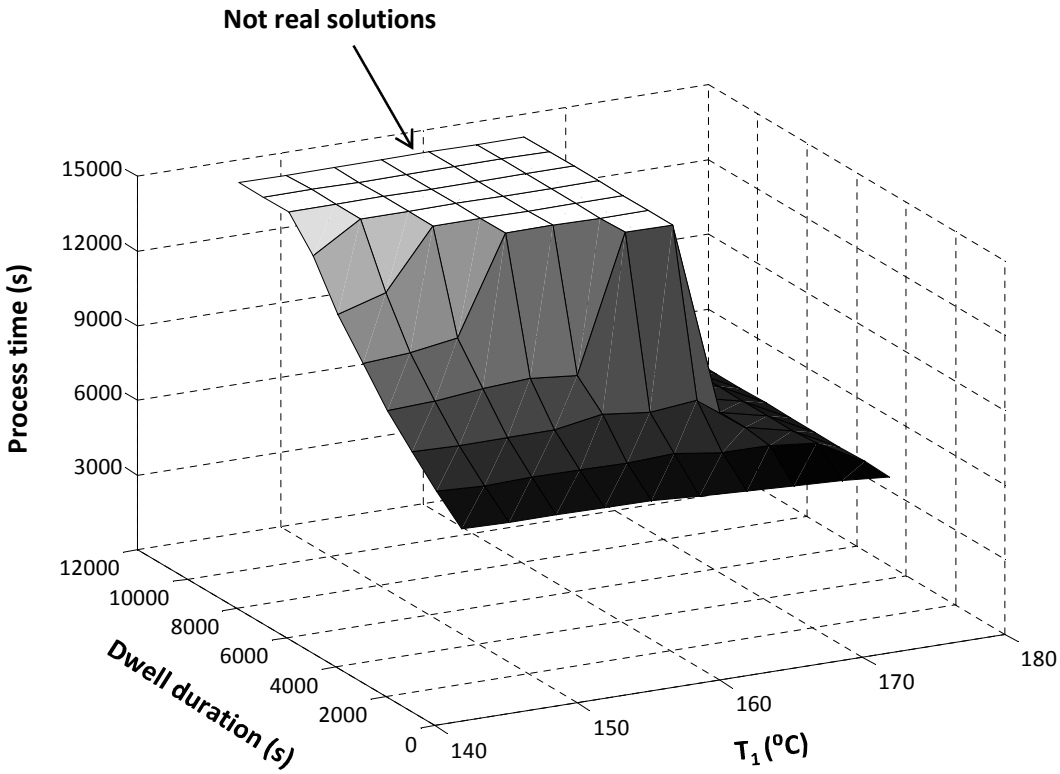

b)

Figure 5-11 Landscape of the cure problem: Dwell duration vs Temperature first dwell a) Temperature overshoot b) Process time

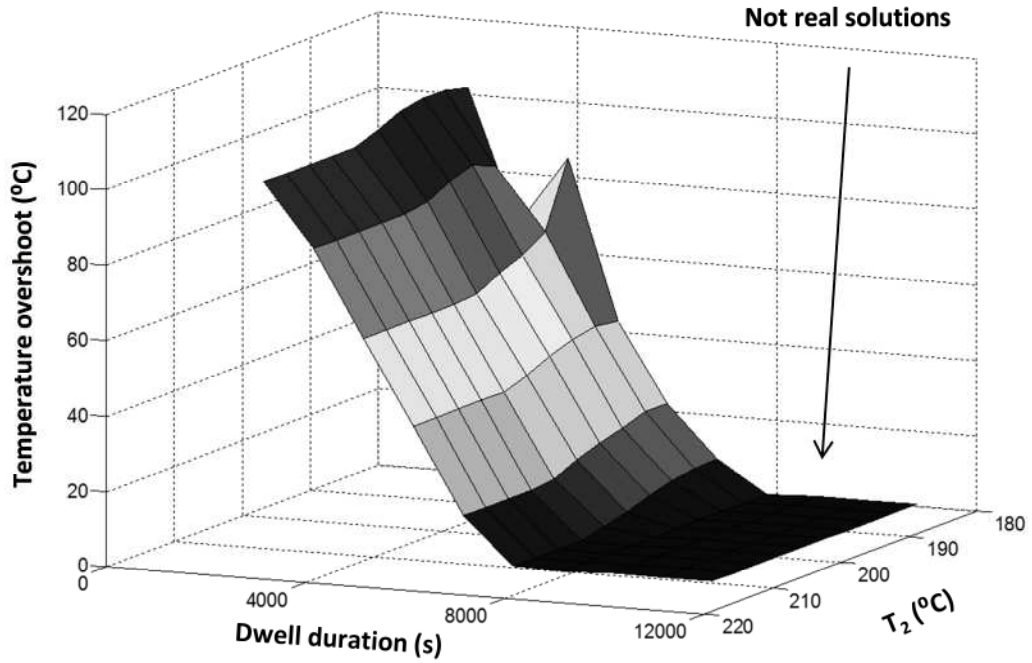

a)

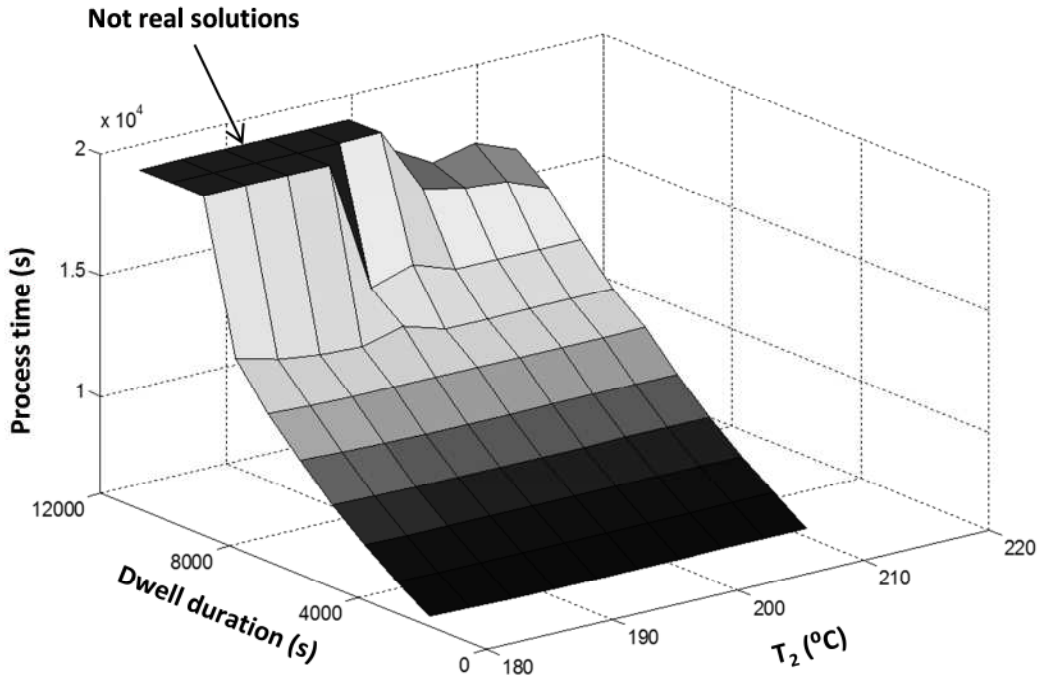

b)

Figure 5-12 Landscape of the cure problem: Dwell duration vs Temperature second dwell a) Temperature overshoot b) Process time

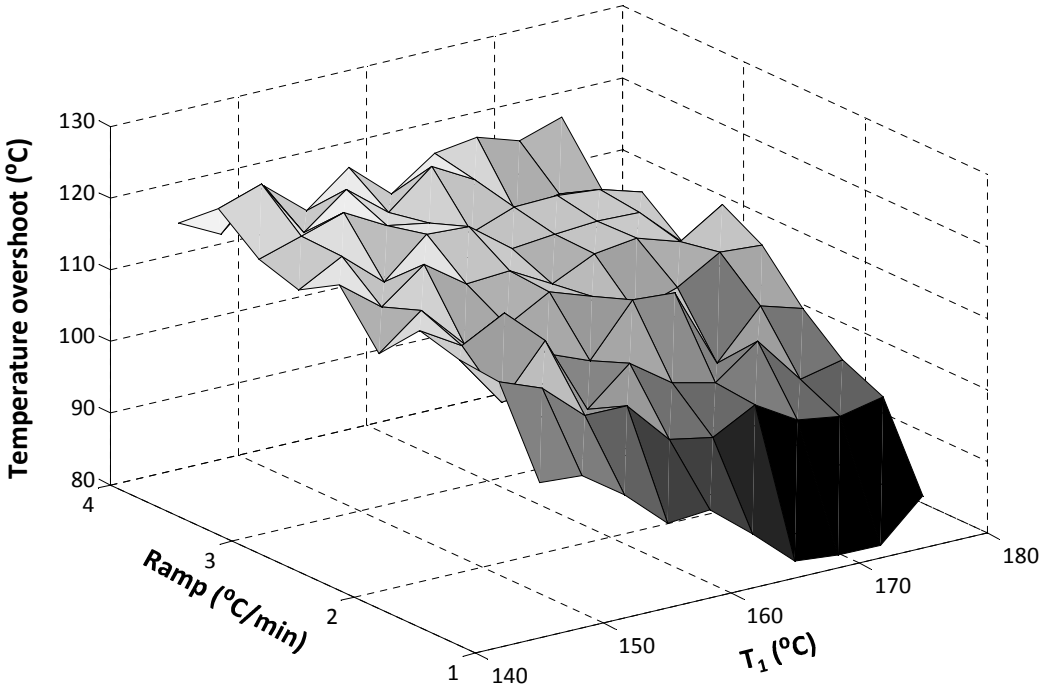

a)

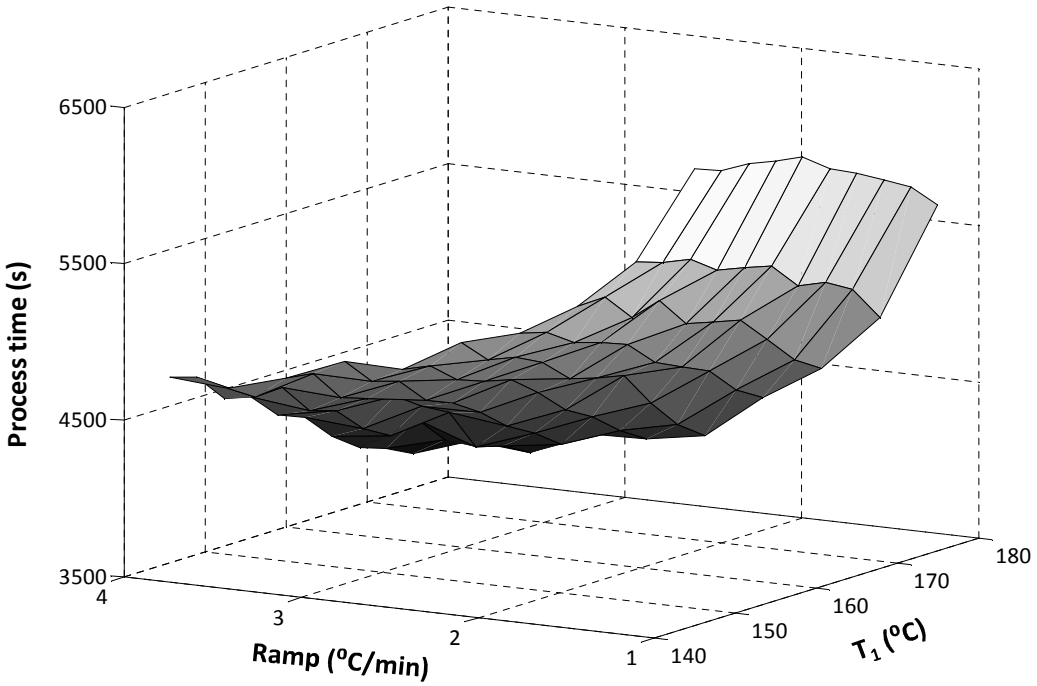

b)

Figure 5-13 Landscape of the cure problem: Ramp rate vs Temperature first dwell a) Temperature overshoot b) Process time

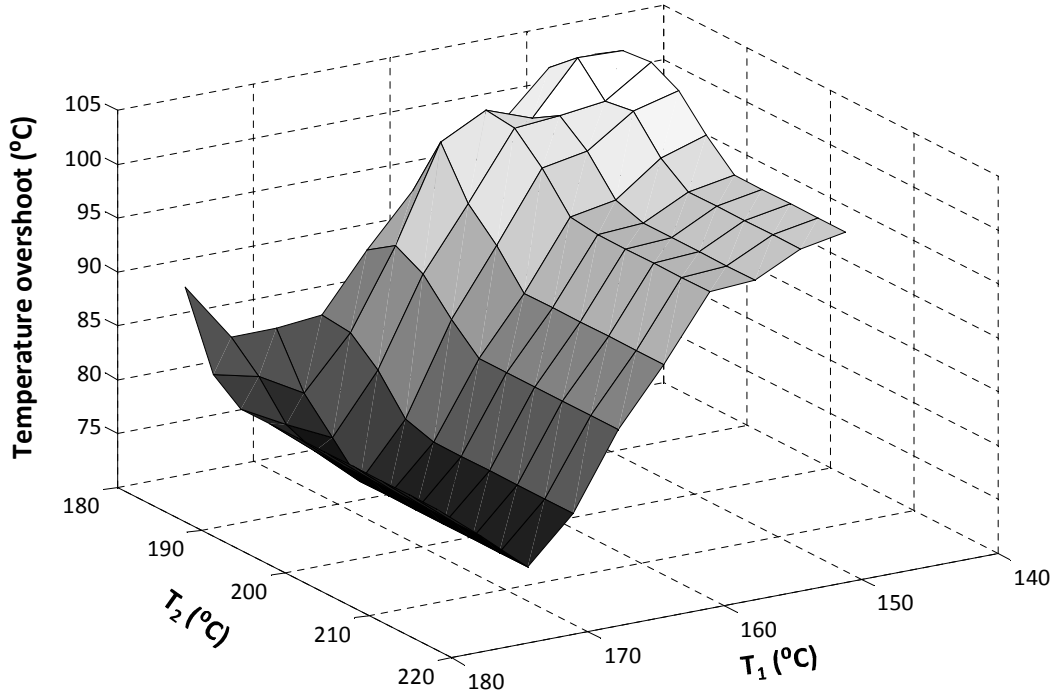

a)

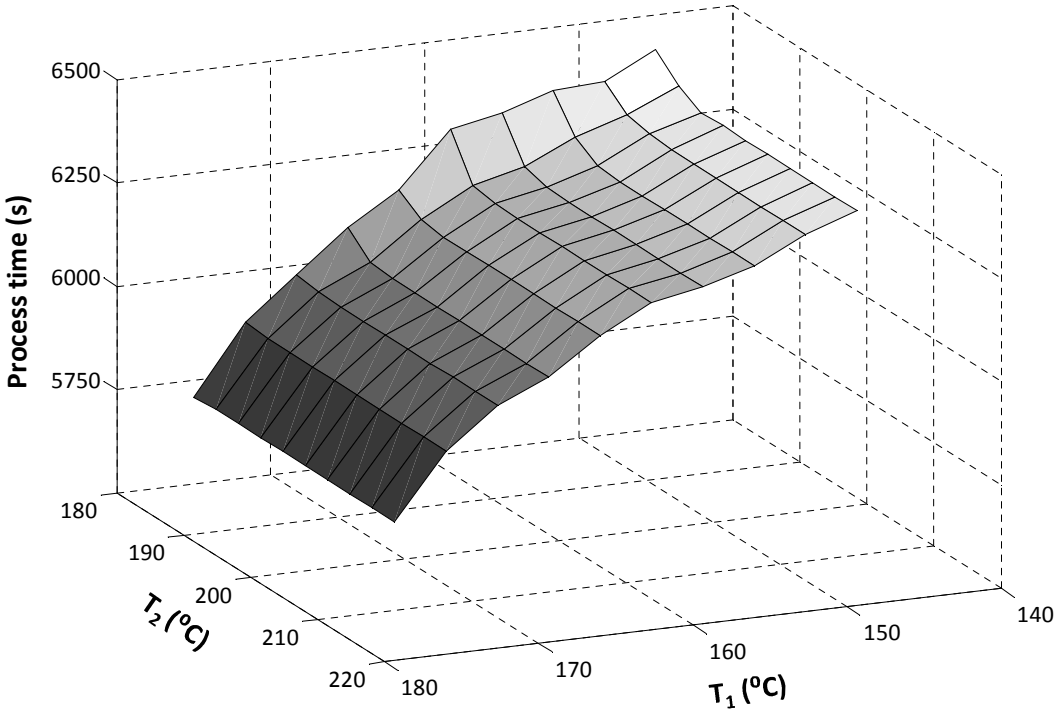

b)

Figure 5-14 Landscape of the cure problem: Temperature first dwell vs Temperature second dwell a) Temperature overshoot b) Process time

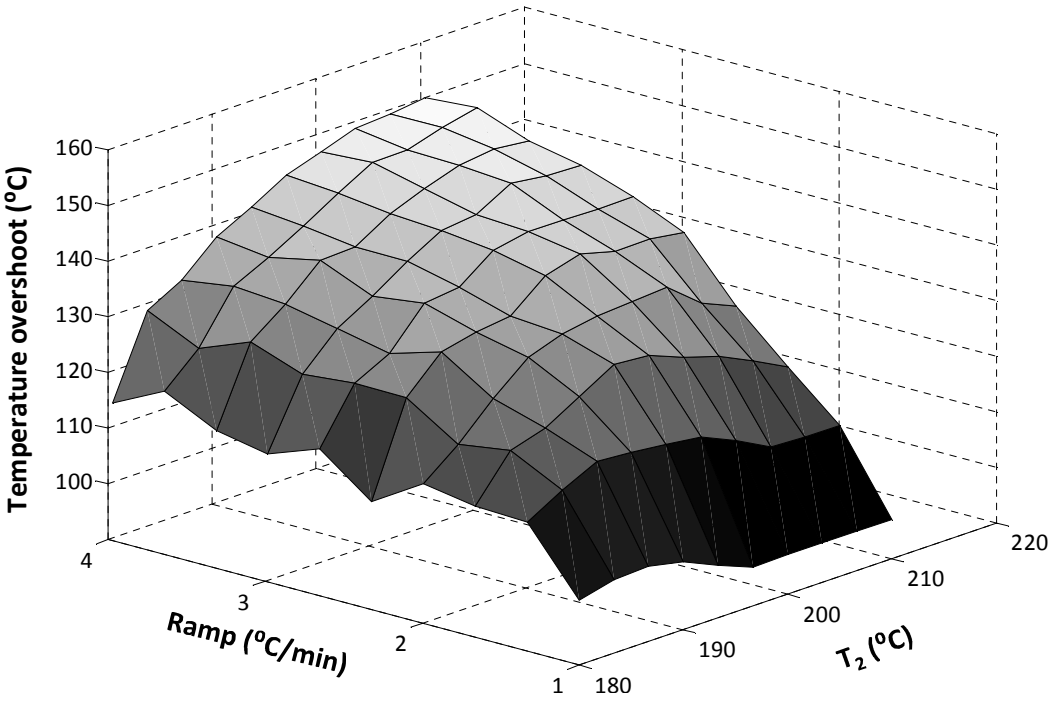

a)

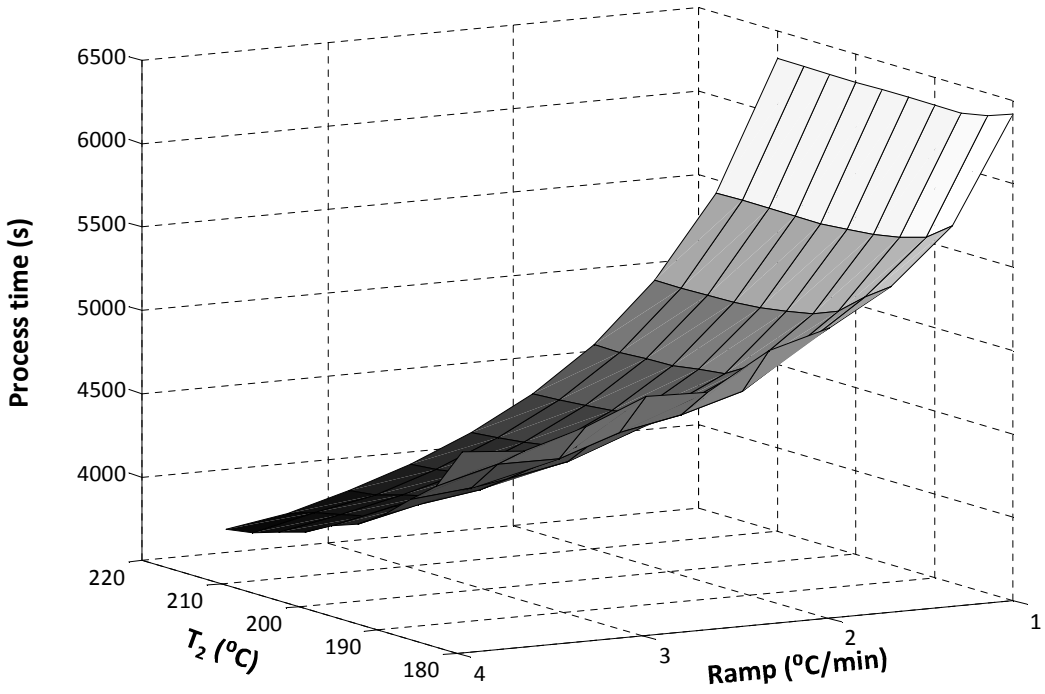

b)

Figure 5-15 Landscape of the cure problem: Ramp rate vs Temperature second dwell a) Temperature overshoot b) Process time

A stability analysis of three solutions belonging to the Pareto front has been performed to evaluate the robustness of process designs. The three points selected are representative of three different regions of the Pareto front: the horizontal zone, the vertical zone and the corner zone. The design parameters have been incremented to investigate how slight differences in parameter setting can affect the value of the objectives. The results are illustrated in Tables 5-7 whilst Figure 5-16 shows the position of the selected point in the Pareto set. In Table 5-6 the process parameters of the chosen points are reported. The values are very similar with differences in ramp rate determining significant change in temperature overshoot and process time. The process is sensitive to ramp rate and first dwell temperature presenting in all the three regions the larger variations in the objectives. The horizontal part has a total variation of about 3 ºC in temperature overshoot and 430 s in process time. In the corner zone 500 s and 18 ºC variations occur, for changes in ramp rate and 700 s and 30 ºC for changes in first dwell temperature. In the vertical zone both ramp rate and first dwell temperature result in 100 s variation in process time and 5 ºC and 10 ºC respectively in temperature overshoot. Therefore, the sensitivity tends to decrease moving towards the horizontal bit of the Pareto. This part shows the most robust behaviour with respect to nominal value variations. All three zones have a robust and reliable behaviour with respect to first dwell duration and temperature of second dwell with variations of about 100 s in process time and less than 3 ºC in temperature overshoot. It is also necessary to point out that the horizontal zone is the part in which the standard cure profile result falls, assuring therefore robust results even though not optimised. A more methodical procedure could be set in order to attribute a robustness degree to each zone.

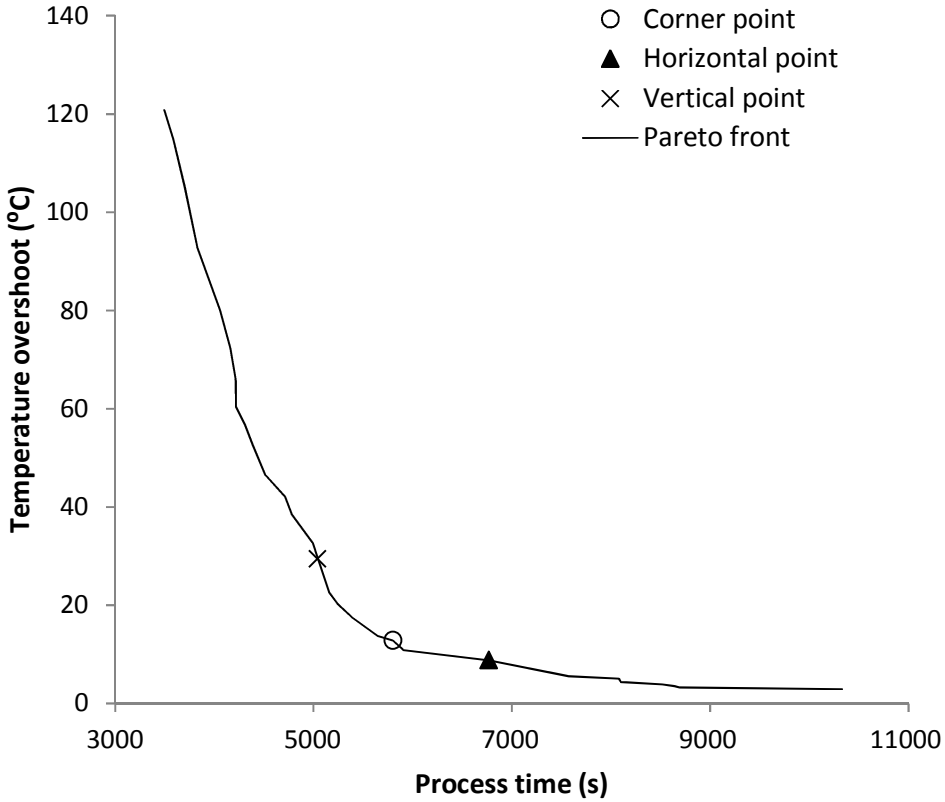

Figure 5-16 Points for stability analysis

Table 5-6 Objectives and related design parameters for chosen points

Points	T_1 (ºC)	T_2 (ºC)	Rate (ºC/min)	Dwell time (s)	Process time (s)	Overshoot (ºC)
Horizontal	164.7	210.1	1.9	3997	6769	8.8
Corner	167.8	209.4	3.5	3926	5801	12.8
Vertical	169.7	209.4	4	3572	5043	29.4

Table 5-7 Stability analysis

Points	Parameters	Swing	ΔProcess time (s)	ΔOvershoot (ºC)
Horizontal	Dwell time (s)	+30 s	-42	1.2
		-30 s	45	-1.2
	Rate (ºC/min)	+0.1 ºC/min	312	-1.5
		-0.1 ºC/min	-121	1.2
	Temp 1 (ºC)	+1 ºC	-42	3.7
		-1 ºC	6	-1
	Temp 2 (ºC)	+1 ºC	0	1
		-1 ºC	1	-0.7
Corner	Dwell time (s)	+30 s	64	-2
		-30 s	-52	1.2
	Rate (ºC/min)	+0.1 ºC/min	-375	17.2
		-0.1 ºC/min	-159	0.4
	Temp 1 (ºC)	+1 ºC	-64	4.2
		-1 ºC	-619	26.2
	Temp 2 (ºC)	+1 ºC	-0.8	0.7
		-1 ºC	1.2	-0.8
Vertical	Dwell time (s)	+30 s	60	-1.4
		-30 s	26	-2.4
	Rate (ºC/min)	+0.1 ºC/min	132	-3.4
		-0.1 ºC/min	12	1.2
	Temp 1 (ºC)	+1 ºC	95	4.6
		-1 ºC	49	-5.4
	Temp 2 (ºC)	+1 ºC	-1	0.6
		-1 ºC	2	-1.4

5.6 Conclusions

An optimisation procedure capable to design an optimal cure profile to minimise process time and temperature overshoot in Vacuum Assisted Resin Transfer Moulding using a GA strategy has been developed and tested. Three geometries, a flat panel, an L-shape and a T-joint, have been chosen to address the problem with three different thicknesses, 3 mm 24 mm and 48 mm, for each geometry. All the optimisations resulted in an L-shape Pareto front suggesting a process design close to the corner direction to minimise both overshoot temperature and process time. From a comparison with standard cure profile results it emerged that significant improvement can be obtained in both objectives applying a set of parameters corresponding to a Pareto front point, especially a corner's point. Significant reduction in process time, up to 60%, can be reached for 3 mm and 24 mm thick components. A reduction in temperature overshoot, up to 80%, can be achieved for ultra-thick components, with subsequent improvement of final product quality. A comparison with a 10,000 evaluation exhaustive search showed the capability of the GA to find a better Pareto front. Analysis of the landscape allowed to identify the presence of many local maxima and minima which justify the GA choice. Stability analysis showed that standard cure profiles lie in the area of higher stability corresponding to the horizontal part of the Pareto front, and that there is a strong sensitivity to ramp rate and first dwell temperature. In contrast the second dwell temperature and first dwell duration do not affect significantly the solution.

6 Multi-objective optimisation of filling stage using genetic algorithm

6.1 Introduction

The filling stage in LCM, such as RTM and VARTM, involves several challenging aspects regarding product quality and cost. These have to be treated simultaneously as both contribute significantly to a successful process. One factor that can define the success of filling is the generation of dry spots. An improper selection of design parameters may lead to the formation of unsaturated regions with obvious detrimental effects to the quality of the part. Therefore, an optimisation of the filling stage can be very useful to solve this issue identifying a set of parameters that can exclude the formation of dry spots. Dry spots are due to two main reasons: a non-optimal arrangement of the gate and vent location and a slow filling stage causing a rise in viscosity level up to a point where the flow is clogged and the resin can no longer reach every region of the part. An optimisation problem can be set up either dealing with gate and vents location or with mould temperature aiming to avoid significant cure progress before the end of the filling whilst speeding up the filling. Additional defects are governed by the different scale of two flows developing in the VARTM process: the flow between fibre tows driven by Darcy's law and the flow within the tows controlled by capillary effects. Mismatch between the speeds of the two flows can lead to the formation of micro voids. Alongside quality challenges cost reasons drive the requirement to keep the filling as fast as possible. The problem considered involves parameters that compete with each other and an optimisation is required in order to highlight hidden trade-off and exploit the full set of possibilities in the process design. Single-objective infusion optimisation has been addressed in the literature using gradient based techniques, GAs and the bound and search method [84; 88; 89; 91; 92; 97]. Multi-objective optimisation of the RTM filling problem has been investigated using GAs [110; 111; 113]. The optimisation of the VARTM process has not been addressed yet in the literature. The present chapter reports a procedure to find optimal non-isothermal filling and gate configuration using the GA

developed in this work to minimise both filling time and degree of cure at the end of the filling stage. The methodology is applied to the filling of a C-composite section.

6.2 Filling optimisation methodology

The GA reported in Chapter 3 has been used as optimiser. The goal of the optimisation is to find the best gate location configuration, temperature profile during the filling of the part and initial resin temperature in order to minimise filling time and degree of cure at the end of the filling stage. A set of feasible gate locations is provided for the optimisation. For every individual in the population the optimiser selects a gate location among the ones provided, initial resin temperature and a temperature profile determined by five parameters: temperature of first and second dwell, duration of first and second dwell and duration of the ramp which can be either a ramp-up or down. The generic shape of the profile is depicted in Figure 6-1. The two objectives taken into account deal with two aspects of the process: minimising filling time which is related with process cost and the minimisation of degree of cure at the end of the filling which is related to the formation of dry spots and hence both to the quality of the final product and the likelihood of process failure.

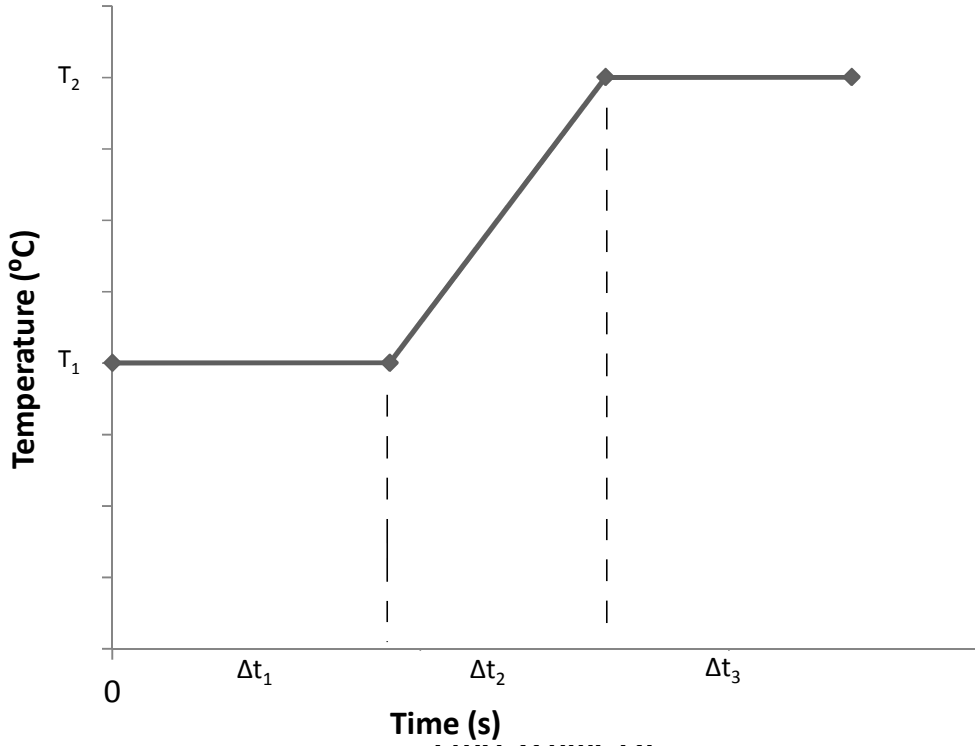

Figure 6-1 Non-isothermal filling profile

An interface able to link the PAM-RTM® solver, used in this study to perform the filling simulation, and the GA algorithm has been developed. The interface communication is illustrated in Figure 6-2. The GA generates a set of parameters (dwell temperature, segment durations and gate locations) which are fed directly to the interface. The interface reads the input file generated by the component under study in PAM-RTM® with nominal values for the design parameters. The location in PAM-RTM® input file where the new process parameters have to be inserted are identified. Consequently a new input file with the new parameters output by the GA replacing the nominal values is generated. A script command is used to run the execution of PAM-RTM® with the brand new input file. The output file of PAM-RTM® is opened and read. The locations where the quantities of interest (objectives) are stored are identified and the objectives read. The outputs are then sent to the GA and a new set of parameters can be output by the GA for a new cycle.

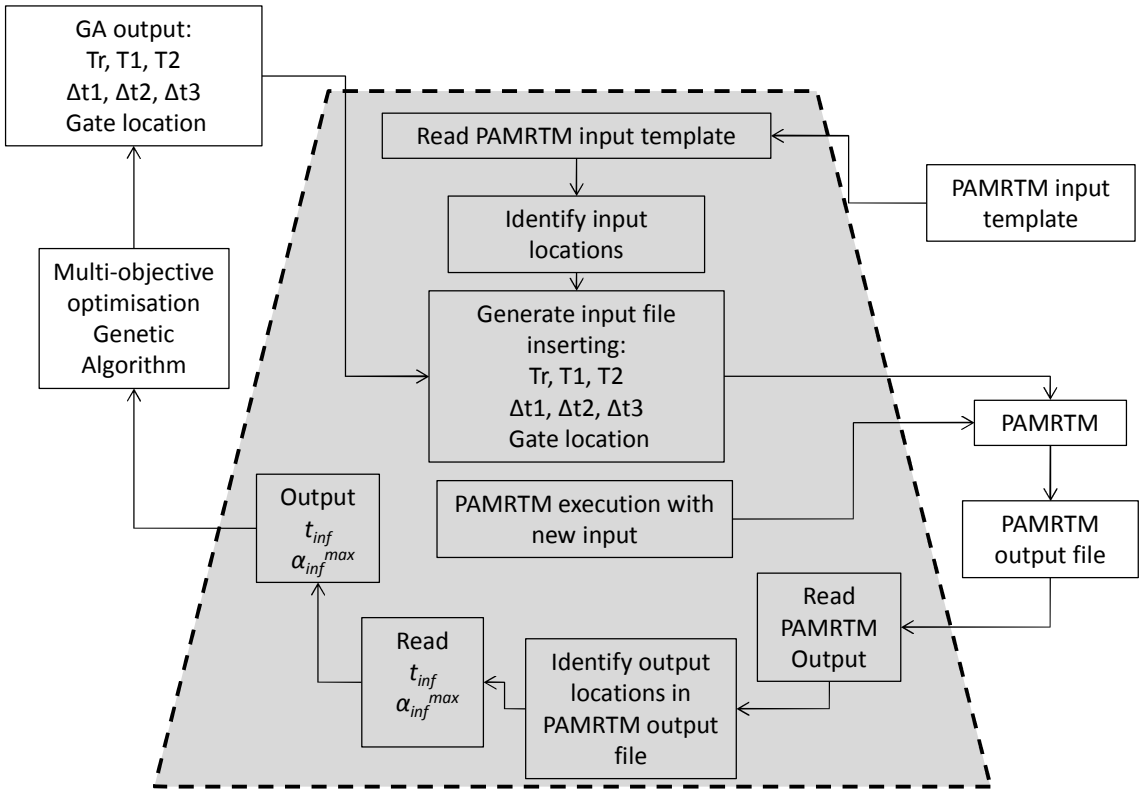

Figure 6-2 Infusion interface

The parameters of the optimisation are reported in Table 6-1 whilst the parameters range applied are reported in Table 6-2. The values for the optimisation input and parameters ranges have been fine-tuned according to the results of several simulations of the part.

Table 6-1 Optimisation input

GA input	Values
Number of generations	20
Individuals per population	15
Individuals per reproduction	10
Elite individuals	4
Size of Pareto	25
Mutation probability	0.005
Cross-over probability	0.5

Table 6-2 Design parameters range

Design Parameters	Ranges
Δt_1 (s)	60-150
Δt_2 (s)	90-210
t_3 (s)	4000
T_1 (^{0}C)	120-190
T_2 (^{0}C)	120-190
T_{resin} (^{0}C)	70-140
Gates number	3

6.3 Part description

A 2D section of a C-stiffener (Figure 6-3) has been chosen for the infusion optimisation problem. The C-stiffener is part of a 3D belly fairing module composed by a flat panel and four C-stiffener along each edge. Due to symmetry only one C-stiffener has been selected out of the four and after identifying the through thickness direction as the one of interest the final part resulted in a 2D section of the stiffener. The part is 6 cm high and 13 cm wide whilst the thicknesses involved are lower than 5 mm. The lay-up was $[+45\ -45]_{2s.}$ The materials were carbon fibres G1157 unidirectional [143] and RTM6 epoxy resin [141]. The injection strategy is a single injection with three candidate gate locations.

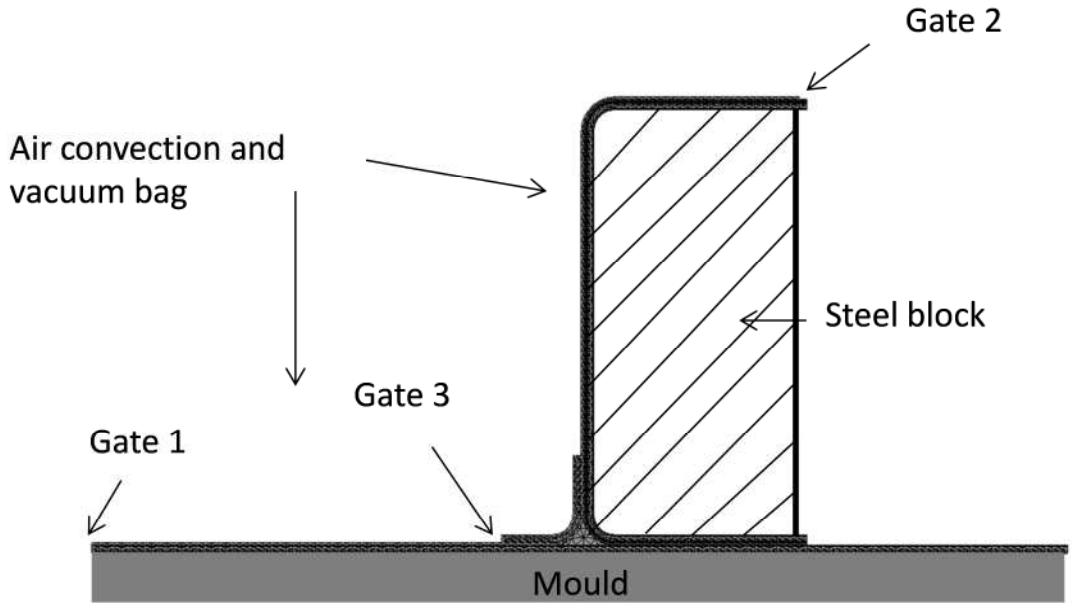

Figure 6-3 C-section model built in PAM-RTM®

6.4 Model description

The model has been built using PAM-RTM® 2010. Table 6-3 reports the permeability for the carbon reinforcement used, Table 6-4 summarises the material properties of both resin and fibres. The model is built with 1909 nodes and 2557 elements. The fibre volume fraction was set to 60%. The porous medium was a PTFE coated glass fibre fabric, with fibre volume fraction of 25%, and permeability equal to 10^{-10} m^2. Material properties for the porous medium and steel block are reported in Table 6-4 [154]. An air convection boundary condition with a surface heat transfer coefficient equal to 5 $W/m^2 \cdot K$ has been used on the bag side of the model and a prescribed temperature boundary condition, dictated by the optimisation, has been applied to the lower boundary part of the C-stiffener. Three feasible gate locations have been pre-selected as shown in Figure 6-3. The initial degree of cure has been set to 6%, initial fibres and the initial tool temperature have been set equal to the initial temperature of the non-isothermal profile.

Table 6-3 Permeability values of carbon fibres

	K_1	K_2	K_3
G1157 permeability (m^2)	$6.0 \cdot 10^{-13}$	$2.5 \cdot 10^{-13}$	$4.0 \cdot 10^{-15}$

Table 6-4 Material properties

	Steel block	**Porous media**
ρ (kg/m^3)	7900	2560
K (W/m·ºC)	35	1.04
C_p (J/kg·ºC)	500	670

6.5 Filling optimisation results

Figure 6-4 shows the results of the multi-objective optimisation depicting the Pareto front at different generations. The GA is able to approach the final Pareto set successfully showing a high rate of convergence, within 10 generations. The parameter ranges chosen are reported in Table 6-2. The duration of the second dwell (t_3) has been assigned a high value. This has been

done to avoid a duration of the filling longer than the duration of the non-isothermal profile. The duration of the first dwell (Δt_1) and the ramp (Δt_2) have been chosen according to the duration of the filling process in order to have all the individuals undergoing the three segments of the non-isothermal profile. The temperatures of the two dwells have been selected starting from the standard infusion at 120 ºC up to 190 ºC. The same ranges have been selected in order to allow both ramp-up and ramp-down. The resin temperature has been taken between 70 ºC and 140 ºC with the purpose of investigating the effect of variation in initial resin temperature at the gate which by standard for RTM6 is set to 80 ºC.

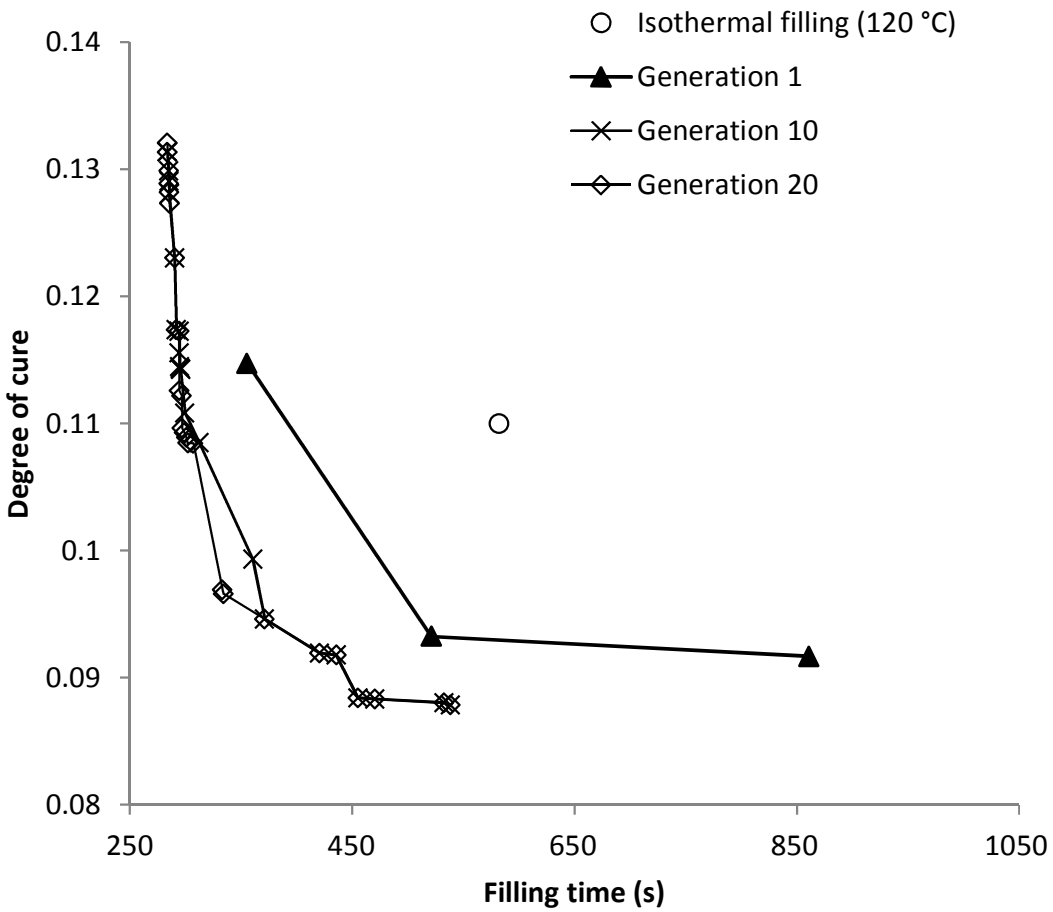

Figure 6-4 Pareto front at different generations

Since the Pareto front of the last generation only includes solutions with gate number 3, it has been chosen to report only the standard results corresponding to this gate. Standard VARTM infusion for RTM6 epoxy resin is carried out with

the tool plate kept at 120 ^{0}C and the resin injected at 80 ^{0}C. Standard infusion result has a filling time equal to 582 s and a final degree of cure at the end of the cure equal to 0.11. The L-shape of the final Pareto set suggests a preferential direction towards the corner that allows to improve both filling time and degree of cure. Furthermore, it highlights two distinct zones, the horizontal part and the vertical part. Moving along the horizontal part it is possible to achieve significant improvements in filling time, while along the vertical part it is possible to achieve significant improvements in final degree of cure. The standard isothermal infusion lies away from these two zones allowing improvements in both objectives. Choosing a design point at the corner of the Pareto front it is possible to achieve a 42% reduction in filling time and a 14% reduction in final degree of cure. The resin temperature at this corner point is 115 ^{0}C while the temperatures of the first and second dwell are 157 ^{0}C and 159 ^{0}C, respectively. This suggests that increasing the resin and dwell temperature affect positively both filling time and degree of cure as long as the filling is fast enough to keep the reaction of the resin still at the beginning of its overall development.

Analysing the design parameters space provides interesting insights. Table 6-5 reports design parameters and filling times for the horizontal part of the front associated with low final degree of cure (<0.1). The improvement in the degree of cure in this zone is about 20%. The first dwell duration for these individuals is very close to the upper limit of the range (135 s) whilst the ramp duration is around 100 s. The second dwell temperature is in the range of 142-146 ºC. Regarding the first dwell temperature the range is wider (140-160 ^{0}C). Furthermore, the selection of ramp-down profile results in better filling time leading to 25-35% reduction with respect to the standard solution. The vertical part is characterised by higher values of temperature for the first dwell around 174 ºC and either a ramp-up to about 177 ºC or ramp-down to about 160 ºC. The individual solutions in this region are generally characterised by shorter first dwell (shorter than 90 s) and longer ramp duration (longer than 150 s).

Table 6-5 Design parameters and filling times corresponding to the horizontal section of the Pareto front presented in Figure 6-4

T_1 (^{0}C)	T_2 (^{0}C)	T_{resin} (^{0}C)	Filling time (s)
144	146	115	470
139	143	115	532
139	143	115	538
156	142	114	420
156	142	115	435
146	146	115	455
160	146	115	371

An exhaustive search has been carried out in order to investigate the design space and verify the efficiency and accuracy of the GA solution. In this case having six active parameters playing a role forced to use a relatively coarse grid for the discretisation in order to limit the total number of evaluations to about 10000. Each parameter range has been then divided in five increments with the exception of gate location which only has three values. Figures 6-5, 6-6 illustrate the objective space allowing a comparison of the GA optimisation and the exhaustive search results. The approximation achieved by the GA is more accurate than the one found by the exhaustive search. The exhaustive search evaluation required about 15 times the computational effort required for the GA execution, although the exhaustive search was carried out using a coarse grid. A much finer discretisation would be needed (about 10^9) for the exhaustive search to achieve an accuracy similar to the GA.

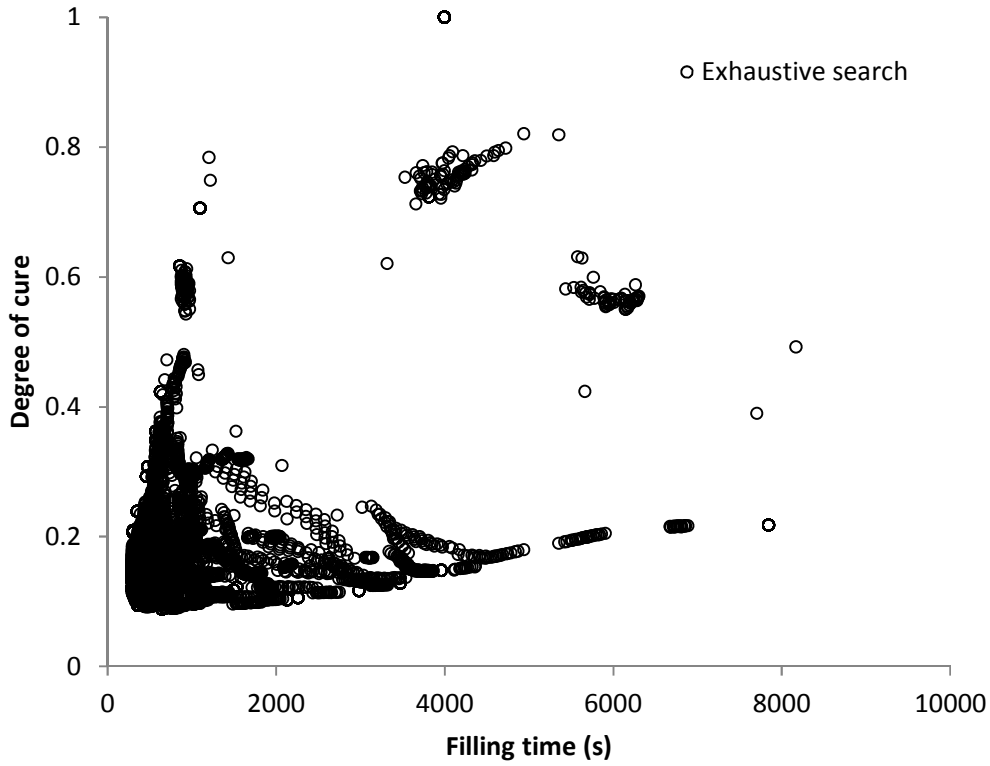

Figure 6-5 Objective space

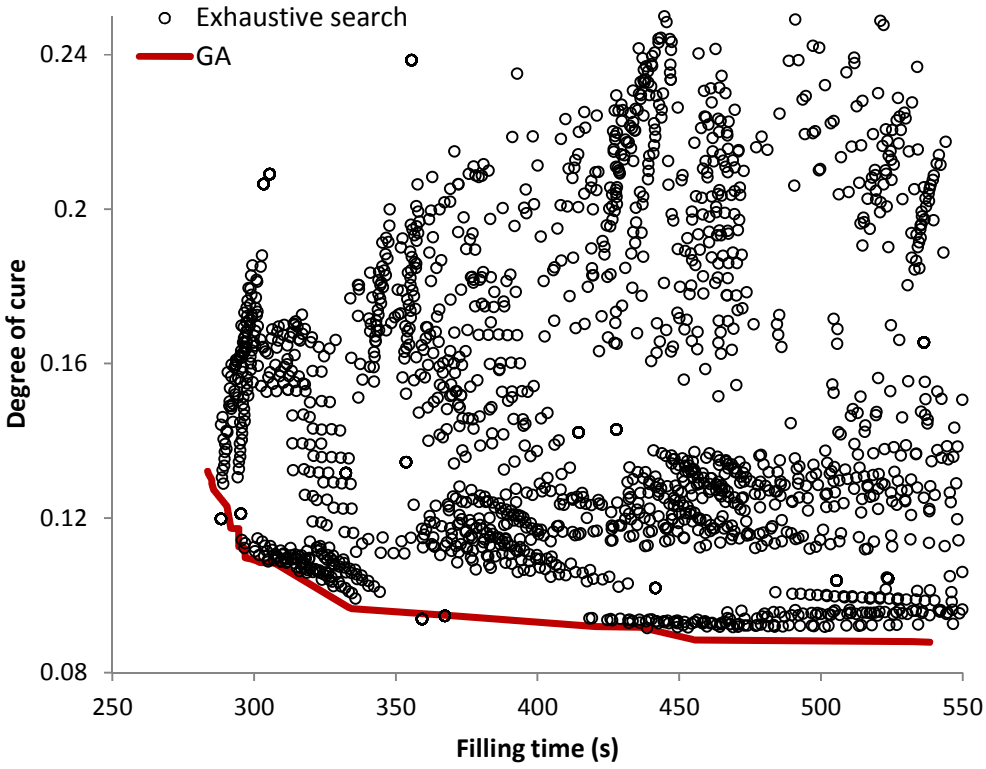

Figure 6-6 Exhaustive search vs GA

Investigation of the optimisation landscape for the filling stage has been undertaken based on the data obtained from the exhaustive search. The two objectives, degree of cure and filling time have been plotted against every possible pair of process parameters (Figures 6-7 – 6-21). A degree of cure of 0.3 has been set as limit for acceptable results as for higher degree of cure the filling was incomplete. Figure 6-7 illustrates the dependence of the objectives on ramp duration and first dwell duration. The degree of cure dependence on these parameters is shown to be complex with the presence of many local maxima and minima (Figure 6-7 a)), whilst the filling time behaviour follows a linear trend (Figure 6-7 b)). Furthermore, a comparison of the behaviour of filling time and final degree of cure shows the competitive nature of the two objectives since high final degrees of cure correspond to low filling time and vice versa. Figure 6-8 illustrates the dependence on gate location and first dwell duration change and Figure 6-12 to the dependence on gate location and second dwell duration. In these pairs of process parameters the major effect is due to the gate selection which produces a clear maximum in both degree of cure and filling time. Figure 6-9 illustrates the objectives with respect to variations in first dwell duration and first dwell temperature. Filling time varies by about 300 s as the first dwell temperature spans from its minimum to its maximum (Figure 6-9 a)) and the final degree of cure ranges by about 0.15 (Figure 6-9 b)). Again the plots show the competitive nature of the objectives as the increase in first dwell temperature produces two opposing effects: it increases the final degree of cure (Figure 6-9 a)) but it decrease the filling time as the viscosity drops at higher temperature (Figure 6-9 b)). Figure 6-10 illustrates the dependence on first dwell duration and second dwell temperature. Some unfeasible solutions appear in this case. These are penalised because the set of parameters leads to incomplete filling. Figure 6-10 a) and b) depicts a strong dependence on second dwell temperature, which results in minima in the landscape and a weak dependence on first dwell duration. Figures 6-11, 6-15 illustrate the dependence of the objectives on resin temperature and first dwell duration and resin temperature and ramp duration showing that the initial resin temperature is a critical parameter as it can make the difference between a successful filling and

an incomplete one. Figures 6-13, 6-14 show the dependence on ramp duration and first dwell temperature and ramp duration and second dwell temperature respectively. Ramp duration has a weak effect compared to the first dwell temperature which has a significant role in both the degree of cure evolution also causing local minima (Figure 6-13 a)) and filling time evolution causing with its variation an overall change in filling time of about 200 s (Figure 6-13 b)). The second dwell temperature influences the two objectives even more producing local minima in final degree of cure (Figure 6-14 a)) and in process time (Figure 6-14 b)). Figure 6-15 shows the influence of ramp duration and resin temperature pointing out the significant role played by the resin temperature. Figures 6-16, 6-19 and 6-20 present the influence of gate and first dwell temperature, gate and second dwell temperature, gate and resin temperature, respectively. Variations in gate location cause maxima in the landscape; the combination with first and second dwell temperature makes the landscape even more complex since new local minima appear as the first dwell temperature (Figure 6-16 a)) second dwell temperature (Figure 6-19 a)) and resin temperature (Figure 6-20 a) and b)) change. Figure 6-17 illustrates the dependence of the objectives on the temperature of the first and second dwell. The two parameters have a strong non-linear influence on the two objectives. A ramp-up from 130 ºC to 190 ºC can end in a filling time about 3000 s and degree of cure of about 0.15 whilst a ramp-down from 190 ºC to 130 ºC produces a filling time of about 800 s and a degree of cure of about 0.4. Figure 6-18 depicts the dependence on resin temperature and first dwell temperature. Once again local minima appear in the landscape in both filling time and degree of cure. Furthermore, careful selection of the two parameters must be carried out as curing might result in incomplete filling. The interdependencies on resin temperature and second dwell temperature reported in Figure 6-21 are even more delicate as tolerance in the selection of these two parameters is smaller.

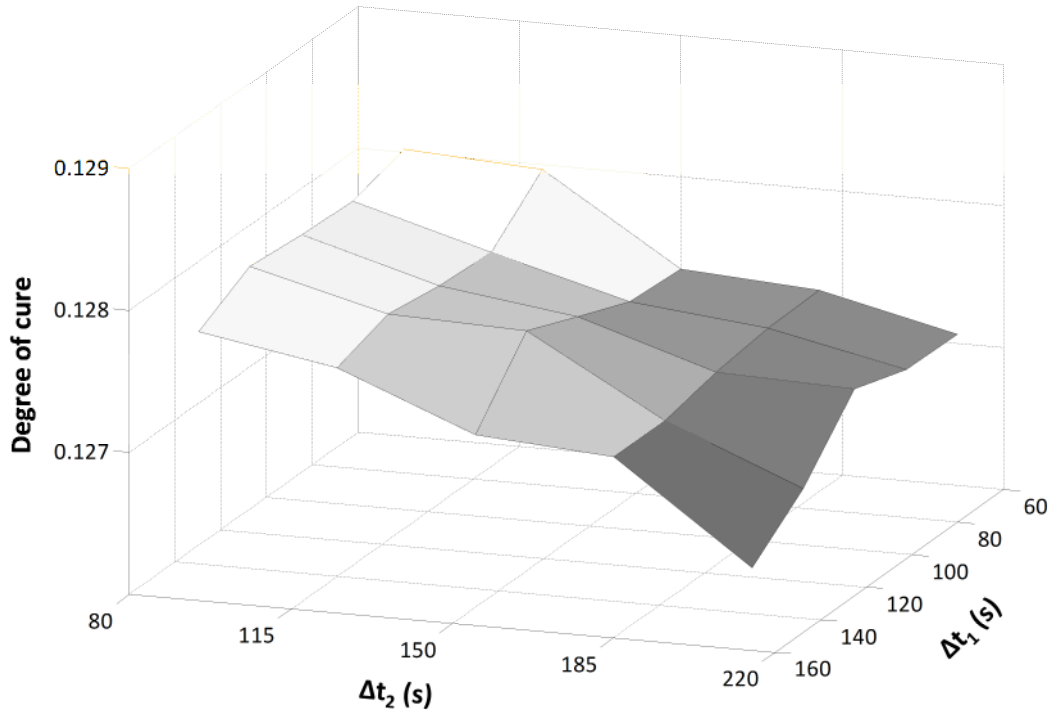

a)

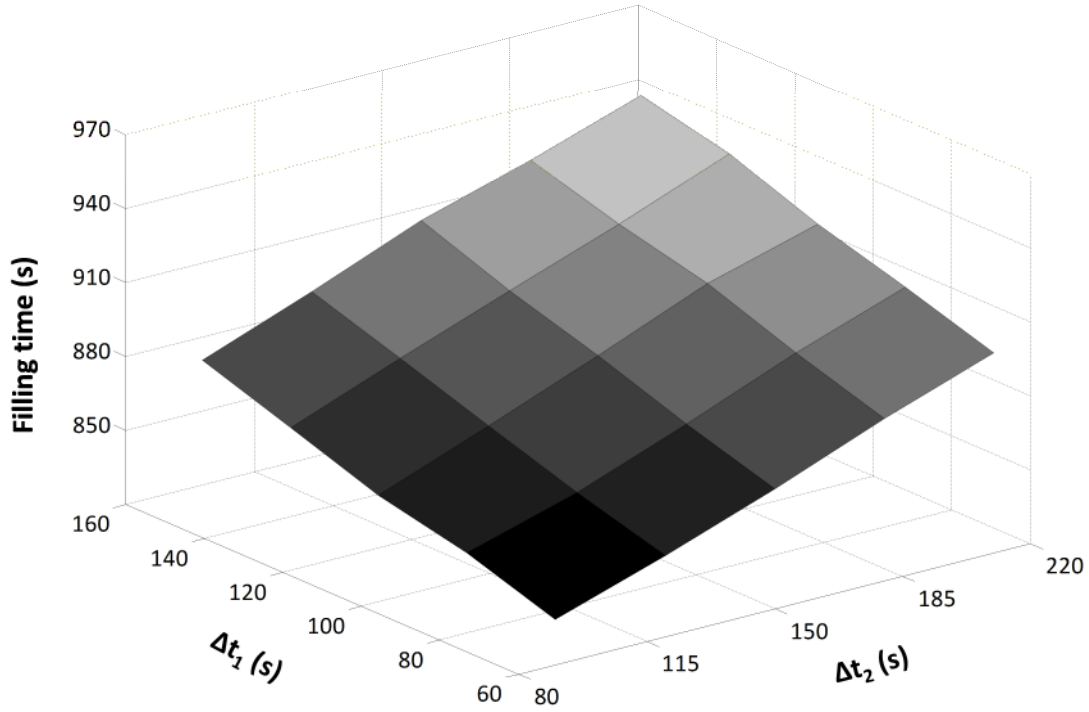

b)

Figure 6-7 Landscape of the infusion problem for gate 3: First dwell duration Vs Ramp duration a) Degree of cure b) Filling time

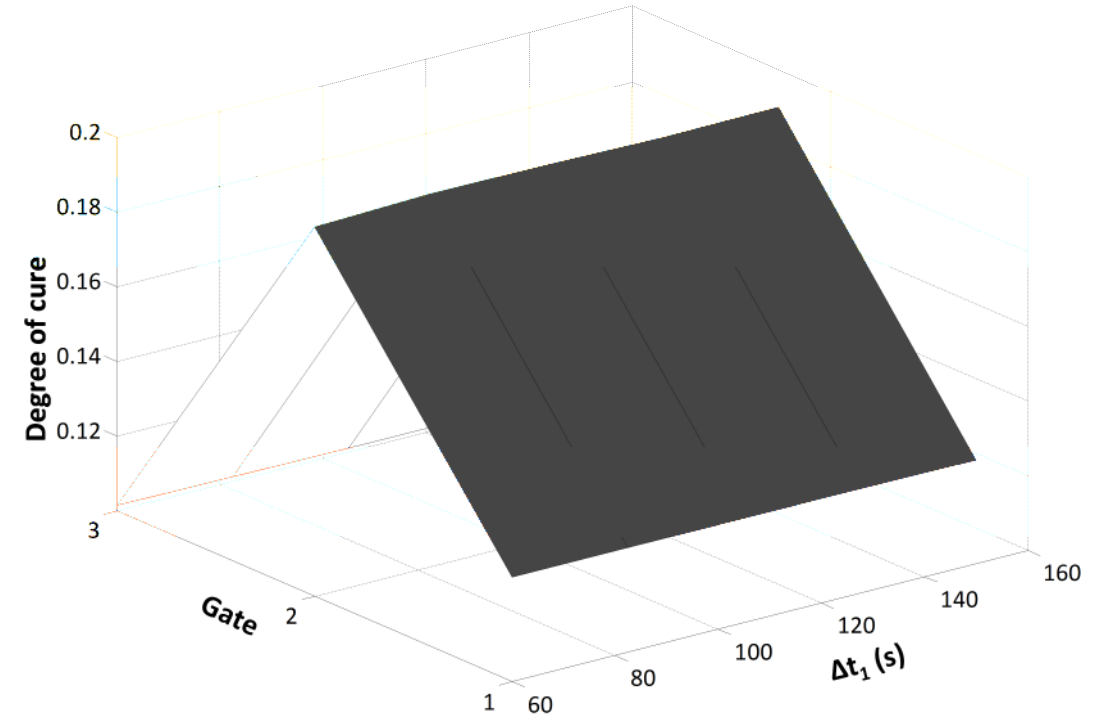

a)

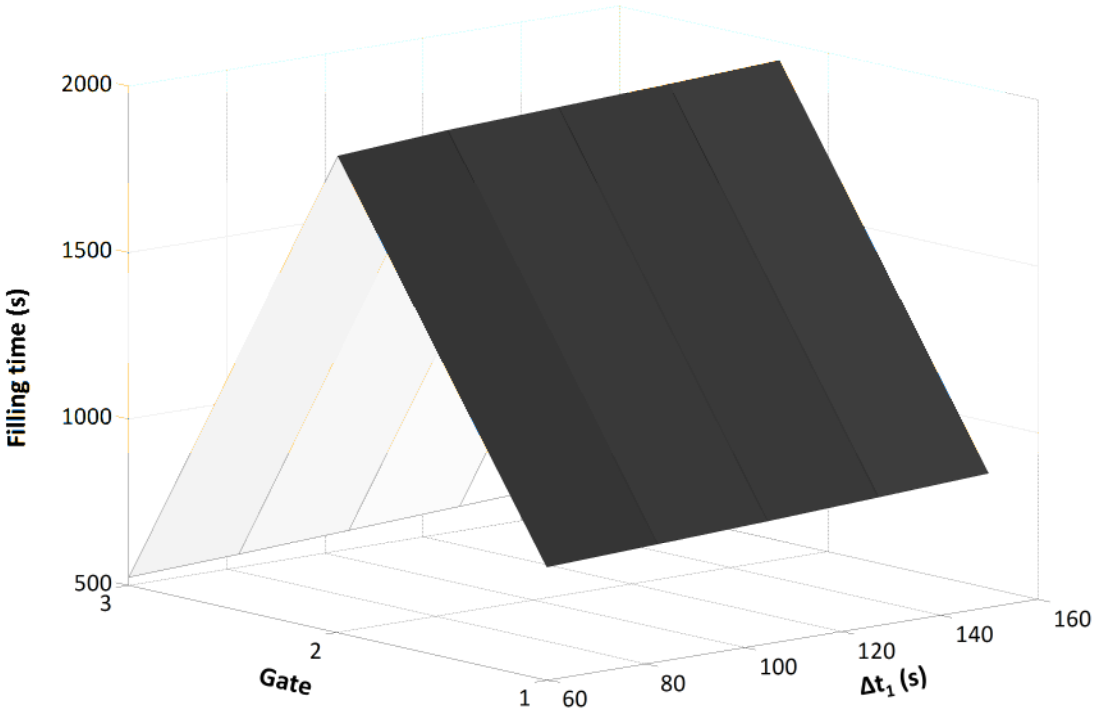

b)

Figure 6-8 Landscape of the infusion problem: First dwell duration Vs Gate location a) Degree of cure b) Filling time

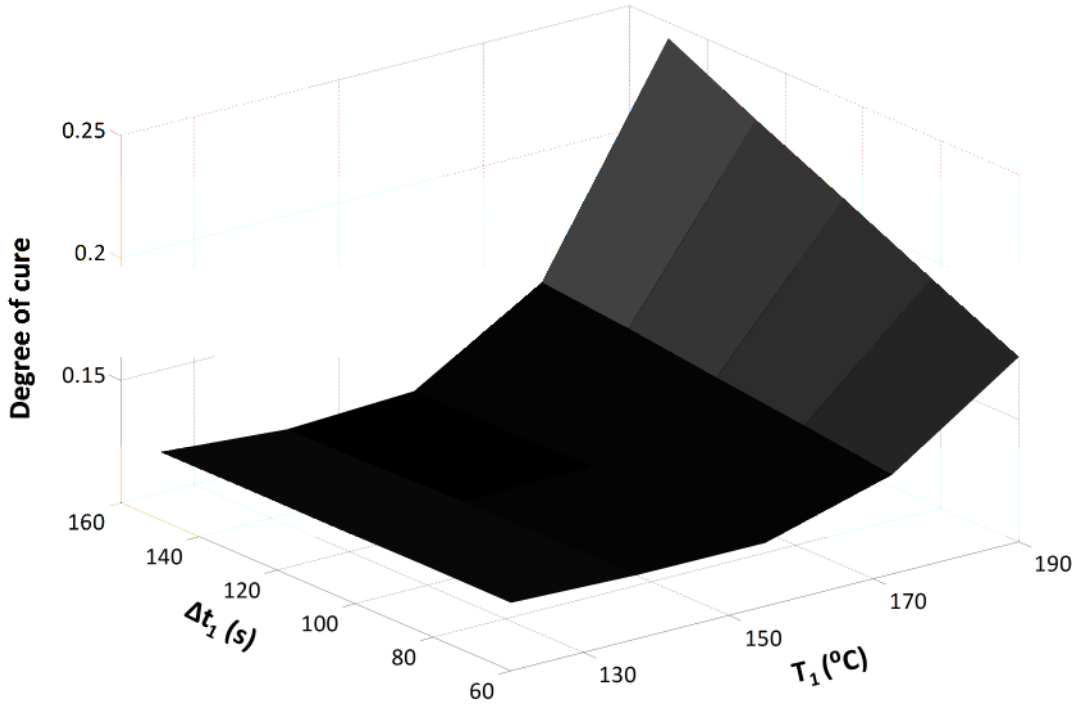

a)

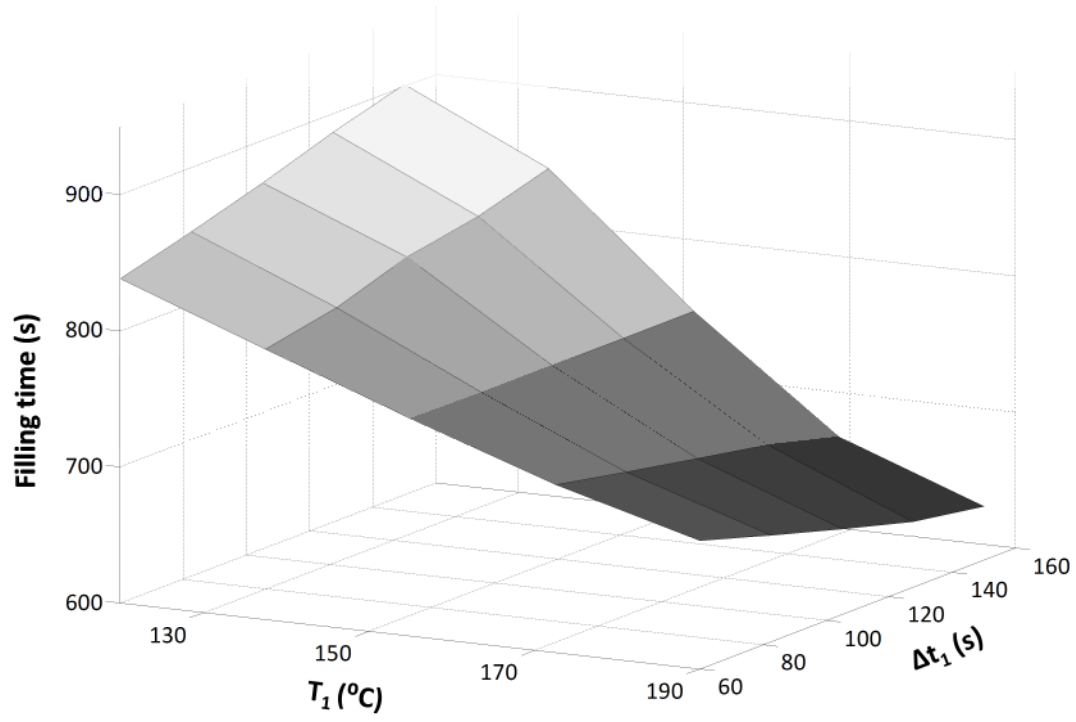

b)

Figure 6-9 Landscape of the infusion problem for gate 3: First dwell duration Vs First dwell temperature a) Degree of cure b) Filling time

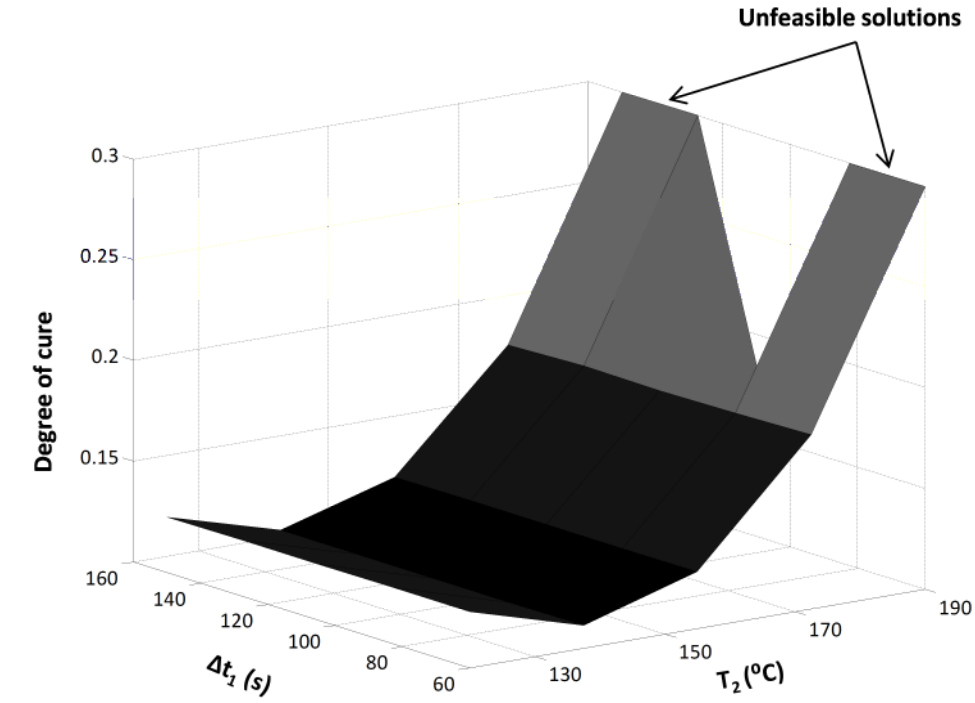

a)

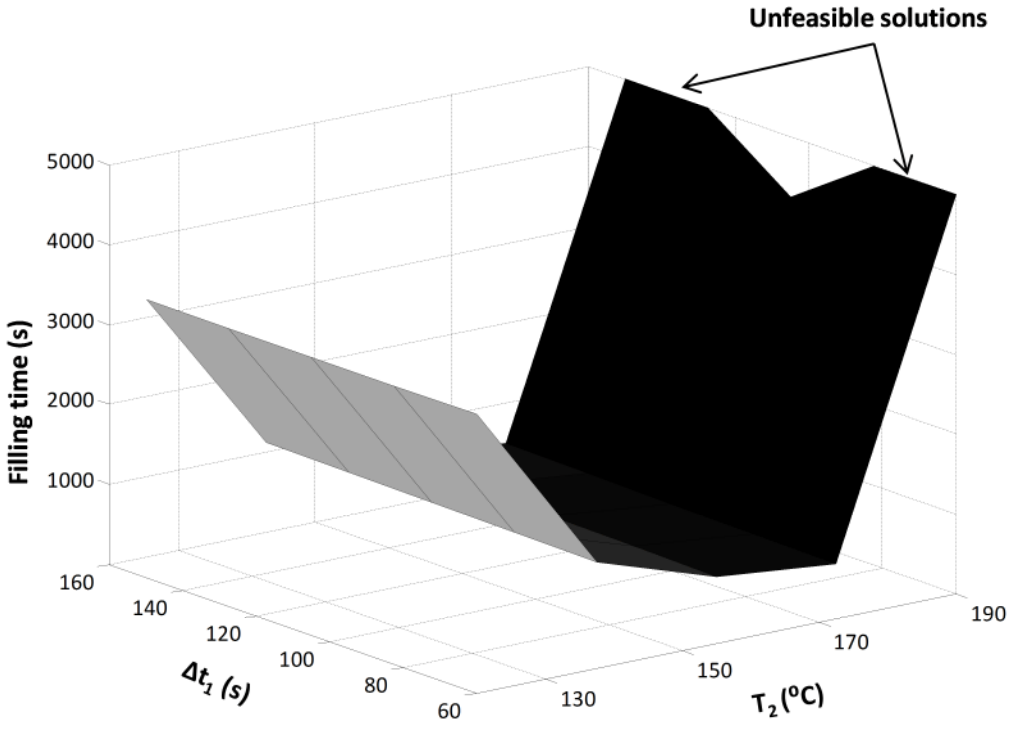

b)

Figure 6-10 Landscape of the infusion problem for gate 3: First dwell duration Vs Second dwell temperature a) Degree of cure b) Filling time

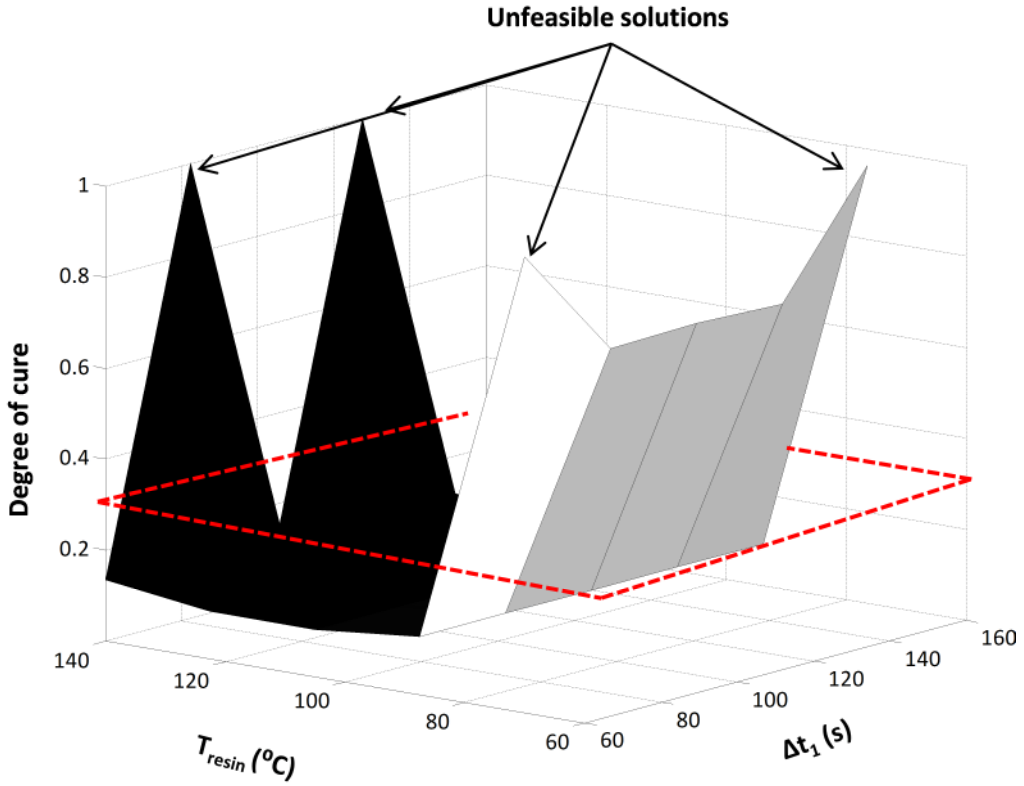

a)

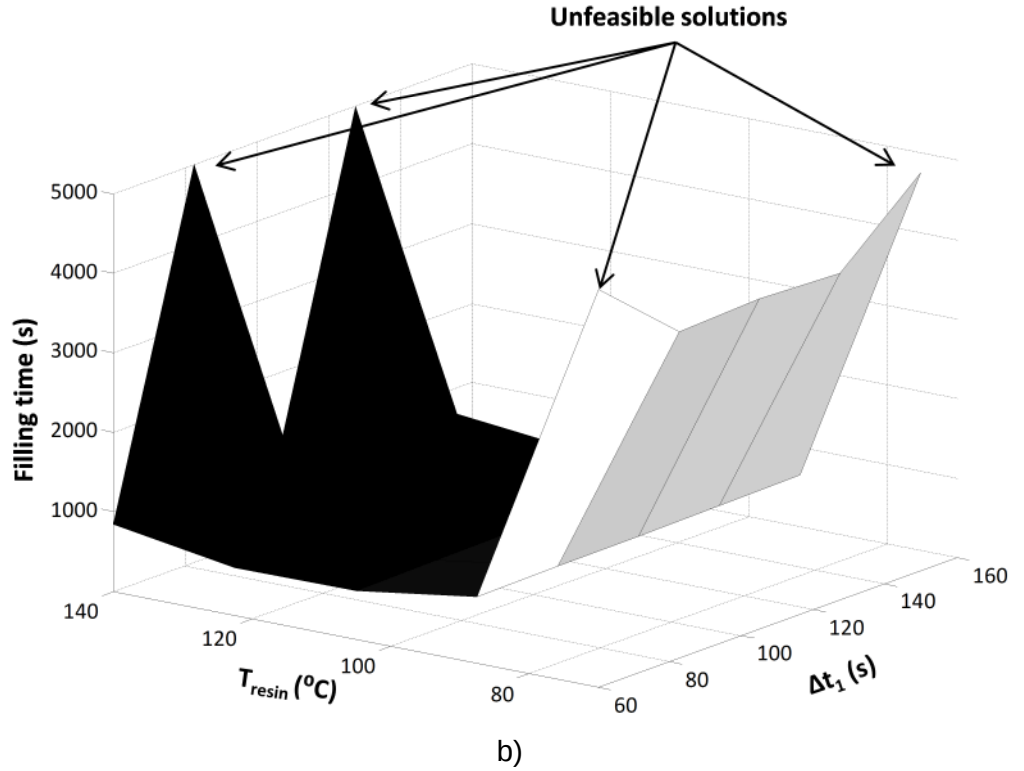

b)

Figure 6-11 Landscape of the infusion problem for gate 3: First dwell duration Vs Resin temperature a) Degree of cure b) Filling time

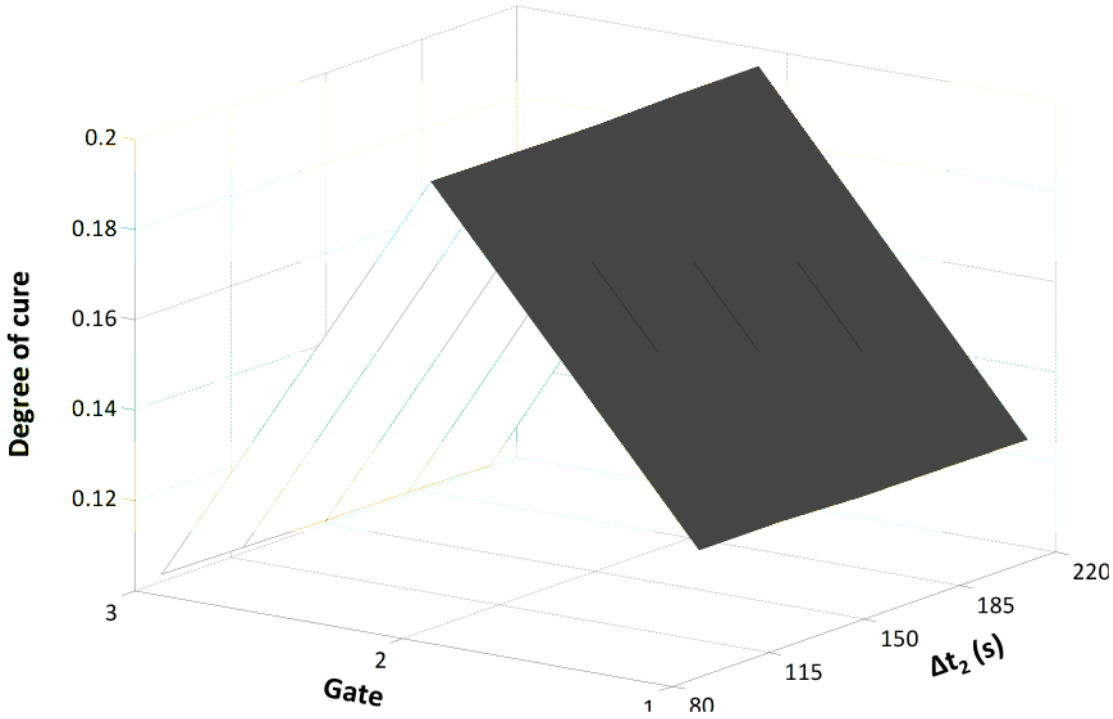

a)

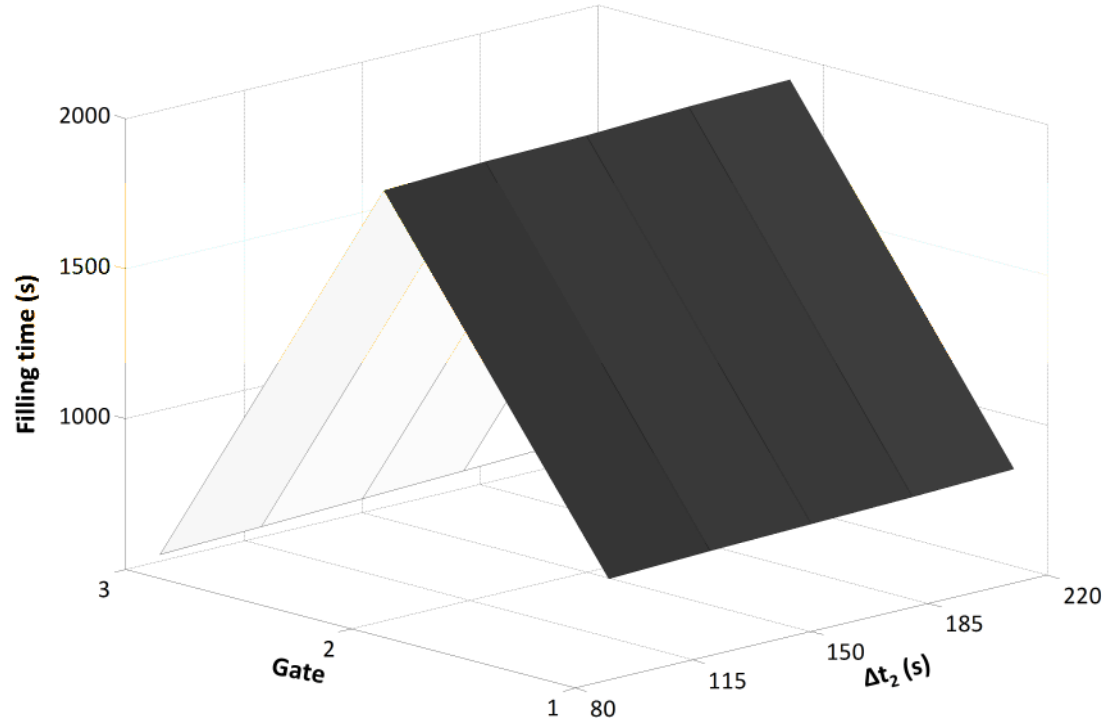

b)

Figure 6-12 Landscape of the infusion problem: Ramp duration Vs Gate location a) Degree of cure b) Filling time

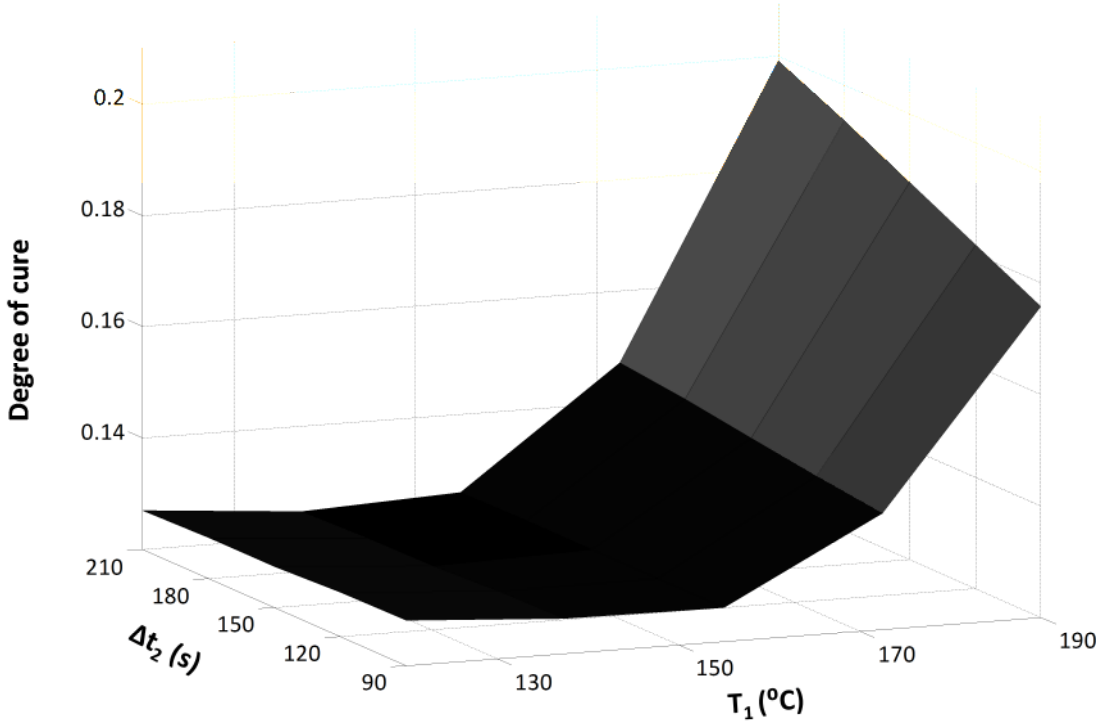

a)

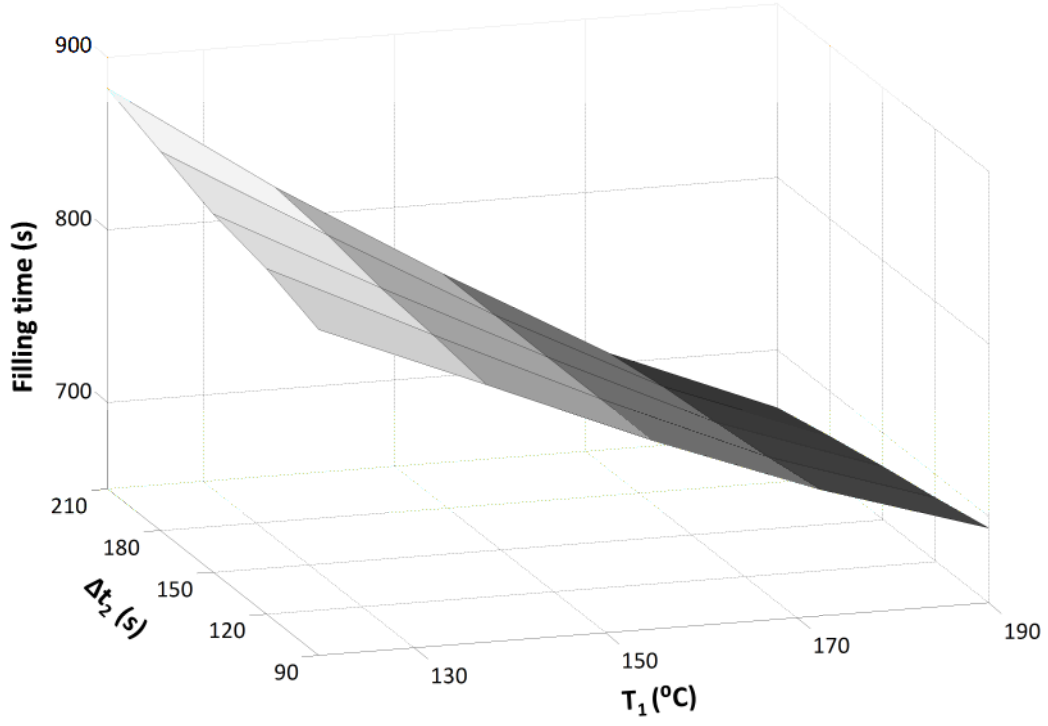

b)

Figure 6-13 Landscape of the infusion problem for gate 3: Ramp duration Vs First dwell temperature a) Degree of cure b) Filling time

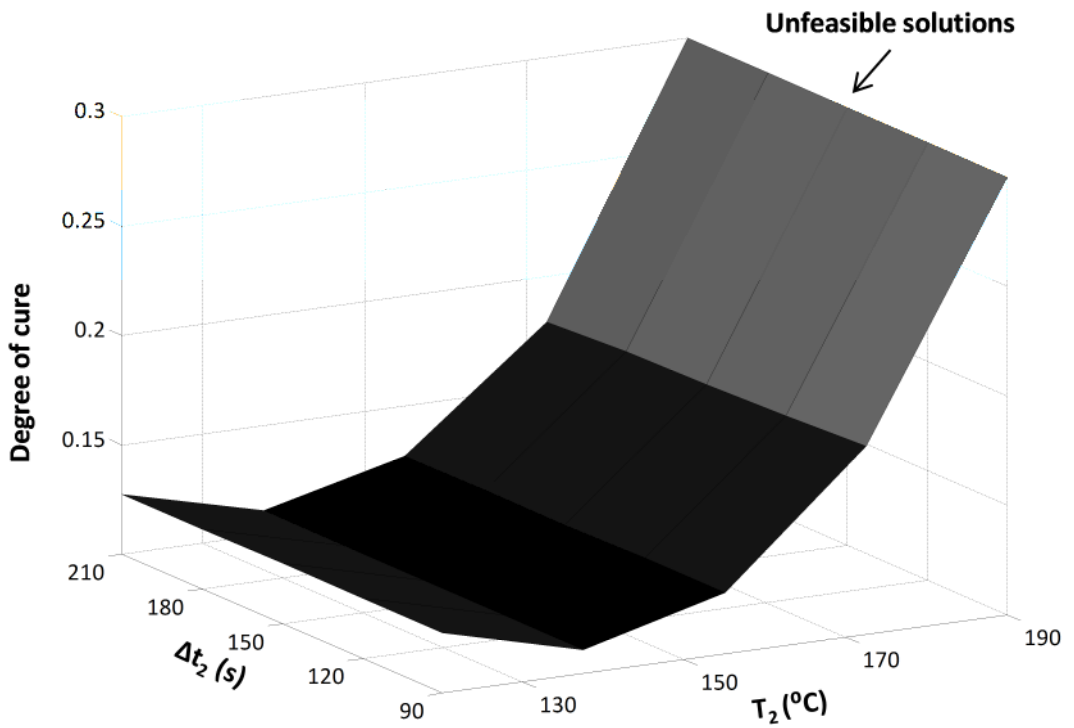

a)

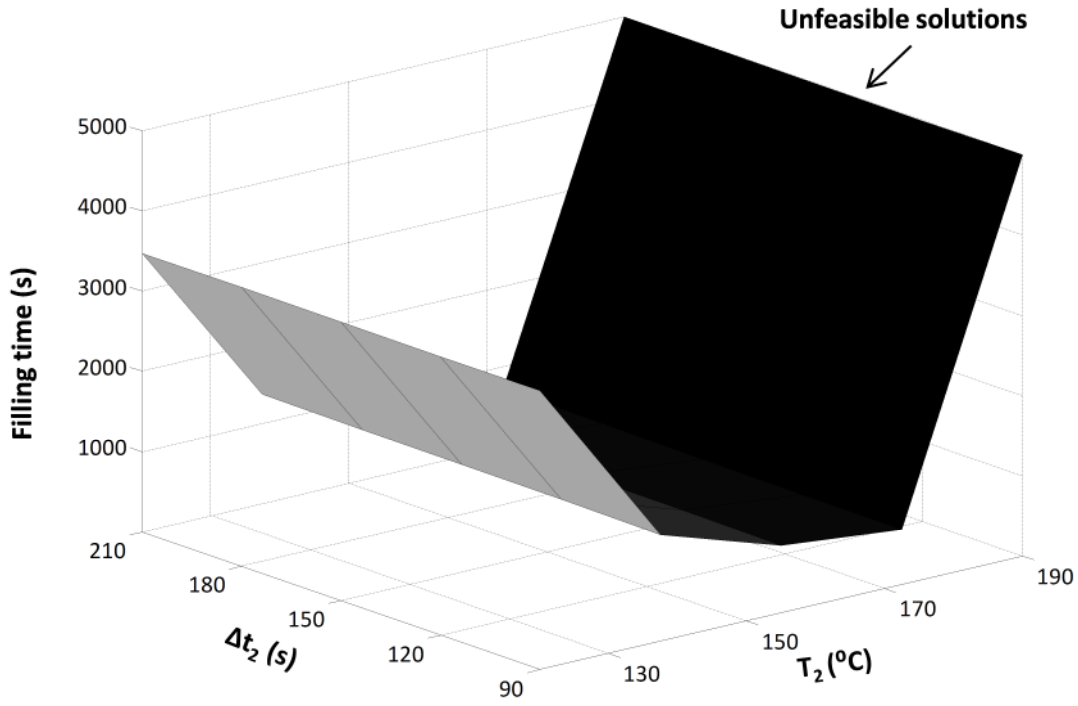

b)

Figure 6-14 Landscape of the infusion problem for gate 3: Ramp duration Vs Second dwell temperature a) Degree of cure b) Filling time

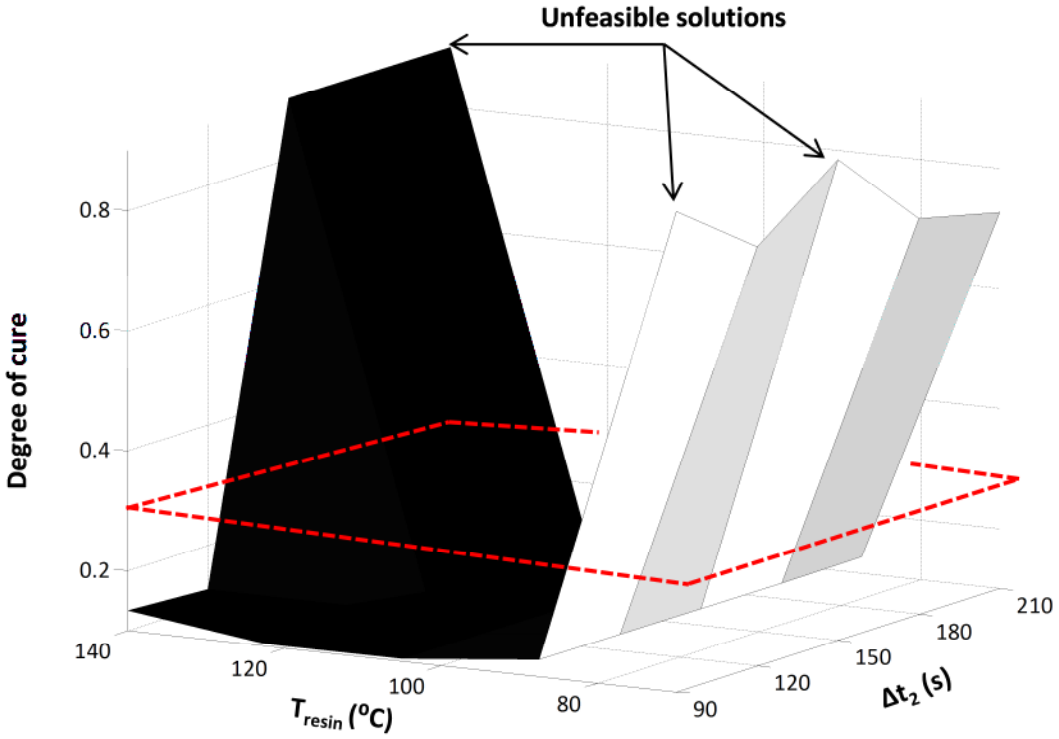

a)

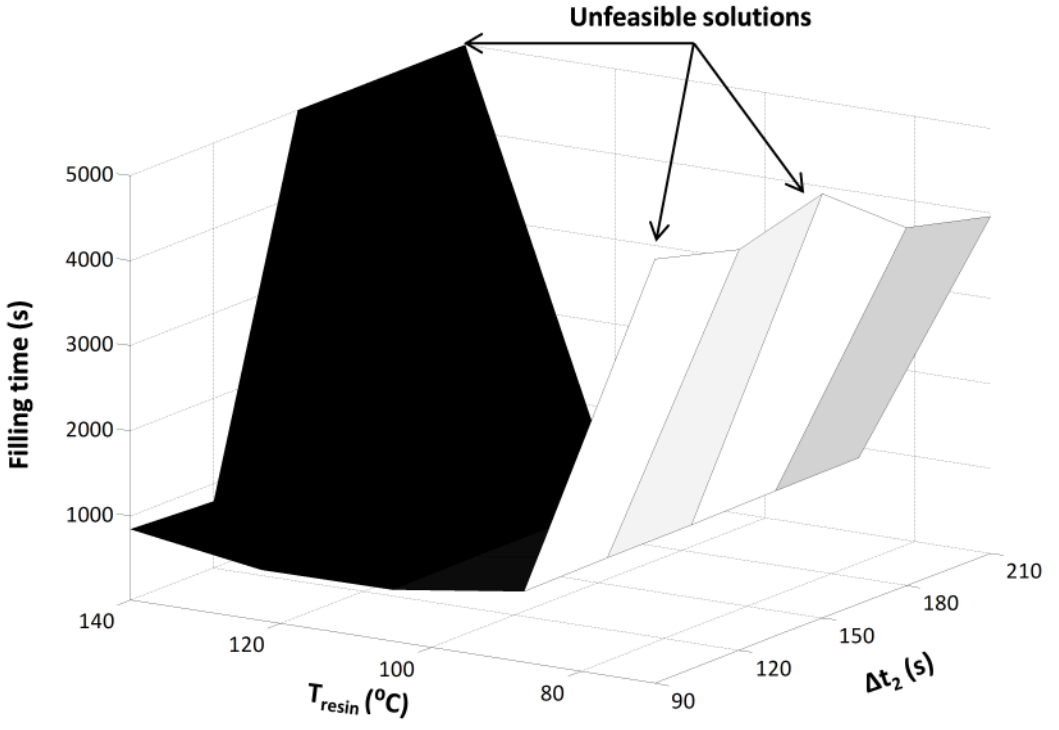

b)

Figure 6-15 Landscape of the infusion problem for gate 3: Ramp duration Vs Resin temperature a) Degree of cure b) Filling time

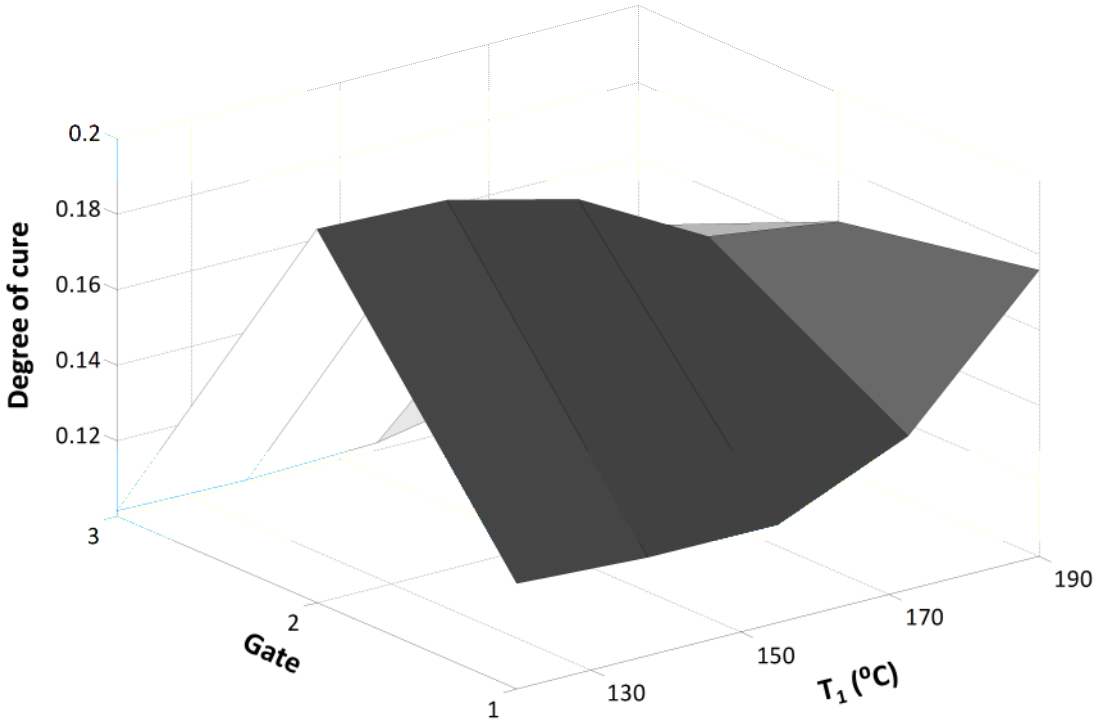

a)

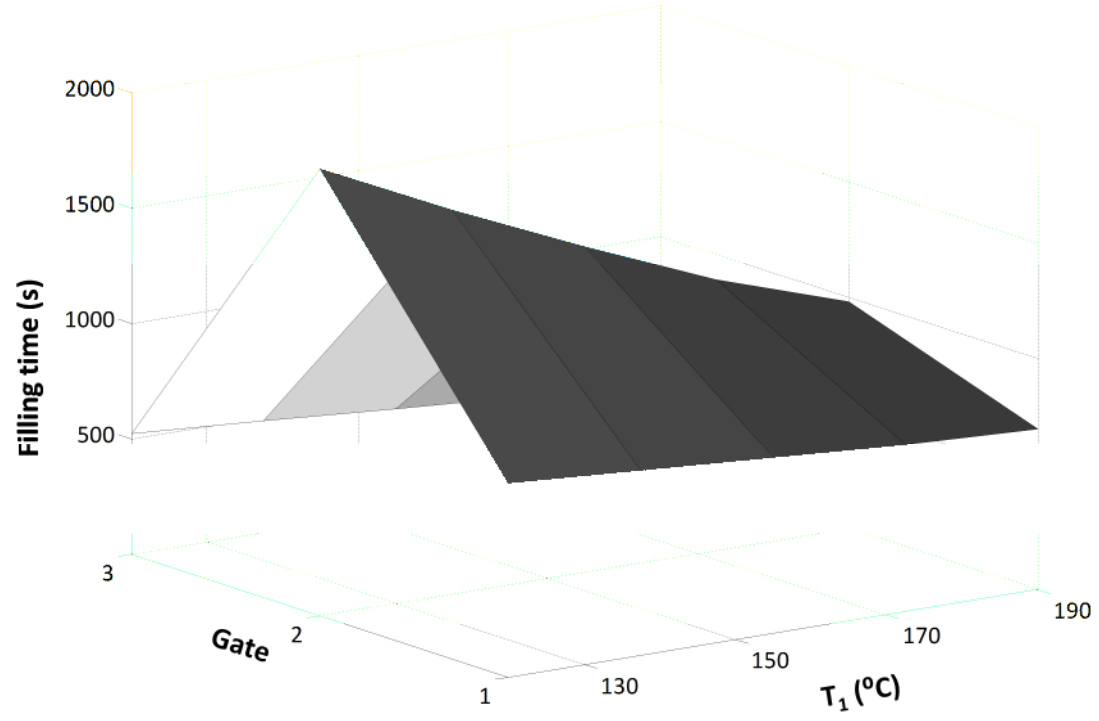

b)

Figure 6-16 Landscape of the infusion problem: Gate location Vs First dwell temperature a) Degree of cure b) Filling time

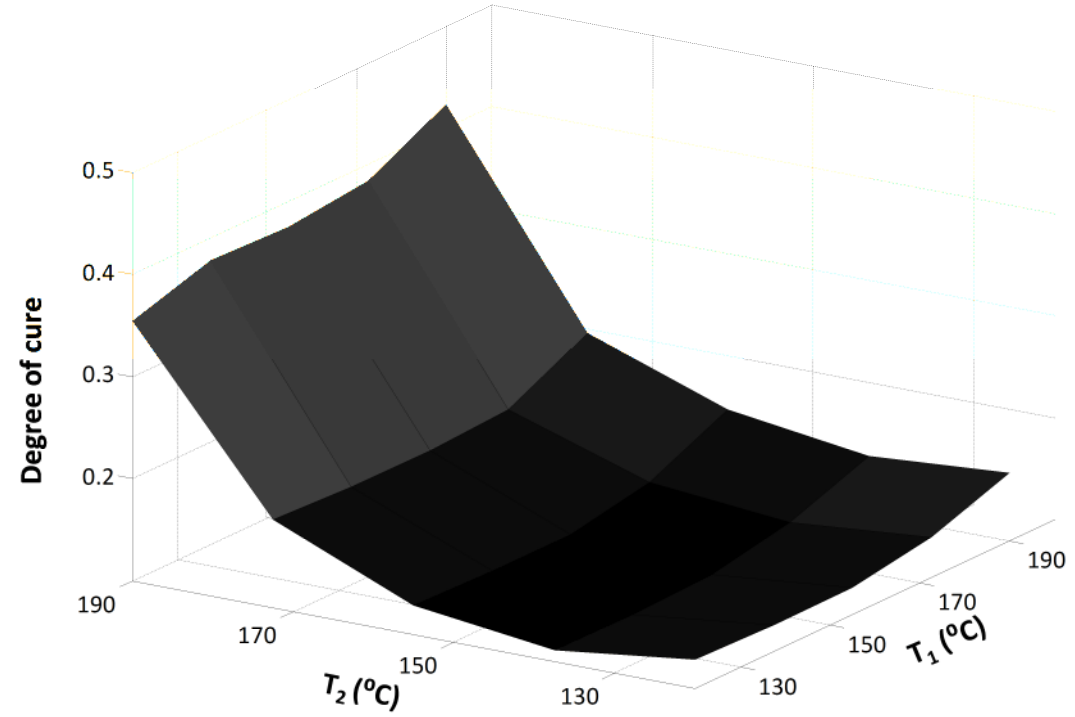

a)

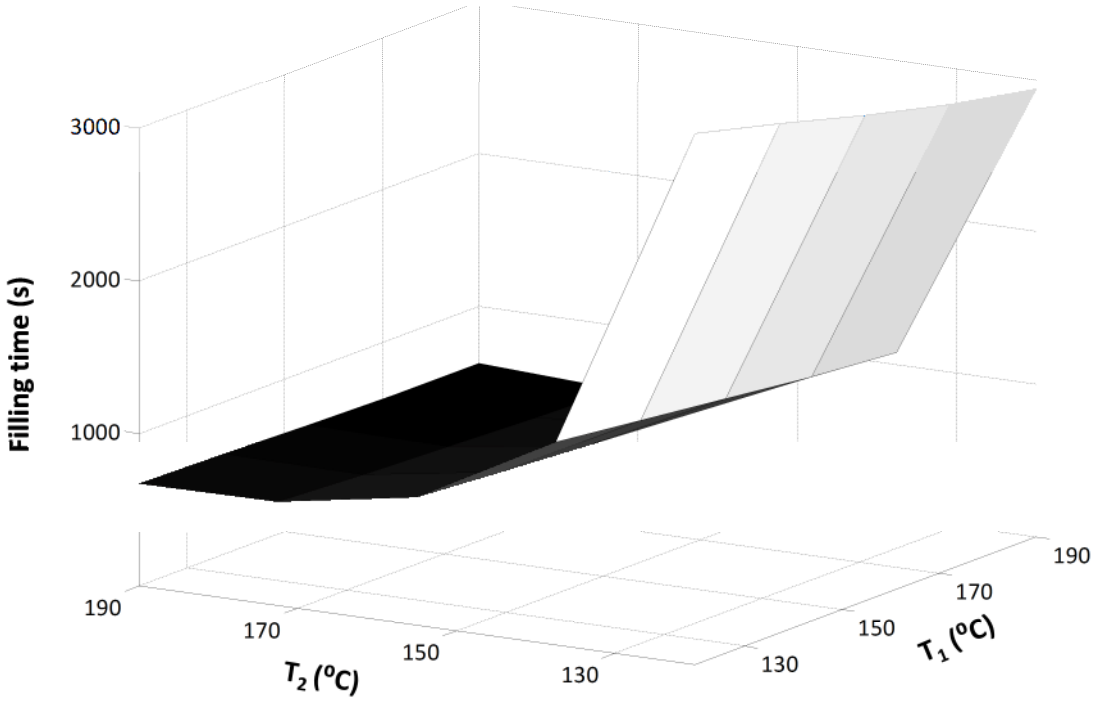

b)

Figure 6-17 Landscape of the infusion problem for gate 3: First dwell temperature Vs Second dwell temperature a) Degree of cure b) Filling time

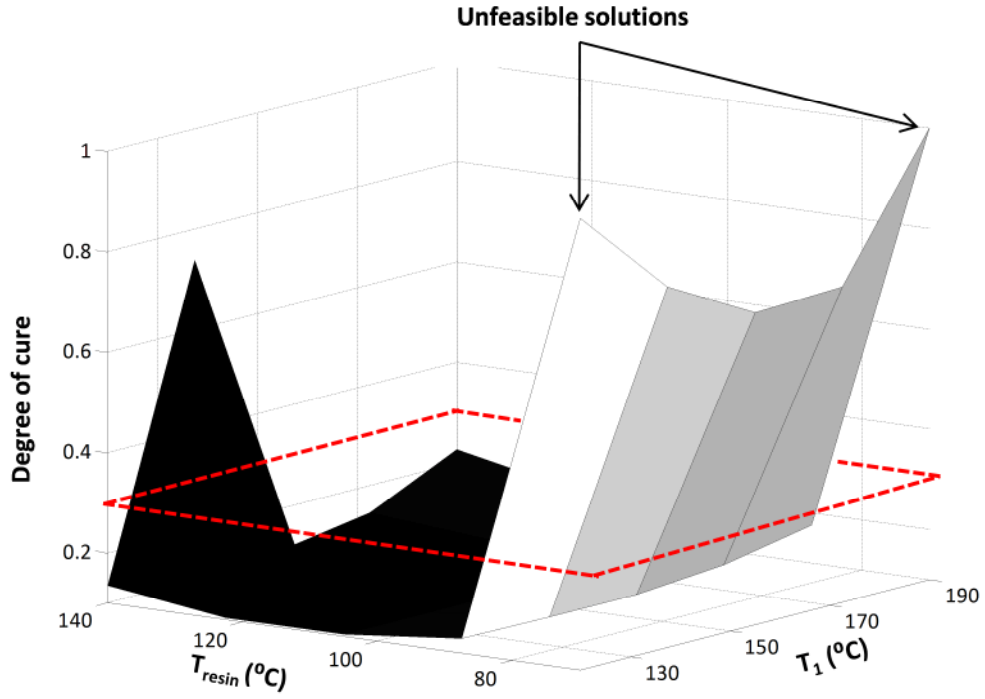

a)

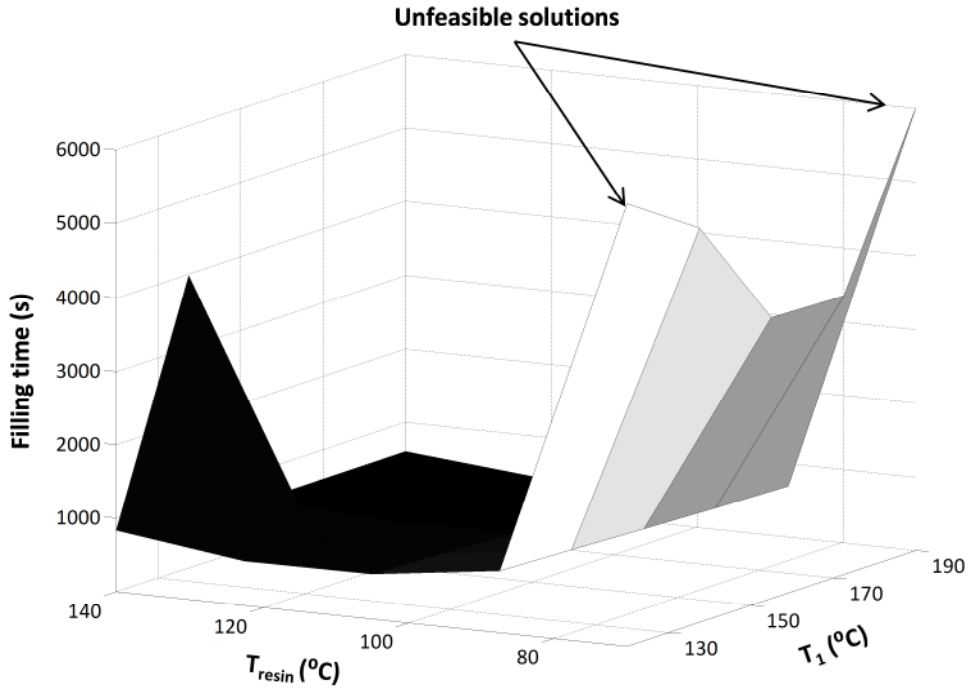

b)

Figure 6-18 Landscape of the infusion problem for gate 3: First dwell temperature Vs Resin temperature a) Degree of cure b) Filling time

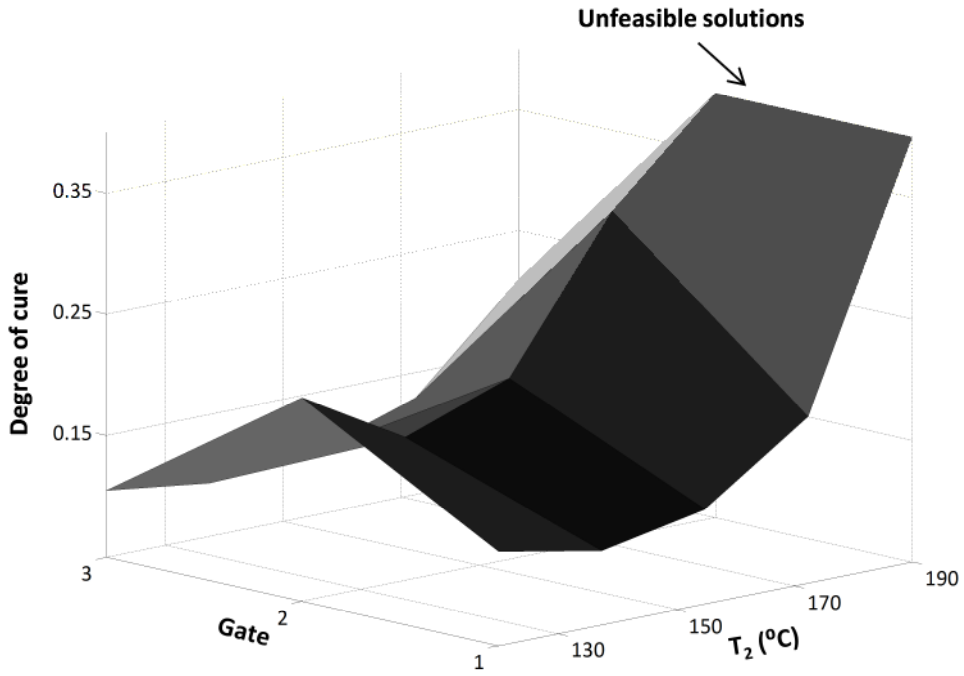

a)

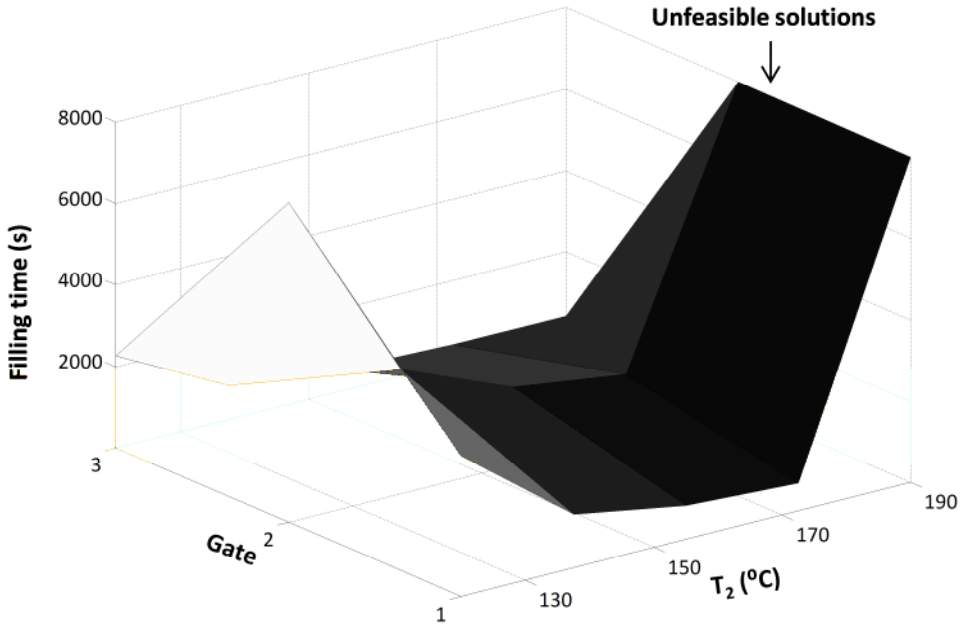

b)

Figure 6-19 Landscape of the infusion problem: Second dwell temperature Vs Gate location a) Degree of cure b) Filling time

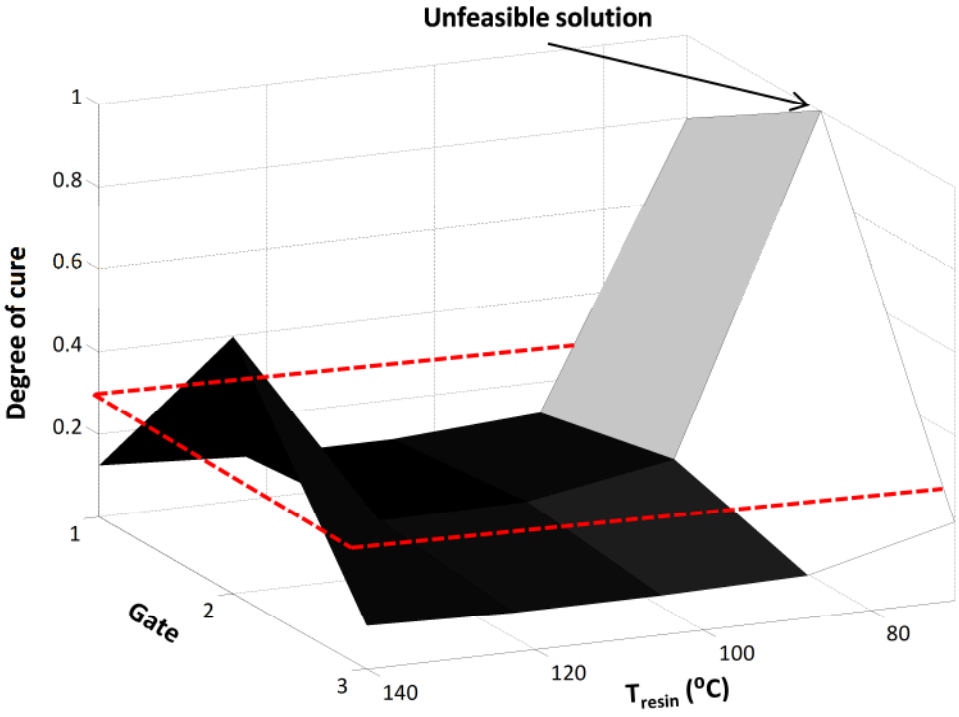

a)

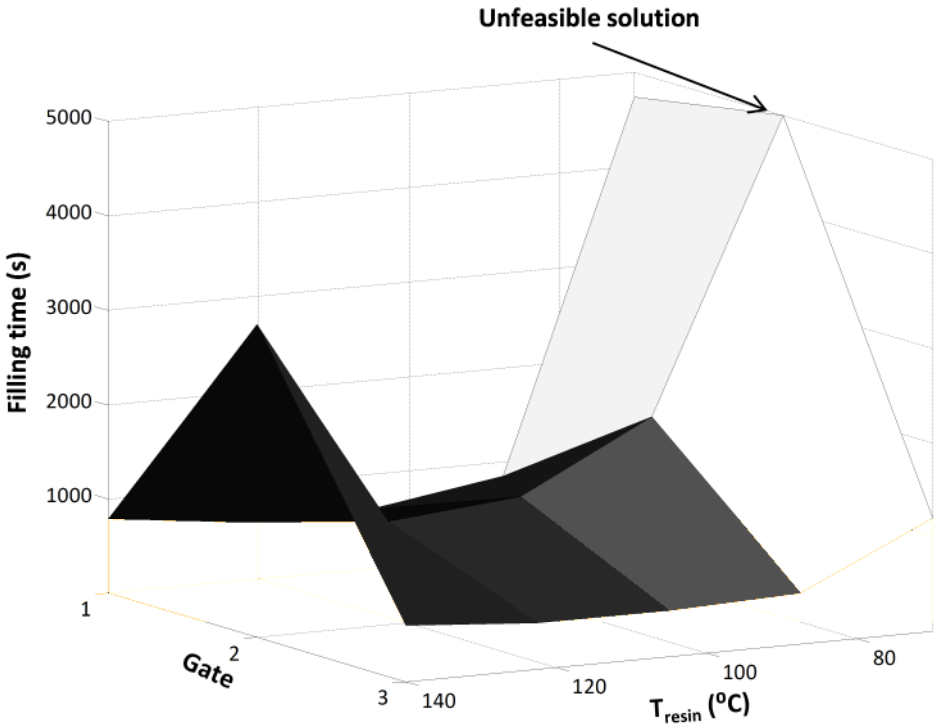

b)

Figure 6-20 Landscape of the infusion problem: Resin temperature Vs Gate location a) Degree of cure b) Filling time

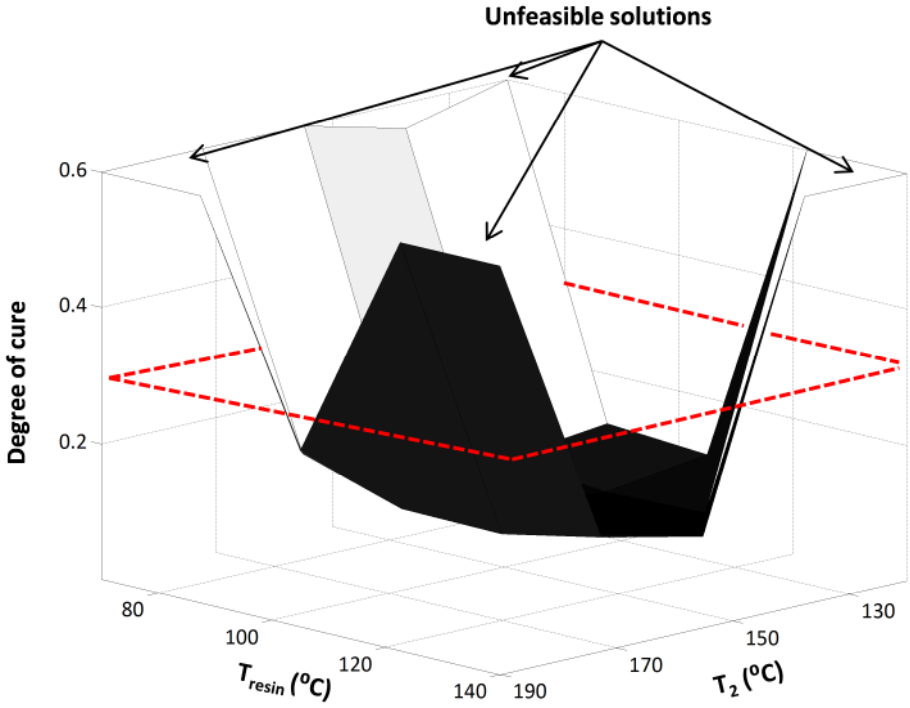

a)

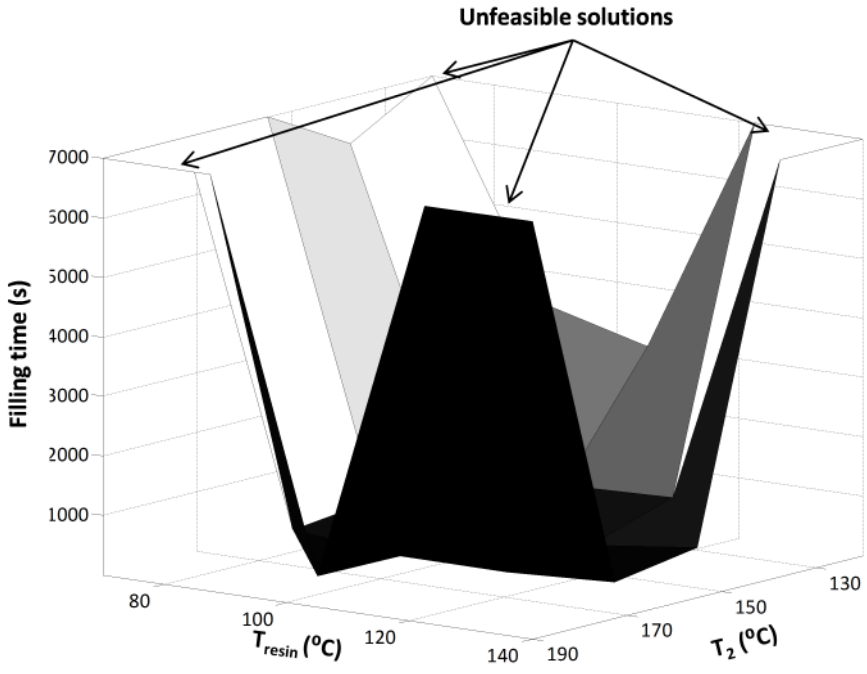

b)

Figure 6-21 Landscape of the infusion problem for gate 3: Resin temperature Vs Second dwell temperature a) Degree of cure b) Filling time

Examination of the surfaces shows that the design parameters must be chosen carefully since the line between a successful filling and an incomplete one is fine. Gate location, resin temperature, first and second dwell temperature in particular proved to be the most critical parameters concerning this. The irregular nature of the objective space, unveiling the presence of many local maxima and minima, justifies the choice of a GA for the solution of the optimisation problem.

6.6 Conclusions

The optimisation procedure developed in this work can be used to optimise gate locations, initial resin temperature and a non-isothermal temperature profile in a VARTM process in order to minimise filling time and degree of cure at the end of filling. The two objectives show a clear trade off resulting in an L-shaped Pareto front. This typical shape gives the opportunity to select a certain combination of design parameters able to provide significant improvements, up to 42% of filling time reduction and up to 14% reduction in final degree of cure with respect to the standard solution. The exhaustive search undertaken provided a better understanding of the process pointing out the critical dependence of the objectives towards changes in initial resin temperature and gate locations. Furthermore, the landscape analysis highlighted the complex nature of the design space proving that the problem studied has no trivial solutions confirming therefore the efficiency, reliability and robustness of the GA used.

7 Multi-objective optimisation: Industrial case study

7.1 Introduction

In this chapter an industrial case study has been addressed in the context of multi-objective process performance and cost optimisation. The aim is to achieve high quality final product manufactured by VARTM combined with cost efficiency. The task has been carried out within the INFUCOMP European project using a cost model developed by the University of Patras University based on a part typical of that produced by Bombardier Aerospace.

7.2 Optimisation methodology

The optimisation methodology is based on the developments presented in Chapter 3 and the strategy reported in Chapter 5 to obtain an optimal cure profile aiming to minimise process cost and maximum temperature overshoot. In order to achieve this two independent interfaces have been built. The cure interface is identical to that described in Section 5.2 with the addition of the surface heat transfer convection coefficient as a new parameter. This implements the link between the cure model built using the MSC.Marc® solver and the optimiser. The addition of the heat transfer coefficient allows further opportunity for optimising the process through the selection of an appropriate tooling and cooling set up. The cost interface implements the link to the cost model developed by the University of Patras. The cost model which is implemented in Microsoft Excel and is specific for the part under study follows the methodology described in [155] and divides the overall process in seven sub-models which take into account different sources of costs for the process:

- Material supply;
- Loading dry fabric in cutting machine, cutting, labelling, wrapping plies and preparing surfboarding;
- Unload of plies, positioning and bagging of panel, panel preforming;
- Positioning, bagging and preforming of the two forwards;
- Join L-stringers and clamp, placing, bagging and preforming T-section;
- Loading T-stringers and bagging, preform panel with stringers;

- Load panel and bagging, tool preparation, curing in autoclave;
- Demolding, rework, inspection and paint.

It has to be pointed out that only the curing in autoclave is a sensitive cost for the optimisation whilst the others act as fixed cost. Each and every sub-model is characterised by a number of cost drivers which are fed to the model as user input. The cost drivers are classified in four categories:

- Part data (i.g. part area, part volume, complexity);
- Process data (i.g. number of workers, infusion profile and cure profile parameters);
- Cost data (i.g. material cost, cost of worker per hour, cost of autoclave operation per hour);
- Depreciation data (i.g. estimated equipment life).

The cost interface is shown schematically in Figure 7-1. A set of inputs is given to the cost model in order to define the location and values of input and output in the Excel worksheets. The path where the Excel file is located is given as well as the number of inputs and outputs. An array is dedicated to the storage of each new input value (InputVal[]), and two more arrays store the location of each of these inputs in the Excel worksheet, one storing the row (InputRow[]), and one the column (InputCol[]). The location of the output is stored in OutputRow[] and OutputCol[]. The inputs are:

- Path of the Excel file;
- Number of inputs (Ninput);
- Number of output (Noutput);
- Array storing input value (InputVal[Ninput]);
- Array storing input row location (InputRow[Ninput]);
- Array storing input column location (InputCol[Ninput]);
- Array storing output row location (OutputRow[Noutput]);
- Array storing output column location (OutputCol[Noutput]).

The output of the cost model is:

- ✓ Process cost ($K_{process}$).

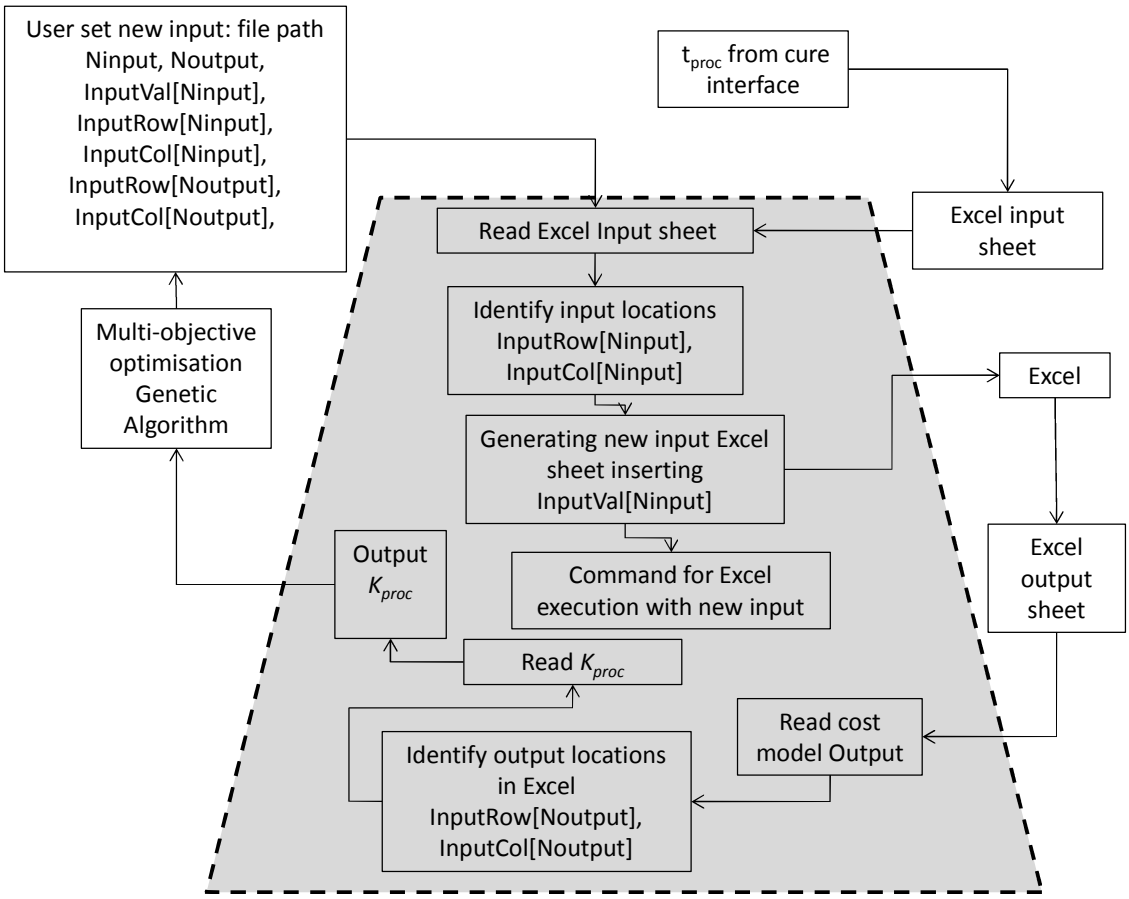

Figure 7-1 Cost interface

Design parameters describing the process are provided directly to the interface (file path, Ninput, Noutput, InputVal[Ninput], InputRow[Ninput], InputCol[Ninput], InputRow[Noutput], InputCol[Noutput]). Then interface opens the Excel file, reads the location where the inputs values are located (InputRow[], InputCol[]) and the Excel worksheet is updated. This is followed by the Excel calculation with the updated inputs. The output worksheet and location are identified (OutputRow[], OutputCol[]) and the interface reads the output, process cost, and sends it to the GA. Among the costs involved in the model the one associated to the autoclave operation has been identified as a characteristic cost for the optimisation. This specific cost for the autoclave operation is fed to the cost model. This specific cost is calculated by multiplying the process time by the cost of the operation per hour of the autoclave and the cost per hour of the workers which are two inputs of the cost model. The process time is withdrawn from the cure interface presented in Chapter 5 and fed at the right

location in the cost model. The cure interface has as input the parameters describing the cure profile, temperature of first and second dwell, duration of first dwell and ramp rate plus the convection coefficient. The general cure profile adopted in this study is presented in Figure 7-2. It is a two dwells cure profile with the two ramps rates at the same rate.

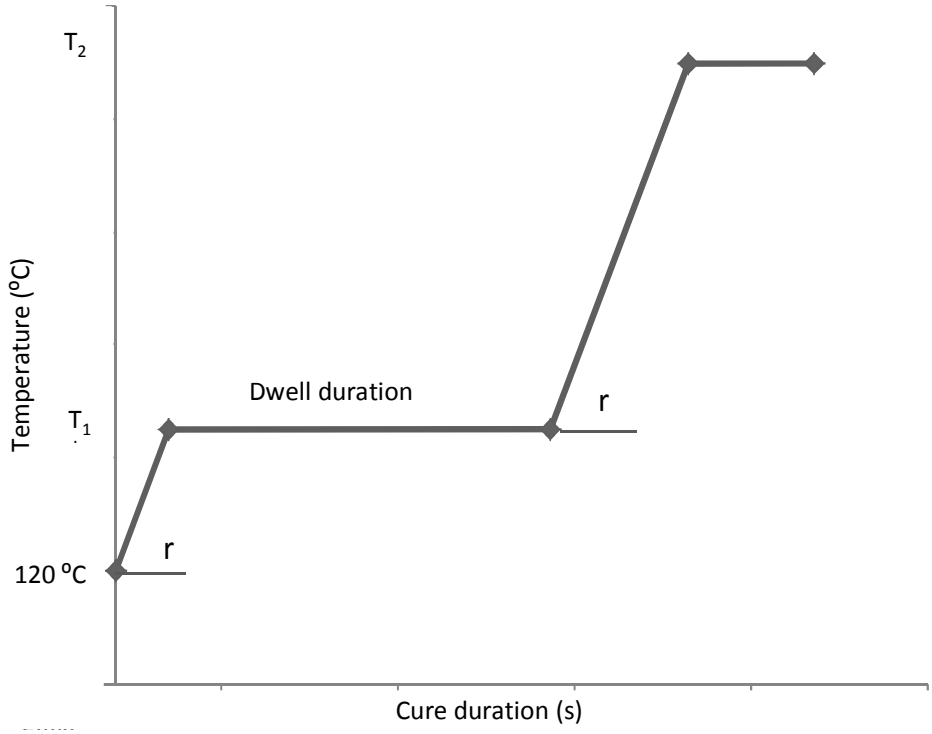

Figure 7-2 Cure profile

The optimisation solution aims to achieve a compromise between process cost and quality of the final part. The process time necessary to evaluate the cost is taken as the time in which the minimum degree of cure reached is 0.85. The parameters chosen to optimise are the cure profile, defined by four parameters (ramp rate, two dwell temperatures and duration of the first dwell) plus the convection coefficient accounting for different insulation/cooling levels. The two objectives chosen for this investigation are process cost which is sent from the cost interface illustrated in Figure 7-1 and maximum temperature overshoot within the part which is sent from the cure interface illustrated in Figure 5-2.

The ranges assigned to each parameter are reported in Table 7-1. The temperature range has been chosen according to the resin system used and its

standard cure profile. The standard cure profile for 890RTM epoxy resin is a 2 h dwell at 180 ºC. Table 7-2 reports the inputs of the optimiser applied for this case study. The number of individuals per generation has been chosen equal to 40 and in order to allow variety to the population a high number for the individuals selected for reproduction has been chosen. The maximum generation number has been chosen to be high. A Pareto size of thirty individuals has been considered large enough to show the Pareto front.

Table 7-1 Values range of parameters

Design Parameters	Ranges
T_1 (^{0}C)	180-210
T_2 (^{0}C)	210-240
Dwell time (s)	1800-10800
Ramp (^{0}C/min)	1-4
H (W/m$^{2.0}$C)	1-10

Table 7-2 Optimisation parameters

GA input	Values
Generations	40
Individuals per population	40
Individuals for reproduction	30
Elite	4
Pareto size	30
Cross-over probability	0.5
Mutation probability	0.005

7.3 Part description

A stiffened panel formed by a skin with three stringers has been selected as a case study. The materials used were carbon fibre G1157 UD [143] and 890 RTM epoxy resin [142]. Due to symmetry reasons a 2D section has been used and only one stringer attached to skin has been considered. The skin is 610 mm

wide and 2616 mm long with 3.6 mm of thickness. The web of the stringer is 4.3 mm thick and the foot is 2 mm thick, whilst the stringer is 3 cm high. Three different lay-up have been designed. According to Figure 7-3 (b), section A-A was [90/0/90/0/0/-45/+45/0/+45/-45/0/0/90/0/90], section B-B [90/0/0/-45/+45/0/90/0/-45/+45] and section C-C [90/0/0/+45/-45/0/90/0].

7.4 Model description

The 2D section of a stiffened panel has been modelled using Marc Mentat®. The overall model comprises 2996 nodes and 1396 elements. In its thickest section the part has a thickness of 5.6 mm. The initial temperature condition was set to 120 ºC and the initial degree of cure at 0.02. The boundary conditions were a prescribed temperature on the tool side in accordance with the cure profile set by the optimisation and air convection on the bag side.

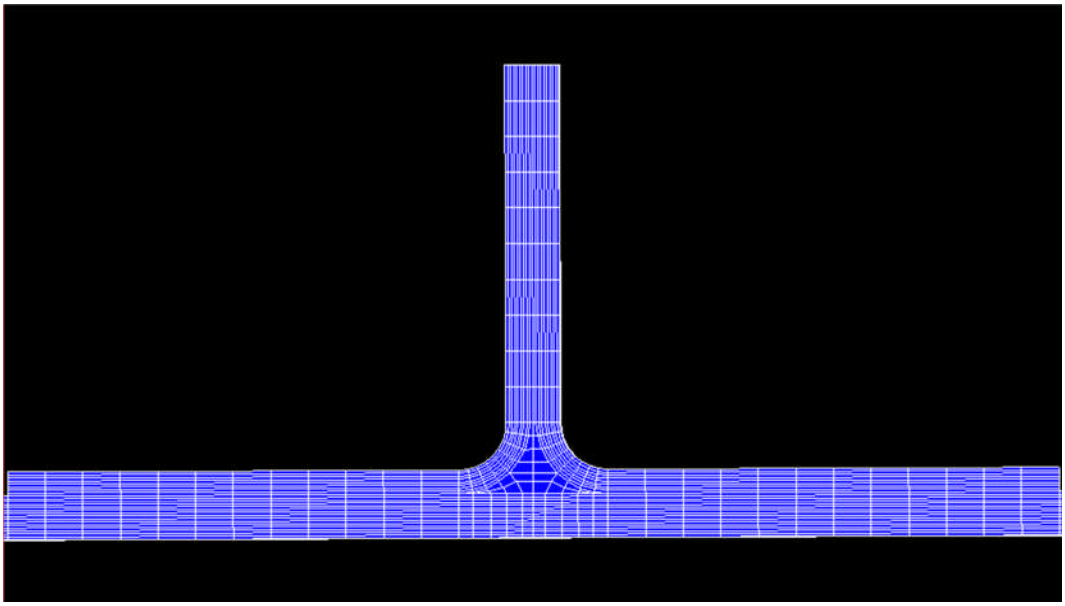

(a)

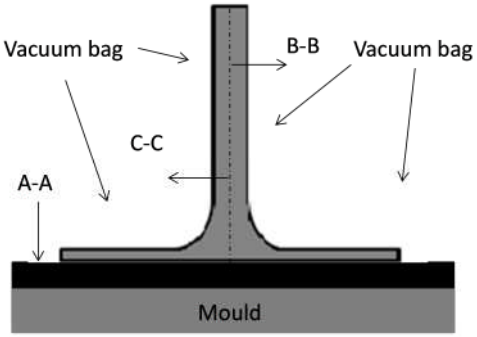

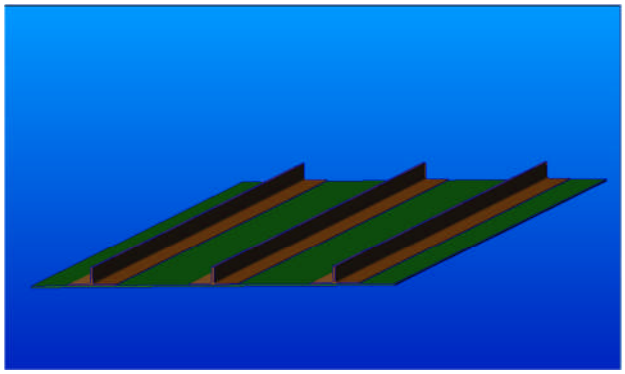

(b) (c)

Figure 7-3 Test case: (a) Finite element model; (b) Cross-section; (c) Isometric view

7.5 Optimisation results

The evolution of the Pareto front for the optimisation of the 2D section of the stiffened panel has been carried out and the results reported in Figure 7-4. The problem addressed is relatively easy from an optimisation point of view. It is still noticeable how better design points are achieved increasing the number of generations. At the first generation the Pareto points are essentially spread horizontally representing benefits only with respect to process cost. When the optimisation reaches the 20th generation the Pareto is enriched with far more

points which occupy more consistently the objective space. The L-shape identifies clearly the presence of a trade-off between process costs and temperature overshoot which relates to part quality. The L-shape front suggests a preferential direction to minimise both process cost and overshoot temperature. It also identifies one region where significant improvement in process cost can be reached without almost affecting the overshoot temperature and vice versa. In the generations after the 20th the optimisation is still able to add some improvements to the final Pareto front slightly moving backward and downward few points belonging to the corner of the L-shape.

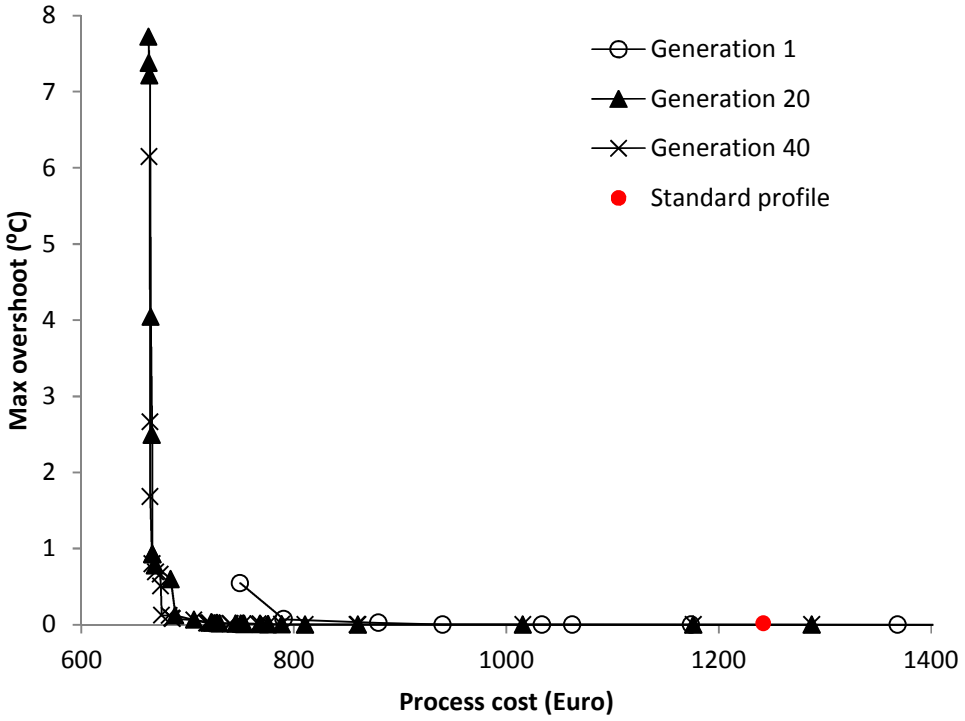

Figure 7-4 Evolution of the Pareto front in the cost/performance optimisation

The L-shape identifies two different areas. A good candidate to represent the typical solution for the horizontal section could be point B, Figure 7-5. These points have first dwell temperature about 200 ºC and second dwell temperature about 230 ºC. The horizontal part away from the corner, represented by point A, is characterised by a very long first dwell around 185 ºC lasting around 9000 s. For these points the process reaches the target of 0.85 degree of cure before the ramp-up toward the second dwell. These are therefore single dwell profiles. These points correspond to the higher process cost (greater than 1000 €). All

the points belonging to the horizontal region (points A and B) have a convection coefficient of around 5 $W/m^{2\circ}C$. Points lying on the vertical section represented by point C have a first dwell temperature of about 210 ºC and second dwell of about 240 ºC and characterised by lower convection coefficients (less than 3 $W/m^{2\circ}C$) which are achievable by increasing the level of insulation of the curing part with the surrounding environment, for instance using an insulating blanket. The combination of both higher dwell temperature with higher insulation produce a quicker process but with higher temperature overshoot. Nevertheless, the overshoots involved in the process are not extraordinary (lower than 7 ºC); therefore the whole Pareto front can be considered as a valid and efficient solution for the process considering both overshoot and process cost.

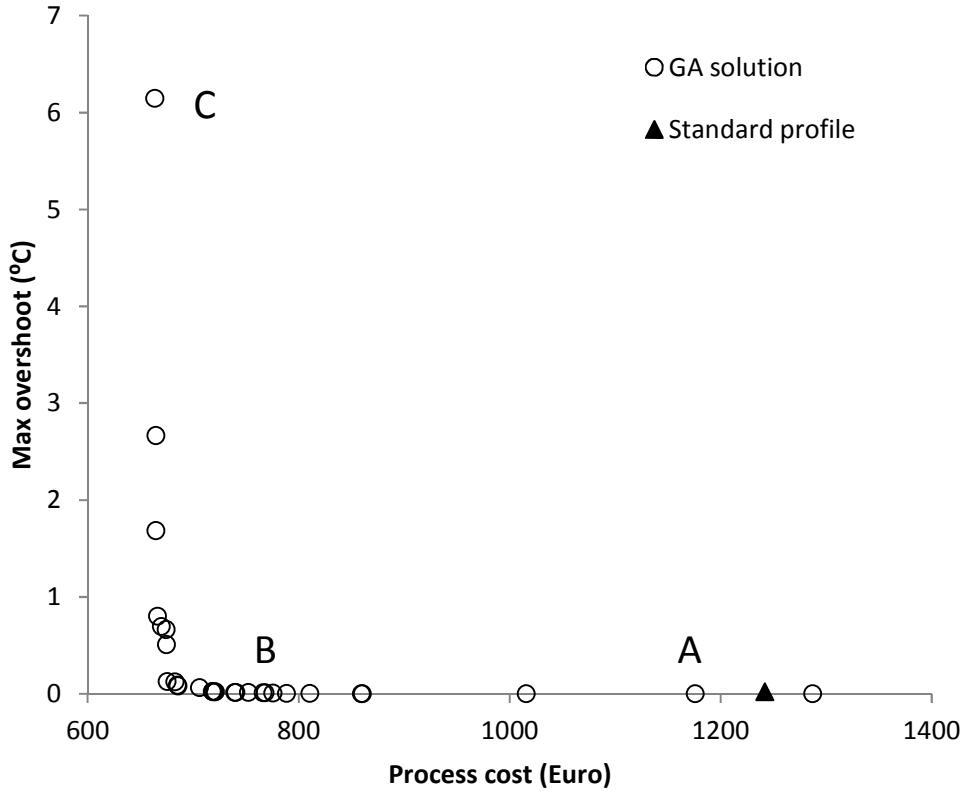

Figure 7-5 Candidate solution for common behaviours

From a comparison with standard profile normally adopted for this resin it is possible to notice a significant reduction in process cost of around 500 €, see Figure 7-5. The standard profile result is in the horizontal part of the Pareto representing large margins for improvements in process cost. The standard

profile is away from the corner confirming that the standard solution usually adopted in manufacturing corresponds to a mild cure profile to ensure that the solution stays as far as possible from the vertical zone, where sudden increase in temperature overshoot can occur. Furthermore, the stability analysis performed in Section 5.5 showed that the points belonging to the horizontal region are more robust toward variability in parameter values. The results of the optimisation also point out that this specific case is not critical with respect to maximum temperature due to the small thickness involved and to the large area influenced by the air convection. This results in a Pareto front where every individual could be used as design point without affecting dramatically the quality of the part

When the standard cure profile is applied the part reaches the desired degree of cure in about 4 hours. Figure 7-6 details the solution found with standard cure profile. It can be noticed that the cure evolves very uniformly along the web. This occurs since there is no significant thermal gradient in the part as all the nodes undergo a similar cure profile with differences in the order of few degrees. This results in a similar evolution of the reaction rate and degree of cure. As shown in Figure 7-6 a) no temperature overshoot occurs confirming the mild nature of the reaction. The individuals belonging to the final Pareto front have design parameters characterised by higher temperature and ramp rate and lower convection coefficient suggesting that the optimisation recognises the mild nature of the reaction in the model and tries to take advantage of that in order to produce a better final Pareto front. Comparing the reaction rate in Figure 7-6 b) with the one presented in Figure 5-8 b), it can be pointed out that the peak in magnitude of the reaction rate is, in this case, smaller (0.0002 1/s).

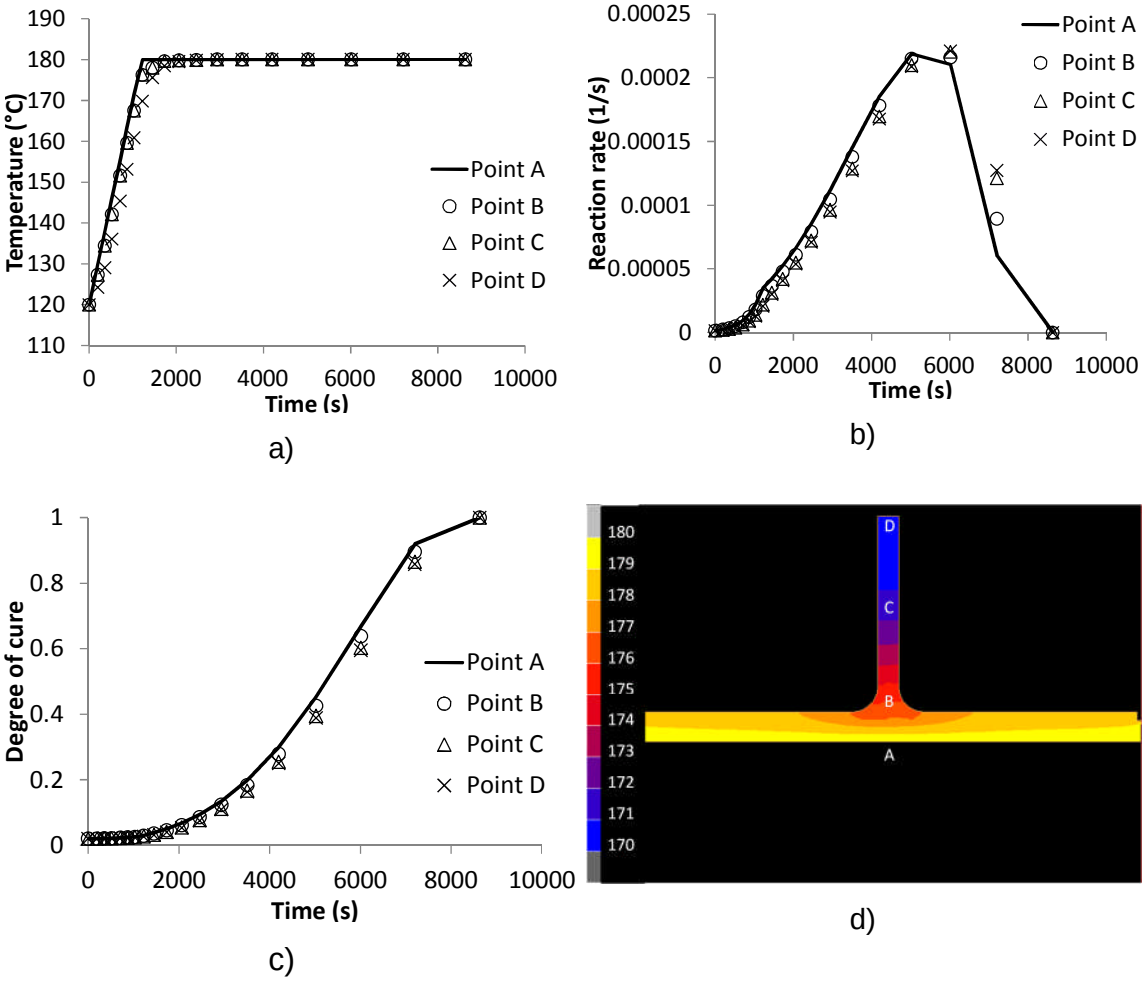

Figure 7-6 Behaviour investigation a) Temperature profile b) Rate of reaction c) Degree of cure (d) Temperature contour map

7.6 Conclusions

Consideration of process cost and quality is necessary as the complexity of parts and corresponding process increases. The methodology presented here can address both these aspects in a multi-objective optimisation context providing a tool to the designer as well as interesting insight of the VARTM highlighting how the current manufacturing procedure can be improved with respect to both quality and cost. The optimisation investigates and reveals new efficient and optimised cure profiles which could lead to significant improvement in the quality and efficiency of the manufacturing industry. A set of efficient optimised solutions has been found able to reduce the process cost by 500 €

without affecting significantly the quality of the part compared with the results obtained using a standard cure profile. This result demonstrates clearly the potential effectiveness of using multi-objective optimisation in the context of process design.

8 Monitoring of infusion process and inverse flow modelling

8.1 Introduction

In this chapter an inverse procedure for the infusion problem is reported based on the GA already illustrated in Chapter 3. The inversion procedure is able to determine an optimal set of three values of permeability, two for the dry fabric and one for the flow media. The inverse procedure arrives eventually to an optimal set by minimising a fitness function which takes into account the difference in arrival times between data from sensors and from model. This allows the on-line estimation of potentially uncertain variable that controls the process using the results obtained by in situ process monitoring.

8.2 Inverse scheme methodology for optimal permeability

An inverse scheme algorithm to estimate permeability values of a fabric and porous media is presented. The assembly comprises the fabric and a layer of porous media to speed up the infusion. The porous media is considered isotropic while the fabric is anisotropic with different permeability in the fibre and transverse directions. The permeability of flow media and fabric in general are subject to a significant variation in terms of both measurement techniques as well as inherent variability in the materials involved [156]. The geometry selected for this study is a flat panel of 30 mm thickness and 210 mm length. The omega infusion pipe is placed along the whole width of the flat panel so that the flow profile is uniform in the width direction. For symmetry reasons the dimension of the problem treated here is reduced to 2D in which through thickness and longitudinal permeability are considered for the fabric. Since the thickness of the part is 30 mm the injection is a single central gate, Figure 8-1.

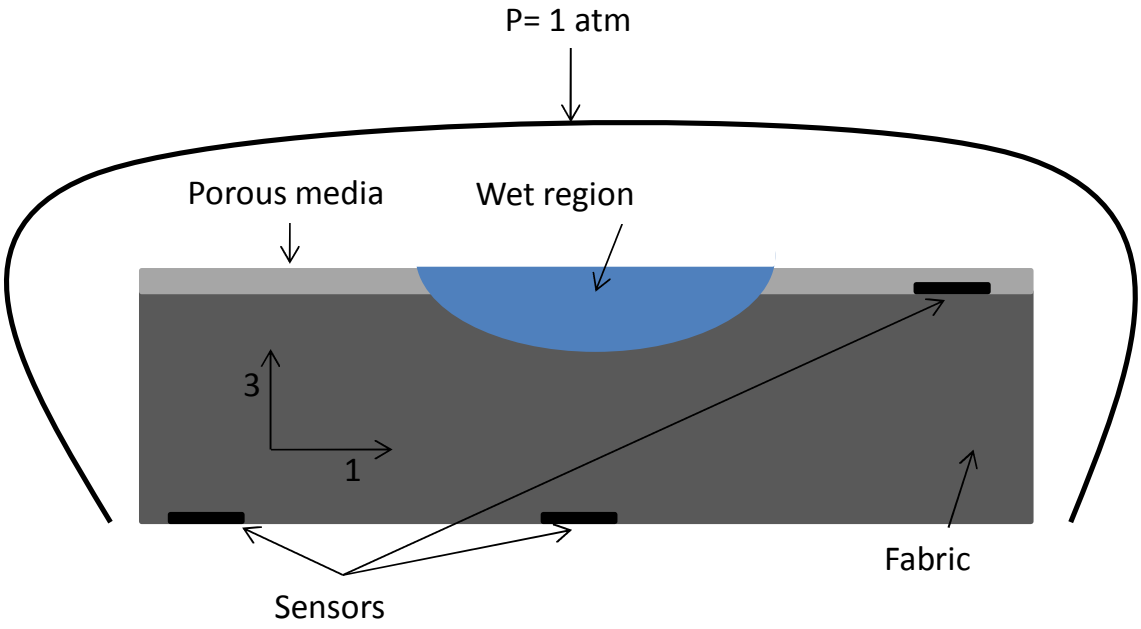

Figure 8-1 Domain of the inverse problem in case of infusion of a flat panel

Three dielectric sensors have been used to signal the resin arrival time at specific locations. A fitness function has been formulated to take into account the difference between the arrival time from the experiment and the arrival time predicted by the model. The minimisation of the fitness function, *D*, constitutes the inverse problem.

$$D = \frac{\sqrt{\sum_i \left(t^i_{model} - t^i_{monitoring}\right)^2}}{n} \tag{8-1}$$

where *n* is the number of sensors the resin has arrived at, t^i_{model} and $t^i_{monitoring}$ are respectively the arrival time at a specific sensors predicted by the model and from the monitoring experiment. Three variables are estimated based on the minimisation of this difference as follows:

- ✓ Longitudinal permeability (K_1);
- ✓ Through thickness permeability (K_3);
- ✓ Flow media permeability (K_{media}).

Table 8-1 reports the permeability range set for the inverse problem.

Table 8-1 Permeability ranges

Permeability	Permeability ranges (m^2)
Longitudinal permeability (K_1)	$1{\cdot}10^{-11}$-$1{\cdot}10^{-10}$
Through thickness permeability (K_3)	$1{\cdot}10^{-13}$-$1{\cdot}10^{-12}$
Flow media permeability (K_{media})	$1{\cdot}10^{-10}$-$1{\cdot}10^{-9}$

The solution of the inverse problem involves the communication among three separate codes. The FEM software Proflot® which uses the viscosity model introduced in Section 4.5.5, the GA optimiser presented in Chapter 2 and the Cranfield Measurements and control system (CMC) which acquires the measurement from the sensors and writes them in a text file which constitutes the output of the system. Figure 8-2 reports the interface to handle the inverse problem. The three parameters values (longitudinal, through thickness and flow media permeability) are produced by the GA and are directly fed to the interface. The interface reads the input file generated by the solver Proflot®. Subsequently the locations where the new parameters must be inserted in the old input file are identified and the input file modified. After that command for the execution of Proflot® using the new input file is generated and run. Once the simulation is terminated the interface opens and reads the output file generated. The locations where the output are stored (arrival times at sensors locations) are identified and the values are withdrawn. Impedance data from sensors are fed to the interface through an ASCII file generated by CMC during the infusion. The impedance data are evaluated by the interface to evaluate whether the resin has reached the sensor. Then the fitness function is computed and evaluated and the result is sent to the GA. In order to handle the described problem effectively, the interface must be able to handle the unknown parameters (three permeabilities), the minimisation of the fitness function *D* and the data coming from the monitoring (impedances) between Proflot®, the optimiser GA and the CMC system. At this stage the methodology has been tested by means of an artificial experiment in which artificial noise from sensors is modelled as a normally distributed variable. Noise is expected to alter the

sensor response resulting in a deviation of arrival times measured from the real ones. The purpose of the tests carried out here is to evaluate the quality, reliability and robustness of permeability approximation depending on noise level.

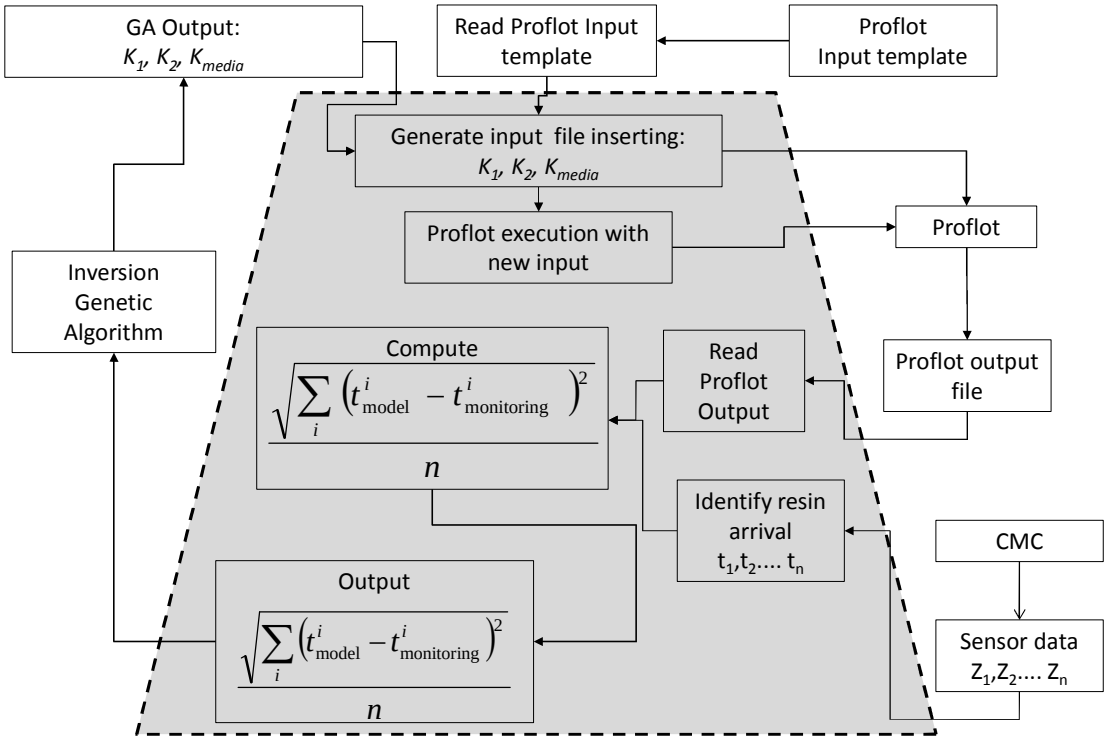

Figure 8-2 Structure of the interface between Proflot®, the inversion GA and CMC

8.3 Part description

The materials used are G1157 carbon fibres [143] and RTM6 epoxy resin system [141]. Central injection is used. The stack of carbon reinforcement is topped by a glass fibre PTFE coated porous media used to enhance the flow speed. The part close to the edges has been left uncovered. The volume fibre fraction is 60%. The lay-up is unidirectional and the resin temperature at injection is 80 ºC. Two initial conditions are applied: the initial temperature of the fabric is set at 120 ºC and the initial degree of cure at 2%.

8.4 Model description

A 2D section of the 30 mm thick flat panel has been modelled in PAM-RTM®, Figure 8-3. Two boundary conditions are applied to the model illustrated in Figure 8-3: fixed temperature is set at 120 ºC for the nodes at the bottom of the model and natural air convection is applied on top and left side. No boundary condition is applied on the right side as it lies on the line of symmetry.

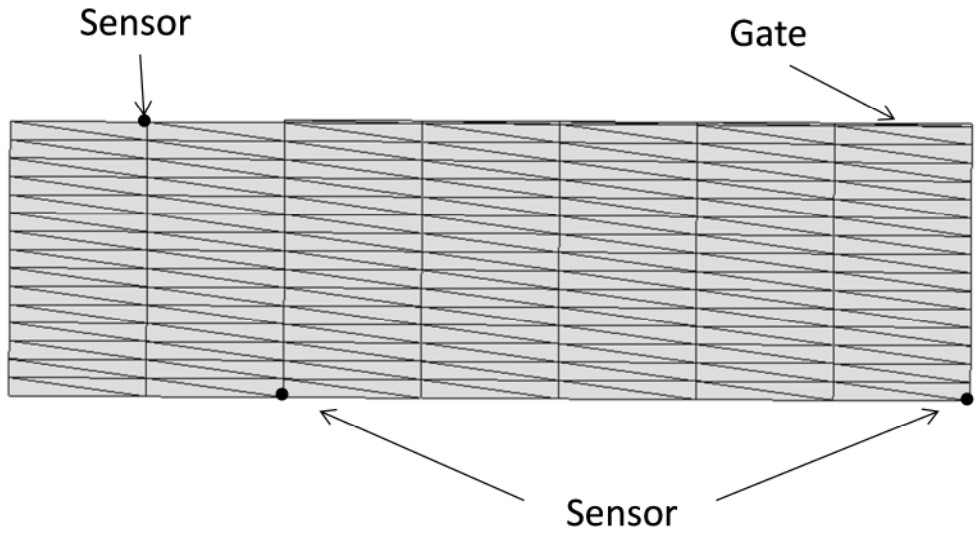

Figure 8-3 Half section of flat panel

8.5 Artificial experiment set up

The performance of the scheme has been tested for three different levels of noise in arrival times: 5 s, 13 s and 25 s. The GA was executed for ten generations. Ten generations have been chosen as a good compromise between convergence and run times. The values utilised for the noisy data were obtained by drawing random numbers for a normal distribution. The aim was to obtain an average value of effective noise from each sensor equal to 5 s, 13 s, 25 s. An effective noise defined as such allows testing of the inverse scheme in different operating conditions regarding the sensors functionality and reliability, i.e. there are different ways to distribute the noise to each sensor and yet having the same total noise, each of these can represent a different working condition. The total noise, calculated as the sum of the noise coming from each sensor, has been set equal to 15 s, 39 s and 75 s. This total effective noise is then divided by the number of sensors, three in this case. Thirty realisations

were used for each noise level. The GA set up is detailed in Table 8-2. The results have been compared at the 10^{th} generation.

Table 8-2 Parameters of the GA

GA input	Values
Number of generations	10
Individuals	40
Individuals used in reproduction	35
Elite individuals	4
Mutation probability	0.005
Cross-over probability	0.5

Three permeability values have been selected as reference to generate a triplet of arrival times at the three sensors (Table 8-3). In order to achieve that the model built in PAM-RTM® has been run to provide the triplet of reference arrival times at the three sensors. The three arrival times obtained using the reference permeability values are 115 s at sensor 1, 605 s at sensor 2 and 657 s at sensor 3.

Table 8-3 Permeability values and ranges utilised in the GA

	Exact values	Lower limit	Upper limit
K_1 (m^2)	$1.5 \cdot 10^{-11}$	$1.0 \cdot 10^{-11}$	$1.0 \cdot 10^{-10}$
K_3 (m^2)	$5.0 \cdot 10^{-13}$	$1.0 \cdot 10^{-13}$	$1.0 \cdot 10^{-12}$
K_p (m^2)	$9.7 \cdot 10^{-10}$	$1.0 \cdot 10^{-10}$	$1.0 \cdot 10^{-9}$

For each noise level 30 different realisations and 30 different arrival times triplets have been drawn and the optimisation run over ten generations. Tables

8-4 – 8-6 report the arrival time triplets along with the permeability output at the last generation for each noise level.

Table 8-4 Arrival times at sensors and permeability output for 5 s noise

Realisations	Arrival time sensor 1 (s)	Arrival time sensor 2 (s)	Arrival time sensor 3 (s)	K_1 (m^2)	K_3 (m^2)	K_p (m^2)
1	109	606	649	$1.5 \cdot 10^{-11}$	$4.97 \cdot 10^{-13}$	$9.65 \cdot 10^{-10}$
2	118	609	665	$1.5 \cdot 10^{-11}$	$4.97 \cdot 10^{-13}$	$9.65 \cdot 10^{-10}$
3	108	605	665	$1.5 \cdot 10^{-11}$	$4.83 \cdot 10^{-13}$	$9.79 \cdot 10^{-10}$
4	106	609	659	$1.5 \cdot 10^{-11}$	$5.11 \cdot 10^{-13}$	$6.60 \cdot 10^{-10}$
5	121	598	655	$1.35 \cdot 10^{-11}$	$5.04 \cdot 10^{-13}$	$9.93 \cdot 10^{-10}$
6	115	596	663	$1.5 \cdot 10^{-11}$	$5.04 \cdot 10^{-13}$	$9.29 \cdot 10^{-10}$
7	112	597	661	$1.5 \cdot 10^{-11}$	$4.97 \cdot 10^{-13}$	$9.57 \cdot 10^{-10}$
8	112	605	669	$1.43 \cdot 10^{-11}$	$4.97 \cdot 10^{-13}$	$9.65 \cdot 10^{-10}$
9	122	606	650	$1.5 \cdot 10^{-11}$	$5.25 \cdot 10^{-13}$	$6.95 \cdot 10^{-10}$
10	121	611	660	$1.5 \cdot 10^{-11}$	$4.97 \cdot 10^{-13}$	$9.65 \cdot 10^{-10}$
11	106	602	654	$1.5 \cdot 10^{-11}$	$4.90 \cdot 10^{-13}$	$8.94 \cdot 10^{-10}$
12	108	608	652	$1.92 \cdot 10^{-11}$	$4.97 \cdot 10^{-13}$	$6.10 \cdot 10^{-10}$
13	108	600	660	$1.5 \cdot 10^{-11}$	$4.83 \cdot 10^{-13}$	$1.00 \cdot 10^{-9}$
14	110	601	651	$1.5 \cdot 10^{-11}$	$5.04 \cdot 10^{-13}$	$8.94 \cdot 10^{-10}$
15	118	613	653	$1.5 \cdot 10^{-11}$	$4.90 \cdot 10^{-13}$	$9.79 \cdot 10^{-10}$
16	111	597	654	$2.2 \cdot 10^{-11}$	$4.83 \cdot 10^{-13}$	$7.66 \cdot 10^{-10}$
17	110	606	666	$1.5 \cdot 10^{-11}$	$4.83 \cdot 10^{-13}$	$9.79 \cdot 10^{-10}$
18	124	600	658	$1.5 \cdot 10^{-11}$	$5.11 \cdot 10^{-13}$	$9.22 \cdot 10^{-10}$
19	103	603	658	$1.5 \cdot 10^{-11}$	$4.90 \cdot 10^{-13}$	$9.79 \cdot 10^{-10}$
20	117	613	652	$1.5 \cdot 10^{-11}$	$4.90 \cdot 10^{-13}$	$9.79 \cdot 10^{-10}$
21	120	603	649	$1.5 \cdot 10^{-11}$	$5.04 \cdot 10^{-13}$	$8.51 \cdot 10^{-10}$
22	111	609	664	$1.5 \cdot 10^{-11}$	$4.83 \cdot 10^{-13}$	$9.79 \cdot 10^{-10}$
23	108	611	655	$1.64 \cdot 10^{-11}$	$4.83 \cdot 10^{-13}$	$9.50 \cdot 10^{-10}$
24	114	615	661	$1.5 \cdot 10^{-11}$	$4.83 \cdot 10^{-13}$	$1.00 \cdot 10^{-9}$
25	119	607	666	$1.5 \cdot 10^{-11}$	$4.97 \cdot 10^{-13}$	$9.65 \cdot 10^{-10}$
26	125	608	659	$1.5 \cdot 10^{-11}$	$4.97 \cdot 10^{-13}$	$8.80 \cdot 10^{-10}$
27	120	612	660	$1.5 \cdot 10^{-11}$	$4.97 \cdot 10^{-13}$	$9.65 \cdot 10^{-10}$
28	118	607	667	$1.5 \cdot 10^{-11}$	$4.83 \cdot 10^{-13}$	$1.00 \cdot 10^{-9}$
29	121	605	666	$1.5 \cdot 10^{-11}$	$5.04 \cdot 10^{-13}$	$9.22 \cdot 10^{-10}$
30	126	602	656	$1.64 \cdot 10^{-11}$	$4.83 \cdot 10^{-13}$	$8.72 \cdot 10^{-10}$

Table 8-5 Arrival times at sensors and permeability output for 13 s noise

Realisations	Arrival time sensor 1 (s)	Arrival time sensor 2 (s)	Arrival time sensor 3 (s)	K_1 (m^2)	K_3 (m^2)	K_p (m^2)
1	100	610	638	$2.63 \cdot 10^{-11}$	$4.69 \cdot 10^{-13}$	$5.89 \cdot 10^{-10}$
2	125	616	675	$1.35 \cdot 10^{-11}$	$4.83 \cdot 10^{-13}$	$9.93 \cdot 10^{-10}$
3	97	605	678	$1.50 \cdot 10^{-11}$	$4.97 \cdot 10^{-13}$	$9.65 \cdot 10^{-10}$
4	93	616	663	$1.78 \cdot 10^{-11}$	$4.83 \cdot 10^{-13}$	$8.80 \cdot 10^{-10}$
5	130	588	650	$1.35 \cdot 10^{-11}$	$5.11 \cdot 10^{-13}$	$9.72 \cdot 10^{-10}$
6	114	585	675	$1.21 \cdot 10^{-11}$	$4.97 \cdot 10^{-13}$	$9.65 \cdot 10^{-10}$
7	108	587	671	$1.50 \cdot 10^{-11}$	$4.97 \cdot 10^{-13}$	$9.43 \cdot 10^{-10}$
8	111	611	686	$1.50 \cdot 10^{-11}$	$4.97 \cdot 10^{-13}$	$7.24 \cdot 10^{-10}$
9	132	612	642	$1.35 \cdot 10^{-11}$	$4.97 \cdot 10^{-13}$	$9.79 \cdot 10^{-10}$
10	127	624	665	$1.50 \cdot 10^{-11}$	$4.97 \cdot 10^{-13}$	$7.73 \cdot 10^{-10}$
11	94	597	647	$1.92 \cdot 10^{-11}$	$4.90 \cdot 10^{-13}$	$8.09 \cdot 10^{-10}$
12	95	612	645	$2.20 \cdot 10^{-11}$	$4.69 \cdot 10^{-13}$	$8.58 \cdot 10^{-10}$
13	100	590	666	$1.57 \cdot 10^{-11}$	$4.83 \cdot 10^{-13}$	$9.72 \cdot 10^{-10}$
14	102	594	642	$2.28 \cdot 10^{-11}$	$4.76 \cdot 10^{-13}$	$7.09 \cdot 10^{-10}$
15	122	625	645	$2.06 \cdot 10^{-11}$	$5.25 \cdot 10^{-13}$	$1.28 \cdot 10^{-10}$
16	104	586	648	$1.78 \cdot 10^{-11}$	$5.39 \cdot 10^{-13}$	$6.95 \cdot 10^{-10}$
17	101	609	678	$1.50 \cdot 10^{-11}$	$4.83 \cdot 10^{-13}$	$9.65 \cdot 10^{-10}$
18	138	593	661	$1.21 \cdot 10^{-11}$	$5.11 \cdot 10^{-13}$	$9.93 \cdot 10^{-10}$
19	86	599	661	$1.50 \cdot 10^{-11}$	$4.83 \cdot 10^{-13}$	$1.00 \cdot 10^{-9}$
20	120	626	644	$2.06 \cdot 10^{-11}$	$5.25 \cdot 10^{-13}$	$1.57 \cdot 10^{-10}$
21	128	600	636	$2.20 \cdot 10^{-11}$	$4.90 \cdot 10^{-13}$	$6.95 \cdot 10^{-10}$
22	105	616	675	$1.92 \cdot 10^{-11}$	$4.83 \cdot 10^{-13}$	$7.17 \cdot 10^{-10}$
23	95	620	653	$2.06 \cdot 10^{-11}$	$4.83 \cdot 10^{-13}$	$5.11 \cdot 10^{-10}$
24	112	630	668	$1.43 \cdot 10^{-11}$	$4.69 \cdot 10^{-13}$	$9.65 \cdot 10^{-10}$
25	124	610	682	$1.21 \cdot 10^{-11}$	$4.90 \cdot 10^{-13}$	$9.93 \cdot 10^{-10}$
26	143	611	662	$1.35 \cdot 10^{-11}$	$4.97 \cdot 10^{-13}$	$9.43 \cdot 10^{-10}$
27	132	619	665	$1.50 \cdot 10^{-11}$	$5.11 \cdot 10^{-13}$	$6.88 \cdot 10^{-10}$
28	125	610	681	$1.21 \cdot 10^{-11}$	$4.97 \cdot 10^{-13}$	$9.22 \cdot 10^{-10}$
29	127	581	660	$1.50 \cdot 10^{-11}$	$5.39 \cdot 10^{-13}$	$6.53 \cdot 10^{-10}$
30	117	591	634	$2.20 \cdot 10^{-11}$	$4.90 \cdot 10^{-13}$	$6.95 \cdot 10^{-10}$

Table 8-6 Arrival times at sensors and permeability output for 25 s noise

Realisations	Arrival time sensor 1 (s)	Arrival time sensor 2 (s)	Arrival time sensor 3 (s)	K_1 (m^2)	K_3 (m^2)	K_p (m^2)
1	86	615	621	$2.35 \cdot 10^{-11}$	$4.61 \cdot 10^{-13}$	$9.22 \cdot 10^{-10}$
2	132	623	697	$1.21 \cdot 10^{-11}$	$4.83 \cdot 10^{-13}$	$9.01 \cdot 10^{-10}$
3	80	604	696	$1.50 \cdot 10^{-11}$	$4.97 \cdot 10^{-13}$	$7.24 \cdot 10^{-10}$
4	73	625	670	$2.20 \cdot 10^{-11}$	$4.40 \cdot 10^{-13}$	$9.36 \cdot 10^{-10}$
5	145	572	645	$1.50 \cdot 10^{-11}$	$5.82 \cdot 10^{-13}$	$6.39 \cdot 10^{-10}$
6	113	567	692	$1.10 \cdot 10^{-11}$	$5.04 \cdot 10^{-13}$	$9.65 \cdot 10^{-10}$
7	100	573	685	$1.50 \cdot 10^{-11}$	$4.97 \cdot 10^{-13}$	$1.00 \cdot 10^{-9}$
8	107	620	709	$1.43 \cdot 10^{-11}$	$4.69 \cdot 10^{-13}$	$9.29 \cdot 10^{-10}$
9	144	624	630	$1.80 \cdot 10^{-11}$	$5.39 \cdot 10^{-13}$	$2.84 \cdot 10^{-10}$
10	135	643	674	$1.43 \cdot 10^{-11}$	$4.83 \cdot 10^{-13}$	$8.30 \cdot 10^{-10}$
11	73	590	639	$2.35 \cdot 10^{-11}$	$4.76 \cdot 10^{-13}$	$9.22 \cdot 10^{-10}$
12	77	618	633	$2.91 \cdot 10^{-11}$	$4.69 \cdot 10^{-13}$	$1.50 \cdot 10^{-10}$
13	86	576	674	$2.20 \cdot 10^{-11}$	$4.69 \cdot 10^{-13}$	$9.36 \cdot 10^{-10}$
14	93	582	627	$2.13 \cdot 10^{-11}$	$4.90 \cdot 10^{-13}$	$1.00 \cdot 10^{-9}$
15	129	642	633	$2.06 \cdot 10^{-11}$	$5.18 \cdot 10^{-13}$	$1.21 \cdot 10^{-10}$
16	94	567	641	$2.13 \cdot 10^{-11}$	$4.83 \cdot 10^{-13}$	$9.79 \cdot 10^{-10}$
17	89	611	700	$1.50 \cdot 10^{-11}$	$4.97 \cdot 10^{-13}$	$8.30 \cdot 10^{-10}$
18	161	583	664	$1.21 \cdot 10^{-11}$	$5.46 \cdot 10^{-13}$	$6.53 \cdot 10^{-10}$
19	60	594	666	$6.31 \cdot 10^{-11}$	$3.41 \cdot 10^{-13}$	$9.36 \cdot 10^{-10}$
20	123	645	630	$2.06 \cdot 10^{-11}$	$5.18 \cdot 10^{-13}$	$1.78 \cdot 10^{-10}$
21	141	596	617	$1.50 \cdot 10^{-11}$	$5.39 \cdot 10^{-13}$	$7.38 \cdot 10^{-10}$
22	95	628	689	$1.50 \cdot 10^{-11}$	$4.97 \cdot 10^{-13}$	$7.73 \cdot 10^{-10}$
23	77	634	649	$2.49 \cdot 10^{-11}$	$4.26 \cdot 10^{-13}$	$8.30 \cdot 10^{-10}$
24	108	654	676	$1.50 \cdot 10^{-11}$	$4.47 \cdot 10^{-13}$	$9.93 \cdot 10^{-10}$
25	132	613	707	$1.21 \cdot 10^{-11}$	$4.90 \cdot 10^{-13}$	$8.65 \cdot 10^{-10}$
26	169	616	667	$1.50 \cdot 10^{-11}$	$5.39 \cdot 10^{-13}$	$3.20 \cdot 10^{-10}$
27	145	634	673	$1.50 \cdot 10^{-11}$	$5.11 \cdot 10^{-13}$	$4.90 \cdot 10^{-10}$
28	128	614	710	$1.21 \cdot 10^{-11}$	$4.69 \cdot 10^{-13}$	$1.00 \cdot 10^{-9}$
29	138	557	661	$1.07 \cdot 10^{-11}$	$5.32 \cdot 10^{-13}$	$1.00 \cdot 10^{-9}$
30	119	578	613	$2.20 \cdot 10^{-11}$	$4.90 \cdot 10^{-13}$	$9.29 \cdot 10^{-10}$

Figure 8-4 illustrates the evolution of the permeability values over the ten generations run. It can be observed that the inverse scheme under study is able to successfully achieve the correct estimation of fabric longitudinal and through thickness permeabilities. Concerning longitudinal permeability for a total level of noise up to 13 s the final value found is close to the exact value (10% difference), while for 25 s of noise the results separate around 20% from the exact value. Regarding through thickness permeability the results are even better with a maximum difference at 25 s noise level of 2% from the exact value. As concern the flow media permeability the results are more sensitive to the noise factor having already at 5 s noises a difference of 6% from the exact value. The GA proved to be effective in all cases. The biased behaviour in non-converging cases is due to the asymmetry of the parameter range used in the GA.

Figure 8-5 illustrates the dependence of final permeability values on noise. It can be observed that the estimation of fabric permeability is highly robust, whereas that of the porous media more challenging. This is probably due to geometrical reasons. The flow in the porous media is much faster than in the fabric therefore changes in flow media permeability have less influence on the arrival time (specifically on the arrival time at sensor 1) in a way that the information about flow media permeability from the arrival time at sensor 1 will be screened by the other two arrival times when computed in the fitness function. Bearing this in mind it can be concluded that higher changes in flow media permeability are allowed affecting the arrival time less. This results in weak influence of this measurement on the fitness function. A way to make this information significant would be weighing the information from sensor 1 allowing it to play a more significant role in the fitness function.

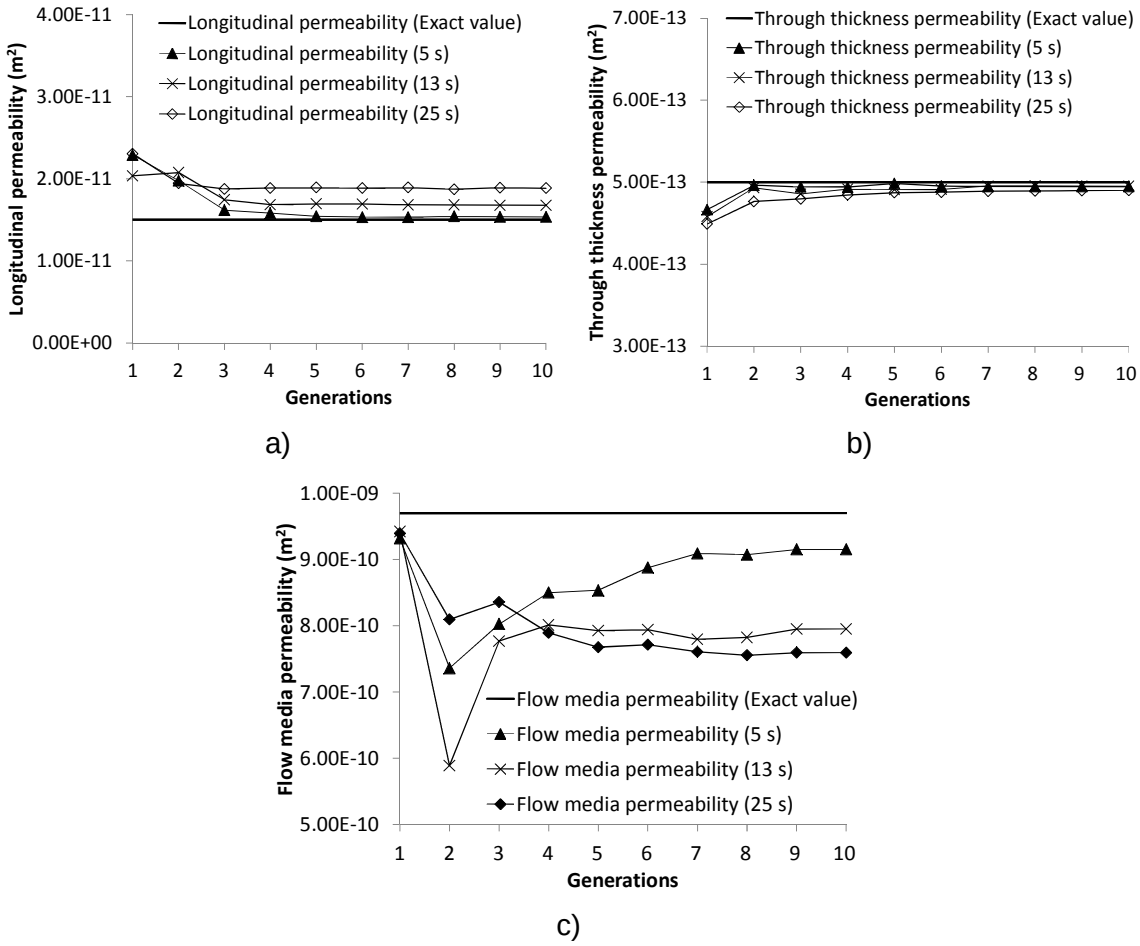

Figure 8-4 Average permeability convergence: (a) Longitudinal permeability; (b) Through thickness permeability; (c) Flow media permeability.

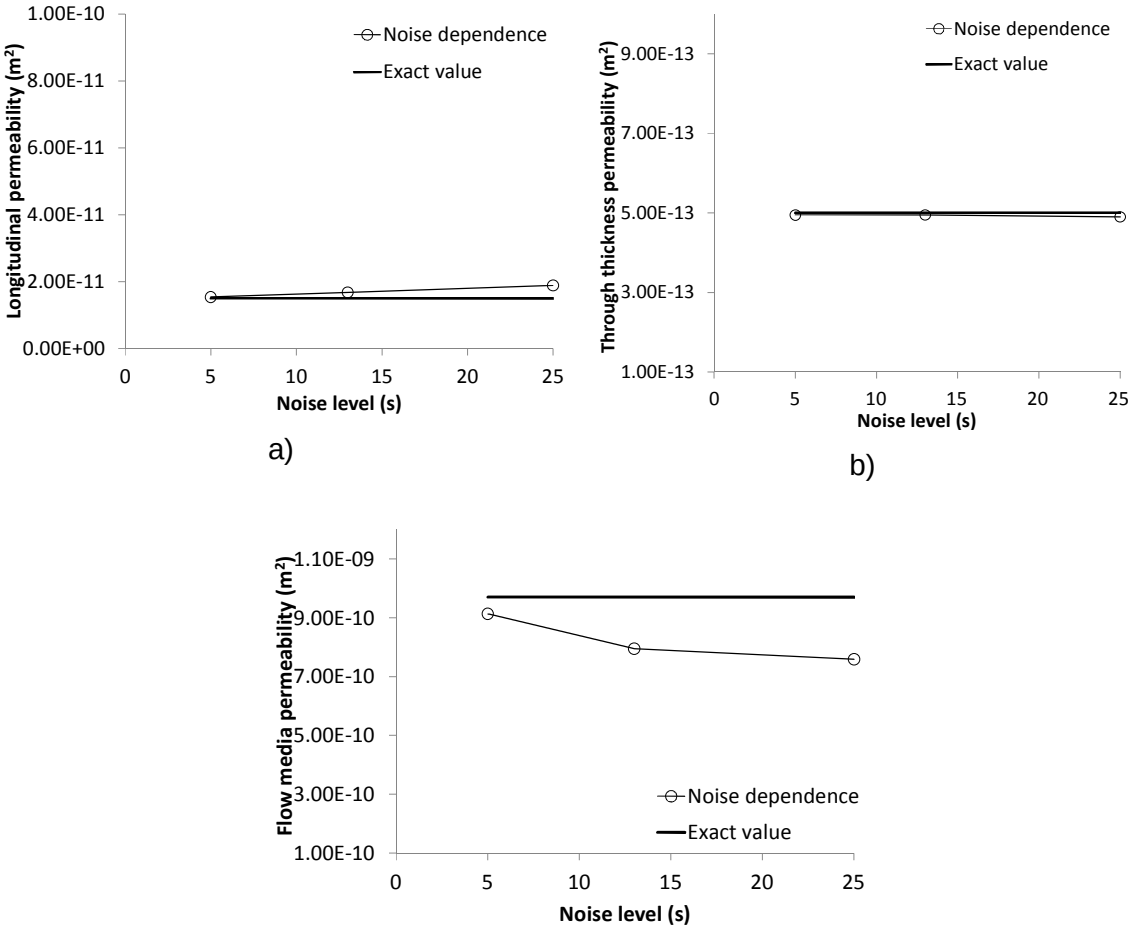

Figure 8-5 Average estimated permeability dependence on noise: (a) Longitudinal permeability; (b) Through thickness permeability; (c) Flow media permeability.

The permeability distributions at the 10th generation for each case (longitudinal, through thickness and flow media permeability) have been plotted in a box whiskers plot (Figure 8-6). It can be observed that in all cases the average value is very close to the correct one even though as the noise level increase the solution becomes more noisy. Nevertheless, the average values of all distribution lie close to the exact value meaning that the majority of the results are close to the correct theoretical ones.

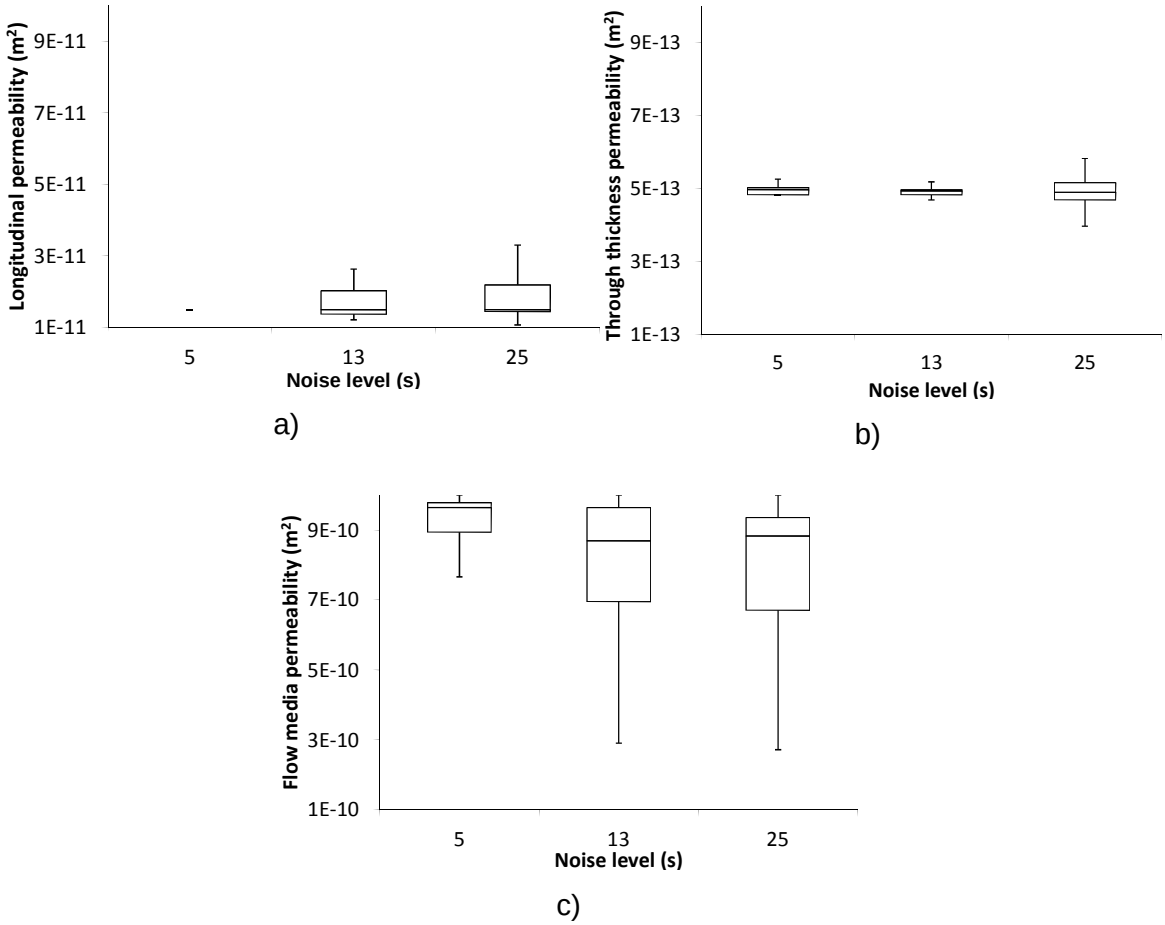

Figure 8-6 Box whisker plot: (a) Longitudinal permeability; (b) Through thickness permeability; (c) Flow media permeability.

8.6 Conclusions

An inversion procedure for the Infusion stage of a VARTM process able to find uncertain permeability values of dry fabric and porous media has been developed and applied to artificial experimental data. The inverse scheme has been tested building several different possible scenarios accounting for three possible different level of noise in the response of flow sensors. The scheme showed good results concerning accuracy up to 5 s of noise associated to each measurement, while for values of noise over 10 s per measurement the estimation is affected resulting in poor accuracy especially in the flow media permeability evaluation.

9 Overall discussion

The investigation addressed in this thesis concerned the development of new methodologies for the optimisation of the VARTM process to improve both filling and cure stage. Until now optimisation of the VARTM process has been addressed neither in a multi-objective optimisation fashion nor in single-objective optimisation. The present study constitutes the first work regarding the optimisation of the VARTM process. The optimisation has been addressed in a multi-objective fashion with the intent to tackle both quality and cost of the process. The extensive literature survey undergone proved that GAs have been mainly used to deal with multi-objective problems. In the light of this a GA strategy has been chosen, developed and tested against four different benchmarks for the purpose of this work. The GA proved to be a reliable and a robust tool capable to handle both convex and non-convex problems. The VARTM process involves two different stages, the filling and the cure stage which have been addressed separately. Cost and quality related objectives have been selected together with sensitive parameters for both stages. The application of the optimisation methodology successfully dealt with the two problems producing meaningful trade-off between the objectives and providing to the designer a set of new feasible design points which compared with the ones obtained by applying standard profile showed significant improvements. When the cost model of the process has been directly implemented a substantial reduction of the process cost was achieved (up to 500 €). Nevertheless a stability analysis showed that not all the individuals in the Pareto front own the same degree of stability and robustness toward parameter swing. Therefore the designer has to pick the design points according to the quality of the equipment available. Furthermore an investigation of the problem landscape pointed out the complex nature of the relationship between the chosen parameters and objectives ending in a domain rich of local minima and maxima in which a gradient technique could be trapped, enforcing the GA choice. One of the most difficult aspects involved in the filling stage to obtain a good accord between experiment and model prediction is related to the estimation of the permeability of the fabric. For this purpose an inverse scheme to estimate dry

fabric and flow media permeabilities has been developed. The inversion procedure has been tested by means of artificial experiments aiming to prove the robustness of the procedure when dealing with noisy measurements. Flexibility of the interfaces developed also allows the methodologies to be able to deal with different FEM packages.

The application of the new methodologies to the manufacturing process unveiled qualitatively and quantitatively the relationships between the objective and design spaces manifesting themselves in the form of trade-offs between objectives. The trade-offs have a characteristic L-shape which points out the competitive relationship between the objectives taken into account. The shape of the Pareto front also explicitly depicts the presence of three different regions in which three different design strategies can be selected according to the requirements of the specific end user. The trade-offs found represent compromise points between cost and quality so that the process can be set in accordance with resource availability and quality requirements. The discovery of trade-offs together with the unfolding of the unknown landscape brings a new knowledge of the process and new awareness in terms of decision making. The methodologies developed here can serve as a starting point for development of more controllable and easier to design processes accompanied by predictive knowledge of cost and product quality.

Nowadays, the need to predict, understand and quantify the consequences of design choices on the final product in terms of cost and quality compliance has been intensified. A process design procedure in which conformity inspections and checks can be carried out only at the end of the process chain cannot reach its maximum efficiency. Process cost and quality of the final product are put in the process at the very first design stage right after that the designer has made his/her choices. However the lack of knowledge about the overall manufacturing line does not allow predicting what these two fundamental variables will be at the end of the process. The two methodologies developed here moves towards the direction of eliminating the gap that divides the design stage from the end product. These methodologies constitute a powerful tool in

the designer's hands which is capable to predict how different configurations at the design stage will impact quality and cost in the final manufacture. Also the quantitative evaluation of trade-off accommodates for a variety of different end users as companies operating in different fields have to cope and deal with different requirements in terms of cost and quality. The methodologies developed here can make available to the designer the whole spectrum of optimal design solutions concerning the specific case study. A systematic use of such a tool in industry can bring enormous advantage in different aspects. Delivery delays can be reduced as the need of remanufacturing a part because of poor quality can be drastically reduced. Cost can also be reduced as the need to introduce modifications after process completion can be minimised. Eliminating the remanufacturing issues can boost the efficiency of the manufacturing chain and improve the accuracy of planning. Furthermore the methodologies developed here contribute towards more sustainable and environmentally friendly manufacture as energy consumption, emission of pollutants and scrap rates can be minimised. In summary application of multi-objective optimisation in the composite manufacturing chain can bring about benefits in three fronts: cost reduction, high quality standard and low environmental impact.

A few issues need to be resolved before applying the methodology in every day industrial activities. The traditional reluctance of the aeronautic field to change procedures that have become standard over the years needs to be overcome. Standard procedures for VARTM cure and infusion have been proven to be a conservative and robust solution, which prevents large variation if a swing in design parameters should occur. However, this does not deny the existence of better and optimised solutions with the same level of reliability. The optimisation results obtained in this work showed the existence of better solutions in terms of both quality and cost with respect to the solution found applying standard processing conditions. However it is of the same importance having stable solutions. Stability analysis indicates that standard cure profiles result in solutions lying in the region of low sensitivity with respect to variation in design parameters. The methodology should take into account the degree of

robustness obtained in the standard solution. Furthermore the methodology needs to be validated and fine-tuned by a number of experiments aiming to prove the actual effectiveness and efficiency of the new optimised design parameters and possible discrepancies between model predictions and experiments accounting for margin of tolerance with respect of models outcome. The experiments would also serve the purpose to evaluate the constitutive material models here implemented.

Therefore, one of the most crucial development steps for this methodology will be the introduction of automated robustness analysis. The goal of a robustness analysis is to quantify the sensitivity of the objectives (output) with respect to the variability in design parameters (input). In order to do that, variability, uncertainty and tolerances must be taken into account in the robust design optimisation. These factors can have different sources, whether from different environmental conditions, equipment inaccuracy or human error but nevertheless they have to be considered in a robust design since they are unavoidable. A robust design optimisation aims not to eliminate the uncertainty but to make the process insensitive to these variations. The trade-offs identified in this study showed the presence of stable regions and unstable regions where it would not be possible to place the design set parameters since the sensitivity would be too high. Ideal and unstable Pareto front are useless for practical purposes. A feasible solution usable in industry might not be located at a peak in the landscape but rather in a plateau guaranteeing a less sensitivity to variations. Robustness considerations will introduce the analysis of the design objectives space under uncertainty accounting for variations in the design parameters set.

Although the methodology was shown to solve successfully the optimisation problems under study there are some limitations which are necessary to point out. The Pareto front found at the end of the optimisation procedure for the all three cases showed to place individuals preferentially on the vertical area of the Pareto leaving the horizontal part with few individuals, this is probably due to the fact that is possible to achieve zero exotherm whilst zero process duration

cannot occur. As the stability analysis proved that individuals belonging to the horizontal region are the more stable it would be better to exploit this part of the Pareto rather than the other. Among the other benefits the introduction of a stability analysis and therefore having a robust optimisation procedure could naturally improve this aspect. A redefinition of the sharing ranking could also help toward this direction.

10 Conclusions

The main outcomes from this study are as follows:

Genetic Algorithm:

- The Genetic algorithm adapted and tested against benchmarks proved to be reliable and robust to treat both convex and non-convex multi-objective problems;
- The Genetic algorithm tested against established software showed accuracy comparable when the problem resulted in a convex Pareto front and better in non-convex Pareto front;
- The in-house Genetic algorithm efficiency is comparable with the established software.

Curing of VARTM:

- A methodology able to handle curing optimisation of the VARTM process has been developed and implemented. This tool is able to fill the knowledge gap between the design of the cure stage and the manufacture of the final part;
- Process time and overshoot temperature within the model have been identified as two competitive objectives which need to be treated simultaneously;
- The cure profile has been parameterised and it proved to affect the objectives of the optimisation;
- The final L-shape Pareto front provides a preferential direction toward which it is possible to optimise both objectives simultaneously;
- Landscape investigation showed the complex nature of the cure problem with the presence of many local minima. The GA provides an accurate and efficient solution requiring 25% of the effort necessary to run an exhaustive search. In the corner zone the Pareto found by the GA improves the one found by the exhaustive search by a maximum reduction of 6% in process time and 20% in temperature overshoot;

- Stability analysis illustrated the presence of regions of the final Pareto front with higher robustness to variations in the input.

Infusion of VARTM:

- A methodology able to handle infusion optimisation of the VARTM process has been developed and implemented. This constitutes a crucial tool in the hand of the designer for the filling stage;
- Filling time and degree of cure at the end of the filling have been identified as two competitive objectives which need to be optimised simultaneously;
- Seven parameters affecting the two objectives have been identified and chosen as input of the optimisation. These are gate locations, resin temperature and five parameters describing the non-isothermal filling profile;
- The optimisation resulted in an L-shape Pareto front. Investigation of the landscape highlighted the strong relationship between the parameters involved and the competitive nature between the objectives;
- The optimised filling profile suggests that increasing the resin and dwell temperature affect positively both filling time and degree of cure.

Cost of VARTM

- A methodology able to assess the cost related to the cure stage of the VARTM process has been developed and implemented;
- A reduction in process cost up to 500 € without affecting quality compared to standard solution has been found;
- The optimisation highlighted that the study case is not critical under the point of view of maximum temperature reached.

Permeability estimation and inverse scheme

- A methodology for an inverse scheme to estimates permeability of dry fabric and flow media has been developed and implemented;
- The inverse scheme has been tested against different level of noise showing that accuracy of the solution is guaranteed up to a 5 s level of noise from each sensor.

11 Suggestions for further investigations

The genetic algorithm developed and implemented here is suitable to treat multi-objective optimisation problems. The tests against four benchmarks revealed its accuracy, reliability and reproducibility with slightly better performance regarding non-convex problems. Further investigations can bring further improvements. More specifically testing it over a wider number of benchmarks especially with non-convex landscapes can allow fine-tuning the algorithm.

The optimisation methodology of the VARTM process could be integrated with stability analysis. The search for a stable and robust Pareto front is crucial. Having a Pareto front in which some individuals may be an unstable solution, meaning that small variation in the parameters values leads to big changes in the objective solution is an acceptable theoretical solution but not appropriate for real world applications. This update is necessary since the equipment and instruments used during manufacturing are affected by uncertainty. However, the robust Pareto front will be above the theoretical one (for a minimisation problem) meaning the applicable set up will lead to worse solutions. The complexity of the landscape poses a further complication to this problem calling for a more sophisticated implementation. This could be achieved either by automatically varying the nominal parameter values in a certain range and then selecting (according to a degree of robustness) the most stable or defining the parameters values as a normal distributed function in which the degree of robustness could be characterised by the multiples of standard deviation away from the exact value. Another possibility could be to treat the degree of robustness as one objective. Having a set of different Pareto fronts, each one relative to a different degree of robustness and stability, would allow the designer to pick his own curve according to the quality of the equipment at his/her disposal.

Further investigation is required to incorporate more competitive objectives (i.e. micro-voids/macro-voids and filling time, residual stresses and process time, spring in and process time). An extension in the number of objectives treated by

the genetic algorithm could give an overall flavour of the process. Interesting results could also come from integrating the infusion stage with curing stage having an interface able to deal with both that could point out links between the two processes that might be hidden when addressed separately.

The cure simulations in this work focused on thermal analysis. This could be extended to a mechanical-thermal analysis which could account for spring-in and deviation of the geometry from the one expected after removal from the curing assembly. Investigations on influence of residual stresses upon the mechanical performance could provide a direct link between process design and product performance.

The inverse procedure is currently working off-line. It is required to improve the real time operation of the inverse algorithm in order to use it on-line. This can be achieved by bringing improvements both in the model and in the inversion algorithm. Furthermore, the number of individuals per generation must be refined and optimised. The inversion procedure can be applied currently to the filling stage of VARTM. The artificial experiment has already proved the potential of the scheme. The inverse procedure could be adapted to the cure stage as well for the measurement of on-line thermal properties as the estimation of anisotropic thermal conductivities.

REFERENCES

[1] Deo, R. B., Starnes, J. H. and Holzwarth, R. C. (2001), "Low-cost composite materials and structures for aircraft applications", *RTO AVT Specialists on Low Composite Structures,* 7-11 May, Loen, Norway, pp. 1.

[2] Marsh, G. (2010), "Airbus 350-XWB update", *Reinforced plastics,* vol. 54, no. 6.

[3] Rudd, C. D., Long, A. C., Kendall, K. N. and Mangin, C. G. (1997), *Liquid moulding technologies,* Woodhead, Cambridge.

[4] Parnas, R. S. (2000), *Liquid composite molding,* Hanser, Munich.

[5] Advani, S. and Hsiao, K. T. (2012), "Vacuum assisted resin transfer molding (VARTM) in polymer matrix composites", in *Manufacturing techinques for polymer matrix composites (PMCs),* Woodhead, Cambridge.

[6] Ruiz, E., Achim, V., Soukane, S., Trochu, F. and Bréard, J. (2006), "Optimization of injection flow rate to minimize micro/macro-voids formation in resin transfer molded composites", *Composites Science and Technology,* vol. 66, no. 3-4, pp. 475-486.

[7] Yuan, Y. (2006), "A new stepsize for the steepest descend method", *Journal of computational mathematics,* vol. 24, no. 2, pp. 149-156.

[8] Arora, J. S. (2004), *Introduction to optimum design,* 2nd ed, Elsevier, Boston.

[9] Kirkpatrick, S., Gelatt, C. D. and Vecchi, M. P. (1983), "Optimization by Simulated Annealing", *Science,* vol. 220, no. 4598, pp. 671-680.

[10] Goldberg, D. E. (1989), *Genetic algorithms in search, optimization and machine learning,* Addison-Wesley, Boston.

[11] Schaffer, J. D. (1985), "Multiple objective optimisation with vector evaluated genetic algorithms", *Proceedings of the first international conference on genetic algorithms and their applications,* July 24-26, Pittsburgh, US, pp. 93.

[12] Fonseca, C. M. and Fleming, P. J. (1993), "Multiobjective genetic algorithms: formulation, discussion and generalization", *IEE colloquium on genetic algorithms for control systems engineering,* vol. 6, pp. 1-5.

[13] Srinivas, N. and Deb, K. (1994), "Multiobjective Optimization Using Nondominated Sorting in Genetic Algorithms", *Evolutionary computation,* vol. 2, no. 3, pp. 221-248.

[14] Hojjati, M. and Hoa, S. V. (1994), "Curing simulation of thick thermosetting composites", *Composites Manufacturing,* vol. 5, no. 3, pp. 159-169.

[15] Ciriscioli, P. R., Springer, G. S. and Lee, W. I. (1991), "Expert system for autoclave curing of composites", *Journal of Composite Materials,* vol. 25, no. 12, pp. 1542-1587.

[16] Pitchumani, R. and Yao, S. (1993), "Non-dimensional analysis of an idealized thermoset composites manufacture", *Journal of Composite Materials,* vol. 27, no. 6, pp. 613-636.

[17] Dusi, M. R., Lee, W. I., Ciriscioli, P. R. and Springer, G. S. (1987), "Cure kinetics and viscosity of fiberite 976 resin.", *Journal of Composite Materials,* vol. 21, no. 3, pp. 243-261.

[18] Suratno, B. R., Lin, Y. and Mai, Y. W. (1998), "Simulation of temperature and curing profiles in pultruded composite rods", *Composites Science and Technology,* vol. 58, no. 2, pp. 191-197.

[19] Behzad, T. and Sain, M. (2007), "Finite element modeling of polymer curing in natural fiber reinforced composites", *Composites Science and Technology,* vol. 67, no. 7–8, pp. 1666-1673.

[20] Blest, D. C., McKee, S., Zulkifle, A. K. and Marshall, P. (1999), "Curing simulation by autoclave resin infusion", *Composites Science and Technology,* vol. 59, no. 16, pp. 2297-2313.

[21] Karkanas, P. I. and Partridge, I. K. (1996), "Modeling the cure of a commercial epoxy resin for application in resin transfer moulding", *Polymer International,* vol. 41, pp. 183-191.

[22] Karkanas, P. I. and Partridge, I. K. (2000), "Cure modeling and monitoring of epoxy/amine resin systems. II. Network formation and chemoviscosity modeling", *Journal of Applied Polymer Science,* vol. 77, no. 10, pp. 2178-2188.

[23] Karkanas, P. I. and Partridge, I. K. (2000), "Cure modeling and monitoring of epoxy/amine resin systems. I. Cure kinetics modeling", *Journal of Applied Polymer Science,* vol. 77, no. 7, pp. 1419-1431.

[24] Mohan, R. V. and Grentzer, T. H. (1995), "Process simulation in thermoset composites for cure response and stress prediction", *Journal of Reinforced Plastics and Composites,* vol. 14, no. 1, pp. 72-84.

[25] Kim, Y. K. and Scott, R. W. (1997), "Process-induced stress relaxation analysis of AS4/3501-6 laminate", *Journal of Reinforced Plastics and Composites,* vol. 16, no. 1, pp. 2-15.

[26] Kim, K. S. and Hahn, H. T. (1989), "Residual stress development during processing of graphite/epoxy composites", *Composites Science and Technology,* vol. 36, no. 2, pp. 121-132.

[27] Plepys, A., Vratsanos, M. S. and Farris, R. J. (1994), "Determination of residual stresses using incremental linear elasticity", *Composite Structures,* vol. 27, no. 1–2, pp. 51-56.

[28] Guemes, J. A. (1994), "Curing residual stresses and failure analysis in composite cylinders", *Journal of Reinforced Plastics and Composites,* vol. 13, no. 4, pp. 409-419.

[29] White, S. R. and Zhang, Z. (1993), "The effect of mandrel material on the processing induced residual stresses in thick filament wound composite cylinders", *Journal of Reinforced Plastics and Composites,* vol. 12, no. 6, pp. 698-711.

[30] Bogetti, T. A. and Gillespie Jr., J. W. (1992), "Process-induced stress and deformation in thick-section thermoset composite laminates", *Journal of Composite Materials,* vol. 26, no. 5, pp. 626-660.

[31] Shojaei, A., Reza, G. and Mohammad Hossein Karimian, S. (2004), "Three-dimensional process cycle simulation of composite parts manufactured by resin transfer molding", *Composite Structures,* vol. 65, no. 3–4, pp. 381-390.

[32] Šimáček, P. and Advani, S. G. (2006), "Role of acceleration forces in numerical simulation of mold filling processes in fibrous porous media", *Composites Part A: Applied Science and Manufacturing,* vol. 37, no. 11, pp. 1970-1982.

[33] Maier, R. S., Rohaly, T. F., Advani, S. G. and Fickie, K. D. (1996), "A fast numerical method for isothermal resin transfer mold filling", *International Journal for Numerical Methods in Engineering,* vol. 39, no. 8, pp. 1405-1417.

[34] Hamdan, M. H. (1994), "Single-phase flow through porous channels a review of flow models and channel entry conditions", *Applied Mathematics and Computation,* vol. 62, no. 2–3, pp. 203-222.

[35] Gibson, A. G. (1992), "Modification of Darcy's law to model mould interface effects in composites processing", *Composites Manufacturing,* vol. 3, no. 2, pp. 113-118.

[36] Trochu, F., Gauvin, R. and Gao, D. (1993), "Numerical analysis of the resin transfer molding process by the finite element method", *Advances in Polymer Technology,* vol. 12, no. 4, pp. 329-342.

[37] Trochu, F., Ruiz, E., Achim, V. and Soukane, S. (2006), "Advanced numerical simulation of liquid composite molding for process analysis and optimization", *Composites Part A: Applied Science and Manufacturing,* vol. 37, no. 6 SPEC. ISS., pp. 890-902.

[38] Yan, X. (2006), "Consolidation and cure simulations for laminated composites", *Journal of Composite Materials,* vol. 40, no. 20, pp. 1853-1869.

[39] Gutowski, T. G., Morigaki, T. and Cai, Z. (1987), "Consolidation of laminates composites", *Journal of Composite Materials,* vol. 21, no. 2, pp. 172-188.

[40] Li, M. and Tucker III, C. L. (2002), "Modeling and simulation of two-dimensional consolidation for thermoset matrix composites", *Composites Part A: Applied Science and Manufacturing,* vol. 33, no. 6, pp. 877-892.

[41] Saunders, R. A., Lekakou, C. and Bader, M. G. (1999), "Compression in the processing of polymer composites 1. A mechanical and microstructural study for different glass fabrics and resins", *Composites Science and Technology,* vol. 59, no. 7, pp. 983-993.

[42] Saunders, R. A., Lekakou, C. and Bader, M. G. (1999), "Compression in the processing of polymer composites 2. Modelling of the viscoelastic compression of resin-impregnated fibre networks", *Composites Science and Technology,* vol. 59, no. 10, pp. 1483-1494.

[43] Potluri, P., Sharma, S. and Ramgulam, R. (2001), "Comprehensive drape modelling for moulding 3D textile preforms", *Composites Part A: Applied Science and Manufacturing,* vol. 32, no. 10, pp. 1415-1424.

[44] Bickerton, S., Šimáček, P., Guglielmi, S. E. and Advani, S. G. (1997), "Investigation of draping and its effects on the mold filling process during manufacturing of a compound curved composite part", *Composites Part A: Applied Science and Manufacturing,* vol. 28, no. 9–10, pp. 801-816.

[45] Trochu, F., Hammami, A. and Benoit, Y. (1996), "Prediction of fibre orientation and net shape definition of complex composite parts", *Composites Part A: Applied Science and Manufacturing,* vol. 27, no. 4, pp. 319-328.

[46] Tam, A. S. and Gutowski, T. G. (1990), "The kinematics for forming ideal aligned fibre composites into complex shapes", *Composites Manufacturing,* vol. 1, no. 4, pp. 219-228.

[47] Dong, L., Lekakou, C. and Bader, M. G. (2001), "Processing of composites: simulations of the draping of fabrics with updated material behaviour law", *Journal of Composite Materials,* vol. 35, no. 2, pp. 138-163.

[48] McEntee, S. P. and Ó Brádaigh, C. M. (1998), "Large deformation finite element modelling of single-curvature composite sheet forming with tool contact", *Composites Part A: Applied Science and Manufacturing,* vol. 29, no. 1-2, pp. 207-213.

[49] Cherouat, A. and Billoët, J. L. (2001), "Mechanical and numerical modelling of composite manufacturing processes deep-drawing and laying-up of thin pre-impregnated woven fabrics", *Journal of Materials Processing Technology,* vol. 118, no. 1–3, pp. 460-471.

[50] Nguyen, M., Herszberg, I. and Paton, R. (1999), "The shear properties of woven carbon fabric", *Composite Structures,* vol. 47, no. 1–4, pp. 767-779.

[51] Li, J., Joshi, S. C. and Lam, Y. C. (2002), "Curing optimization for pultruded composite sections", *Composites Science and Technology,* vol. 62, no. 3, pp. 457-467.

[52] Lam, Y. C., Li, J. and Joshi, S. C. (2003), "Simultaneous Optimization of Die-Heating and Pull-Speed in Pultrusion of Thermosetting Composites", *Polymer Composites,* vol. 24, no. 1, pp. 199-209.

[53] Joshi, S. C., Lam, Y. C. and Win Tun, U. (2003), "Improved cure optimization in pultrusion with pre-heating and die-cooler temperature", *Composites Part A: Applied Science and Manufacturing,* vol. 34, no. 12, pp. 1151-1159.

[54] Carlone, P., Palazzo, G. S. and Pasquino, R. (2007), "Pultrusion manufacturing process development: Cure optimization by hybrid computational methods", *Computers and Mathematics with Applications,* vol. 53, no. 9, pp. 1464-1471.

[55] Mawardi, A. and Pitchumani, R. (2004), "Cure cycle design for thermosetting-matrix composites fabrication under uncertainty", *Annals of Operations Research,* vol. 132, no. 1-4, pp. 19-45.

[56] Nelder, J. A. and Mead, R. (1965), "A simplex method for function minimization", *Computer Journal,* vol. 7, no. 4, pp. 308-313.

[57] Acquah, C., Datskov, I., Mawardi, A., Zhang, F., Achenie, L. E. K., Pitchumani, R. and Santos, E. (2006), "Optimization under uncertainty of a composite fabrication process using a deterministic one-stage approach", *Computers and Chemical Engineering,* vol. 30, no. 6-7, pp. 947-960.

[58] Safonov, A. and Suvorova, Y. V. (2009), "Optimization of the pultrusion process for a rod with a large diameter", *New Technology in Machinery Manufacture,* vol. 38, no. 6, pp. 572-578.

[59] Santos, L. S., Pagano, R. L., Biscaia, E. C. and Calado, V. M. A. (2009), "Optimum heating configuration of pultrusion process", *Computer Aided Chemical Engineering,* vol. 27, pp. 705-710.

[60] Liu, X. L. (2001), "Numerical modeling on pultrusion of composite I beam", *Composites Part A: Applied Science and Manufacturing,* vol. 32, no. 5, pp. 663-681.

[61] Pillai, V., Beris, A. N. and Dhurjati, P. (1996), "Heuristics guided optimization of a batch autoclave curing process", *Computers and Chemical Engineering,* vol. 20, no. 3, pp. 275-294.

[62] Li, M., Zhu, Q., Geubelle, P. H. and Tucker III, C. L. (2001), "Optimal curing for thermoset matrix composites: Thermochemical considerations", *Polymer Composites,* vol. 22, no. 1, pp. 118-131.

[63] Li, M. and Tucker III, C. L. (2002), "Optimal curing for thermoset matrix composites: Thermochemical and consolidation considerations", *Polymer Composites,* vol. 23, no. 5, pp. 739-757.

[64] Udaykumar, H. S. and Shyy, W. (1993), "Optimal cure cycles for thermoset composites manufacture", *29th National Heat Transfer Conference,* Vol. 241, 8-11 August, Atlanta, US, pp. 23.

[65] Chang, M. H., Chen, C. L. and Young, W. B. (1996), "Optimal design of the cure cycle for consolidation of thick composite laminates", *Polymer Composites,* vol. 17, no. 5, pp. 743-750.

[66] Yang, Z. L. and Lee, S. (2001), "Optimized curing of thick section composite laminates", *Materials and Manufacturing Processes,* vol. 16, no. 4, pp. 541-560.

[67] Skordos, A. A. and Partridge, I. K. (2004), "Inverse heat transfer for optimization and on-line thermal properties estimation in composites curing", *Inverse Problems in Science and Engineering,* vol. 12, no. 2, pp. 157-172.

[68] Rai, N. and Pitchumani, R. (1997), "Optimal cure cycles for the fabrication of thermosetting-matrix composites", *Polymer Composites,* vol. 18, no. 4, pp. 566-581.

[69] Watson, G. A. (2007), "A Levenberg-Marquardt method for estimating polygonal regions", *Journal of Computational and Applied Mathematics,* vol. 208, no. 2, pp. 331-340.

[70] Dufour, P., Michaud, D. J., Touré, Y. and Dhurjati, P. S. (2004), "A partial differential equation model predictive control strategy: application to

autoclave composite processing", *Computers & Chemical Engineering,* vol. 28, no. 4, pp. 545-556.

[71] Mawardi, A. and Pitchumani, R. (2003), "Optimal temperature and current cycles for curing of composites using embedded resistive heating elements", *Journal of Heat Transfer,* vol. 125, no. 1, pp. 126-136.

[72] Carlone, P. P., G.S. (2011), "A simulation based metaheuristic optimization of the thermal cure cycle of carbon epoxy composite laminates", *The 14th International ESAFORM Conference on Material Forming: ESAFORM 2011,* 27–29 April 2011, Belfast, UK, pp. 5-10.

[73] White, S. R. and Hahn, H. T. (1993), "Cure cycle optimization for the reduction of processing-induced residual stresses in composite materials", *Journal of Composite Materials,* vol. 27, no. 14, pp. 1352-1378.

[74] Olivier, P. and Cottu, J. P. (1998), "Optimisation of the co-curing of two different composites with the aim of minimising residual curing stress levels", *Composites Science and Technology,* vol. 58, no. 5, pp. 645-651.

[75] Gopal, A. K., Adali, S. and Verijenko, V. E. (2000), "Optimal temperature profiles for minimum residual stress in the cure process of polymer composites", *Composite Structures,* vol. 48, no. 1, pp. 99-106.

[76] Bailleul, J. L., Sobotka, V., Delaunay, D. and Jarny, Y. (2003), "Inverse algorithm for optimal processing of composite materials", *Composites Part A: Applied Science and Manufacturing,* vol. 34, no. 8, pp. 695-708.

[77] Head, J. D. and Zerner, M. C. (1985), "A Broyden—Fletcher—Goldfarb—Shanno optimization procedure for molecular geometries", *Chemical Physics Letters,* vol. 122, no. 3, pp. 264-270.

[78] Zhu, Q. and Geubelle, P. H. (2002), "Dimensional accuracy of thermoset composites: Shape optimization", *Journal of Composite Materials,* vol. 36, no. 6, pp. 647-672.

[79] Khorsand, A. R., Raghavan, J. and Wang, G. (2008), "Tool-shape optimization to minimize warpage in autoclave processed L-shaped composite part", *International SAMPE Technical Conference,* 8-11 September, Memphis, US, pp. 79-93.

[80] Mahale, A. D., Prud'homme, R. K. and Rebenfeld, L. (1993), "Characterization of voids formed during liquid impregnation of non-woven multifilament glass networks as related to composite processing", *Composites Manufacturing,* vol. 4, no. 4, pp. 199-207.

[81] Patel, N. and Lee, L. J. (1996), "Modeling of void formation and removal in liquid composite molding. Part I: wettability analysis", *Polymer Composites,* vol. 17, no. 1, pp. 96-103.

[82] Kessels, J. F. A., Jonker, A. S. and Akkerman, R. (2007), "Optimising the flow pipe arrangement for resin infusion under flexible tooling", *Composites Part A: Applied Science and Manufacturing,* vol. 38, no. 9, pp. 2076-2085.

[83] Jiang, S., Zhang, C. and Wang, B. (2002), "Optimum arrangement of gate and vent locations for RTM process design using a mesh distance-based approach", *Composites - Part A: Applied Science and Manufacturing,* vol. 33, no. 4, pp. 471-481.

[84] Mychajluk, G., Manoochehri, S. and Parnas, R. S. (1996), "Resin transfer molding process optimization for minimum cycle-time", *Journal of Advanced Materials,* vol. 28, no. 1, pp. 9-18.

[85] Ye, X., Zhang, C., Liang, Z. and Wang, B. (2004), "Heuristic algorithm for determining optimal gate and vent locations for RTM process design", *Journal of Manufacturing Systems,* vol. 23, no. 4, pp. 267-277.

[86] Lin, M. Y., Murphy, M. J. and Hahn, H. T. (2000), "Resin transfer molding process optimization", *Composites Part A: Applied Science and Manufacturing,* vol. 31, no. 4, pp. 361-371.

[87] Young, W. B. (1994), "Gate location optimization in liquid composite molding using genetic algorithms", *Journal of Composite Materials,* vol. 28, no. 12, pp. 1098-1113.

[88] Zhang, C., Jiang, S. and Wang, B. (2000), "Performance modeling and optimization of composite manufacturing processes", *American Society of Mechanical Engineers, Manufacturing Engineering Division, MED,* vol. 11, pp. 1055-1059.

[89] Kim, B. Y., Nam, G. J. and Lee, J. W. (2002), "Optimization of filling process in RTM using a genetic algorithm and experimental design method", *Polymer Composites,* vol. 23, no. 1, pp. 72-86.

[90] Kim, B. Y., Nam, G. J., Ryu, H. S. and Lee J.W. (2000), "Optimization of filling process in RTM using genetic algorithm", *Korea-Australia Rheology Journal,* vol. 12, no. 1, pp. 83-92.

[91] Luo, J., Liang, Z., Zhang, C. and Wang, B. (2001), "Optimum tooling design for resin transfer molding with virtual manufacturing and artificial intelligence", *Composites Part A: Applied Science and Manufacturing,* vol. 32, no. 6, pp. 877-888.

[92] Gokce, A., Hsiao, K. -. and Advani, S. G. (2002), "Branch and bound search to optimize injection gate locations in liquid composite molding processes", *Composites Part A: Applied Science and Manufacturing,* vol. 33, no. 9, pp. 1263-1272.

[93] Lam, Y. C., Britton, G. A. and Liu, D. S. (2004), "Optimisation of gate location with design constraints", *International Journal of Advanced Manufacturing Technology,* vol. 24, no. 7-8, pp. 560-566.

[94] Gokce, A. and Advani, S. (2003), "Combinatorial search to optimize vent locations in the presence of disturbances in liquid composite molding processes", *Materials and Manufacturing Processes,* vol. 18, no. 2, pp. 261-285.

[95] Gokce, A. and Advani, S. G. (2005), "Modeling, optimization and control of resin flow during manufacturing of textile composites with liquid molding", in Long, A. (ed.) *Design and Manufacture of Textile Composites,* Woodhead, Cambridge.

[96] Gokce, A. and Advani, S. G. (2004), "Vent location optimization using map-based exhaustive search in liquid composite molding processes", *Materials and Manufacturing Processes,* vol. 19, no. 3, pp. 523-548.

[97] Gokce, A. and Advani, S. G. (2004), "Simultaneous gate and vent location optimization in liquid composite molding processes", *Composites Part A: Applied Science and Manufacturing,* vol. 35, no. 12, pp. 1419-1432.

[98] Henz, B. J., Mohan, R. V. and Shires, D. R. (2007), "A hybrid global-local approach for optimization of injection gate locations in liquid composite molding process simulations", *Composites Part A: Applied Science and Manufacturing,* vol. 38, no. 8, pp. 1932-1946.

[99] Le Riche, R., Saouab, A. and Bréard, J. (2003), "Coupled compression RTM and composite layup optimization", *Composites Science and Technology,* vol. 63, no. 15, pp. 2277-2287.

[100] Drozdov, A. D. and Kalamkarov, A. L. (1995), "Optimization of winding process for composite pressure vessels", *International Journal of Pressure Vessels and Piping,* vol. 62, no. 1, pp. 69-81.

[101] Di Vita, G., Marchetti, M. and Nappi, M. (1998), "Code to analyse the structural-technological design of filament wound pressure vessels", *International SAMPE Symposium and Exhibition,* 1-3 June, Anaheim, US, pp. 1238.

[102] Koussios, S., Bergsma, O. K. and Beukers, A. (2006), "Filament winding: kinematics, collision control and process optimisation through

application of dynamic programming", *Composites Part A: Applied Science and Manufacturing,* vol. 37, no. 11, pp. 2088-2104.

[103] Wilson, E., Karr, C. and Messimer, S. (2003), "Genetic algorithm optimization of a filament winding process modeled in WITNESS", *Materials and Manufacturing Processes,* vol. 18, no. 3, pp. 509-521.

[104] Skordos, A. A., Monroy Aceves, C. and Sutcliffe, M. P. F. (2005), "Drape optimisation in woven composite manufacturing", *Proceeding of the 5th international conference on inverse problems in engineering: theory and practice,* July 11-15, 2005, Cambridge, UK, pp. S09.

[105] Long, A., Skordos, A. A., Harrison, P., Clifford, M. and Sutcliffe, M. P. F. (2006), "Optimisation of sheet forming for textile composites using variable peripheral force", *27th International conference SAMPRE EUROPE,* March 26-27, Paris, France, pp. 340-344.

[106] Svanberg, K. (1987), "Method of moving asymptotes: a new method for structural optimization", *Journal for Numerical Methods in Engineering,* vol. 24, no. 2, pp. 359-373.

[107] Kaufmann, M., Zenkert, D. and Åkermo, M. (2010), "Cost/weight optimization of composite prepreg structures for best draping strategy", *Composites Part A: Applied Science and Manufacturing,* vol. 41, no. 4, pp. 464-472.

[108] Chen, X., Xie, H., Chen, H. and Zhang, F. (2010), "Optimization for CFRP pultrusion process based on genetic algorithm-neural network", *International Journal of Material Forming,* vol. 3, no. SUPPL. 2, pp. 1391-1399.

[109] Coelho, R. M. L. and Calado, V. M. A. (2002), "An optimization procedure for the pultrusion process based on a finite element formulation", *Polymer Composites,* vol. 23, no. 3, pp. 329-341.

[110] Ratle, F., Achim, V. and Trochu, F. (2009), "Evolutionary operators for optimal gate location in liquid composite moulding", *Applied Soft Computing Journal,* vol. 9, no. 2, pp. 817-823.

[111] Mathur, R., Fink, B. K. and Advani, S. G. (1999), "Use of genetic algorithms to optimize gate and vent locations for the resin transfer molding process", *Polymer Composites,* vol. 20, no. 2, pp. 167-178.

[112] Li, J., Zhang, C., Liang, R. and Wang, B. (2008), "Robust design of composites manufacturing processes with process simulation and optimisation methods", *International Journal of Production Research,* vol. 46, no. 8, pp. 2087-2104.

[113] Mouton, S., Ledoux, Y., Teissandier, D. and Sébastian, P. (2010), "Genetic algorithm for design and manufacture optimization based on numerical simulations applied to aeronautic composite parts", *AIP Conference Proceedings,* Vol. 1252, pp. 1150-1159.

[114] Skordos, A. A., Sutcliffe, M. P. F., Klintworth, J. W. and Adolfsson, P. (2006), "Multi objective optimisation of woven composite draping using genetic algorithm", *27th International Conference SAMPE EUROPE,* 27-29 March, Paris, France, pp. 494-499.

[115] Yu, H. W. and Young, W. B. (1997), "Optimal design of process parameters for resin transfer molding", *Journal of Composite Materials,* vol. 31, no. 11, pp. 1113-1140.

[116] Michaud, D. J., Beris, A. N. and Dhurjati, P. S. (2002), "Thick-sectioned RTM composite manufacturing, Part II. Robust cure cycle optimization and control", *Journal of Composite Materials,* vol. 36, no. 10, pp. 1201-1232.

[117] Pantelelis, N. G. (2005), "Towards the dynamic optimisation for the cure control of thermoset-matrix composite materials", *Composites Science and Technology,* vol. 65, no. 7-8, pp. 1254-1263.

[118] Pantelelis, N., Vrouvakis, T. and Spentzas, K. (2002), "Cure cycle design for composite materials using computer simulation and optimisation tools", *Forschung im Ingenieurwesen/Engineering Research,* vol. 67, no. 6, pp. 254-262.

[119] Pantelelis, N. G. (2003), "Optimised cure cycles for resin transfer moulding", *Composites Science and Technology,* vol. 63, no. 2, pp. 249-264.

[120] Ruiz, E. and Trochu, F. (2006), "Multi-criteria thermal optimization in liquid composite molding to reduce processing stresses and cycle time", *Composites Part A: Applied Science and Manufacturing,* vol. 37, no. 6 SPEC. ISS., pp. 913-924.

[121] Ruiz, E. and Trochu, F. (2005), "Comprehensive thermal optimization of liquid composite molding to reduce cycle time and processing stresses", *Polymer Composites,* vol. 26, no. 2, pp. 209-230.

[122] Mitchell, M. (1998), *An introduction to genetic algorithms,* MIT Press, USA.

[123] Zitzler, E., Deb, K. and Thiele, L. (2000), "Comparison of multiobjective evolutionary algorithms: Empirical results", *Evolutionary computation,* vol. 8, no. 2, pp. 173-195.

[124] Fonseca C.M., F. P. J. (1995), "Multiobjective genetic algorithms made easy: Selection, sharing and mating restriction", *Proceeding of 1st International Conference on Genetic Algorithms in Engineering Systems: Innovations and Applications (GALESIA),* 12-14 September, Sheffield, UK, pp. 45-52.

[125] Erickson, M., Mayer, A. and Horn, J. (2002), "Multi-objective optimal design of groundwater remediation systems: application of the niched Pareto genetic algorithm (NPGA)", *Advances in Water Resources,* vol. 25, no. 1, pp. 51-65.

[126] Zitzler, E. (1999), *Evolutionary algorithms for multiobjective optimization: Methods and applications*.

[127] Back, T. (1996), *Evolutionary Algorithms in Theory and Practice,* Oxford Press, Oxford.

[128] Deb, K. (2001), *Multi-Objective Optimization using Evolutionary Algorithms,* Wiley, West Sussex.

[129] D'Souza, G., Sekaran, K. and Kandasamy, A. (2010), "Improved NSGA-II based on a novel ranking scheme", *Journal of computing,* vol. 2, no. 2, pp. 91-95.

[130] Horn, J. and Nafpliotis, N. (1994), "Multi objective optimisation using the niched pareto genetic algorithm ", *IEEE World Congress on Computational Intelligence,* 27-29 June, Illinois, US, pp. 82-114.

[131] Dias, A. and Vasconcelos, A. (2002), "Multiobjective genetic algorithms applied to solve optimisation problems", *IEEE transaction on magnetics,* vol. 38, no. 2, pp. 1133-1136.

[132] Tan, K. C., Lee, T. H. and Khor, E. F. (2001), "Evolutionary algorithm for multi objective optimisation: Performance assessments and comparisons", *IEEE Congress on Evolutionary Computation,* May 27-30, Seoul, Korea, pp. 979-986.

[133] Bleuler, S., Laumanns, M., Thiele, L. and Zitzler, E. (2003), "PISA-A platform and programming language independent interface for search algorithms", *EMO'03 Proceedings of the 2nd international conference on Evolutionary multi-criterion optimization,* April 8–11, Faro, Portugal, pp. 494-508.

[134] Zitzler, E., Laumanns, M. and Thiele, L. (2001), "SPEA2: Improving strength pareto evolutionary algorithm for multiobjective optimisation", *Evolutionary Methods for Design, Optimization and Control with Applications to Industrial Problems. Proceedings of the EUROGEN 2001,* 19-21 September, Athens, Greece, pp. 95-100.

[135] Deb, K., Agrawal, S., Pratab, A. and Meyarivan, T. (2000), " A fast elitist non-dominated sorting genetic algorithms for multiobjective optimization: NSGA II.", *Evolutionary computation,* vol. 6, no. 2, pp. 182-197.

[136] Marc® (2011), *Volume A: Theory and user information,* www.mscsoftware.com.

[137] Marc® (2011), *Volume B: Elements library,* www.mscsoftware.com.

[138] Marc® (2011), *Volume D: User subroutine and special routines,* www.mscsoftware.com.

[139] PAM-RTM® (2011), *The virtual manufacturing solution for liquid composite molding,* www.esi-group.com.

[140] Drapier, S., Celle, P. and Bergheau, J. M. (2008), "Numerical model for fluid infusion during infusion-based processes", *The 9th International Conference on Flow Processing in Composite Materials,* 8-10 July, Montreal, Canada.

[141] Hexcel® (2009), *RTM 6 180°C epoxy system for Resin Transfer Moulding monocomponent system Product Data,* www.hexcel.com.

[142] Cycom® (2012), *890 RTM Resin system technical data sheet,* www.cytec.com.

[143] HexForce® (2013), *G1157 D1300 INJ 2F Carbon fabric,* www.hexcel.com.

[144] Wise, C. W., Cook, W. D. and Goodwin, A. A. (1997), "Chemico-diffusion kinetics of model epoxy-amine resins", *Polymer,* vol. 38, no. 13, pp. 3251-326.

[145] Farmer, J. D. and Covert, E. E. (1996), "Thermal conductivity of a thermosetting advanced composite during its cure", *Journal of Thermophysics and Heat Transfer,* vol. 10, no. 3, pp. 467-475.

[146] Yamane, T., Katayama, S., Todoki, M. and Hatta, I. (2000), "The measurement of thermal conductivity of carbon fibers", *Journal of Wide Bandgap Materials,* vol. 7, no. 4, pp. 294-305.

[147] Khoun, L., Centea, T. and Hubert, P. (2010), "Characterization methodology of thermoset resins for the processing of composites materials - Case study: CYCOM 890RTM epoxy resin", *Journal of Composite Materials,* vol. 44, no. 11, pp. 1397-1415.

[148] Fylstra, D., Lasdon, L., Watson, J. and Waren, A. (1998), "Design and use of the microsoft excel solver", *Interfaces,* vol. 28, no. 5, pp. 29-55.

[149] Skordos, A. A., Kergomard, Y. D., Marquette, P. and De Luca, P. (2012), "Methodology applied to integrate a viscosity model for liquid composite molding simulation in PAMRTM", *ASME 2012 11th Biennal Conference on Engineering System Design and Analysis,* July 2012, Nantes, France, pp. 11-19.

[150] Cartié, D. D. R., Dell'Anno, G., Poulin, E. and Partridge, I. K. (2006), "3D reinforcement of stiffener-to-skin T-joints by Z-pinning and tufting", *Engineering Fracture Mechanics,* vol. 73, no. 16, pp. 2532-2540.

[151] Wood, M. D. K., Tong, L., Luo, Q., Sun, X., Katzos, A. and Adrian, R. (2009), "Failure of stitched composite L-joints under tensile loading-experiment and simulation", *Journal of Reinforced Plastics and Composites,* vol. 28, no. 6, pp. 715-742.

[152] Koh, T. M., Feih, S. and Mouritz, A. P. (2011), "Experimental determination of the structural properties and strengthening mechanisms of z-pinned composite T-joints", *Composite Structures,* vol. 93, no. 9, pp. 2222-2230.

[153] Formicola, C., De Fenzo, A., Zarrelli, M., Frache, A., Giordano, M. and Camino, G. (2009), "Synergistic effect of zinc borate and aluminium trihydroxide on flammability behaviour of aerospace epoxy system", *Polymer Letter,* vol. 3, no. 6, pp. 376-384.

[154] Liu, X. L. and Hillier, W. (1999), "Heat transfer and cure analysis for the pultrusion of a fiberglass-vinyl ester I beam", *Composite Structures,* vol. 47, no. 1–4, pp. 581-588.

[155] Weiland, F., Weimer, C., Dumount, F. and Katsirpoulos, C. (2013), "Process and cost modelling applied to manufacture of complex aerospace composite part", *Plastics, Rubber and Composites,* vol. 42, no. 10, pp. 427-436.

[156] Lundström, T. S., Stenberg, R., Bergström, R., Partanen, H. and Birkeland, P. A. (2000), "In-plane permeability measurements: a nordic round-robin study", *Composites Part A: Applied Science and Manufacturing,* vol. 31, no. 1, pp. 29-43.

APPENDICES

Appendix A Interfaces code

A.1 Interface code for the cure problem

The cure model interface can be used on any MSC.Marc® cure model. Nevertheless the cure model must follow a specific strategy in the input of the temperature profile followed and the process time in output is defined as the time where every element in the model has reached a minimum target degree of cure. This is performed through a series of user subroutines in MSC.Marc®.

Subroutine FORCDT, Figure A-1, contains the thermal profile input block appropriate for the definition of a generic profile. The parameters of the cure profile are written by the interface in the text file (lines 7-10).

```
      SUBROUTINE FORCDT (X1,X2,X3,F,T,TIME,DTIME,NDEG,NODE,X4,XORD
     1        ,NCRD,IACFLG,INC,IPASS)
              IMPLICIT REAL *8 (A-H, O-Z)
             include '../common/creeps'
             DIMENSION F(NDEG),T(NDEG),XORD(NCRD)
             COMMON StoredINC, Tbound, DTmax,amin,Zeroflag,writeflag,tcure,Temp,TI
             T1=160
             T2=180
             Dt=3600
             r=3
             r=r/60
             if (TIME<=(T1-120)/r) then
                     T=120+r*TIME
             end if
             if (TIME>(T1-120)/r.AND.TIME<=Dt+(T1-120)/r) then
                     T=T1
             end if
             if (TIME>Dt+(T1-120)/r.AND.TIME<=(T2-T1)/r+Dt+(T1-120)/r) then
                     T=T1+r*(TIME-(Dt+(T1-120)/r))
             end if
             if (TIME>(T2-T1)/r+Dt+(T1-120)/r.AND.TIME<=(T2-T1)/r+Dt+
     1       (T1-120)/r+67200) then
                     T=T2
             end if
             Tbound=T(1)
      RETURN
      END
```

Figure A-1 Cure Interface: Thermal profile definition in MSC.Marc® user subroutine FORCDT

The maximum overshoot temperature within the model is identified by means of UPSTNO subroutine that picks out every nodes temperature, Figure A-2. The difference between the nodes temperature (*Temp*) and the one at the boundary (*Tbound*) is then computed for each node and the difference is stored in *DTmax* if it is higher than the former.

```
SUBROUTINE UPSTNO (NQCODE,NODEID,VALNO,NQNCOMP,NQTYPE,
1       NQAVER,NQCOMPTYPE,NQDATATYPE,NQCOMPNAME)
        IMPLICIT REAL*8 (A-H,O-Z)
        COMMON StoredINC, Tbound, DTmax,amin,Zeroflag,writeflag,tcure,Temp,
1       TIME,Tempstore
        include '../common/concom'
        include '../common/creeps'
        include '../common/blnk'
        include '../common/lass'
        DIMENSION VALNO(*)
        CHARACTER*24 NQCOMPNAME(*)
        call nodvar(14,NODEID,Temp,NQNCOMP,NQDATATYPE)
        VALNO(1)=Temp
        if (Temp-Tbound>DTmax .AND.amin<0.88) then
                DTmax=Temp-Tbound
                open (unit=1,file="DTmax_148.txt",form="formatted"
1               ,status="replace",action="write")
                write (unit=1,fmt=*),DTmax
                close (unit=1)
        endif
        if (Temp-Tbound>DTmax .AND.amin>=0.88) then
                DTmax=Temp-Tbound
                open (unit=1,file="DTmax_148.txt",form="formatted"
1               ,status="replace",action="write")
                write (unit=1,fmt=*),DTmax
                close (unit=1)
        end if
RETURN
```

Figure A-2 Cure Interface: Maximum temperature computation in MSC.Marc® using subroutine UPSTNO

Subroutine UEDINC is executed at the end of each increment and is used to compute cure time, Figure A-3. The routine compares the minimum degree of cure value stored in *amin* with a predefined limit (0.88) and mark the time at which this limit is exceeded.

```
SUBROUTINE UEDINC (INC1,INCSUB1)
 IMPLICIT REAL *8 (A-H, O-Z)
 COMMON StoredINC, Tbound, DTmax,amin,Zeroflag,writeflag,tcure,Temp,TIME,
 1       Tempstore
 include '../common/concom'
 include '../common/creeps'
 if (amin>0.88.AND.writeflag==0.0) then
                tcure=CPTIM
                open (unit=2,file="tcure_148.txt",form="formatted"
 1              ,status="replace",action="write")
                write (unit=2,fmt=*),tcure
                close (unit=2)
                writeflag=1.0

 end if
 if (amin<0.88.AND.CPTIM>19799.0) then
                tcure=40000
                open (unit=2,file="tcure_148.txt",form="formatted"
 1              ,status="replace",action="write")
                write (unit=2,fmt=*),tcure
                close (unit=2)
 endif
  RETURN
END
```

Figure A-3 Cure Interface: Cure time computation in MSC.Marc® using subroutine UEDINC

These subroutines are facilitated by the PLOTV subroutine, Figure A-4, which operates in the element loop at the end of each increment and resets the values temperature difference and minimum degree of cure when necessary, i.e.

compares the current minimum degree of cure with the degree of cure at each element and replaces when appropriate.

```
 SUBROUTINE PLOTV (V,S,SP,ETOT,EPLAS,ECREEP,T,M,NN,KCUS,NDI,
+ NSHEAR,JPLTCD)
   IMPLICIT REAL *8 (A-H, O-Z)
   DIMENSION S(*),SP(*),ETOT(*),EPLAS(*),ECREEP(*),T(*),
+ M(2),KCUS(2)
   COMMON StoredINC, Tbound, DTmax,amin,Zeroflag,writeflag,tcure,Temp,TIME
   include '../common/concom'
   include '../common/creeps'
   if (INC==0.AND.Zeroflag==0) then
          DTmax=-8065014
          amin=8065014
          Zeroflag=1
   end if
   if (INC>StoredInc) then
          amin=8065014
          StoredInc=INC
   end if
   call elmvar(285,M,NN,KCUS,conv)
   if (conv<amin) then
          amin=conv
   end if
   RETURN
  END
```

Figure A-4 Cure Interface: Implementation of PLOTV subroutine

The two solutions are written in two text files (Figures A-2, A-3) one for cure duration and the other for maximum overshoot temperature. Furthermore a subroutine named UCURE for the cure kinetics solution is defined.

```
      subroutine ucure(m,n,nn,kc,matus,dt,ak,density,volumi,curedat,
1     tempbeg,tempend,deltime,time,curerate)
      include '../common/implicit'
      include '../common/concom'
      include '../common/mrcparm'
      dimension curedat(*),matus(2)
      real K1
      real K2
      real K1c
      real K2c
      real Kd
      real A1
      real A2
      real Ad
      real ni
      real nl
      real mi
      real E1
      real E2
      real Ed
      real H
      real R
      real vf
      real l
      real b
      real Tginf
      real Tg0
      real f
      A1=1.7580E4
      A2=2.1525E4
      Ad=6.48E18
        E1=70.5E3
        E2=59.05E3
        Ed=136.8E3
        ni=1.8
        nl=1.32
      mi=1.16
      l=0.435
        b=0.467
      Tginf=206+273.15
      Tg0=-11+273.15
      H=465000.0
        R=8.3144
        vf=0.6
      f=4.8e-4*((tempbeg+273.15)-Tg0-(Tginf-Tg0)*l*dt/(1-(1-l)*dt))+0.025
      K1c=A1*exp(-E1/R/(tempbeg+273.15))
      K2c=A2*exp(-E2/R/(tempbeg+273.15))
      Kd=Ad*exp(-Ed/R/(tempbeg+273.15))*exp(-b/f)
      K1=1/(1/Kd+1/K1c)
      K2=1/(1/Kd+1/K2c)
      curerate=K1*(1-dt)**ni+K2*dt**mi*(1-dt)**nl
      curedat(9)=H*(1-vf)
      volumi=1.0
      ak=dt+deltime*curerate
      if (ak>0.999) then
              curerate=0.0
              ak=1.0
      end if
    end
```

Figure A-5 Cure Interface: Implementation of UCURE subroutine for RTM6 epoxy resin

Concerning the cure problem addressed in Chapter 5 a different resin system has been used, 890RTM epoxy resin, as consequence the UCURE subroutine looked differently caused the cure kinetics of the two resins are different, Figure A-6. Furthermore, a new subroutine named UFILM has been implemented to manage the convection coefficient, Figure A-7.

```
subroutine ucure(m,n,nn,kc,matus,dt,ak,density,volumi,curedat,
1   tempbeg,tempend,deltime,time,curerate)
        include '../common/implicit'
        include '../common/concom'
        include '../common/mrcparm'
        dimension curedat(*),matus(2)
        real A
        real nl
        real ml
        real E
        real H
        real R
        real vf
        real c
        real ac
        real at
        real k
        real f
        A=58500
        E=68970
        nl=0.72
        ml=0.83
        c=28.5
        ac=-3.73
        at=0.0103
        H=425000.0
        R=8.3144
        vf=0.6
        k=dt-ac-at*(tempbeg+273.15)
        f=(A*exp(-E/R/(tempbeg+273.15)))/(1+exp(c*k))
        curerate=f*(1-dt)**nl*dt**ml
        curedat(9)=H*(1-vf)
        volumi=1.0
        ak=dt+deltime*curerate
        if (ak>0.999) then
        curerate=0.0
        ak=1.0
        end if
end
```

Figure A-6 Cure interface: implementation of UCURE for 890RTM epoxy resin

```
  SUBROUTINE UFILM (UHFILM,UTSINK,UHNATUR,UEXPNAT,
  1       UEFFVIEW,UEMISS,UQFLUX,TS,N,TIME,INC)
          IMPLICIT REAL*8 (A-H,O-Z)
          DIMENSION TS(*),N(*)
          UHNATUR=0
          UTSINK=25
          UHFILM=0
          UEXPNAT=1
          UEFFVIEW=1
          UEMISS=0
          UQFLUX=0
  RETURN
  END
```

Figure A-7 Cure interface: Implementation of UFILM subroutine

```
double *marc_run(double T1, double T2,double dt1,double r)
{
int i;
string line;
string line1;
double tcure=806541;
double maxtemp=806541;
ifstream oldinput;
oldinput.open("z:\\Giacomo\\My_work\\Composites_joint\\Marc_model\\usub_24.f");
ofstream newinput;
newinput.open("z:\\Giacomo\\My_work\\Composites_joint\\Marc_model\\usub_24_new.f");
for ( i=0;i<6;i++)
{
        getline(oldinput,line);
        newinput<<line<<endl;
    }
    getline(oldinput,line);
    newinput<<line.substr(0,19);
    newinput<<T1<<endl;
    getline(oldinput,line);
    newinput<<line.substr(0,19);
    newinput<<T2<<endl;
    getline(oldinput,line);
    newinput<<line.substr(0,19);
    newinput<<dt1<<endl;
    getline(oldinput,line);
    newinput<<line.substr(0,18);
    newinput<<r<<endl;
for ( i=10;i<172;i++)
{
        getline(oldinput,line);
        newinput<<line<<endl;
    }
oldinput.close();
newinput.close();
system ("\"C:\\Program Files (x86)\\Intel\\Composer XE 2011 SP1\\bin\\ifortvars.bat\" intel64 & C:\\MSC.Software\
        Marc_Classic\\2011\\marc2011\\tools\\run_marc -jid Z:\\Giacomo\\My_work\\Composites_joint\\Marc_model\
        flatpanel_sub24mm_flattherm.dat -u Z:\\Giacomo\\My_work\\Composites_joint\\Marc_model\\usub_24_new  -back no")
ifstream outfile0;
outfile0.open("Z:\\Optimisation_algorithm\\Cure\\Cure\\DTmax_24.txt");
getline(outfile0,line);
line1=line.substr(3,19);
maxtemp=strtod(line1.c_str(), NULL);
outfile0.close();
ifstream outfile2;
outfile2.open("Z:\\Optimisation_algorithm\\Cure\\Cure\\tcure_24.txt");
getline(outfile2,line);
line=line.substr(3,19);
tcure=strtod(line.c_str(), NULL);
outfile2.close();
label:
    double *output;
    output = new double[1];
    output[0] = tcure;
    output[1] = maxtemp;
    return output;
}
```

Figure A-8 C++ implementation of the cure interface

The cure interface is reported in Figure A-8. It operates in the following steps:

- Initialisation of the two outputs (*tcure, maxtemp*);
- Definition of the file template and the modified one;
- Replacement with new parameters at the appropriate locations of the template file;
- Opening specific output files and reading the values of the variables written by Msc.Marc® subroutine;
- Exiting an array with the two outputs.

A.2 Interface code for the infusion problem

The interface receives process parameters (*thermal profile parameters and gate selection*) from the GA, it modifies the input file of PAM-RTM®, it executes the solution, it reads the output files to withdraw the information related to the GA objectives and output these to the GA. File paths relevant to PAM-RTM® run, input file line numbers to allow modification of input file, run parameters and penalty factor are included in the arguments of the interface function:

- ✓ Path: Old (template) input file;
- ✓ Path_new: New input file;
- ✓ Path_bat: Batch file;
- ✓ Path_inj: Injection report output file;
- ✓ Path_cure: Cure output file.

Whilst the array of integers (*InputValue) transfer the following variables:

- ✓ *InputValue: Number of elements in the model;
- ✓ *InputValue+1: Penalty filling time applied in the case incomplete filling;
- ✓ *InputValue+2: Number of gates;
- ✓ *InputValue+3: Line of initial temperature input;
- ✓ *InputValue+4: Beginning of thermal profile definition block;
- ✓ *InputValue+5: End of thermal profile definition block;
- ✓ *InputValue+6: Gate activation reference line;
- ✓ *InputValue+7: Number of lines of the input file.

An example of the location of the lines related to PAM-RTM® input is given in Figure A-9.

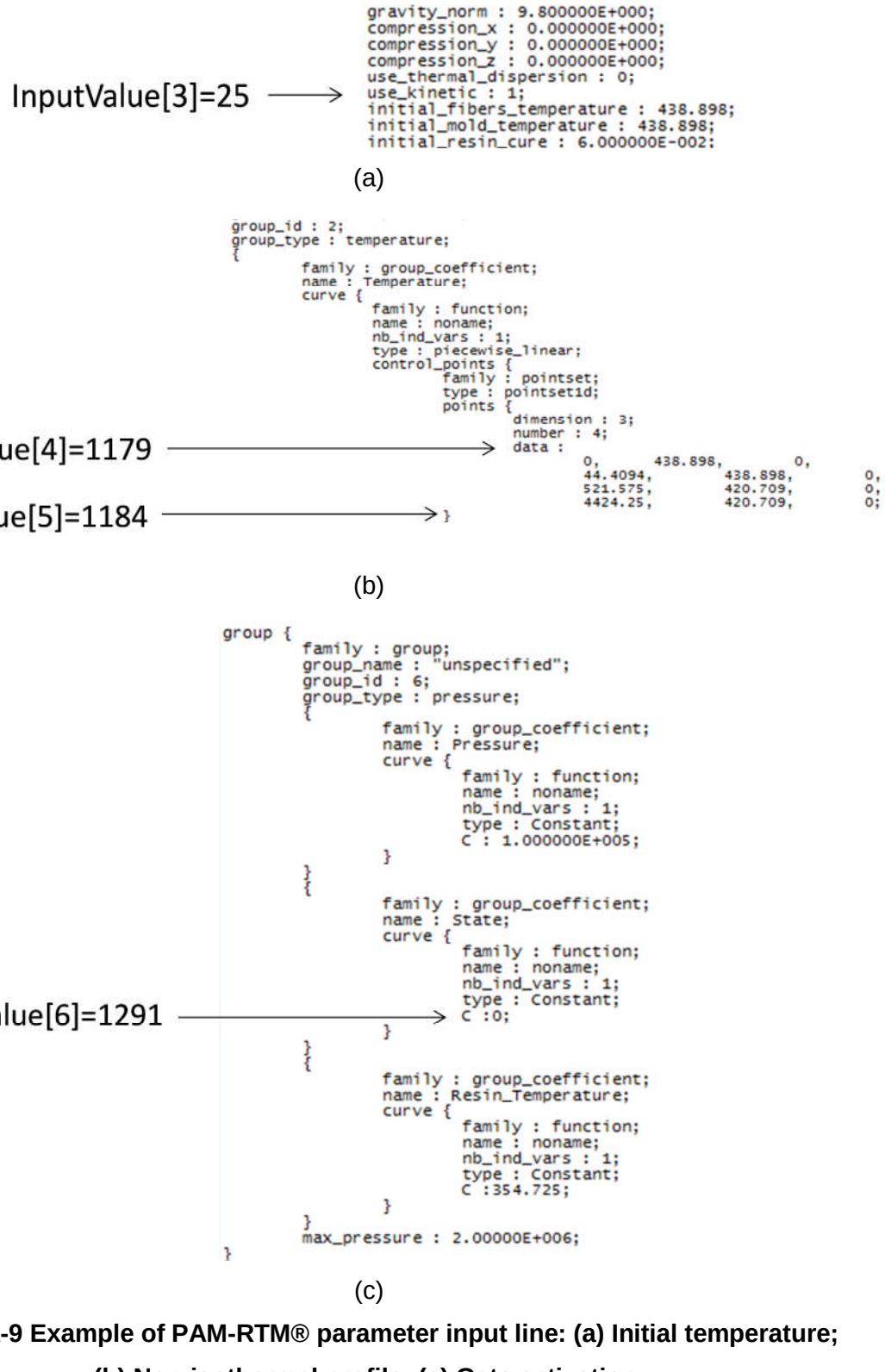

Figure A-9 Example of PAM-RTM® parameter input line: (a) Initial temperature; (b) Non-isothermal profile; (c) Gate activation.

An example of the definition of these variables is given in Figure A-10.

```
void individual::CalculateFitness()//calculate fitness for all criteria
{
    double Tr;
    double T2;
    double T1;
    double dt1;
    double dt2;
    double selection;
    std::string path;
    std::string path_new;
    std::string path_bat;
    std::string path_inj;
    std::string path_cure;
double *pResults = new double[1];
    Tr= cChromosome.GetParameter(0);
    T2= cChromosome.GetParameter(1);
    T1= cChromosome.GetParameter(2);
    dt1= cChromosome.GetParameter(3);
    dt2= cChromosome.GetParameter(4);
    selection= cChromosome.GetParameter(5);
 path="Z:\\Infusion_optimisation\\Optimisation_C_section_gate.dtf";
 path_new="Z:\\Infusion_optimisation\\Optimisation_C_section_gate_new.dtf";
 path_bat="Z:\\Infusion_optimisation\\infusion_gate.bat";
 path_inj="Z:\\Infusion_optimisation\\Optimisation_C_section_gate_new_injection_report.dat";
 path_cure="z:\\Infusion_optimisation\\Optimisation_C_section_gate_new_cure_filling.unv";
int Ninput=8;
double *InputValue=new double[Ninput-1];
 InputValue[0]=2445;
 InputValue[1]=40000;
 InputValue[2]=3;
 InputValue[3]=25;
 InputValue[4]=1179;
 InputValue[5]=1184;
 InputValue[6]=1291;
 InputValue[7]=1435;
  pResults=PAMRTM_run(Tr,T2,T1,dt1,dt2,selection,path,path_new,path_bat,path_inj,path_cure,Ninput,InputValue);
    cPartialFitness[0] = pResults[0];
    cPartialFitness[1] = pResults[1];
}
```

Figure A-10 Definition of input for the infusion interface

The interface itself starts defining and initialising variables, after that the non-isothermal profile for the infusion is defined. Subsequently, the interface starts modifying the input file according to the new parameters set starting from setting the new initial temperature and the new non-isothermal profile, Figure A-11. After that a selection is done by the user regarding the potential number of gates which address the interface to three different sections. Resin temperature is also modified according to new input from GA as shown in Figures A-12 – A-14. Then PAM-RTM® is called and executed, once the simulation has terminated the interface open the output file and picks out the information needed regarding the objectives of the optimisation. These values are then sent to GA, Figure A-15.

```
double *PAMRTM_run(double Tr,double T2,double T1,double dt1,double dt3,double selection,string path,
      string path_new,string path_bat,string path_inj,string path_cure,int Ninput,double *InputValue)
{
const char *myfile=path.c_str();
const char *myfile_new=path_new.c_str();
const char *myfile_bat=path_bat.c_str();
const char *myfile_inj=path_inj.c_str();
const char *myfile_cure=path_cure.c_str();
double time1;
double Temp1;
double time2;
double Temp2;
double time3;
double Temp3;
double time4;
double Temp4;
double acure;
double check;
double size=0;
double curefilelength=0;
int i;
int k=0;
int ab=0;
int b=0;
int c=0;
string line;
string line1;
string line12;
double tfill=806541;
double acuremax=-806541;
double dt2=InputValue[1];
time1=0;
Temp1=T1;
time2=dt1;
Temp2=T1;
time3=dt3+time2;
Temp3=T2;
time4=time2+time3+dt2;
Temp4=T2;
ifstream oldinput;
oldinput.open(myfile);
ofstream newinput;
newinput.open(myfile_new);
for ( i=0;i<InputValue[3];i++)
{
        getline(oldinput,line);
        newinput<<line<<endl;
    }
        getline(oldinput,line);
        newinput<<line.substr(0,30)<<Temp1<<";"<<endl;
        getline(oldinput,line);
        newinput<<line.substr(0,28)<<Temp1<<";"<<endl;
for ( i=InputValue[3]+2;i<InputValue[4];i++)
{
        getline(oldinput,line);
        newinput<<line<<endl;
    }
getline(oldinput,line);
    newinput<<line.substr(0,6);
    newinput<<time1<<","<<line.substr(0,1)<<Temp1<<","<<line.substr(0,1)<<"0,"<<endl;

    getline(oldinput,line);
    newinput<<line.substr(0,6);
    newinput<<time2<<","<<line.substr(0,1)<<Temp2<<","<<line.substr(0,1)<<"0,"<<endl;

    getline(oldinput,line);
    newinput<<line.substr(0,6);
    newinput<<time3<<","<<line.substr(0,1)<<Temp3<<","<<line.substr(0,1)<<"0,"<<endl;

    getline(oldinput,line);
    newinput<<line.substr(0,6);
    newinput<<time4<<","<<line.substr(0,1)<<Temp4<<","<<line.substr(0,1)<<"0;"<<endl;
```

Definition and variable initialisation

Non-isothermal profile definition

New initial temperature

New non isothermal profile

Figure A-11 Infusion optimisation interface: Variable initialisation and thermal profile

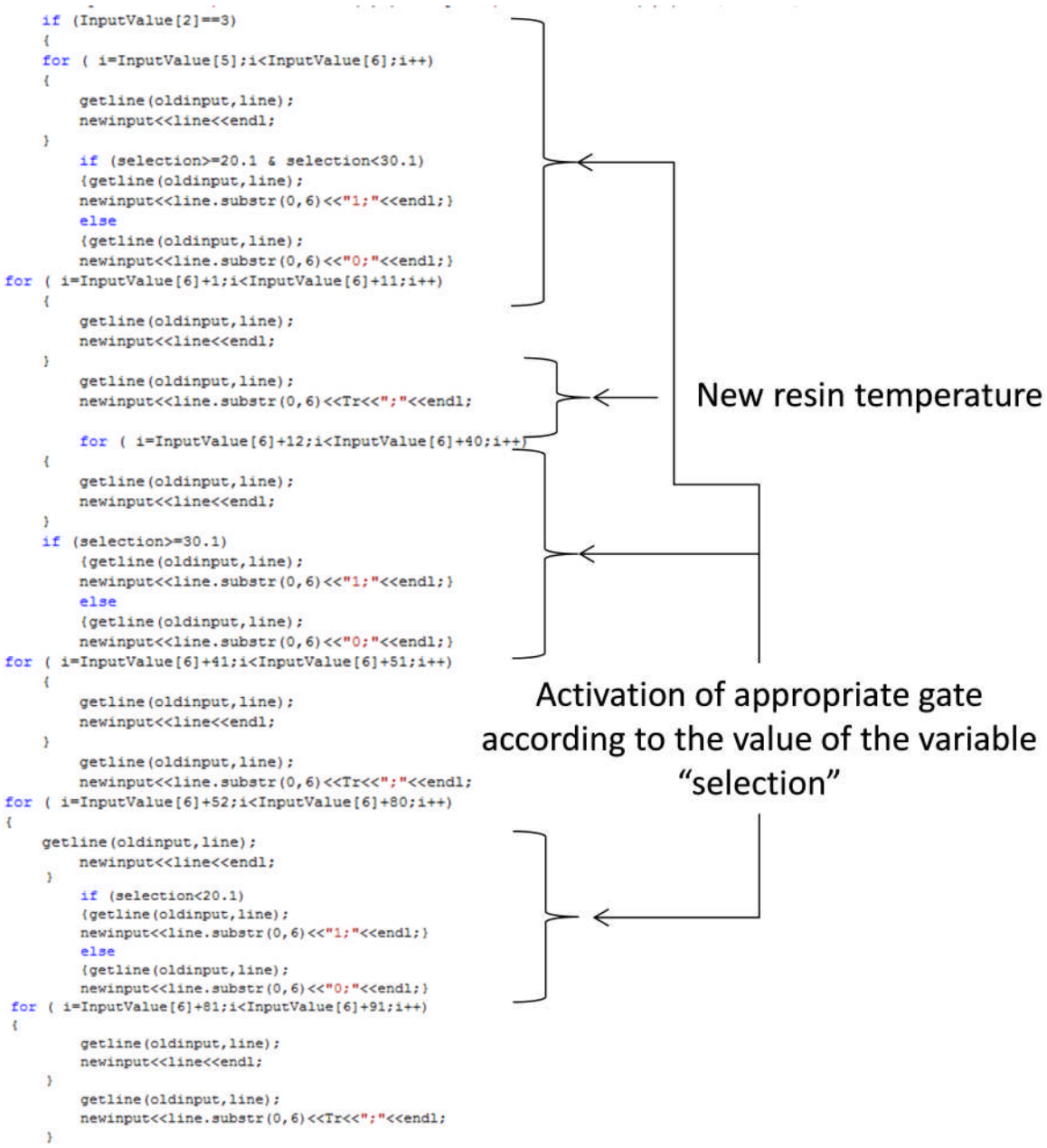

Figure A-12 Infusion optimisation interface: Three potential gates case

```
if (InputValue[2]==2)
{
    for ( i=InputValue[5];i<InputValue[6];i++)
    {
        getline(oldinput,line);
        newinput<<line<<endl;
    }
        if (selection>=25.0)
        {getline(oldinput,line);
        newinput<<line.substr(0,6)<<"1;"<<endl;}
        else
        {getline(oldinput,line);
        newinput<<line.substr(0,6)<<"0;"<<endl;}
    for ( i=InputValue[6]+1;i<InputValue[6]+11;i++)
    {
        getline(oldinput,line);
        newinput<<line<<endl;
    }
        getline(oldinput,line);
        newinput<<line.substr(0,6)<<Tr<<";"<<endl;
    for ( i=InputValue[6]+12;i<InputValue[6]+40;i++)
    {
        getline(oldinput,line);
        newinput<<line<<endl;
    }
    if (selection<25)
        {getline(oldinput,line);
        newinput<<line.substr(0,6)<<"1;"<<endl;}
        else
        {getline(oldinput,line);
        newinput<<line.substr(0,6)<<"0;"<<endl;}
    for ( i=InputValue[6]+41;i<InputValue[6]+51;i++)
    {
        getline(oldinput,line);
        newinput<<line<<endl;
    }
        getline(oldinput,line);
        newinput<<line.substr(0,6)<<Tr<<";"<<endl;
        for ( i=InputValue[6]+52;i<InputValue[6]+80;i++)
    {
    getline(oldinput,line);
        newinput<<line<<endl;
    }
        {getline(oldinput,line);
        newinput<<line.substr(0,6)<<"0;"<<endl;}
    for ( i=InputValue[6]+81;i<InputValue[6]+91;i++)
    {
        getline(oldinput,line);
        newinput<<line<<endl;
    }
        getline(oldinput,line);
        newinput<<line<<endl;
}
```

Third gate off

Figure A-13 Infusion optimisation interface: Two potential gates case

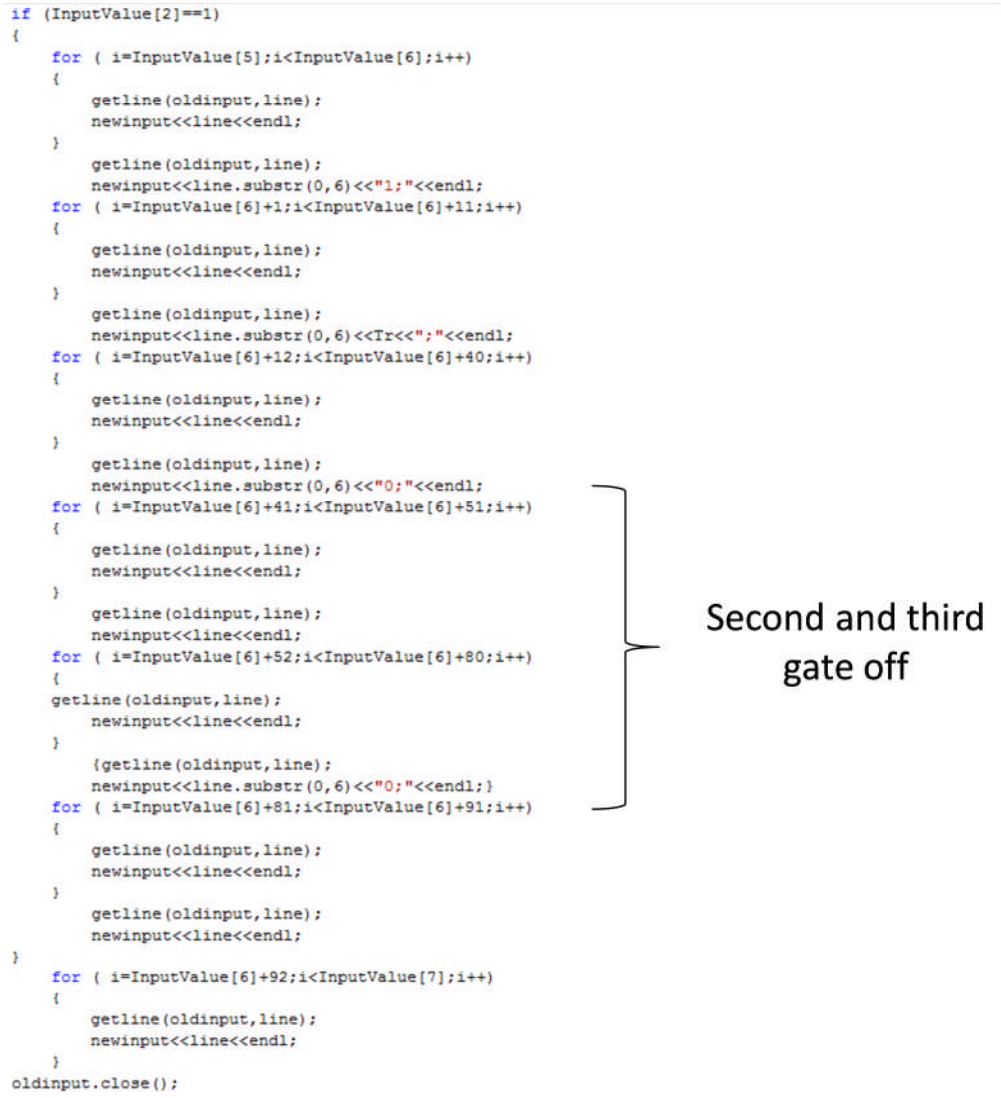

Figure A-14 Infusion optimisation interface: One potential gate case

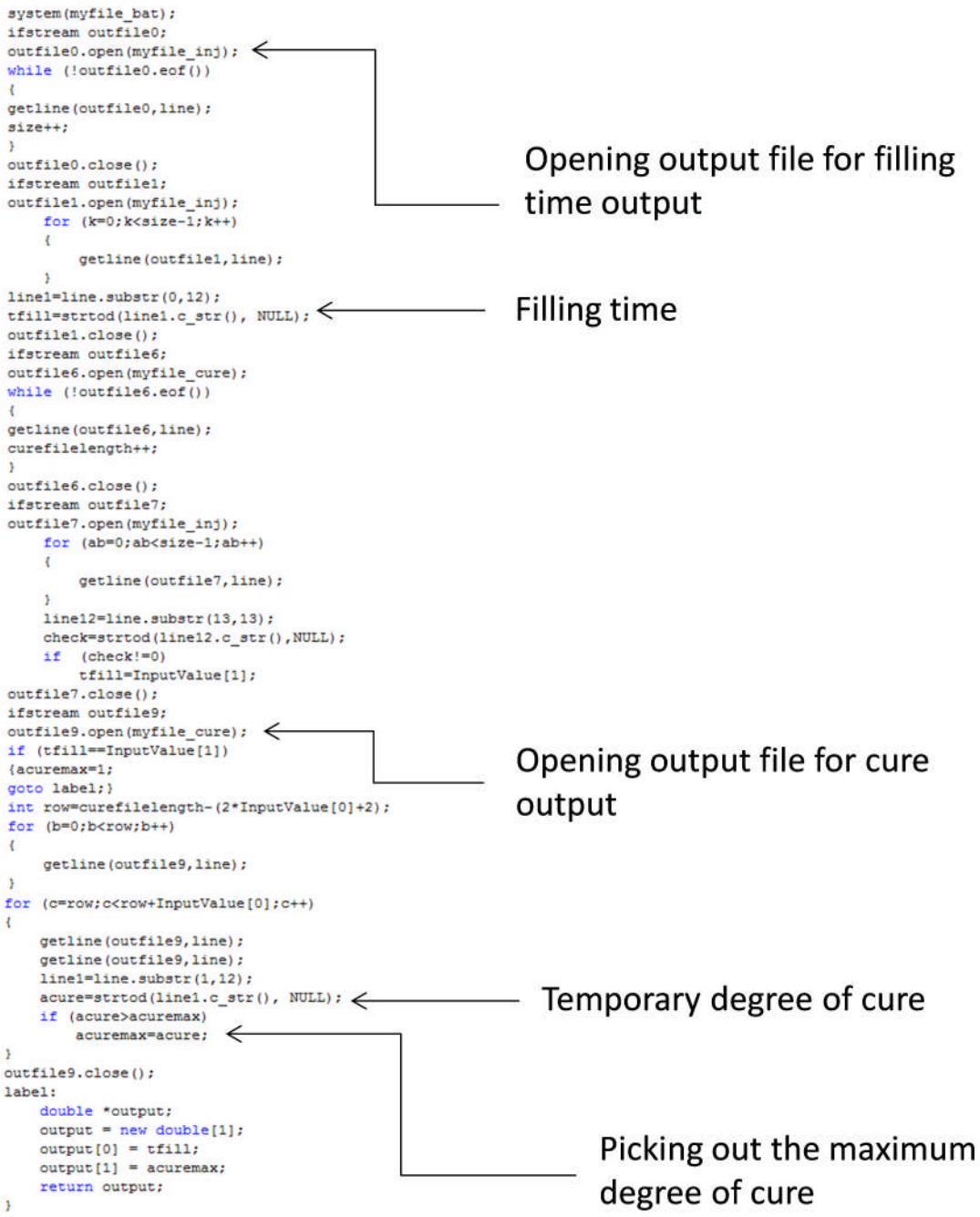

Figure A-15 Infusion optimisation interface: Execution, post processing and output

A.3 Interface code for the cost problem

The cost code interface here developed aim to link the GA with Microsoft Excel environment where a cost model has been built. The interface will be used to write the new input for the cost model at appropriate locations defined by the user in the Excel spreadsheet. An array will store the value of each new input (*InputVal[]*), and two more arrays will store the input location in the Excel sheet (*InputRow[],* (*InputCol[]*). Two arrays will store the output location (*OutputRow[],* (*OutputCol[]*) so that the interface can locate and withdraw the cost output. The user has to input the file path, the location of the input of interest and the corresponding values and the location of the output. The inputs are listed in Section 7.2. The parameter section implemented in C++ is reported in Figure A-16.

The cost interface that is illustrated in Figure A-17 operates performing the following steps:

- ✓ Activate Microsoft Excel;
- ✓ Open cost model Excel file;
- ✓ Define input and output sheets;
- ✓ Output input values at the defined row/column locations;
- ✓ Read cost model output;
- ✓ Exit with cost value.

```
    std::string path="\"Z:\\Giacomo\\My_work\\Cost_objective\\Cost_mod_bomb_withcure.xlsx\"";
    int Ninput=5;
    int Noutput=1;
    double *InputValue=new double[Ninput-1];
    double *InputRow=new double[Ninput-1];
    double *InputCol=new double[Ninput-1];
    double *outputRow=new double[Noutput-1];
    double *outputCol=new double [Noutput-1];
    InputValue[0]=T1;
    InputRow[0]=14;
    InputCol[0]=7;
    InputValue[1]=T2;
    InputRow[1]=15;
    InputCol[1]=7;
    InputValue[2]=dt1/3600;
    InputRow[2]=16;
    InputCol[2]=7;
    InputValue[3]=r*60;
    InputRow[3]=13;
    InputCol[3]=7;
    double curetime=pResultscure[1]/3600;
    double time1=(T1-120)/(r*60) +dt1/3600;
    double time2=(T1-120)/(r*60) +dt1/3600+(T2-T1)/(r*60);
    if (curetime>time2)
    {
    InputValue[4]=curetime-time2;
    }
    if (curetime>time1 & curetime<time2)
    {
    InputValue[4]=0;
    int deltatime=(curetime-time1);
    InputValue[1]=(r*60*(curetime-time1))+T1;
    }
    if (curetime<time1)
    {
    InputValue[4]=0;
    InputValue[1]=InputValue[0];
    InputValue[2]=curetime-(T1-120)/(r*60);
    }
    InputRow[4]=17;
    InputCol[4]=7;
    outputRow[0]=12;
    outputCol[0]=10;
    pResults = cost_run(Ninput,Noutput,path,InputValue,InputRow,InputCol,outputRow,outputCol);
    cPartialFitness[0] = pResultscure[0];
    cPartialFitness[1] = pResults[0];
}
```

Figure A-16 Parameter section of the cost-cure interface

```
double *cost_run(int Ninput,int Noutput,string path,double *InputValue,double *InputRow,
                 double *InputCol,double *outputRow,double *outputCol)
{
double cost;
const char *myfile= path.c_str();
 CoInitialize(NULL);
        Excel::_ApplicationPtr mpXL;
        mpXL.CreateInstance(L"Excel.Application");
        mpXL->PutDisplayAlerts(0, FALSE);
        Excel::_WorkbookPtr pBook  = mpXL->Workbooks->Open(myfile);
        Excel::_WorksheetPtr pWksheet1 = mpXL->Sheets->Item[2];
        Excel::_WorksheetPtr pWksheet2 = mpXL->Sheets->Item[11];
        Excel::RangePtr pRange1 = pWksheet1->Cells;
        Excel::RangePtr pRange2 = pWksheet2->Cells;
        int count;
        for (count=0;count<Ninput;count++)
        {
        pRange1->Item[InputRow[count]][InputCol[count]] = InputValue[count];
        }
        int k;
        for (k=0;k<Noutput;k++)
        {
         cost=pRange2->Item[outputRow[k]][outputCol[k]];
        }
        mpXL->Quit();
label:
    double *output;
    output = new double[0];
    output[0] = cost;
    return output;
}
```

Figure A-17 Cost model spreadsheet interface

A.4 Interface code for the inverse scheme

The interface obtains the process parameters values (longitudinal, through thickness and flow media permeability) from the GA. It identifies the location of the aforementioned parameters in the Proflot® input file and updates it. Subsequently it executes the solution and opens the relevant output file to withdraw the resin arrival time at the sensors location. Meanwhile interface reads a text file generated by CMC and obtains the arrival time from the experiment. A fitness function is defined capable to evaluate the agreement between data from experiment and model. This result is then fed to the GA which performs the necessary operations for minimising the error.

A set of additional information provided by the user is required. It comprises strings and a set of 11 long integers. The strings are defined as follows:

- ✓ Path: Old input file;
- ✓ Path_new: New input file;
- ✓ Path_bat: Batch file;
- ✓ Path_filling: Filling report output file;

While the array of integers (* InputValue) transfers the following values:

- ✓ *InputValue: Element number associate to sensor 1;
- ✓ *InputValue+1: Element number associate to sensor 2;
- ✓ *InputValue+2: Element number associate to sensor 3;
- ✓ *InputValue+3: Reference line to input K1 and K3;
- ✓ *InputValue+4: Reference line to input Kp;
- ✓ *InputValue+5: Number of lines of the input file;
- ✓ *InputValue+6: Noise for sensor 1;
- ✓ *InputValue+7: Noise for sensor 2;
- ✓ *InputValue+8: Noise for sensor 3;
- ✓ *InputValue+9: Number of sensors;
- ✓ *InputValue+10: Threshold jump allowed to identify arrival time from impedance measurements.

In Figure A-18 is an example of modification of the PAM-RTM® input file.

InputValue[3]=189 →

```
reinforcement_type : fabric;
permeability_curve_k1 {
        family : function;
        name : noname;
        nb_ind_vars : 1;
        type : Constant;
        C : 6.88189e-011;
}
permeability_curve_k2 {
        family : function;
        name : noname;
        nb_ind_vars : 1;
        type : Constant;
        C : 4.54331e-013;
}
permeability_curve_k3 {
        family : function;
        name : noname;
        nb_ind_vars : 1;
        type : Constant;
        C : 5.000000E-013;
}
```

(a)

InputValue[4]=631 →

```
reinforcement_type : fabric;
permeability_curve_k1 {
        family : function;
        name : noname;
        nb_ind_vars : 1;
        type : Constant;
        C : 7.66142e-010;
}
permeability_curve_k2 {
        family : function;
        name : noname;
        nb_ind_vars : 1;
        type : Constant;
        C : 7.66142e-010;
}
permeability_curve_k3 {
        family : function;
        name : noname;
        nb_ind_vars : 1;
        type : Constant;
        C : 7.66142e-010;
}
```

(b)

Figure A-18 Example of PAM-RTM® parameter input line: (a) Fabric permeability; (b) Flow media permeability

An example of input variables definition is given in Figure A-19

```
void individual::CalculateFitness()
{
    double K1;
    double K3;
    double Kp;
    std::string path;
    std::string path_new;
    std::string path_bat;
    std::string path_filling;
    std::string path_cmc;
    double *pResults = new double[0];
    K1= cChromosome.GetParameter(0);
    K3= cChromosome.GetParameter(1);
    Kp= cChromosome.GetParameter(2);
    path="z:\\Model_monitoring\\Flat_30_2D_210mm_proflot_half.dtf";
    path_new="z:\\Model_monitoring\\Flat_30_2D_210mm_proflot_half_new.dtf";
    path_bat="Z:\\Model_monitoring\\Infucomp_wp31.bat";
    path_filling="z:\\Model_monitoring\\Flat_30_2D_210mm_proflot_half_new.dtf_result_filling.unv";
    path_cmc="z:\\Model_monitoring\\Sensor_output.txt";
    int Ninput=11;
    double *InputValue=new double[Ninput-1];
    InputValue[0]=234;
    InputValue[1]=799;
    InputValue[2]=794;
    InputValue[3]=189;
    InputValue[4]=631;
    InputValue[5]=1050;
    InputValue[6]=57;
    InputValue[7]=57;
    InputValue[8]=57;
    InputValue[9]=3;
    InputValue[10]=3;
```

Figure A-19 Parameter definition

A.4.1 Interaction with CMC

The interface reads the resin arrival times at sensors from a text file generated by CMC. The file has a column for the time and a column with impedance values for each sensor. When a drop in impedance bigger than a threshold occur interface withdraw the corresponding arrival time. In Figure A-20 is reported the piece of code doing this task.

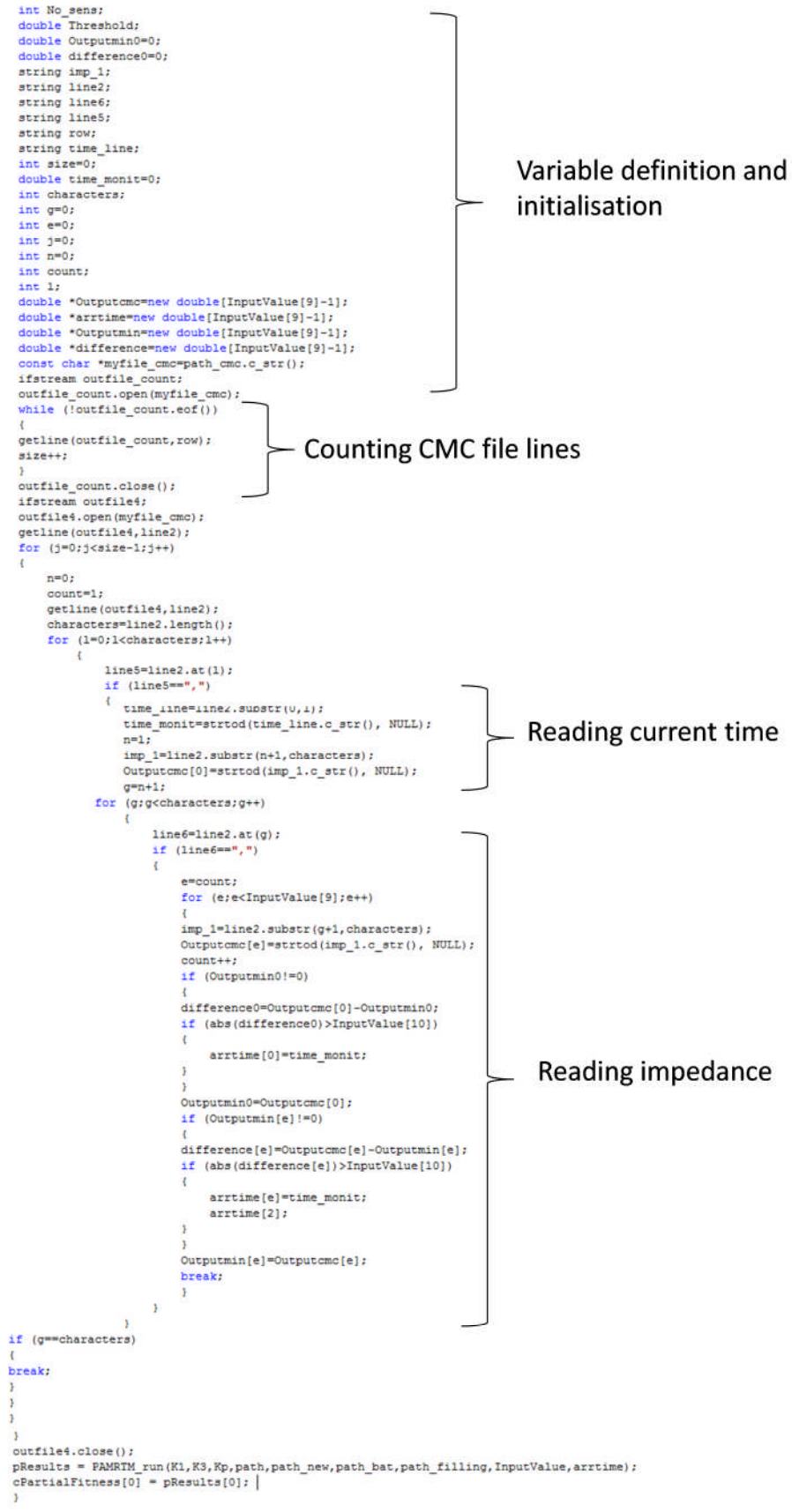

Figure A-20 Interaction with CMC file

A.4.2 Interface functions

The interface for the monitoring follows the subsequent steps:

- ✓ Variables and output definition and initialisation, in Figure A-21;
- ✓ Writing of the new input file by replacing the new permeability values both for fabric and flow media in the appropriate location, Figure A-22;
- ✓ Execution of the new solution by running Proflot®, Figure A-22;
- ✓ Opening filling output file for reading, Figure A-23;
- ✓ Arrival time from sensors with normal distributed noise, Figure A-24;
- ✓ Definition and evaluation of fitness function, Figure A-24.

```
double *PAMRTM_run(double K1,double K3, double Kp,string path,string path_new,string path_bat,
                   string path_filling,double *InputValue,double *arrtime)
{
const char *myfile=path.c_str();
const char *myfile_new=path_new.c_str();
const char *myfile_bat=path_bat.c_str();
const char *myfile_filling=path_filling.c_str();
//arrtime[0];
int sensor_reached=0;
int s1=0;
int s2=0;
int s3=0;
double t=((double) rand() / (RAND_MAX));
double w=((double) rand() / (RAND_MAX));
double v=((double) rand() / (RAND_MAX));
double r=((double) rand() / (RAND_MAX));
double b=((double) rand() / (RAND_MAX));
double d=((double) rand() / (RAND_MAX));
double sens_1=0;
double sens_2=0;
double sens_3=0;
double sensavg_1=0;
int i=0;
int k=0;
int h=0;
int sens;
int size=0;
string row;
string line;
string line1 ("Filling");
string line3;
string line4;
string time;
string numb;
string fill;
double element=InputValue[0];
double element1=InputValue[1];
double element2=InputValue[2];
double stdv_1= InputValue[6];
double stdv_2= InputValue[7];
double stdv_3= InputValue[8];
double time_1=0;
double time_2=0;
double time_3=0;
double id=0;
double unit=0;
double fitness=0;
```

Figure A-21 Variables initialisation

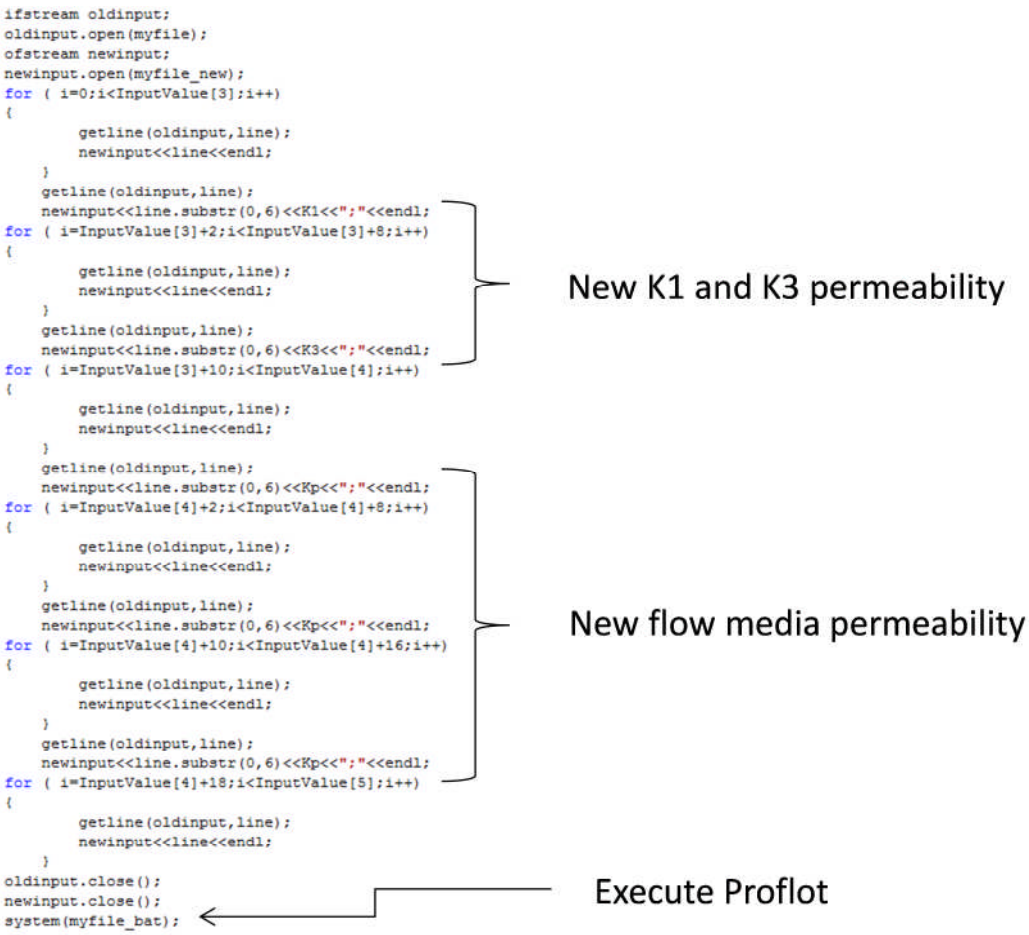

Figure A-22 New input file and Proflot® execution

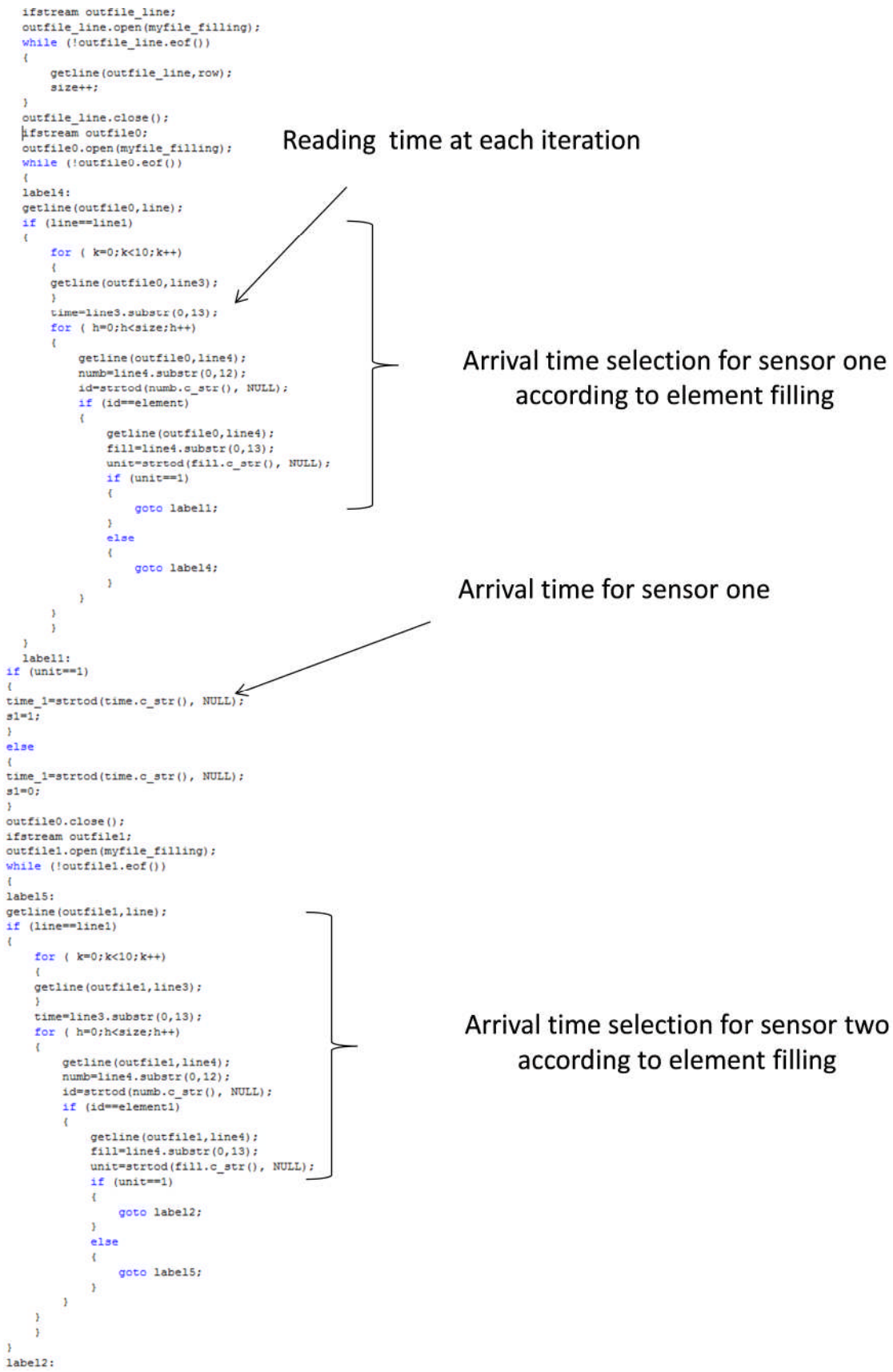


```
ifstream outfile_line;
outfile_line.open(myfile_filling);
while (!outfile_line.eof())
{
    getline(outfile_line,row);
    size++;
}
outfile_line.close();
ifstream outfile0;
outfile0.open(myfile_filling);
while (!outfile0.eof())
{
label4:
getline(outfile0,line);
if (line==line1)
{
    for ( k=0;k<10;k++)
    {
    getline(outfile0,line3);
    }
    time=line3.substr(0,13);
    for ( h=0;h<size;h++)
    {
        getline(outfile0,line4);
        numb=line4.substr(0,12);
        id=strtod(numb.c_str(), NULL);
        if (id==element)
        {
            getline(outfile0,line4);
            fill=line4.substr(0,13);
            unit=strtod(fill.c_str(), NULL);
            if (unit==1)
            {
                goto label1;
            }
            else
            {
                goto label4;
            }
        }
    }
    }
}
label1:
if (unit==1)
{
time_1=strtod(time.c_str(), NULL);
s1=1;
}
else
{
time_1=strtod(time.c_str(), NULL);
s1=0;
}
outfile0.close();
ifstream outfile1;
outfile1.open(myfile_filling);
while (!outfile1.eof())
{
label5:
getline(outfile1,line);
if (line==line1)
{
    for ( k=0;k<10;k++)
    {
    getline(outfile1,line3);
    }
    time=line3.substr(0,13);
    for ( h=0;h<size;h++)
    {
        getline(outfile1,line4);
        numb=line4.substr(0,12);
        id=strtod(numb.c_str(), NULL);
        if (id==element1)
        {
            getline(outfile1,line4);
            fill=line4.substr(0,13);
            unit=strtod(fill.c_str(), NULL);
            if (unit==1)
            {
                goto label2;
            }
            else
            {
                goto label5;
            }
        }
    }
    }
}
label2:
```

Figure A-23 Reading of arrival times in the model

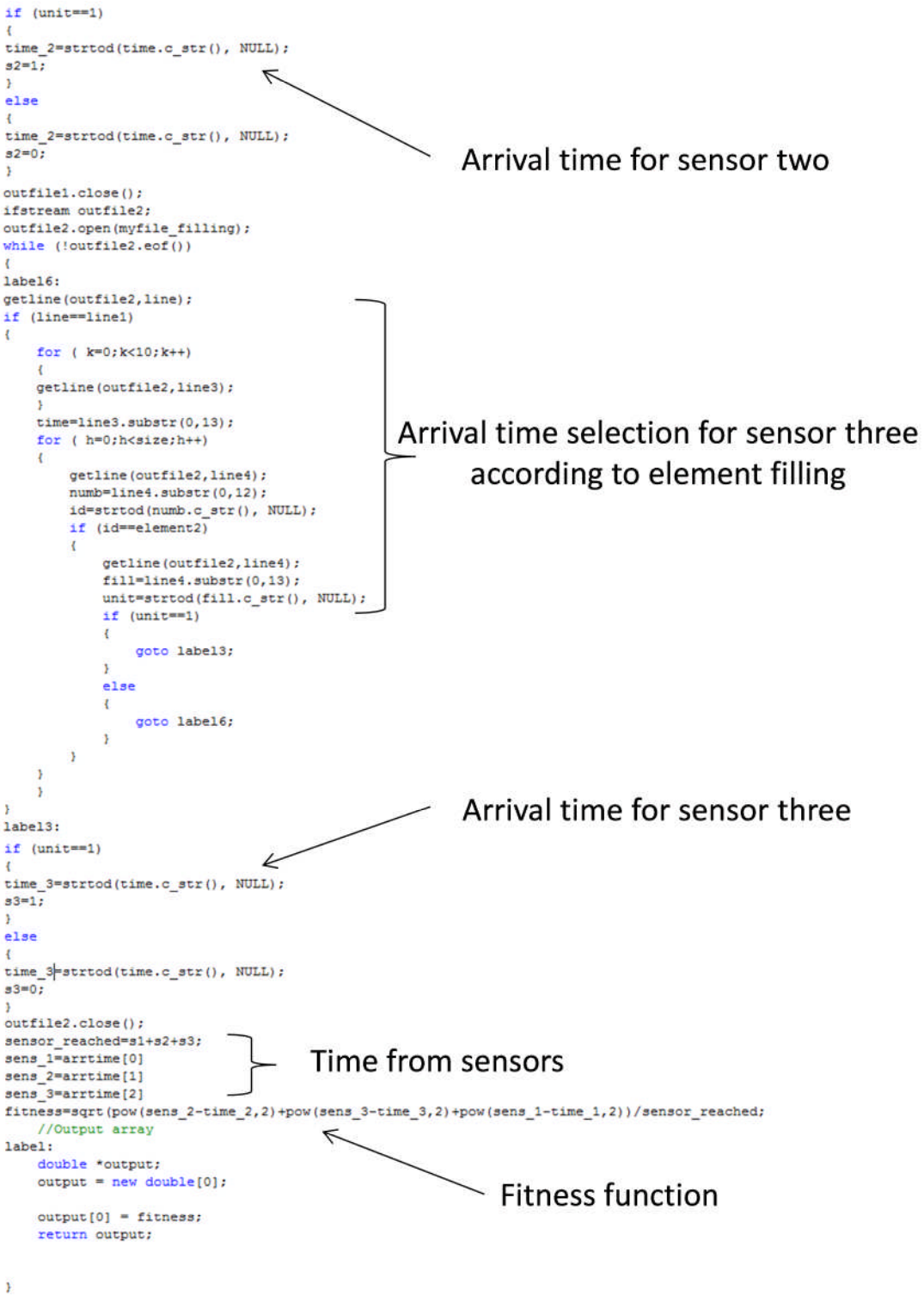


```
if (unit==1)
{
time_2=strtod(time.c_str(), NULL);
s2=1;
}
else
{
time_2=strtod(time.c_str(), NULL);
s2=0;
}
outfile1.close();
ifstream outfile2;
outfile2.open(myfile_filling);
while (!outfile2.eof())
{
label6:
getline(outfile2,line);
if (line==line1)
{
    for ( k=0;k<10;k++)
    {
    getline(outfile2,line3);
    }
    time=line3.substr(0,13);
    for ( h=0;h<size;h++)
    {
        getline(outfile2,line4);
        numb=line4.substr(0,12);
        id=strtod(numb.c_str(), NULL);
        if (id==element2)
        {
            getline(outfile2,line4);
            fill=line4.substr(0,13);
            unit=strtod(fill.c_str(), NULL);
            if (unit==1)
            {
                goto label3;
            }
            else
            {
                goto label6;
            }
        }
    }
    }
}
label3:
if (unit==1)
{
time_3=strtod(time.c_str(), NULL);
s3=1;
}
else
{
time_3=strtod(time.c_str(), NULL);
s3=0;
}
outfile2.close();
sensor_reached=s1+s2+s3;
sens_1=arrtime[0]
sens_2=arrtime[1]
sens_3=arrtime[2]
fitness=sqrt(pow(sens_2-time_2,2)+pow(sens_3-time_3,2)+pow(sens_1-time_1,2))/sensor_reached;
    //Output array
label:
    double *output;
    output = new double[0];

    output[0] = fitness;
    return output;


}
```

Figure A-24 Sensor arrival times